To the Graduate Council:

I am submitting herewith a dissertation written by David C. Huang entitled "Extrudate Swell of Polymer Melts and Compounds in Various Die Geometries and the Screw Extrusion of Rubber Compounds." I recommend that it be accepted in partial fulfillment of the requirements for the degree of Doctor of Philosophy, with a major in Polymer Engineering.

J. L. White, Major Professor

We have read this dissertation
and recommend its acceptance:

Accepted for the Council:

Vice Chancellor
Graduate Studies and Research

X

EXTRUDATE SWELL OF POLYMER MELTS AND COMPOUNDS IN VARIOUS DIE GEOMETRIES AND THE SCREW EXTRUSION OF RUBBER COMPOUNDS

A Dissertation

Presented for the

Doctor of Philosophy

Degree

The University of Tennessee, Knoxville

David C. Huang

March 1981

ACKNOWLEDGEMENT

The author wishes to express his appreciation to the many people who have contributed to the completion of this dissertation.

Foremost of all, Professor James L. White, the author's advisor, has been a constant source of guidance and inspiration. Sincere appreciation is extended to Professor White for his many critical suggestions and encouragement on the various aspects of this work.

Appreciation is also extended to Professor H. F. Johnson, Head of the Department of Chemical, Metallurgical and Polymer Engineering.

This work was supported in part by a Fellowship from the Phillips Petroleum Company and from the National Science Foundation under grants NSF GK43921 and ENG 76-19815. Support also came from a Teaching Assistantship and the Industrial Polymer Consortium.

Thanks is also due to the Mechanical and Instrument shops. Special thanks is extended to Mr. H. B. Thompson and his co-workers for producing numerous dies of different geometries which were used in this work.

The author expresses his appreciation to all the faculty members, especially the "Polymer Engineering and Science Group".

Appreciation is extended to Professor D. C. Bogue for useful comments on this work. Thanks are also extended to V. M. Lobe and W. Minoshima for providing some experimental data.

To all these people, the author expresses his deepest gratitude and appreciation.

ABSTRACT

A comparative experimental and theoretical study is presented for extrudate swell and dies of various cross-sectional geometries and lengths. The geometries studied included slit, capillary, rectangular and trapezoidal dies. We also present an experimental and theoretical study of screw extrusion of rubber compounds.

The swell from slit dies is greater than the swell from capillaries. At low die wall shear rates the swell of homogeneous melts goes to a value of about 1.2 for slit dies as opposed to about 1.1 found for capillary dies. The swell from short dies is greater than the swell from long dies.

A theoretical study of extrudate swell based on unconstrained elastic recovery from poiseuille flow is developed for long dies. The argument is made that elongational flow existing in the die entry region determines extrudate swell for short dies. A theory of swell based on unconstrained recovery from the entrance flow is developed. A theory is also proposed for the swell of filled polymer melts. This involves consideration of the gel-like character of these materials.

The screw extrusion of rubber compounds has also been studied. A new model is developed which considers the slip of the rubber compounds in the region near the hopper.

TABLE OF CONTENTS

CHAPTER		PAGE
1.	INTRODUCTION	1
2.	HISTORICAL BACKGROUND	3
	A. Constitutive Equation B. Rheological Properties of Polymer Melts C. Rheological Properties of Filled Polymer melts D. Die Flow E. Screw Extrusion	
3.	MATERIALS AND APPARATUS	40
	A. Materials B. Apparatus	
4.	EXTRUSION PRESSURE LOSS OF POLYMER MELTS FLOWING THROUGH RECTANGULAR AND TRAPEZOIDAL DIES	53
	A. Theory B. Experimental C. Results and Interpretation	
5.	EXTRUDATE SWELL FOR LONG SLIT AND CAPILLARY DIES	67
	A. Experimental Approach B. Theory of Extrudate Swell C. Interpretation of Experiments D. Conclusions	
6.	EXTRUDATE SWELL FROM SHORT SLIT AND CAPILLARY DIES	95
	A. Experimental B. Results C. Discussion and Analysis D. Theory of Extrudate Swell from Short Dies E. Conclusions	

CHAPTER PAGE

7. EXTRUDATE SWELL FROM DIES OF COMPLEX GEOMETRIES 120

A. Theory
B. Experimental
C. Results and Interpretation
D. Conclusions

8. EXTRUDATE SWELL OF FILLED POLYMER MELTS 139

A. Theoretical
B. Experimental
C. Results and Discussion
D. Conclusions

9. SCREW EXTRUSION OF RUBBER COMPOUNDS 171

A. General
B. Theoretical Model
C. Experimental
D. Discussion
E. Conclusion

LIST OF REFERENCES 221

VITA 238

LIST OF TABLES

TABLE		PAGE
3-1.	Typical recipes for rubber compounds.	45
4-1.	Dimensions of dies for experiment in Ch. 4. . .	61
5-1.	Dimensions of dies for experiment in Ch. 5. . .	69
5-2.	Shear rates and shear stresses at distortion occurrence.	79
6-1.	Dimensions of dies for experiment in Ch. 6. . .	97
8-1.	Dimensions of dies for experiment in Ch. 8. . .	161

LIST OF FIGURES

FIGURE		PAGE
2-1.	Schwedoff model representing rheological behavior of filled polymers	10
3-1.	Viscosity-shear rate behavior of polymer melts studied	41
3-2.	Principal normal stress difference-shear stress behavior for polymer melts studied . . .	42
3-3.	Viscosity and principal normal stress difference-shear stress behavior for polymer melts studied	43
3-4.	Sandwich testing device	49
3-5.	Screw extruder used for studying screw extrusion of rubber compounds	51
4-1.	Die dimension: (a) rectangle, (b) trapezoid. .	57
4-2.	Plots of Q vs. $(\Delta P_d H/2L)$ for rectangular die. .	62
4-3.	Plots of Q vs. $(\Delta P_d H/2L)$ for trapezoidal die. .	65
5-1.	Photographs of unannealed cross sections of extrudates from capillary and slit dies	71
5-2.	Influence of annealing on cross-sectional shape	72
5-3.	Photographs of polystyrene (PS) and polypropylene (PP) extrudates from capillary and slit dies in unstable flow region	74
5-4.	Extrudates swell d/D and h/H as a function of of die wall shear for melts for unannealed extrudates (correlated to 180°C).	75
5-5.	Influence of annealing and extrudate swell-shear ratio function.	77
5-6.	Extrudate swell for slit and capillary dies as a function of ratio of principal normal stress difference to shear stress at the die wall.	89

FIGURE PAGE

5-7. Plot of extrudate swell for slit and capillary dies vs. die wall shear stress for polystyrene comparison with Eqs. (5-21) and (5-22). 93

6-1. Extrudate swell B as a function of die length for PS 98

6-2. Comparison of extrudate swell B from short (L/D, L/H→0) and long (L/D, L/H→∞) slit and capillary dies. 100

6-3. Influence of die entry geometry on extrudate swell of PP 103

6-4. Influence of die entry geometry on extrudate swell of PS 104

6-5. Elongational flow character of die entrance region. 105

6-6. $\bar{\tau} = N_1/2\,\sigma_{12}\dot{\gamma}$ as a function of $\dot{\gamma}$ for PS and PP. 109

6-7. Plot B vs. Weissenberg number $\tau_{ch}\, V_{ch}/L_{ch}$ for 30° and 120° angle dies 111

6-8. Comparison of theory and experiment for swell swell of PS from a 180° entrance angle die. . . 118

7-1. Die and extrudate cross sections for capillary: (a) D=0.762 mm, (b) D=1.702 mm; for slit: (c) aspect ratio 16.7, (d) aspect ratio 10.0; (e) rectangle, (f) trapezoid. . . . 118

7-2. Comparison between unannealed and annealed extrudate dimension for (a) rectangular (b) trapezoidal dies. 129

7-3. Extrudate swell-wall shear stress behaviors for polystyrene of various die geometries . . . 132

7-4. Extrudate swell-wall shear stress behaviors for polypropylene of various die geometries . . 133

7-5. Comparison of predicted (inner solid line) observed (outer solid line) PS extrudate dimension from rectangular die at $\Delta P_{die} H/2L =$ 1.1×10^5 pascal. 136

FIGURE PAGE

7-6. Comparison of predicted (inner solid line) observed (outer solid line) PS extrudate dimension from trapezoidal die at $\Delta P_{die} H/2L = 1.1 \times 10^5$ pascal. 137

8-1. Model for filled polymer melts. 140

8-2. Viscosity-shear rate behavior for the rubber compounds used 159

8-3. Viscosity-shear stress behavior for the rubber compounds used 160

8-4. Capillary extrudate swell as a function of die length for tread compound 162

8-5. Extrudate swell-wall shear stress for side wall compound 163

8-6. Viscosity and principal normal stress difference as a function of shear stress of TiO_2 filled polystyrene with various solid volume fraction 165

8-7. Extrudate swell-wall shear stress for tread compound. 166

8-8. Extrudate swell-wall shear stress behavior for TiO_2 filled polystyrene with various volume fraction 168

8-9. Extrudate swell as a function ratio of principal normal stress difference to shear stress at the die wall. 169

9-1. Rectanglized screw channel. 174

9-2. An infinitesimal element at barrel surface. . . 181

9-3. Flow patterns of isothermal flow in screw channel with various slip conditions. 186

9-4. Comparison of Q^* vs. G_r behaviors of isothermal Newtonian flow at various barrel and screw surface slippage conditions 187

9-5. Comparison of Q^* vs. G_r behaviors of isothermal flow in screw channel with variable slip conditions. 189

FIGURE PAGE

9-6. Flow patterns of Bingham fluid in a screw channel at various conditions 195

9-7. Comparison of Q^* vs. G_r behaviors between Newtonian and Bingham fluid and non-slip at wall 196

9-8. Rectangular opening at the screw hopper 197

9-9. (a) Output rate-RPM (b) head pressure-RPM behaviors for the screw extrusion of tread compound at various conditions. 201

9-10. (a) Output rate-RPM (b) head pressure-RPM behaviors for the screw extrusion of side wall compound at various conditions 202

9-11. Output rate-head pressure behaviors for cold feed continuous strip of tread compound at various RPM 204

9-12. Output rate-head pressure behaviors for hot feed pieces of tread compound at various RPM. . 205

9-13. Output rate-head pressure behaviors for cold feed pieces of tread compound at various RPM. . 206

9-14. Output rate-head pressure behaviors for hot feed side wall compound at various RPM. 207

9-15. Output rate-head pressure behaviors for cold feed side wall compound at various RPM. 208

9-16. Output rate-head pressure behaviors for polystyrene 209

9-17. Output rate-head pressure behaviors for polypropylene 210

9-18. Comparison of Q^* vs. G_b behaviors of cold feed continuous strip at various RPM. 212

9-19. Comparison of Q^* vs. G_b behaviors of tread compound at 60 RPM and various feeding conditions. 213

9-20. Comparison of Q^* vs. G_b behaviors of side wall compound at various RPM and feeding conditions. 214

FIGURE PAGE

9-21. (a) Screw opening (b) backup flow at screw opening of rubber compounds 216

9-22. Q^* vs. G_b behaviors of polystyrene at various various RPM 217

9-23. Q^* vs. G_b behaviors of polypropylene at various RPM 218

CHAPTER 1

INTRODUCTION

No process or apparatus is more important than screw extrusion in the polymer processing industry.

The screw extruder is a continuous pumping device which can transfer heat, mix polymer systems and build up high pressure to push polymer melts through a die. The die may have various geometries ranging from circular to slit, annular, rectangular or trapezoid depending on the frozen shape of final product.

The extrusion process has been a subject of extensive study for more than one hundred years. However to the present many practical problems are still solved by engineering art and trial and error experience. This is because practical problems are generally very complicated and the available studies are usually for specific and simple cases.

This problem of extrudate swell and character of melts emerging from dies has been of considerable concern in the polymer industry for a half century or more. Most of these studies have involved flow through capillary dies and indeed only a few investigators report studies on cross sections other than circular and these results are only qualitative. The more limited literature on polymer compounds relates largely to qualitative descriptions.

Studies of screw extrusion of polymers in the literature generally consider simple metering screw pump behavior or combine it with a plasticating melting model. There has been little attention given for the peculiar characteristics of rubber compounds, even though this was the first type of polymer system commercially processed in a screw extruder and continues to be important to this day.

Our purpose in this dissertation is to present a broad based study of flow through dies and in the screw extruder for pure and filled polymer melts and elastomers. We compare the theoretical and experimental pressure loss vs. extrusion rate relationship for dies of various geometries. A major purpose of the present dissertation is to present a joint theoretical and experimental study of extrudate swell of homogeneous and filled polymer melts emerging from dies of various geometries including slit, capillary, trapezoidal and rectangular dies. The influence of die length and entrance geometry will be considered. We conclude by presenting a fundamental new theoretical and experimental study of screw extrusion of rubber compounds.

CHAPTER 2

HISTORICAL BACKGROUND

A. CONSTITUTIVE EQUATION

Polymer melts show a wide variety of responses in flow conditions, such as non-Newtonian viscosity, recoil, extrudate swell and Weiseenberg effect. They exhibit the combined behavior of the properties of solids and liquids and show elastic as well as viscous response to applied stresses. There have been many attempts to express the relation between the strain history and stress in visco-elastic fluid. These are generally termed constitutive equations (54, 246).

Two types of constitutive equations of viscoelastic materials have been developed. These are differential type models (rate theory) and integral type models (integral theory). As early as 1867 Maxwell (144) had presented a simple model to represent the viscoelastic materials. This model generates a basic one dimensional differential type constitutive equation,

$$\sigma + \tau \frac{d\sigma}{dt} = G\tau\dot{\gamma} \qquad (2\text{-}1)$$

where σ is the stress, $\dot{\gamma}$ is the strain rate, G is the elastic modulus and τ denotes the relaxation time (144).

This theory is linear and does not predict normal stresses or non-Newtonian viscosity. Maxwell's theory

was generalized to large deformation and a three-dimensional form by Zaremba (284). Zaremba's theory predicts both normal stresses and non-Newtonian viscosity. Various modified and non-linear forms have been proposed by Hencky (99), de Witt (69), Oldroyd (183), Williams and Bird (273), Spriggs and Bird (218, 219) and notably White and Metzner (269). The White and Metzner formulation which is most widely used has the form

$$\sigma_{ij} = - P \delta_{ij} + \underline{P}_{ij} \tag{2-2}$$

$$\underline{P}_{ij} + \tau(\mathrm{II}_d) \frac{\delta \underline{P}_{ij}}{\delta t} = 2 G \tau(\mathrm{II}_d) d_{ij} \tag{2-3}$$

$$\frac{\delta \underline{P}_{ij}}{\delta t} = \frac{D \underline{P}_{ij}}{Dt} - V_{,m}{}^{i} \underline{P}_{mj} - V_{,m}{}^{j} \underline{P}_{im} \tag{2-4}$$

where II_d is secondary invariant of deformation tensor d_{ij}. $\delta/\delta t$ is the contravarient form of Oldroyd's convected derivative (182) which physically is expressing the rate of change of stress as viewed from a rotating and deforming coordinate system.

In 1874 Boltzmann (29) established the general constitutive equation, the so-called superposition integral equation, for a viscoelastic material which is subjected to small deformations. This has the one dimensional form

$$\sigma = \int_{-\infty}^{t} G(t-s) \dot{\gamma}(s) \, ds \tag{2-5}$$

where G (t) is a fading memory function of t, known as the relaxation modulus, $\dot{\gamma}$ is the strain rate and s is the time.

The basic concept is that the stress is a sum of all past strain history weighted with a "memory" function. This memory function is exponential in form and recent strain experience is more important than past experience, which the material gradually "forgets". If the memory is very large, the material becomes an elastic solid. If the memory goes to zero it becomes a Newtonian fluid.

Integration of Eq. (2-5) by parts and taking the present state (s=t) as the standard state to make $\gamma(t)=0$, gives

$$\sigma(t) = \int_{-\infty}^{t} \Phi(t - s)\, \gamma(s)\, ds$$

$$\Phi(t - s) = - \frac{d\, G\, (t - s)}{ds} \qquad (2\text{-}6)$$

The Maxwell equation is a special case of the Boltzmann equation for

$$G\,(t) = G\, e^{-t/\tau} \quad \text{and} \quad (t) = \frac{G}{\tau}\, e^{-t/\tau} \qquad (2\text{-}7)$$

The relaxation spectrum $H\,(\tau)$ is introduced to represent G(t) as a generalized Maxwell fluid as follows:

$$G\,(t) = \int_{-\infty}^{\infty} H\,(\tau)\, e^{-t/\tau}\, d \ln \tau \qquad (2\text{-}8)$$

The Boltzmann equation predicts Newtonian viscosity and is limited to small deformations. Generalization of the Boltzmann theory to large strains was first attempted by Lodge (128). Green and Rivlin (90) have proposed a general three dimensional form of the hereditary functional for large strains. The nonlinear integral theory approach

of Green and Rivlin (90) is certainly general enough to explain the nonlinear phenomena observed in viscoelastic polymer fluids. An equivalent formulation has been proposed by Coleman and Noll (54, 179).

Zapas and Craft (282, 283) have shown on the basis of multistep large deformation stress relaxation tests on bulk rubber that a constitutive equation containing only a single integral is more appropriate than one containing double, triple and higher integrals. This result suggests restrictions on constitutive theories.

Bernstein, Kearsley and Zapas (BKZ) (16, 17) proposed a constitutive equation of this form which is able to predict most if not all of the nonlinear phenomena observed in viscoelastic fluid systems. Their theory is motivated by the Finger-Rivlin theory of nonlinear ("rubber") elasticity and involves the introduction of a time dependent scalar function which plays the same role in their theory as the strain energy function does in elasticity theory. Bird and his students (21, 219) used the deformation rate invariant instead of the strain invariant. Bogue (24) proposed a theory later modified by Bogue and White (26, 94), which is intermediate between BKZ and Bird. It involves time averaged rate of deformation variants.

The single integral constitutive equation for isotropic viscoelastic fluids has the general form as (26, 94)

$$\underset{\sim}{\sigma} = - p\underset{\sim}{I} + \int_o^\infty [m_1(z)\underset{\sim}{c}^{-1} - m_2(z)\underset{\sim}{c}]\, dz \qquad (2\text{-}9)$$

where $\underset{\sim}{\sigma}$ is the stress tensor, p is pressure, $\underset{\sim}{I}$ the unit tensor, $\underset{\sim}{c}^{-1}$ and $\underset{\sim}{c}$ the Finger and Cauchy deformation measures and $m_1(z)$ and $m_2(z)$ are memory functions. In general $m_1(z)$ and $m_2(z)$ may depend upon deformation or deformation rates. The Lodge "rubber-like" fluid (129) is the special case of Eq. (2-9) for which $m_2(z)$ is zero and $m_1(z)$ is independent of deformation invariants. In the Bogue-White model

$$m_1(z) = \left[1 + \frac{\epsilon}{2}\right] \sum_i \frac{G_i}{\tau_{ieff}} e^{-z/\tau_{ieff}}$$

$$m_2(z) = - \frac{\epsilon}{2} \sum_i \frac{G_i}{\tau_{ieff}} e^{-z/\tau_{ieff}} \qquad (2\text{-}10)$$

and $$\tau_{ieff} = \frac{\tau_i}{1 + a\tau_i \bar{\mathrm{II}}_d^{\frac{1}{2}}} \qquad (2\text{-}11)$$

where $$\mathrm{II}^{\frac{1}{2}} = \frac{1}{z} \int_o^\infty \left| \mathrm{II}_d(s) \right|^{\frac{1}{2}} ds \qquad (2\text{-}11)$$

$$\mathrm{II}_d = 2 \operatorname{tr} \underset{\sim}{d}^2 = 2\, d_{ij} d_{ji}$$

where τ_{ieff} depends upon the time averaged rate of deformation tensor. The quantity ϵ determines the value of the second normal stress difference. ϵ is reported to have the values of -0.2 to -0.6 (264). $\bar{\mathrm{II}}^{\frac{1}{2}}$ is the time averaged square root second invariant of rate of deformation. The effective time constant τ_{ieff} becomes smaller as the shear rate is increased.

The quantity a is an empirical constant. Generally, the parameters are the same order 0.6 - 1.2 (81) for polymer melts.

Most constitutive equations predict that the elongational viscosity and stress become infinite (279, 39, 64) at high elongation rate. Dealy (62) and Bird et al (22) tabulate some of the more complicated rheological models according to whether or not they predict a bounded elongational viscosity for all finite rates of strain or not. Ide and White (104, 105) showed if $a < 2/\sqrt{3}$ in the Bogue-White model, the elongation viscosity and stress will become unbounded at finite elongation rates.

Constitutive equations based on models of concentrated systems of flexible chains are due to Yamamoto (279, 280) and Lodge (128). Variations of these models have been developed in more recent years by Tanner (227) and by Phan and Tanner (231).

Many polymer processing operations involve large variations in temperature with time (e.g. melt spinning, tubular film extrusion). Therefore the material time constant should be temperature dependent. Replacing τ by $\tau(T)$ or equivalently $\tau(t)$ in Eq. (2-1), we can suggest the form of the non-isothermal Maxwell model through dependence on time; i.e.

$$\sigma + \tau(t) \frac{d}{dt} = G \tau(t) \dot{\gamma} \qquad (2\text{-}12)$$

The solution of Eq. (2-12) is (25),

$$\sigma = G \int_{-\infty}^{t} e^{-\int_{t'}^{t} \frac{dt''}{\tau(t'')}} \dot{\gamma}(t')\, dt' \qquad (2\text{-}13)$$

Matsui and Bogue (137-139) (see also 70, 140) have developed a non-isothermal constitutive equation for non-linear viscoelastic fluids. This has the form

$$\sigma_{ij} = -p\,\delta_{ij} + \sum_n G_n^{\circ} \frac{T(t)}{T_\circ} \cdot \int_{-\infty}^{t} \frac{\exp\left[-\int_{t'}^{t} \frac{dt''}{\tau^*_n[II_d(t''),\ T(t'')]}\right]}{\tau^*_n[II_d(t'),\ T(t')]} \cdot c_{ij}^{-1}\,(t,t')\, dt' \qquad (2\text{-}14)$$

$$\tau^*_n[II_d(\cdot),\ T(\cdot)] = \frac{\tau_n^{\circ} a_T[T(\cdot)]}{1+bII_d^{\frac{1}{2}}(\cdot)a_T[T(\cdot)]\tau_n^{\circ}} \qquad (2\text{-}15a)$$

$$\tau_n(\cdot) = a_T(T(\cdot))\,\tau_n^{\circ} \qquad (2\text{-}15b)$$

where II_d is the second invariant of the deformation rate tensor, and b is a dimensionless empirical parameter. This is similar to the Bogue and White isothermal model (26). Here $a_T(T)$ is the shift factor due to Williams, Landel and Ferry equation (274), which has approximately the form:

$$\log a_T(T) = \frac{-C_1(T-T_\circ)}{C_2+T-T_\circ} \qquad (2\text{-}16)$$

In highly filled polymer melt systems with small particles, a yield value is generally found as in a Bingham plastic fluid (19). The Schwedoff model yield as shown in Figure 2-1, a simple combination of a yield value Y and a Maxwell mdoel has been proposed by Lobe and White (127, 272) to represent the flow behavior of filled polymers. Using

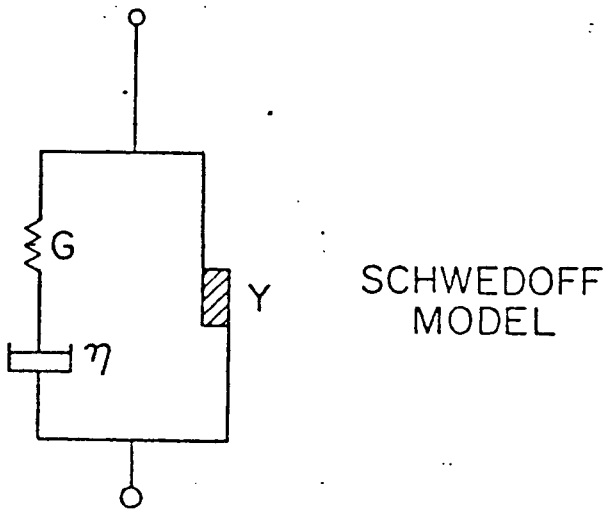

Figure 2-1. Schwedoff model representing rheological behavior of filled polymers.

arguments of the type developed by Hohenemser and Prager (100) and Oldroyd (181) for Bingham plastics and through application of a Von Mises yield criterion, Lobe and White (272, 127) have extended this to a three dimensional constitutive equation as:

$$\sigma = -pI + \underset{\sim}{P} \quad \text{with tr } \underset{\sim}{P} = 0 \tag{2-17}$$

$$\text{tr } \underset{\sim}{P}^2 < 2Y^2 \quad \underset{\sim}{d} = 0 \tag{2-18}$$

$$\text{tr } \underset{\sim}{P}^2 > 2Y^2 \quad \underset{\sim}{P}\left(1-\frac{2Y}{\text{tr}\underset{\sim}{P}^2}\right) = \underset{\sim}{H}\ (\text{deformation history}) \tag{2-19}$$

where a single integral form of H is

$$\int_0^\infty [u_1(z)(\underset{\sim}{c}^{-1}-1/3\ \text{tr}\underset{\sim}{c}^{-1}) - u_2(z)(\underset{\sim}{c}-1/3\ \text{tr}\underset{\sim}{c})]\ dz$$

Here $\underset{\sim}{P}$ is the deviatoric stress tensor, $\underset{\sim}{c}^{-1}$, the Finger deformation tensor, $\underset{\sim}{c}$ the Cauchy deformation tensor, $\underset{\sim}{d}$ the rate of deformation tensor and $u_1(z)$ and $u_2(z)$ are relaxation functions.

B. RHEOLOGICAL PROPERTIES OF POLYMER MELTS

The rheological properties of polymer melt systems are very complex compared to most industrial fluids. The simplest of these fluids is the homogeneous polymer melt. It is generally agreed that this fluid is an isotropic viscoelastic fluid and for small strains obeys the Boltzmann superposition integal (1, 81, 116, 176, 233-238, 271, 272). For large strains and flows, the general features of the response are semi-quantitatively agreed upon those different constitutive equations proposed but no general agreement exists (97, 217, 154, 24, 40, 3, 66, 21).

It is of importance that we consider the rheological characteristics of polymer melts in shear flow for this type of kinematics exists in fully developed flow through a die. Simple shear flow in cartesian coordinates

$$v_1 = v_1(x_2) \qquad v_1 = v_2 = 0 \tag{2-20}$$

The stress response to this flow involves both a shear stress, σ_{12}, which resists flow and normal stresses, σ_{11}, along the streamlines and σ_{22} in the direction of shear. The stress state in flow is determined by the isotropic pressure the shear stress, σ_{12}, and two normal stress differences N_1 and N_2 defined by

$$N_1 = \sigma_{11} - \sigma_{22} \qquad N_2 = \sigma_{22} - \sigma_{33} \tag{2-21}$$

The stress responses σ_{12}, N_1 and N_2 to shear flow may be related to $\dot{\gamma}$ through rheological properties, namely the shear viscosity η and the normal stress coefficients Ψ_1 and Ψ_2

$$\sigma_{12} = \eta(\dot{\gamma})\dot{\gamma} \qquad N_1 = \Psi_1(\dot{\gamma})\dot{\gamma}^2 \qquad N_2 = \Psi_2(\dot{\gamma})\dot{\gamma}^2 \tag{2-22}$$

where η, Ψ_1, and Ψ_2 are functions of the absolute value or square of $\dot{\gamma}$. Generally the principal normal stress coefficient is considered as a product of the viscosity and a characteristic time $\bar{\tau}$.

$$\Psi_1 = 2\eta\bar{\tau} \tag{2-23}$$

where $\bar{\tau}$ is the ratio of the first to the zeroth moment of the relaxation modulus function according to viscoelastic fluid theory.

There have been extensive studies of the viscosity function for molten polymers (11, 125, 95, 97, 180, 267, 268). Usually, at least two viscometers are needed with a capillary viscometer to get high shear rate data and usually a cone-plate (79, 258) to obtain low shear rate data. Typically the viscosity is constant at low shear rates and then decreases with increasing shear rate. In this high shear rate range, data tend to be linear on logarithmic paper indicating power law behavior; i.e.,

$$\sigma_{12} = K\dot{\gamma}^{n} \qquad \eta = K\dot{\gamma}^{n-1} \tag{2-24}$$

Several researchers have measured N_1 as a function of shear rate generally using cone-plate instruments (11, 13, 9, 95, 97, 180, 267, 268). The normal stress data is usually limited to shear rates less than 10 sec^{-1}. The coefficient Ψ_1 like η is a decreasing function of shear rate. However N_1 increases much more rapidly than σ_{12} with $\dot{\gamma}$. A power law relationship of N_1 - σ_{12} is generally valid at low shear rate for polymer melts as follows:

$$N_1 = A\,\sigma_{12}^{a} \tag{2-25}$$

Oda, Clark and White (180) compared a range of commercial polystyrene and found that the N_1 - σ_{12} relationship is a monotonic increasing function independent of temperature and is unique in families of polymers with similar molecular weight distributions.

The ratio N_1/σ_{12} can become quite large for some melts, being often greater than unity by a $\dot{\gamma}$ of 1 sec^{-1}. There has been little study of N_2 but existing results indicate it to be negative and of order 10 to 20 percent of the value of N_1 (125).

Historically, rheological investigations of polymer melts have largely concerned shearing flows. It is only in the past decade that any substantial attention has been given to elongational flow.

Generally, shear flow of all polymer melts follow a similar pattern whereas elongational flows show significant differences for different polymer systems (50).

Several research groups (48-50, 41, 152, 153) and most recently, Ide and White (103-105) have made extensive studies of elongational flow for polymer melts. Some polymer melts show unbounded elongational viscosity, some tend to decrease with elongation rate. Ide and White were able to explain these behaviors quantitatively through the application of Bogue-White constitutive equation.

Biaxial extension experiments have been carried out by Denson, et al (65) and Maerker and Schowalter (131).

C. RHEOLOGICAL PROPERTIES OF FILLED POLYMER MELTS

Polymer melts often contain reinforcing agent or fillers. This addition of particulate solids to polymer melts dates back a century or more when it was widely used

for rubber. Polymers notably rubber and PVC are generally not used or fabricated in the pure state but compounded with large amounts of fillers and oils. The addition of fillers to polymer melts has a major influence on the rheological properties (120, 133, 173, 261, 264, 265). Not only is the influence complex but so is the nature of interaction.

Carbon black is probably the most important of all reinforcing fillers used in polymers, its most important application being with elastomers in compounds used for tire components. Generally carbon black is produced by the thermal decomposition of hydrocarbons produced by impingement or free flame processes (214). The dominant characteristic of black is its high surface area per unit mass, small particle size and surface structure. Common blacks used in tire compounds possess particle diameters in the range of 200-500 Å. Another important characteristic of carbon black is its chemical surface characteristics such as its oxygen content or pH (31).

Other solid fillers usually have larger particles than carbon black. TiO_2, talc and $CaCO_3$ have sizes of thousands of Angstrom units or fractions of a micron. Glass fibers have diameters of several microns and lengths of more than a millimeter.

McCabe and Mueller (145), Hopper (101), Collins and Oetzel (55, 56), Vinogradov, et al. (250), White and Crowder (266), Bagchi and Sirkar (4) and Lobe and White (127) have looked specifically at how carbon black loading and diameter and structure influence the viscosity. In general viscosity and the apparent thixotropic behavior of the compounds is approximately a monotonic increasing function of the total black surface area. Similar behavior is also observed for other fillers notably TiO_2 (168) and glass fiber (38).

Matsumoto, and Onogi (141-143, 184, 185) have investigated the influence of fillers on the dynamic properties of polymer solutions. Filled polymer fluids exhibit apparent yield values at low shear rates. Lobe and White (127) observed apparent yield values for highly filled carbon black-polystyrene at low shear rate.

Matsumoto, Hitomi and Onogi (141) suggested a higher maximum relaxation time in carbon black-filled polymer solutions, using linear viscoelastic low frequency dynamic measurements. However Minagawa and White (168) suggested this results may be influenced by the yield value at such low shear rates and may be not pertinent at moderate and high shear rates.

There are only a few studies of elongational flow for filled polymer melts (176, 38, 127). Serious study is really due to Chan, White and Oyanagi (38) for glass

fiber reinforced polymers and Lobe and White (127) for carbon black-polystyrene. They found that the elongational viscosity is unbounded at low elongation rates and decreases at higher rates.

D. DIE FLOW

The extrusion of molten polymers through dies as an industrial processing operation dates back to 1840 (110). However, fundamental research on this subject is of considerably more recent date.

1. Stable flow

a. Flow into entry

The pressure, Δp, required to force a molten polymer through a series of capillaries of varying L/D ratio at the same wall shear rate may be expressed as the sum of the entrance pressure drop, the capillary pressure drop, and the exit pressure drop (3, 13, 95, 188). The creeping flow of Newtonian fluids through sharp-edged entrances have been studied analytically by Roscoe (200) and Weissberg (257), and experimentally by LaNieve and Bogue (124). The study of die entrance pressure drops for polymers was first discussed by Mooney (171, 172) for rubber compounds and by Bagley (5) for molten plastics. They pointed

out the existence of very large entrance pressure losses (1/3 to 1/2 of the total pressure drop). Philippoff and Gaskins (188) were the first to point out the apparent relationship of the entrance pressure to melt viscoelasticity, particularly normal stresses. This view was taken up by Bagley (9), LaNieve and Bogue (124) and White and Kondo (267). Boles, Davis and Bogue (27, 28) attempted to generalize the LaNieve and Bogue's result to flows in a tapered entrance. Similar studies at pressure drops have also been made by other research groups (90, 115, 232). Han and his co-workers (95, 96) have experimentally separated the end pressure losses into entrance and exit loss contributions.

Visual and birefringent of die entrance flow patterns have been extensively studied. Flow patterns in glycerine and water moving from a reservoir into a small diameter tube exhibit nearly radial flow and a 180° entrance angle has been reported (12, 30, 86, 107). Low density polyethylene (6, 7, 207, 241), polystyrene (11) and various polymer solutions (86, 195, 209) show large circulating flows or vortices at the die entry. Other melts notably high density polyethylene (6, 7), isotactic polypropylene (13) and narrow MWD polybutadiene (249) apparently do not exhibit these vortices. It is found that increasing extrusion rate increases the size of the circulating regions and decreases the entrance angle.

The experimental results of Ballenger and White (13) show that large vortices or small entrance angle correspond to large entrance pressure losses. Bagley and Schreiber (9) and White and Kondo (267) visualized the flow patterns at the entry of tapered dies and found that decreasing the entrance angle decreased the vortex size.

Hydrodynamic analyses have been given by Langlois and Rivlin (123), Kaloni (109), Strauss (221) and others (209, 210). These involve use of asymptotic slow flow acceleration tensor expansions and perturbations about the Newtonian flow solutions which predict radially inward motion in a cone or wedge. Perera and Waltors (187) numerically studied flow of viscoelastic fluids in converging flow into a die.

Cogswell (50) and Metzner and his co-workers (162, 163) were the first to note the elongational flow character of the die entrance region. The former author suggested it could be used for measurements of elongational viscosity of polymer melts. This procedure was used by Shroff, Cancio and Shida (213) where they compared the elongational viscosity measured from converging flow and more direct elongation flow measurements. More detailed discussions about the kinematics of entrance flows were published by Metzner and co-workers (162, 163), Cogswell (49, 51, 52) and White and Kondo (267). Both Cogswell (53) and White and Kondo (267) argued that it is the elongational flow character of polymer melts which gives rise to the vortex-like die entrance flow.

b. Flow through dies

Non-Newtonian flow through an isothermal die has been considered by various investigators for a half century. Most studies have involved flow through cylindrical dies and pressure drop-flow rate relationships have been devised for a number of rheological models including power law and Bingham plastic models which exhibit yield values (23). One may develop scaled equations based upon pressure drop-flow rate data as is implicit in the work of Weissenberg (75, 76, 192) and Mooney (170). A similar literature has been developed for slit dies (94).

Nonisothermal flow of polymer melts through a die has received attention by various researchers. Brinkman (33), Bird (20) and later authors (239, 82-84, 174, 131, 59, 78, 275) have treated this problem for tube flow. The developing temperature field for annular and slit dies has more recently been investigated by Cox and Macosko (59) and numerically calculated by Winter (275). As the temperature profile induced by viscous dissipation and heat conduction and convection varies the viscosity, the energy equation and the force balance become inter-related. Analytical solutions are generally impossible to obtain and numerical solutions must be carried out. The results are sensitive to presumption of boundary conditions.

There has been extensive analytical study of flow through dies with complex cross sections for various

rheological models (77, 89, 123, 259). They concluded, in general, the flow of viscoelastic fluids through a non-circular tube under an uniform pressure gradient cannot be longitudinal. Secondary circulating flows are superposed on the main flow. Langlois and Rivlin (123) have shown that it took a fourth order fluid, Rivlin-Ericksen expansion of acceleration tensors, to yield circulating flow patterns. These flows have been more recently investigated by Pipkin and his students (190, 42) and by Walters and his co-workers (72, 244). Such flow have relatively little influence on the extrusion rate-pressure gradient relationship (42, 72, 260). Experimental observations on polymer solutions by Giesekus (85), Semjonow (211), and Walters and co-workers (72, 244), appear to support theoretical predictions. Han (95) observed the streamline patterns of molten polymers flowing through rectangular duct, but didn't observe a circulating flow. This was probably due the short die used.

The steady, isothermal rectilinear flow of a power law fluid in a rectangular duct of constant cross section has been analyzed numerically to determine velocity fields and pressure gradient-flow rate relations by Schechter (205), Wheeler and Wissler (259, 260), Middleman (165), Arai and Toyoda (2) and Rothemeyer (201-203). Rothemeyer (201, 203) has similarly investigated dies with more complex cross sections.

c. Extrudate swell

The problem of extrudate swell of polymer melts has received considerable attention in the literature mostly experimental (10, 11, 47, 71, 88, 94, 177, 193, 196, 215, 216, 240, 250, 252, 254). Extrudate swell in polymer melts generally (i) increases with increasing extrusion rate, decreases with increasing extrusion temperature; (ii) decreases first rapidly and later slowly until it reaches a constant value with increasing L/D ratio; (iii) first increases then levels off with increasing reservoir to capillary diameter ratio (88, 97, 155-157, 248, 270).

Extrudate swell is a very difficult rheological problem to analyze. For Newtonian fluids Harman (98) showed that a momentum balance led to a B=d/D of 0.866. The first attempt to derive an analytical expression for die swell of polymer solutions presumed high Reynolds number flows where the response is largely determined by momentum fluxes and normal stresses (159-161, 269). However for polymer melts the Reynolds numbers are small and momentum fluxes are negligible compared to rheological forces.

Recently, Tanner and Nickell et al (229, 230, 178) carried out a complex numerical solution using finite element methods for the case of Newtonian creeping flow. They predicted a die swell of B=d/D=1.13 for long tubes.

More recently Reddy and Tanner (196) have shown that similarly for a slit B=h/H is 1.19.

The view that extrudate swell of a polymer melt from long dies is a result of unconstrained recovery from fully developed poiseuille flow is an old one and may be inferred from papers from Dillon and Johnston (71) in the 1930's to Nakajima and Shida (177) among others (155, 247, 88, 8, 228, 254) in recent times. The first reasonably satisfactory treatment of the problem would appear to be that of Tanner (228) who made use of unconstrained elastic recovery calculations by Lodge (129) for an integral Maxwell model with a Finger deformation measure (compare White (263)). The assumptions he made are (i) the flow is isothermal and incompressible; (ii) the die is very long, $L/D \to \infty$; (iii) inertial effects, gravity, other body forces, surface tension forces may be ignored; (iv) the small, slow recovery far from the die may be ignored. These assumptions are realistic for application to extrusion of polymer melts with small inertial forces which are highly viscoelastic. He uses a constitutive equation of the BKZ type and assumes N_2, the second normal stress difference is negligible and that the relaxation function is Maxwellian. Basically he found die swell is a function of the ratio of the first normal stress difference to the shear stress at the wall of a circular die. The recovery expressed by Tanner (228) has the form

$$Z' = (Z/\lambda^2) + g(\gamma)$$

$$\gamma' = \lambda\gamma$$

$$\theta' = \theta \qquad (2\text{-}26)$$

and the deformation tensor is

$$Q = \begin{vmatrix} 1/\lambda^2 & g' & 0 \\ 0 & \lambda & 0 \\ 0 & 0 & \lambda \end{vmatrix} \qquad (2\text{-}27)$$

$$Q\,Q^T = \begin{vmatrix} 1/\lambda^4 + g'^2 & \lambda g' & 0 \\ \lambda g' & \lambda^2 & 0 \\ 0 & 0 & \lambda^2 \end{vmatrix}$$

where $g(r)$ or $g'=dg/dr$ is a shear strain with above formulation, he worked out the swell equation of capillary die as

$$B = \left\{ \frac{\int_o^{D/2} (N_1 + G - \sigma^2/G^2)\,\gamma\, d\gamma}{\int_o^{D/2} Gr\, dr} \right\}^{1/6} \qquad (2\text{-}28)$$

He found agreement between theory and existing experimental data of polystyrene if he added 0.1 to the right side of the above equation to account for viscous effects.

Experimental studies of these and other extrudate swell theories have been reported by Vlachopoulos and his co-workers (251, 252, 254), Utracki, Bakerdjian and Kamal (248), White and Roman (270, 199) and by Racin and Bogue (193, 194). White and Roman (270) developed a modified formulation of Tanner's theory where the melt recovers

from poiseuille flow into a state of uniaxial tension. They found that the swell decreases rapidly with increasing applied pick up force. The theoretical equation which fits data reasonably good has the form:

$$\left[\frac{B}{B_{(o)}}\right]^6 = 1 - \frac{\tau_{eff}}{\eta}\,\frac{4F}{\pi D^2}\,\frac{B^2}{B^6_{(o)}} \qquad (2\text{-}29)$$

where F is the applied force, $B_{(o)}$ is the extrudate swell without pick up stress and is represented by Tanner's swell equation.

White and Roman (270, 199) also compared theory with swell data taken by various methods (i.e. frozen, annealed in hot silicone oil, photographed emerging into air, photographed emerging through 180°C silicon oil). They found that the frozen extrudate data and melts extruded into air account for the theory reasonably well but the annealed and isothermal data are much higher.

An empirical relationship of extrudate swell for shorter dies which has been proposed is (177, 202):

$$B = B_\infty + (B_o - B_\infty)\cdot\exp(-\bar{t}/\lambda^*) \qquad (2\text{-}30)$$

where B_∞ is die swell for $L/D\to\infty$, B_o is the die swell for $L/D=0$ and $\bar{t}$, λ^* are averaged values of residence time and relaxation time. The quantity $\bar{t}$ is largely a function of L/D and extrusion rate and λ^* largely depends on wall shear rate and material properties.

There are no analyses for B_o which seems to relate to the recovery from the entrance flow.

Most studies of polymer extrudate swell have involved flow through capillary dies and indeed only few investigators report studies on cross sections other than circular and these results are only qualitative (94, 122, 201, 202, 253, 277). There is no joint experimental and theoretical study for slit and more complex geometries.

There have been some studies on the extrudate swell behavior for filled polymer systems (38, 94, 145, 168, 214, 266). Generally increasing filler loading decreases die swell rapidly. White and Crowder (266) found the particle size of carbon black has significant effect to the decreasing of extrudate swell. For the same loading, smaller particles gives less die swell. At high loading, extrudate swell can be completely eliminated (38, 127). The most systematic data was given by Minagawa and White (168) and Lobe and White (127) in which they found the normal stress function N_1 decreases with increasing loading but not as rapidly as extrudate swell does.

Studies of extrudate swell for filled polymers have involved efforts to develop a master curve of shear stress versus the corrected die swell $(B/1-\phi)$ (58, 151). The quantity ϕ can be filler volume fraction (142) or modified effective filler volume fraction (4, 119, 120, 151, 191, 266). Bagchi and Sirkar (4) chose to use the swell equation of Bagley and Duffy (8) and an empirical

relation of elastic modulus for highly filled system. They then worked out a swell equation for polymer compounds as follows:

$$\sigma_w = \left(\frac{G_o}{f}\right) \frac{(B^4 - B^{-2})^{\frac{1}{2}}}{(1 - \phi_e)^b} \qquad (2\text{-}31)$$

where σ_w is wall shear stress, b is power index for the filled system with 2.5 for inert spherical filler (34) and f is a non-linear factor for G_o (modulus of unfilled polymer polymers). G_o/f may depends on σ_w and time. Based on Eq. (2-31) Bagchi and Sirkar were able to plot a single curve of σ_w vs. $(B^4-B^{-2})^{\frac{1}{2}}/(1-\phi_e)^b$ for a range carbon black compounds. However there is no theoretical analysis for the extrudate swell of filled polymer systems based on constitutive equations.

2. Unstable flow

The first careful investigation of the nature of emerging extrudates was published by Spencer and Dillon (215). They distinguished three regimes of flow in polystyrene. At the lowest flow rate the melt emerges with a smooth surface. In an intermediate regime more or less regular spirals were produced followed by a grossly distorted extrudate at the highest extrusion rates. The onset of distortion occurred at a critical wall shear stress about 10^6 dynes/cm^2 which is also confirmed by later investigators (11, 12 246).

It is clear from flow visualization studies (262, 12, 6, 13, 241, 267) for molten plastics that the instabilities giving rise to these distorted extrudates develop in the die entry flow region.

It is usually observed that the extent of distortion decreases with increasing L/D ratio (240), but this is not always the case (67, 68). Addition of filler into polymer melts (60, 168, 266) delays the onset of distortion to higher shear rates. This phenomenon is very important to elastomers which usually show distorted extrudates even at extremely low extrusion rate. (250, 18, 60, 266) Minagawa and White (168) found that TiO_2 decreases both the characteristic relaxation time of polymer melts and extrudate swell as well as retarding the occurrence of extrudate distortion. There are a variety of mechanisms which have been proposed through the years for the cause of the initiation of melt flow instabilities in extrusion. These involve hypotheses of fracture of the melt and of hydrodynamic instability (25).

E. SCREW EXTRUSION

Rubber Extruders - General. The use of a screw extruder as a continuous pumping device in the rubber industry originated in 1870-80 as a result of attempts to devise a machine which would operate continuously. After that, improvements were made largely on an intuitive

trial-and-error basis, many of which were subsequently discarded, but the sum effect over the years was a gathering of empirical knowledge (often unrecorded). During that time, empiricism not science held sway, but nevertheless an invaluable body of rules was amassed.

In 1922, Rowell and Finlayson (204) first developed a theory of screw pumps for viscous liquids. Pigott (189) and Carley, Mallouk and McKelvey (36) applied this to the analysis of screw extrusion of polymers. Since that time screw extruders have been extensively studied. The results of these efforts for plastics have been summarized in the monograph of Tadmor and Klein (226).

These models are basically for extrusion of molten plastics which exhibit distinct solid conveying, melting and metering regions. Such a model is not expected to work at all well for rubber compounds. In succeeding sections, we will critically review the extensive literature on screw extrusion of plastics. While realizing that in its present formulation, it will not be adequate for rubber compounds, the concepts of the theories should form the basis for any new analysis.

1. Solid conveying zone

The task of the solid conveying zone is to pick up and convey the solid plastic particles, generally in the form of small cubes of more or less regular form, to the melting zone. Usually, the first few turns (2 - 4

turns) of the screw from the hopper performs the solid conveying function. The conveying capacity of the feeding zone must be at least equal to the metering capacity of the melts conveying zone in terms of mass flow rate. Decker (63) recommends attaining low friction between the screw surface and polymer by polishing the screw and maintaining high friction between polymer and barrel by roughening the barrel surface and requiring a high bulk density for the solids to get higher delivery. More quantitative approaches have been developed by later authors but the first equations that express the solid conveying capacity were developed by Darnell and Mol (61). The Darnell and Mol model involves a force balance along the length of the screw channel with the bed preserved to move as a solid plug between the barrel with coefficient of friction μ_b and the screw with coefficient of friction μ_s. Pressure profiles and flow rates are interrelated with screw geometry, rotation rate N and μ_b and μ_s. The experimental output rates of the solid zone was also found very close to the calculated values. Using a model extruder with a glass barrel, Griffin (92) was able to see that unplastified beads or pellets moved as an unsheared plug. He also showed lower and less steady screw extrusion rates are more likely for small spherical pellet feed particles than for large cubic particles.

The frictional mechanism of Darnell and Mol only applies in a short feeding region where the surrounding is still cold. Once the solid polymer starts to melt on the heated barrel and screw surfaces, the viscous forces instead of frictional forces control the solid conveying function as proposed by Chung (44). According to his experiments, the slip behavior of polymer solids on metal surfaces are represented by two parameters: the friction coefficient below their melting point and the sled stress above their melting point. Modified solid conveying models based on the views of Darnell and Mol were developed by Tadmor and Broyer (35, 223). From their mathematical model, the temperature profile in the solid plug together with the strongly interacting pressure profile can be calculated. Kacir and Tadmor (108) developed a theoretical model for the newly-defined (224, 226) "delay zone" which starts at the end of the solids conveying zone and involves formation of film of melt on the barrel. This continues up to where the "steady state" melting mechanism starts to operate. From their model the length of the delay zone can be calculated. Many experimental investigations (130, 220, 224, 73) have shown that the solid plug is separated from barrel surface by a thin melt film, except for a few turns of the screw near the hopper. Therefore, Chung, Nichols and Kruder (46) suggested that Darnell and Mol's theory was developed based on the assumption that the

solid plug is in direct contact with the barrel surface and thus should not be applied to long sections of the extruders. However, the transfer from the frictional mechanism to the viscous shearing mechanism of polymers on a metal surface is not clearly understood at present. Schneider (206) investigated the frictional behavior of polymers on metal surface for pressures less than 40 psi and sliding speeds of less than 1.3 in./sec. Friche (80) made similar measurements for pressures up to 350 psi. Most recently, Chung, Hennessey and Tusim (45) measured the friction coefficients of several polymers on metal surfaces up to high temperature, pressure and speed to simulate real extrusion conditions found the interrelations are too complicated to make any prediction.

2. Melting zone

The presence of a melting zone is the major distinction of the plasticating extruder. Quite early in the development of extrusion theory it was realized that the energy required for melting the polymer originates from two sources: heat conduction through the hot barrel surface and viscous dissipation.

The melting zone or phase transition zone is defined as that portion of the screw in which solid polymer and melt co-exist. The length of the melting zone is a function not only of the screw geometry, but also of the

operating conditions and the physical properties of the polymer as well. The melting zone does not exactly coincide with the tapered, transition or compression section, although one would often like to design an extruder screw that would complete the melting at the end of the compression section. The position of the melting region varies with screw speed, barrel temperature and polymer properties. It is very difficult in defining and analyzing a two phase system in the melting zone.

The melting mechanism in screw extruders was first investigated by Maddock (130) and Street (220). They developed the experimental techniques which first led to the development of a qualitative mechanism for melting through visual observation. Their basic concept is first to feed the extruder with a mixture of natural and colored (3-5%) polymer. When steady state is reached, they suddenly freeze all conditions by stopping the screw and solidifying the polymer. The screw is then pushed out of the barrel, the polymer is peedled off the screw; and the helically shaped ribbon of polymer is sectioned. The molten and partially mixed polymer will exhibit flow lines, while the unmelted polymer will remain in the initial solid particulate form.

From these kinds of experiments a qualitative melting mechanism can be described as follows. The solid pellets which are fed into the hopper start moving towards

the die in the extruder channel. At a certain point melting starts and forms a thin film on the hot barrel surface. Pellets from this point are no longer loosely packed, since considerable pressure is developed which together with the softening effect of the hot surroundings tend to compact the pellets into a sturdy "solid bed" which has the shape of the helical channel and slides in it. The melt collects in the pool of melt in the rear of the channel in front of the advancing flight. In the melt pool, due to the relative velocity of the barrel and the root of the screw, a circulatory motion is set up.

Streamlines of this circulatory motion can be clearly identified in the experimental cross section. A pressure is developing which, of course, forces the solid bed to segregate in its observed location at the trailing side of the flight. Thus, inspite of the fact that most of the melting occurs at the barrel surface, or rather at the interface of the film of melt and the solid bed, the height of the solid bed does not decrease and the solid bed is continuously rearranged while maintaining a constant height. Consequently, the width of the solid bed is gradually decreasing as it moves down the channel. As the solid bed moves down the channel a situation may arise, where the external forces overcome the strength of the bed and cause it to break up. The breaking up of the solid bed explains the observations

by Marshall, Klein and Uhl (134) of high temperature fluctuation in the melting zone. A secondary, less vigorous, circulatory flow also develops around the broken up solid bed. A theoretical model based on the melting mechanism and a Newtonian fluid was given by Tadmor (222). A dimensionless group in his analysis, the Brinkman number, represents a measure of the importance of viscous heat generation relative to the heat conduction resulting from the imposed temperature difference between barrel and melting point. If Br > 2, there is a maximum temperature at a position intermediate between barrel and solid bed. Models involving non-Newtonian fluid response have also been developed. These are much more complex (111, 112, 135, 226).

There have been various improvements in the melting model theory by considering non-Newtonian viscosity, temperature profiles in the film, overall improved handling of continuity and force balances (43, 46, 223, 113, 114, 126).

Several experimental studies have been carried out. The validity of the model was tested with numerous experiments which were performed with low and high density polyethylene, plasticized polyvinyl chloride, rigid polyvinyl cloride power, polypropylene, ABS and nylon 66. The mathematical model proved to be successful in predicting

pressure and plastic temperature profiles in extruder channel, temperature fluctuation, solids content, and power consumption (113).

3. Melt conveying zone (metering zone)

The term metering zone originates from the common practice of designing the last section of the screw preceding the die to control or "meter" the flow rate of the extruder. Rowell and Finlayson (204) did the first systematic experimental studies of screw pump with a variety of screws, channel depths, and liquids (such as water, soap solutions, petroleum, and oils). The data were correlated on the basis of flow equations which were developed by these authors with the assumption of isothermal, Newtonian flow of an incompressible fluid in a rectangular channel, with screw-barrel clearance effect neglected. Pigott (189) reviewed the theoretical flow equations and also reported some experimental data on rubber compounds. He attempted to modify the analyses to include non-Newtonian viscosity. Further experiments were reported by McKelvey (146-150, 37) and others (15) in which corn syrup was pumped with a two inch diameter screw. From his experiments he showed the two-dimensional flow equations accurately describe the flow behavior of Newtonian liquids in screw extruders.

The error of using a rectangular coordinate system instead of cylindrical coordinate system is contained in McKelvey's (150) "curvature correction factor" for pure drag flow. According to his results, less than 4 percent error is introduced by neglecting the curvature when (outer radius/inner radius) less than 1.3 for a Newtonian fluid, and less than 1.1 for a non-Newtonian fluid with a power law exponent of 0.5. The backward pressure flow which the theory predicts has been confirmed by direct measurements made by Eccher and Valentinotti (74).

To avoid metal to metal friction, most screws have a small clearance between the top of the flight and the barrel surface. The effect of the clearance on performance may be negligible in new equipment. The wearing of the screw with time increases the problem until it reaches beyond a tolerable level (111). Mohr and Mallouk (169) developed extrusion-flow equations considering the leakage flow through the clearance. Mallouk and McKelvey (150) showed that the screw power consumed as irreversible viscous dissipation into heat generation by the viscous dissipation. Barr and Chung (14) showed experimentally output decreased almost linearly with increasing radial clearance at the same screw speeds. Tadmor and Klein (226) developed the basic equation relating extruder output, flight clearance and pressure in isothermal operation.

Numerical solutions for non-Newtonian power law fluids were obtained by Colwell and Nickolls (57). They assumed an unidirection velocity field and didn't include transverse flow. Heat conduction balanced by viscous dissipation heating and neglected heat convection. Middleman and Kroesser (121, 165) derived a theory of a screw pump with a power law viscosity function in isothermal flow in a rectangular duct with a moving wall. Griffith (91) treated the non-Newtonian non-isothermal case including transverse flow. Griffith (91) neglected heat convection in the down channel direction and allows temperature varying only with respect to attitude above the screw flight. The most thorough study of this asymptotic analysis is due to Zamodits and Pearson (281).

Martin (136) took the convective term into account and he also pointed out the relevant Peclet number is larger in the real case (2000~5000). Two physical processes are responsible for the heat transfer between barrel wall and polymer, namely heat conduction and heat convection. According to Jepson (107) the latter mechanism is due to the "wiping effect" of the screw bank. According to a suggestion put forward by Janeschitz-Kriegl and Schiff (106), the critical screw speed N_k above which convection plays a predominant role is given by the relation:

$$\frac{N_k h^2}{\alpha} \approx 150 \qquad (2\text{-}32)$$

N_k = screw speed (rev./sec.)

h = channel depth (cm)

α = thermal diffusivity ($cm^2/sec.$) (10^{-3} for P.E.)

A direct temperature measurement in the screw channel seems almost impossible. However, Schlaffer, Schijf and Janeschitz-Kriegl (208) measured the temperature profile right about 1 cm behind the end of the extruder (30 mm) with a temperature probe. Some results confirmed the transient temperature profile which implied super-imposed steady state never be attained in real case because to get there need extremely low flow rate or extremely long extruder. Worth, Parnaby and Helmy (278) firstly considered the wall slip between metal surface and polymer melts and its influence on screw extrusion.

CHAPTER 3

MATERIALS AND APPARATUS

A. MATERIALS

The polymers used in this dissertation were two "pure" molten plastics plus two rubber compounds.

Polystyrene and polypropylene melts were included in the study of pressure loss-extrusion rate relationship for complex dies and extrudate swell emerging from die of various geometries. The polystyrene was Dow Styron 678U and it was studied at 180°C. The polypropylene was an experimental polymer supplied by the Diamond Shamrock Corporation (now part of ARCO) and investigated at 180°C. The viscosity-shear rate behaviors of those polymers are shown in Figure 3-1, the principal normal stress difference $N_1 = \sigma_{11} - \sigma_{22}$ is shown as a function shear stress σ_{12} in Figure 3-2, and the viscosity and N_1 shown as function of σ_{12} are contained in Figure 3-3.

The polystyrene results are due to V. M. Lobe and was part of the Oda-White-Clark $N_1 - \sigma_{12}$ correlation (180) for this material. The polypropylene data are due to W. Minoshima and part of an extensive rheological study of several polypropylene melts.

Two rubber compounds were prepared. These were a model tread compound based upon SBR 1712 (Texas-US chemical) and a side wall compound based upon SBR 1712

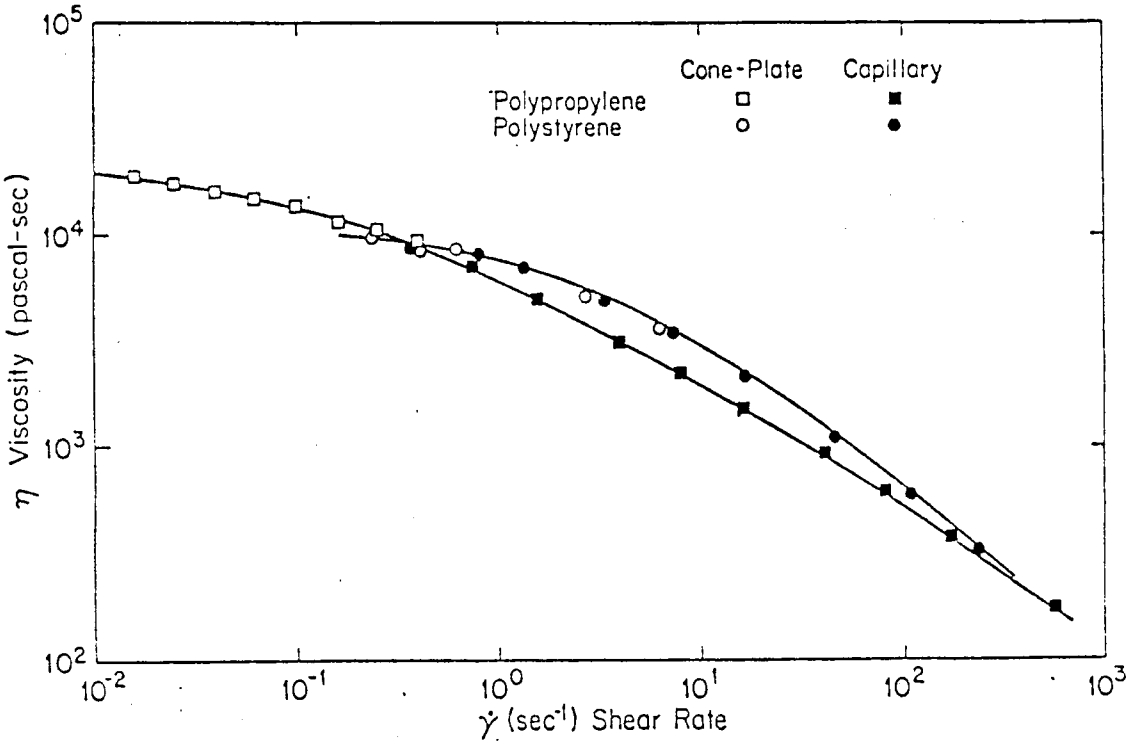

Figure 3-1. Viscosity-shear rate behavior of polymer melts studied.

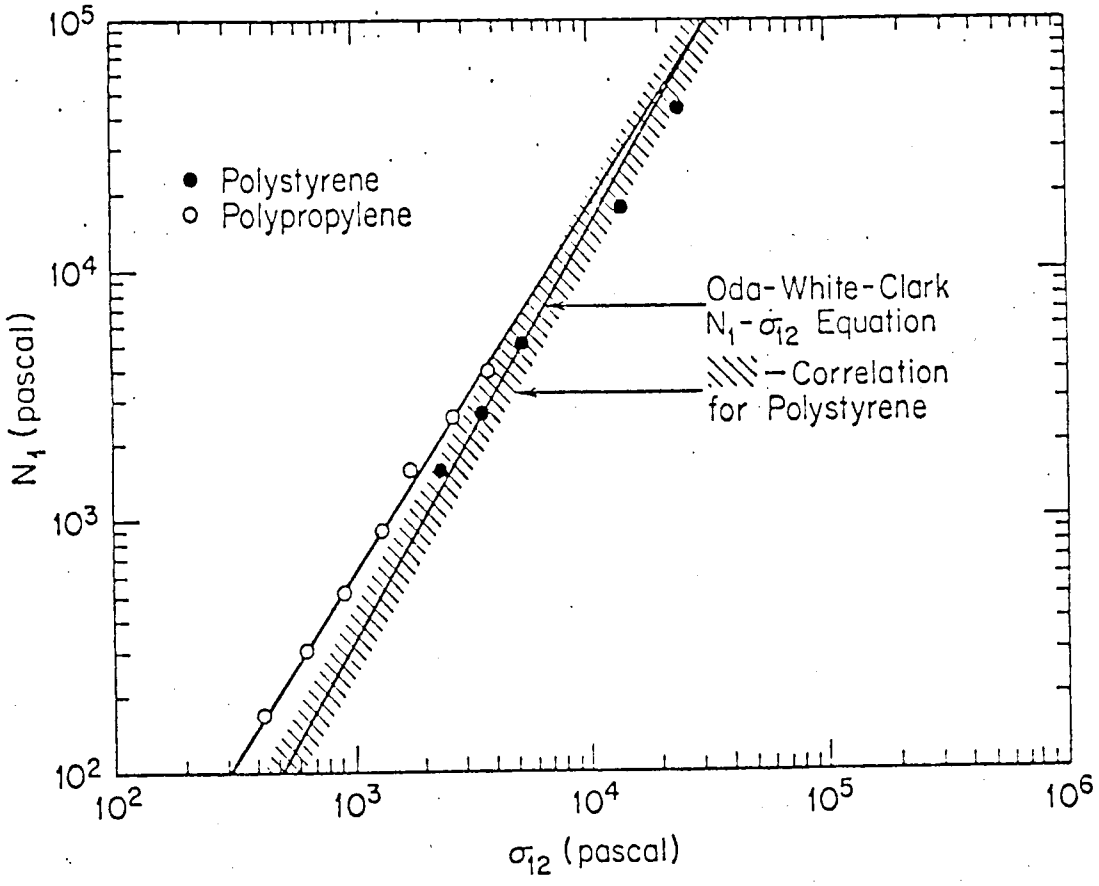

Figure 3-2. Principal normal stress difference-shear stress behavior for polymer melts studied.

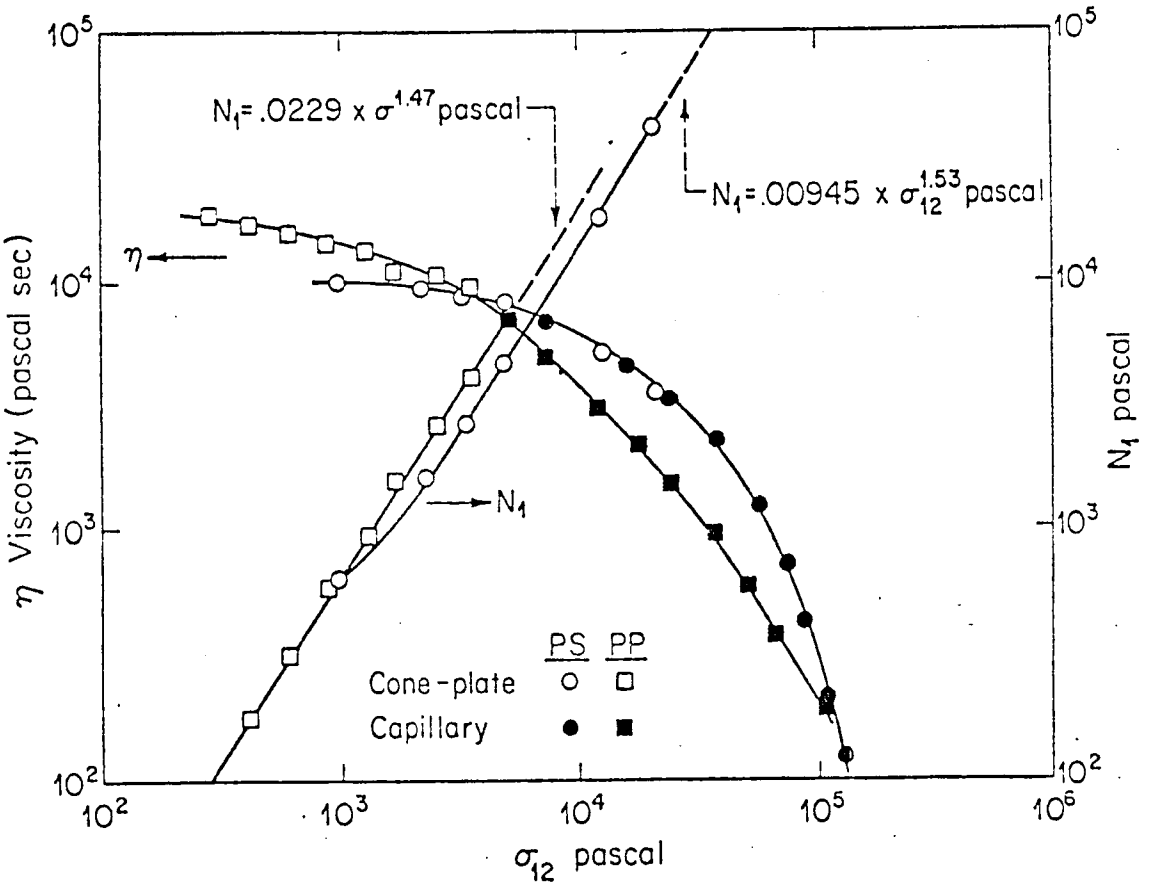

Figure 3-3. Viscosity and principal normal stress difference-shear stress behavior for polymer melts studied.

(Texas-US chemical). Both types of SBR are emulsion polymerized copolymer with about 23.5 weight percent styrene. The recipes are the same as used by Furuta, Lobe and White (81) and shown in Table 3-1. The major difference of these two compounds is the molecular weight of the elastomer and the level of carbon black.

A laboratory roll mill having 3 inches diameter by 7 inches width is used to prepare these compound samples. About 400 grams batches were mixed. The front and rear roll were run at 12 and 16 rpm, respectively and were heated to 50°C. The nip between the rolls need to be adjusted constantly, usually wide in initial rough mixing stage and narrow in the fine dispersing stage. The total compounding time for each batch was about 2 hours.

B. APPARATUS

1. Rheological characterization

a. Mechanical Spectrometer

Rheological measurements in the low shear rate region were carried out on the Mechanical Spectrometer (manufactured by Rheometrics Inc., Union, New Jersey) in the cone-plate configuration.

To obtain the shear stress and the first normal stress difference the following equations are used (26, 129, 166, 258):

Table 3-1. Typical Recipes for Rubber Compounds

	Tread	Sidewall
SBR 1500	--	100
SBR 1712	137.5	--
Anti-Oxidant[1]	1	2
Stearic Acid[2]	2	1.5
ISAF Carbon Black[3]	70	--
FEF Carbon Black[4]	--	65
Aromatic Oil	--	30
Zinc Oxide[5]	3	3

[1]Di-ortho-tolylguanidie (DuPont).

[2]Acid Stearic (Fisher Scientific Co.).

[3]Continex ISAF-LS (N-219).

[4]Continex FEF (N-529).

[5]Lead Free Zinc Oxide (St. Joseph Lead Co.)

$$\dot{\gamma} = \frac{\Omega}{\alpha} \tag{3-1}$$

$$\sigma_{12} = (3T/2\pi R^3) \tag{3-2}$$

$$N_1 = \sigma_{11} - \sigma_{22} = 2F/\pi R^2 \tag{3-3}$$

where

Ω = angular velocity (radians/sec.)

α = cone angle (radians)

T = torque

F = thrust

R = radius of cone

b. Instron Capillary Rheometer

The Instron Rheometer is a capillary viscometer consisting of a barrel about 13 inches long with a three-eighth inch inside diameter and a plunger. The close-fitting plunger is dirven through the barrel at constant speed, extruding the melt through a capillary die fixed to the bottom of the barrel. The plunger speed is controlled discretely from 0.002 inch/min. to 20 inches/min. By recording the steady state plunger force from a load cell and knowing the plunger speed, a total pressure drop and a volumetric flow rate are obtained.

The barrel electrically heated and the temperature is controlled within 0.5°C.

In this experiment the force needed to drive the plunger at a constant speed is measured directly.

Generally, at least three dies with equal diameter and different L/D ratio are needed for the characterization.

The total pressure p_T required to extrude a polymer fluid is the sum of a capillary die pressure loss, plus entrance and exit losses. This is

$$p_T = \Delta p_{die} + \Delta p_{entrance} + \Delta p_{exit} \qquad (3\text{-}4)$$

By a force balance Δp_{die} may be related to $(\sigma_{12})_w$ and $\Delta p_{entrance}$ and Δp_{exit} are usually coupled as Δp_{ends}. This leads to

$$p_T = 4\,(\sigma_{12})_w\, L/D + \Delta p_{ends} \qquad (3\text{-}5)$$

Eq. (3-5) suggests the "Bagley plot" (5, 168, 266) where p_T is plotted versus L/D and $(\sigma_{12})_w$ determined from the slope and p_{ends} from the intercept. This procedure was used in our studies.

The shear rate $\dot{\gamma}_w$ at the die was obtained using Weissenberg's equation (76)

$$\dot{\gamma}_w = \left(\frac{3n' + 1}{4n}\right) \frac{32Q}{\pi D^3} \qquad (3\text{-}6)$$

where Q is the extrusion rate and n' is

$$n' = \frac{d \log (\sigma_{12})_w}{d \log 32Q/\pi D^3} \qquad (3\text{-}7)$$

Here $(\sigma_{12})_w$ is the wall shear stress.

c. Sandwich testing device

A sandwich device based on that devised by Middleman (167) was built for use in our Instron tensile testile testing machine by Furuta et al (81) as shown in Figure

3-4. The two sheared rubber slabs had dimensions 2.54, 3.81, 0.15 cm. This was placed within the grips and heated in a temperature controlled "air" bath. This apparatus was developed by Matsui and Bogue and is described in Matsui's thesis (137).

The uppergrip is moved upward at velocity V producing a constant shear rate $\dot{\gamma}_{12}=V/H$ in the rubber compounds. The shear stress is represented by

$$\sigma_{12} = F/2A \qquad (3\text{-}8)$$

where F = force

A = area of the slab

If V is low enough, a steady state force (F) measurement can be made to give viscosity at low shear rate.

2. Extrudate swell

Extrudate swell measurements were done on Instron Rheometer where polymer samples were heated and then extruded through die of various geometries.

Dies of various cross section are made in our mechanical shop with outer diameter to be close to three-eight inch to fit into the Instron barrel. The detailed cross section will be described in the appropriate chapters.

The unstressed extrudates were either emerging into air or into cold silione oil. The latter procedure was used in the long capillary and slit die study to eliminate gravity effect and will be described in more detail in

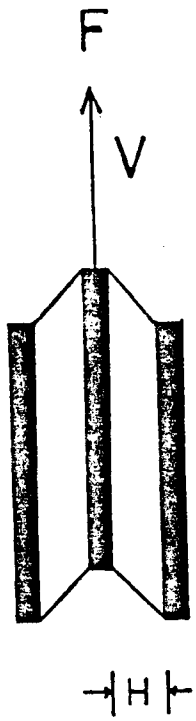

$$\dot{\gamma}_{12} = \frac{V}{H}$$

$$\sigma_{12} = \frac{F}{2A}$$

Figure 3-4. Sandwich testing device.

Chapter 5. In the other studies (Chapter 6 and 7), the extrudate emerged directly into air where we used higher extrusion rates (i.e. wall shear rate > 1 $sec.^{-1}$). At these higher extrusion rate, the gravity effect is negligible.

Extrudate dimensions were measured with a micrometer of accuracy up to 0.0005 inch. The measured value need to be multiplied by a density factor which is defined as $[\rho(\text{room temperature})/\rho(\text{Instron temperature})]^{1/3}$ (155, 270). The density factor has values 1.057 for polypropylene, 1.027 for polystyrene and 1.009 for tread and side wall compounds. Extrudate swell is represented in terms of the ratio of the extrudate dimension to the die dimension i.e.

$$B = d/D \quad \text{or } h/H \quad \text{or } w/W \tag{3-9}$$

where d, h, w are extrudate dimension corresponding to the die dimension, D (capillary diameter), H (small dimension of slit or rectangle), W (large dimension of slit or rectangle).

Extrudates were annealed from 170°C to 180°C in hot silicone oil for five minutes. The annealed extrudate dimensions were then investigated and measured.

3. Screw extrusion

The screw extruder (refer to Figure 3-5) used for studying extrusion of rubber compounds is a 3/4 inch

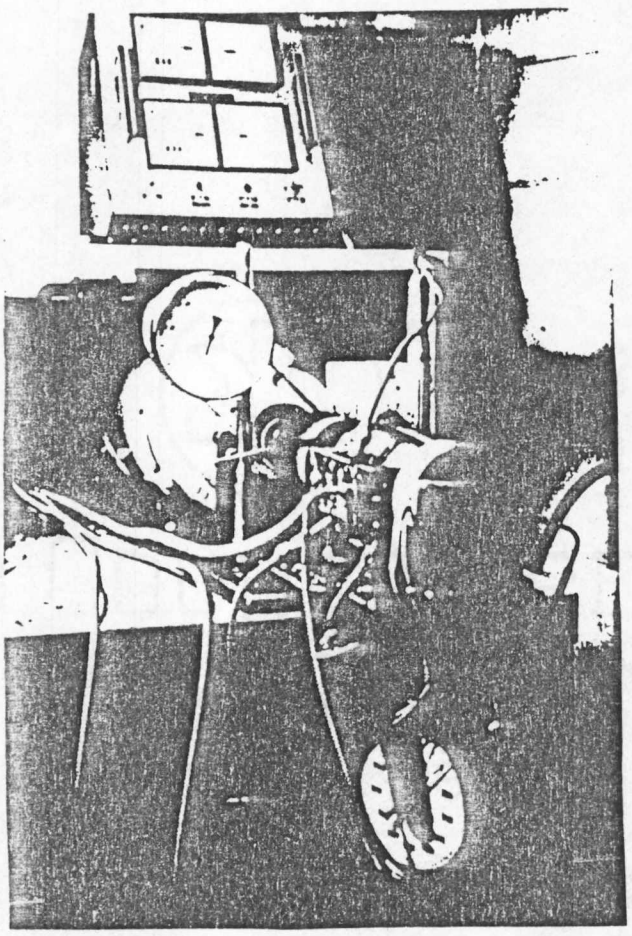

Figure 3-5. Screw Extruder used for studying screw extrusion of rubber compounds.

diameter Brabender Extruder model 1003 made by C. W. Brabender Instruments, Inc. The screw length to diameter ratio is 10 and the helix angle 17.7°. The flight height is 0.15 inch and channel width 0.60 inch with aspect ratio 4. The screw used in this dessertation has a constant flight height from hopper to the end. A pressure gauge (0 - 10,000 psi), silicone type with bleeder valve, is installed in a hole of barrel located at the end of the screw.

Cooling water is circulating around the barrel. The temperature is controlled in the barrel and die by a two zone temperature control console and electric heaters.

The die used in this study had D=1.473 mm and L/D= 4.9, 10.0, 20.0 and 40.0.

CHAPTER 4

EXTRUSION PRESSURE LOSS OF POLYMER MELTS FLOWING THROUGH RECTANGULAR AND TRAPEZOIDAL DIES

Experimental and theoretical studies of extrusion of polymer melts through dies are largely limited to cylindrical cross sections, and a few researchers have reported results for slit dies. However, many industrial processes involve extrusion through more complex cross sections. Studies of flow of polymer melts in this geometry are much more limited.

It is our purpose in this chapter to present a basic study of flow rate-pressure gradient relationships in rectangular and trapezoidal dies. We investigate the limitations of the two dimensional simple shear flow asymptote for polymer melts.

A. THEORY

Consider the fully developed flow of a polymer melt through a conduit. We shall choose "1" as the direction of flow and "2" and "3" as the directions of shear, so that we may write

$$\underset{\sim}{V} = V_1 (x_2, x_3) \underset{\sim}{e}_1 + 0\underset{\sim}{e}_2 + 0\underset{\sim}{e}_3 \qquad (4\text{-}1)$$

As noted earlier in some cases small secondary flows V_2 and V_3 may exist.

We, now turn to the balance of forces, Cauchy's equation of motion (245) and describe how it may be used to determine a velocity field, Cauchy's equation has the form

$$\rho\left[\frac{\partial \underset{\sim}{V}}{\partial t} + (\underset{\sim}{V}\cdot\nabla)\,\underset{\sim}{V}\right] = \nabla\cdot\underset{\sim}{\sigma} + \rho\,\underset{\sim}{g} \tag{4-2}$$

where ∇ represents the del operation (23) for steady state flow in a conduit. The velocity V_1 is independent of position x_1 along the tube and the stress σ_{11} varies along the axis only through the pressure. This allows us to reduce Eq. (4-2) to

$$0 = -\frac{\partial p}{\partial x_1} + \frac{\partial \sigma_{12}}{\partial x_2} + \frac{\partial \sigma_{13}}{\partial x_3} \tag{4-3}$$

The shear stresses, σ_{12} and σ_{13}, depend upon the velocity gradients $\partial V_1/\partial x_2$ and $\partial V_1/\partial x_3$. The inter-relationship is given by

$$\sigma_{12} = \eta\left(\frac{\partial V_1}{\partial x_3}\right), \qquad \sigma_{13} = \eta\left(\frac{\partial V_1}{\partial x_3}\right) \tag{4-4}$$

so that we may write

$$0 = -\frac{\partial p}{\partial x_1} + \frac{\partial}{\partial x_2}\left[\eta\frac{\partial V_1}{\partial x_2}\right] + \frac{\partial}{\partial x_3}\left[\eta\frac{\partial V_1}{\partial x_3}\right] \tag{4-5}$$

The fluids we are considering are non-Newtonian with their viscosity dependent upon shear rate. The viscosity must depend upon $\partial V_1/\partial x_2$ and $\partial V_1/\partial x_3$ in such a manner that it will be independent of coordinate system. This necessitated that η depend upon invariants, and in

particular deformation rate invariants. We may write:

$$\eta = \eta(II_d)$$

with

$$II_d = 2\, t_r\, \underset{\sim}{d}^2, \qquad \underset{\sim}{d} = \frac{1}{2}\left[\nabla \underset{\sim}{V} + (\nabla \underset{\sim}{V})^T\right] \tag{4-6}$$

In particular for a velocity field of the type given by Eq. (4-6)

$$II_d = \left[\left(\frac{\partial V_1}{\partial x_2}\right)^2 + \left(\frac{\partial V_1}{\partial x_3}\right)^2\right]^{1/2} \tag{4-7}$$

The most widely used of viscosity-shear rate relationships for analyzing the flow behavior of polymer fluids is the power law

$$\eta = K\dot{\gamma}^{n-1} \tag{4-8}$$

The dependence of η upon II_d and the $\partial V_1/\partial x_2$ and $\partial V_1/\partial x_3$ velocity gradient components is taken as

$$\eta = K\left[\left(\frac{\partial V_1}{\partial x_2}\right)^2 + \left(\frac{\partial V_1}{\partial x_3}\right)^2\right]^{\frac{n-1}{2}} \tag{4-9}$$

we obtain for the force balance

$$\frac{1}{K}\frac{\partial p}{\partial x_1} = \frac{\partial}{\partial x_2}\left\{\left[\left(\frac{\partial V_1}{\partial x_2}\right)^2 + \left(\frac{\partial V_1}{\partial x_3}\right)^2\right]^{\frac{n-1}{2}}\frac{\partial V_1}{\partial x_2}\right\} + \frac{\partial}{\partial x_3}\left\{\left[\left(\frac{\partial V_1}{\partial x_2}\right)^2 + \left(\frac{\partial V_1}{\partial x_3}\right)^2\right]^{\frac{n-1}{2}}\frac{\partial V_1}{\partial x_3}\right\} \tag{4-10}$$

Solution of Eq. (4-10) is in general difficult and requires numerical procedures. It is the expression which was solved by Schechter (205), Wheeler and Wissler (259),

Middieman (165), Arai and Toyoda (2) and Rothmeyer (203) to give velocity fields and pressure gradient-extrusion rate relationships for conduits of varying cross section.

It is sometimes possible to obtain approximate solutions if one of the velocity gradient components is larger than the other.

$$\frac{\partial V_1}{\partial x_2} >> \frac{\partial V_1}{\partial x_3} \tag{4-11}$$

This allows us to reduce Eq. (4-10) to

$$\frac{1}{K}\frac{\partial p}{\partial x_1} = \frac{\partial}{\partial x_2}\left(\frac{\partial V_1}{\partial x_2}\right)^n \tag{4-12}$$

which has the solution

$$V_1 = \frac{n}{n+1}\left(\frac{1}{K}\frac{\partial p}{\partial x_1}\right)^{\frac{1}{n}}\left(\frac{H}{2}\right)^{\frac{n+1}{n}}\left[1 - \left(\frac{x_2}{H/2}\right)^{\frac{n+1}{n}}\right] \tag{4-13}$$

and

$$\begin{aligned} Q &= 2\int_o^w \int_o^{H(x_3)/2} V_1(x_2)\, dx_2\, dx_3 \\ &= \frac{n}{2(2n+1)}\left(\frac{1}{2K}\frac{\partial p}{\partial x_1}\right)^{1/n}\int_o^w H(x_3)^{\frac{2n+1}{n}}\, dx_3 \\ &= \frac{n}{2(2n+1)}\left(\frac{\Delta P_{die} H_o}{2KL}\right)^{\frac{1}{n}} W H_o{}^2 \int_o^w \left(\frac{H(x_3)}{H_o}\right)^{\frac{2n+1}{n}} \frac{dx_3}{W} \end{aligned} \tag{4-14}$$

where H_o is a characteristic thickness.

For rectangular or trapezoid dies (refer to Figure 4-1) where $\partial V_1/\partial x_2 >> \partial V_1/\partial x_3$ is not valid, a

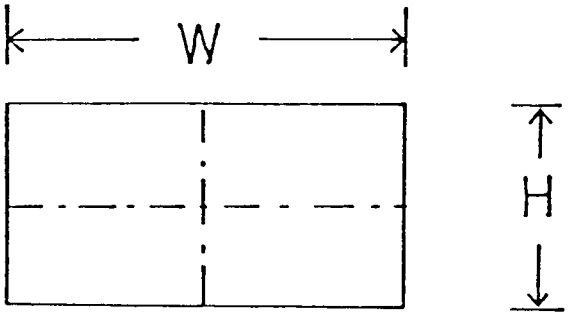

(a) rectangle

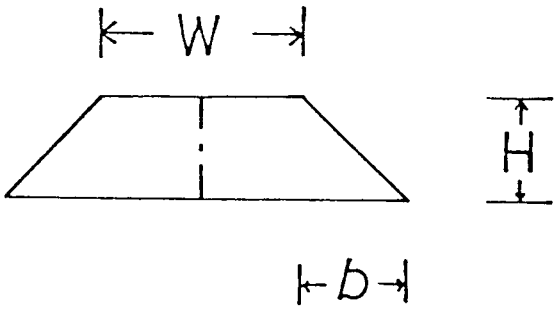

(b) trapezoid

Figure 4-1. Die dimensions: (a) rectangle, (b) trapezoid.

shape factor F_p has traditionally been introduced, i.e.

$$Q = \frac{n}{2(2n+1)} \left(\frac{\Delta P_{die} H}{2KL}\right)^{\frac{1}{n}} WH_o^2 F_p \qquad (4\text{-}15)$$

For a rectangular die and a Newtonian fluid, the shape factor is given as (32),

$$F_p = 1 - \left(\frac{192H}{\pi^5 W}\right) \sum_{g=1,3\ldots}^{\infty} \left(\frac{1}{g^5}\right) \tanh\left(g\pi H/2W\right) \qquad (4\text{-}16)$$

The power law problem has been solved numerically by various investigators (165, 205, 259). Its F_p can be represented approximately as,

$$F_p = \frac{1}{\left(1 + \frac{n^{1/3}\, 3^{1/\phi}}{2}\right)^{1/n}} \qquad (4\text{-}17)$$

where ϕ = aspect ration = W/H.

For the same ϕ, F_p is larger and closer to 1 for Newtonian fluid than that for non-Newtonian fluid. An aspect ratio of about 6 is required for two dimensional flow to be used for a Newtonian fluid. The critical aspect ratio which allows us to take a slit asymptotic approach in solving this problem increases with increasing non-Newtonian behavior or decreasing power index n of the polymer melts.

We will now apply a one-dimensional shear approximation to a trapezoidal die of equal sides. We specify this by,

$$\text{as} \quad -\frac{W}{2} \leq x_3 \leq \frac{W}{2}, \qquad H = H_o \tag{4-18a}$$

$$\text{as} \quad x_3 > \frac{W}{2}, \qquad H = H_o\left[1 - \frac{1}{b}\left(x_3 - \frac{W}{2}\right)\right] \tag{4-18b}$$

The extrusion rate is then

$$Q = Q_w + 2Q_b \tag{4-19a}$$

where

$$Q_w = \frac{n}{2(2n+1)}\left(\frac{\Delta P_{die} H_o}{2KL}\right)^{\frac{1}{n}} W H_o^2 \tag{4-19b}$$

If we insert equation (4-18b) into Eq. (4-14), we get

$$Q_b = \frac{n}{2(2n+1)}\left(\frac{\Delta P_{die} H_o}{2KL}\right)^{\frac{1}{n}} H_o^2 \left(\frac{n}{3n+1}\, b\right) \tag{4-20}$$

Combining Eqs. (4-20) and (4-19b) with (4-19a), we get

$$Q = \frac{3n}{2n+1}\left(\frac{\Delta P_{die} H_o}{2KL}\right)^{\frac{1}{n}} W H_o^2 \left(1 + \frac{2n}{3n+1}\,\frac{b}{W}\right) \tag{4-21}$$

and

$$F_p = 1 + \frac{2n}{(3n+1)}\,\frac{b}{W}$$

For the case b = W/2, which is the trapezoidal die used in this study, we have

$$F_p = \frac{4n+1}{3n+1} \tag{4-22}$$

B. EXPERIMENTAL

1. Meterials

Two polymer melts, polystyrene and polypropylene were used. The reological properties for these two polymers has been described in Chapter 3.

2. Dies

Dies with a range of cross sections were used in these experiments. These are summarized in Table 4-1 which includes channels with rectangular and trapezoidal geometries.

3. Pressure loss-extrusion rate behavior

Pressure losses within die channels were obtained by measuring the pressure required to extrude polymer melts through dies of equivalent cross section and variable length and subtracting out the ends losses with a Bagley plot (5). This has been discussed in Chapter 3.

C. RESULTS AND INTERPRETATION

At high shear rate, power law model can be used to represent polystyrene and polypropylene used in this study. The rheological constants n and K of power law model are:

for polystyrene

$$n = 0.357, \qquad K = 1.1 \times 10^{4} \text{ pascal} * \text{sec}^{-0.357}$$

for polypropylene

$$n = 0.463, \qquad K = 0.52 \times 10^{4} \text{ pascal} * \text{sec}^{-0.463}$$

Plots of Q vs. $(\Delta P_d H/2L)$ are shown in Figure 4-2 for rectangular dies of various aspect ratio and Figure 4-3 for trapezoidal die of both polymer melts at 180°C.

Table 4-1. Dimensions of dies for experiment in Ch. 4

Slit dies:

H (mm)	Aspect Ratio	L/H		
		1	2	3
0.381	16.7	12.53	20.00	29.87
0.635	10.0	12.00	18.18	24.08

Rectangular dies: H = 1.19 mm W/H = 2.0

L/H = 9.89, 15.01, 19.97

Trapezoidal dies: H = b = 1.524 mm W/H = 2.0

L/H = 3.05, 10.32, 31.3

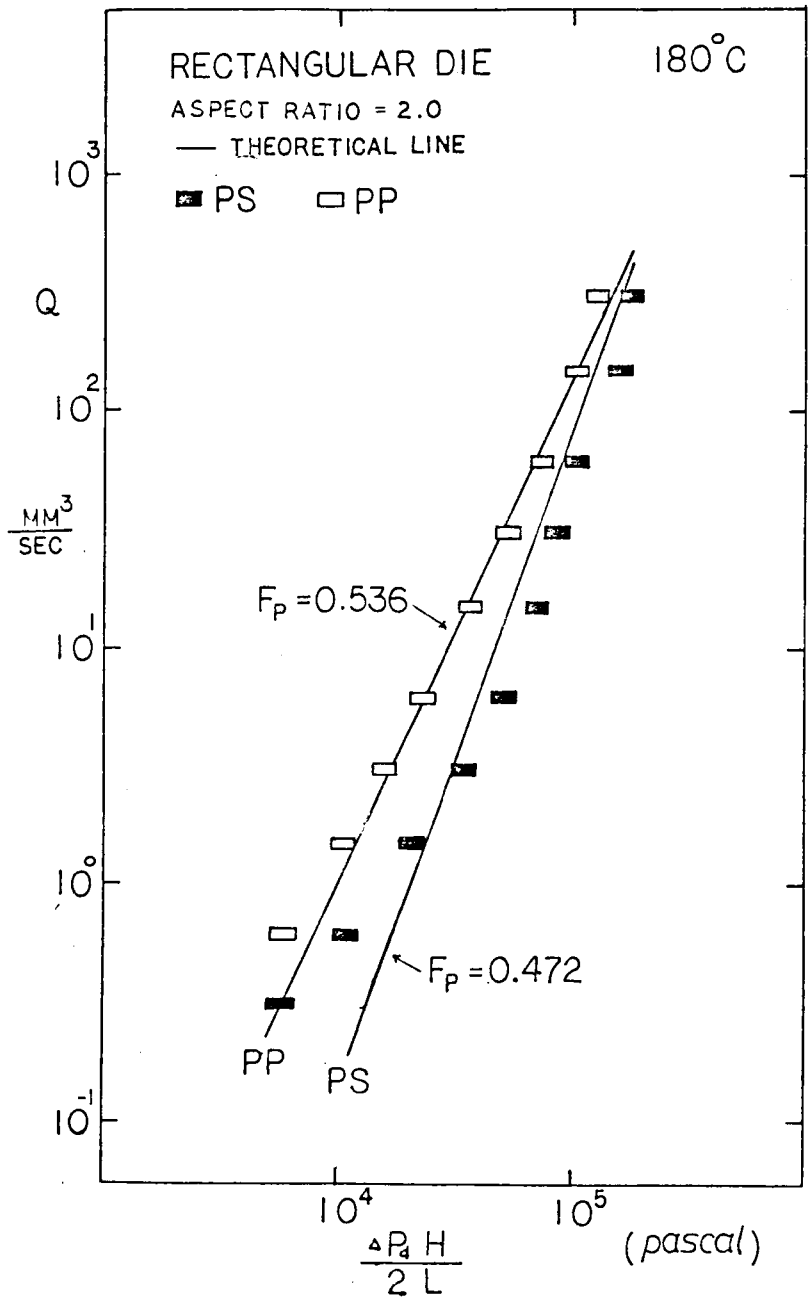

Figure 4-2. Plots of Q vs. ($\Delta P_d H/2L$) for rectangular die.

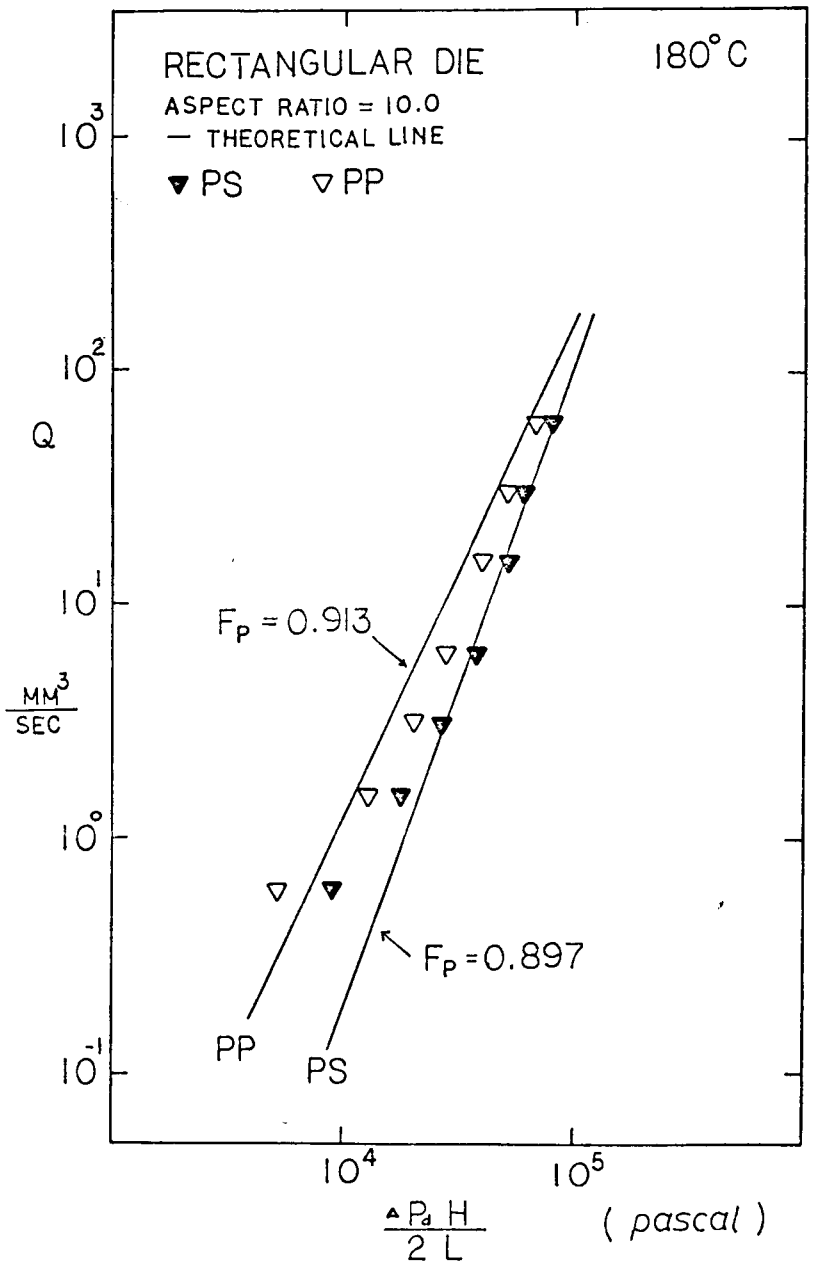

Figure 4-2. (Continued)

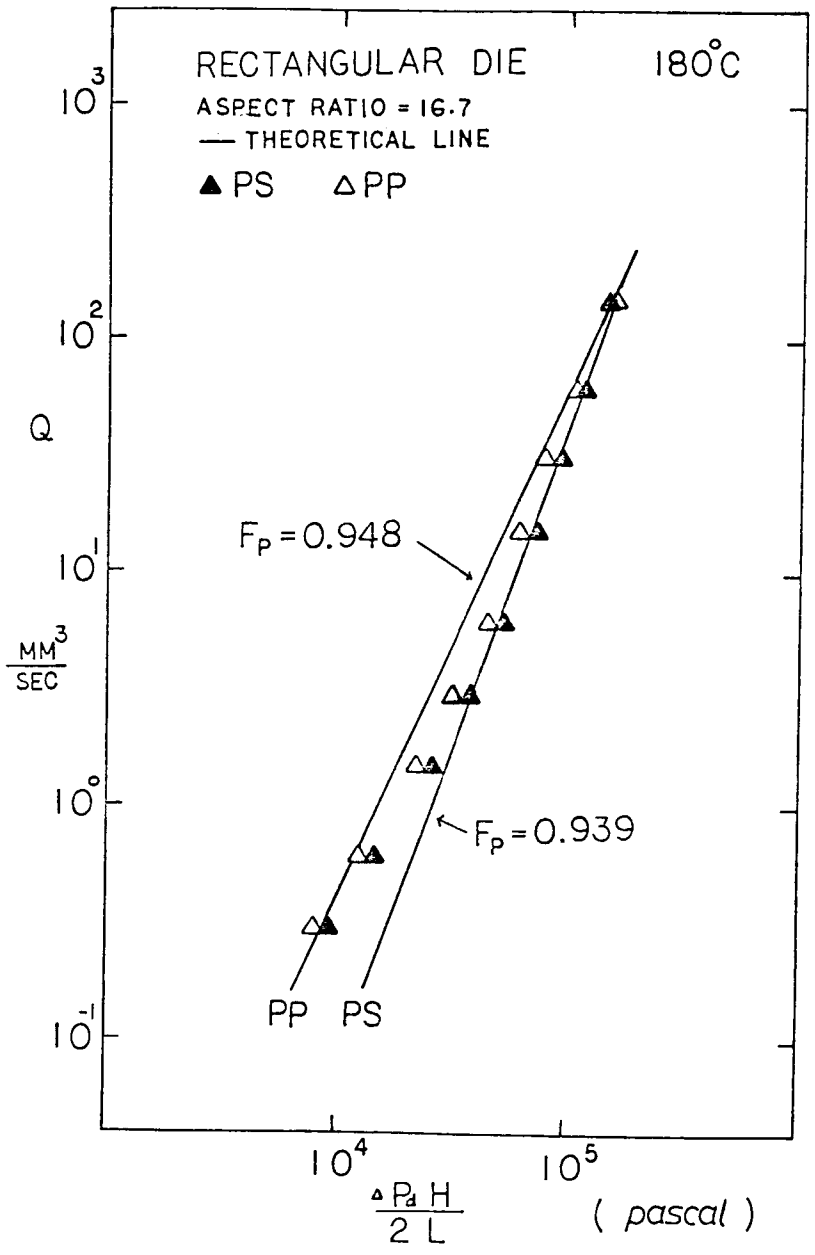

Figure 4-2. (Continued)

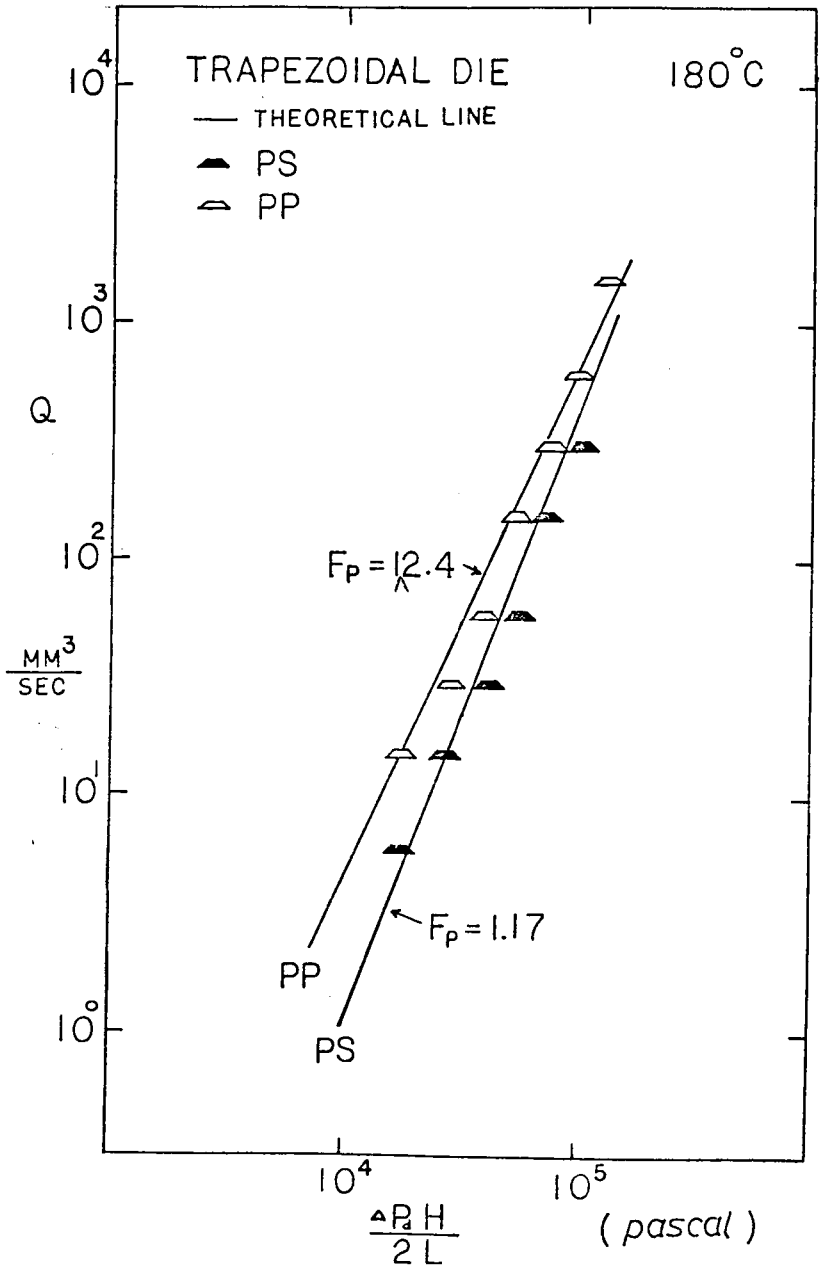

Figure 4-3. Plot of Q vs. ($\Delta P_d H/2L$) for trapezoidal die.

Theoretical lines based on Eqs. (4-15), (4-17) and (4-22) (pp. 57, 59) have also been given for comparison.

Generally, the experimental and computed results are reasonably good. It is striking that the theoretical prediction of trapezoidal die is very good although the theoretical derivation is an approximated analysis. The descrepancy is usually higher at lower flow rate especially polystyrene. This is because the prameters of power law model are chosen at high flow rate. At low flow rate, polymer melts especially polystyrene are closing to be Newtonian fluids. The shape factors F_p are closing to 1 for aspect ratio 10.0 and 16.7 and about 0.5 for aspect ratio 2 of rectangular dies. The role of shape factor is very important in rectangular dies of low aspect ratio, without it the error can go up to 100% or more (refer to Figure 4-2). To calculate the flow field of a complex die like trapezoidal is extremely difficult. Some numerical calculation has been provided by Rothemeyer (203) with applying finite element method. However, there is no evalution of shape factor for dies of this geometry in the literatures. We have accomplished a first order formulation of shape factor for trapezoidal dies. This formulation may be limited to the case where both W/H and b (refer to Figure 4-1 (p. 58)) must not be small (i.e. $W/H \gg 1$ and $b > W$).

CHAPTER 5

EXTRUDATE SWELL FOR LONG SLIT AND CAPILLARY DIES

Numerous studies have been reported for extrudate swell from a capillary die but very limited investigations for other geometries as we have discussed in Chapter 2. Before we turn to the study of swell from more complicated dies, it is necessary to understand the swell behavior from another simple geometry, the slit die. The slit die is a die of rectangular cross section in which the ratio of the larger dimension to the smaller dimension (aspect ratio) is very large. For this geometry, we can treat the problem as a two dimension simple flow. The capillary and slit are the two simplest cases of flow problem but very different in nature.

A comparative experimental study of extrudates from long slit and capillary dies is reported in this chapter for rheologically characterized polystyrene and polypropylene melts. The rheological behavior for these two polymers has been summarized in Figure 3-1 to 3-3 (pp. 41-43).

The experimental results are compared with theories of swell based on unconstrained recovery from Poiseuille flow in these geometries. A detailed analysis of such theories of extrudate swell based on the original work of Tanner has been carried out. The analysis is placed in a more general form which should be valid for a range of die cross sections.

A. EXPERIMENTAL APPROACH

1. Apparatus

Extrudate swell measurements were made at 180°C in an Instron capillary rheometer. The dies used had both rectangular and circular cross sections. The rectangular dies had aspect ratios of 10.0 and 16.7 with small dimensions H of 0.381 mm and 0.635 mm. The dies had ratios of length of channel thickness (L/H) or length to diameter (L/D) as shown in Table 5-1.

2. Experimental procedures and problems

Some difficulties arose with gravitational effects especially with polystyrene melts emerging from slit dies. The melt streams badly necked down on flowing vertically downward from the die. This problem was overcome by extruding into a bath of silicone oil possessing a density approximately equal to those of the melts.

The extrudate swell of the polymer emerging from the slit die were values measured at the center of the cross section. Extrudate swell measurements have been found to vary with observer even in our own laboratories. Reasons for gross variations are discussed by White and Roman (270). Our concern is with smaller changes of order 0.1 in d/D. The problem is that we are interested really in the difference in (d-D)/D and (h-H)/H and are measuring

Table 5-1. Dimensions of dies for experiment in Ch. 5

Slit dies:

H (mm)	Aspect Ratio	L/H		
		1	2	3
0.381	16.7	12.53	20.00	29.87
0.635	10.0	12.00	18.18	24.08

Capillary dies:

Diameter (mm)	L/D			
	1	2	3	4
0.762	8.00	11.95	15.97	---
1.702	5.02	9.98	15.04	20.02

d/D and h/H. Generally the swell was measured at about 5 mm to 25 mm from the initial end of the extrudates as we move from low to high wall shear rate.

For most sets of extrudate swell measurements, the die length we used was long enough to reach the asymptotic value. Exceptions were at very high shear rates where extrapolation is necessary.

Extrudates were annealed from 170°C to 180°C in hot silicone oil for five minutes.

3. Extrudate character - qualitative

Typical cross sections for the unannealed polystyrene and polypropylene extrudates are shown in Figure 5-1 at various extrusion rates within the stable flow region. There is a slight tendency for greater swell at the center of the slit cross-section. As extrusion rate increases, swell likewise increases. The swell decreases as we increase the L/D ratio. The influence of annealing on cross-sectional shape for extrudates from slit dies is shown in Figure 5-2. There are difficulties in measuring swell at low extrusion rates because of a tendency of the melt to interact with the outward face of the die and ball up.

At high extrusion rates, distortion occurs. This has the form of helical extrudates in the melts emerging from the circular dies. It had a somewhat different character for the rectangular/slit dies as shown in

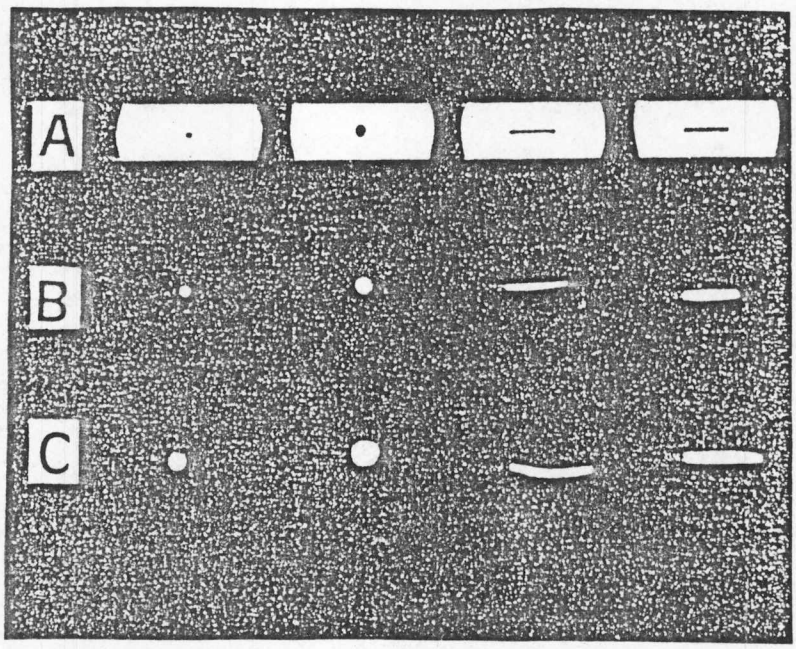

(A) Die cross section

(B) Low shear rate

(C) High shear rate

Figure 5-1. Photographs of unannealed cross sections of extrudates from capillary and slit dies.

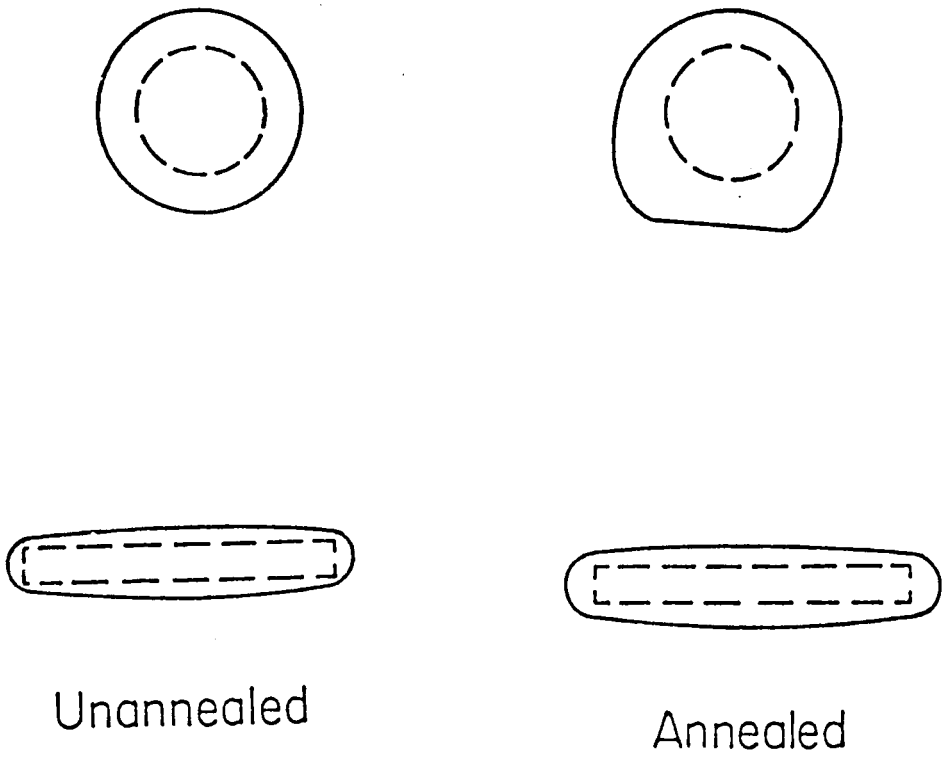

Figure 5-2. Influence of annealing on cross-sectional shape.

Figure 5-3. One forms a ribbed extrudate in which the ribs are parallel to the die exit. The results are similar to those described by Vlachopoulus and Chan (253). Sometimes the slit extrudates also show a twisted shape at high extrusion rate as shown in Figure 5-3. Specifically the distortion always seems initiated at the center of the longer dimension of the slit die. Extrudate distortion is decreased by increasing die length. It can be eliminated by applying a small force or by the extrudates own gravity until very high extrusion rates.

4. Extrudate character - quantitative

Generally extrudate swell for both slit (h/H), and capillary (d/D), decrease with increasing die length achieving eventually asymptotic values. We plot in Figure 5-4 the long die length asymptotic extrudate swell from capillary (d/D) and slit (h/H) dies as a function of wall shear rate $\dot{\gamma}_w$. For the capillary, $\dot{\gamma}_w$ is defined by Eqs. (3-6) and (3-7), and for a slit die is defined by Eqs. (4-25) and (4-26), where we have neglected shearing along the smaller dimensions of the slit channel.

We plot the extrudate swell data in Figure 5-4 as a function of shear rate on semi-logarithmic coordinates. The values of the swell are corrected to 180°C using density changes. This density factor, $[\rho(30°C)/\rho(180°C)]^{1/3}$, is 1.027 for polystyrene and 1.057 for polypropylene.

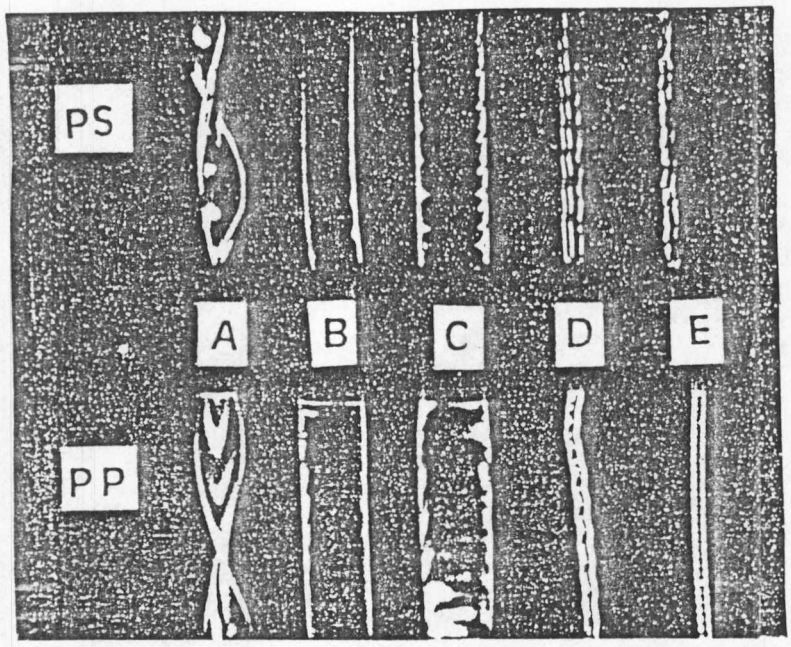

(A) Twisted extrudate from slit die at high shear rate.
(B) Initial distorted extrudate of slit die.
(C) Highly distorted extrudate of slit die.
(D) Initial distorted extrudate of capillary die.
(E) Highly distorted extrudate of capillary die.

Figure 5-3. Photographs of polystyrene (PS) and polypropylene (PP) extrudates from capillary and slit dies in unstable flow region.

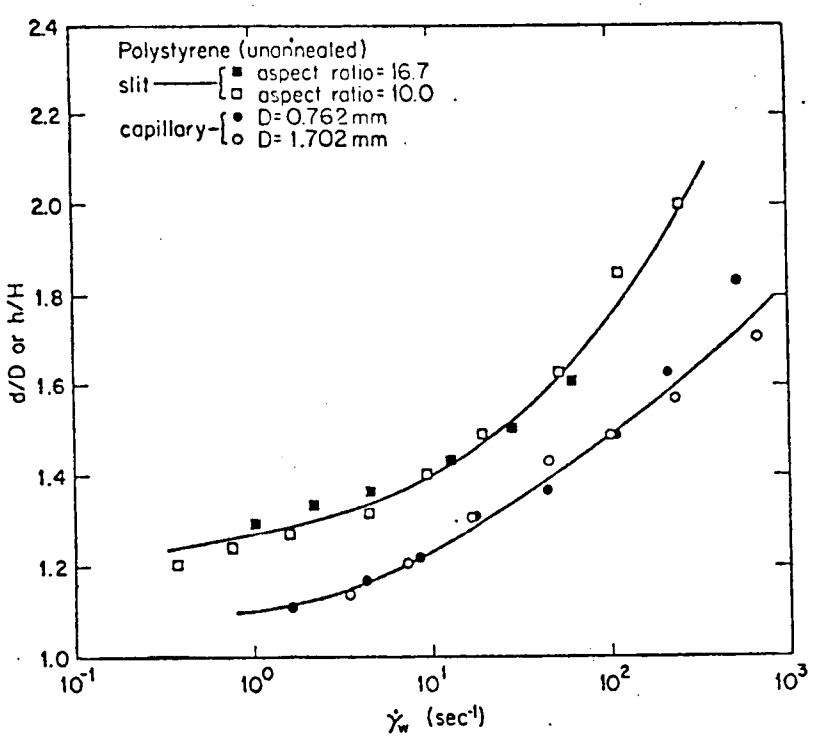

(a) polystyrene

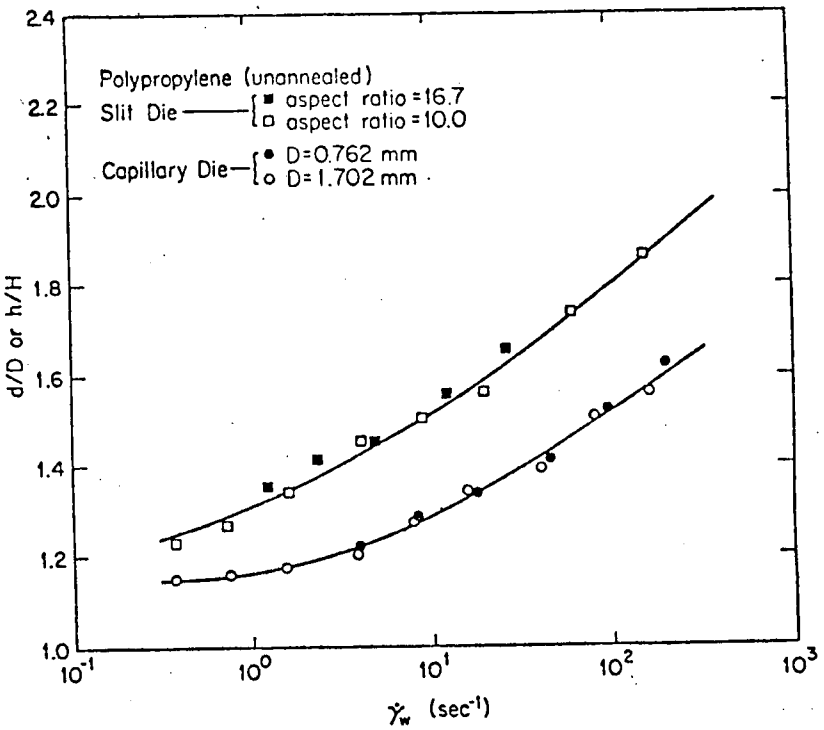

(b) polypropylene

Figure 5-4. Extrudate swell d/D and h/H as a function of die wall shear rate for melts for unannealed extrudates (correlated to 180°C).

The swell is an increasing function of shear rate for both die geometries. At low shear rates the swell goes to asymptotic value for the slit of about 1.2 and for the capillary about 1.1. Generally the polypropylene has a higher swell, but the polystyrene is rising more rapidly at the higher shear rates.

In Figure 5-5 we show the influence of annealing. This generally increases the level of swell. The increase is about the same as found by White and Roman (270) for similar polymer melts.

The onset of extrudate distortion occurred at critical values of $\dot{\gamma}_w$ and σ_w as shown in Table 5-2. Generally these are higher for the capillary and for the lower aspect ratio slit dies as compared to the higher aspect ratio slit die. The extrudate distortion observed for the slit dies is equivalent to the initial "buckling" instability described by Vlachopoulos and Chan (253).

B. THEORY OF EXTRUDATE SWELL

The constitutive equations used here to develop the swell equations is essentially a Bogue-White model with a Maxwellian relaxation function which was presented in Chapter 2 with Eq. (2-8) to (2-10).

We shall proceed in our development by taking ε equal to zero. This is equivalent to the formulation used by White (263) and by White and Roman (270) in earlier

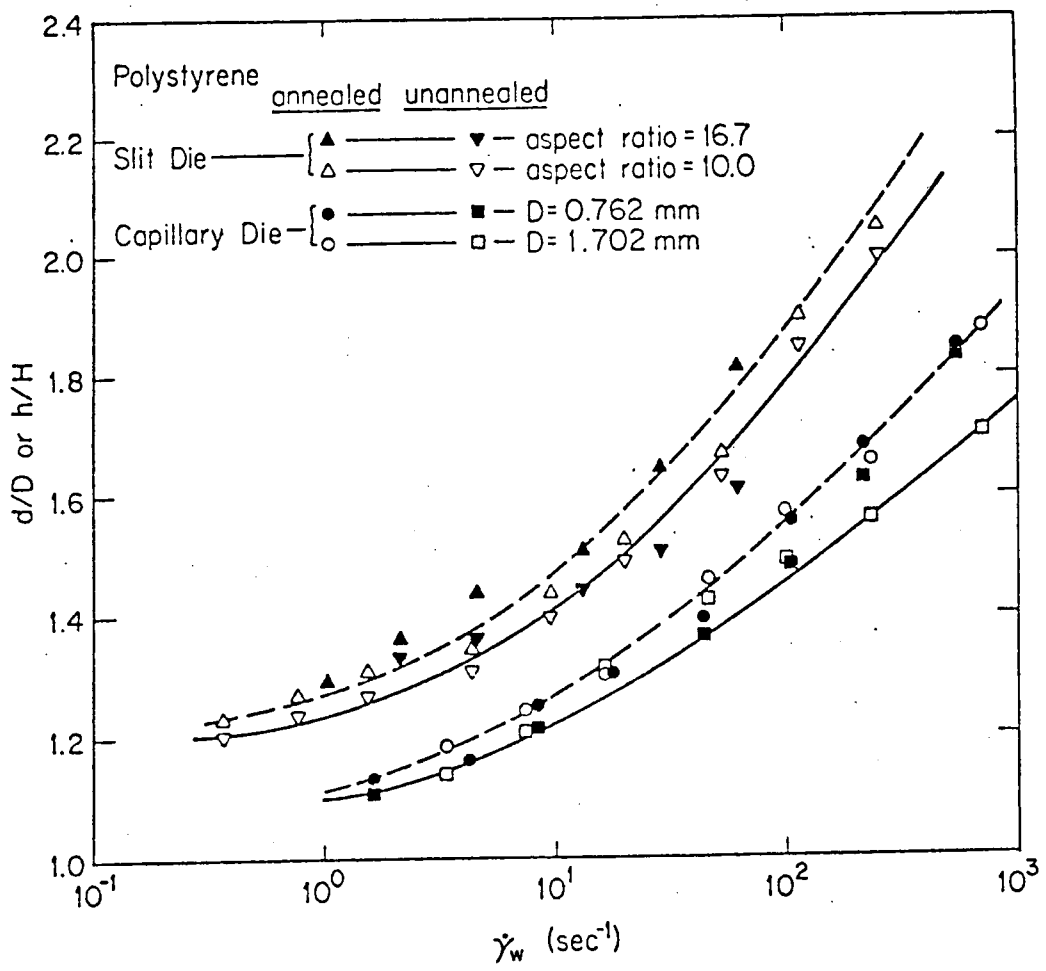

(a) Polystyrene

Figure 5-5. Influence of annealing and extrudate swell-shear ratio function.

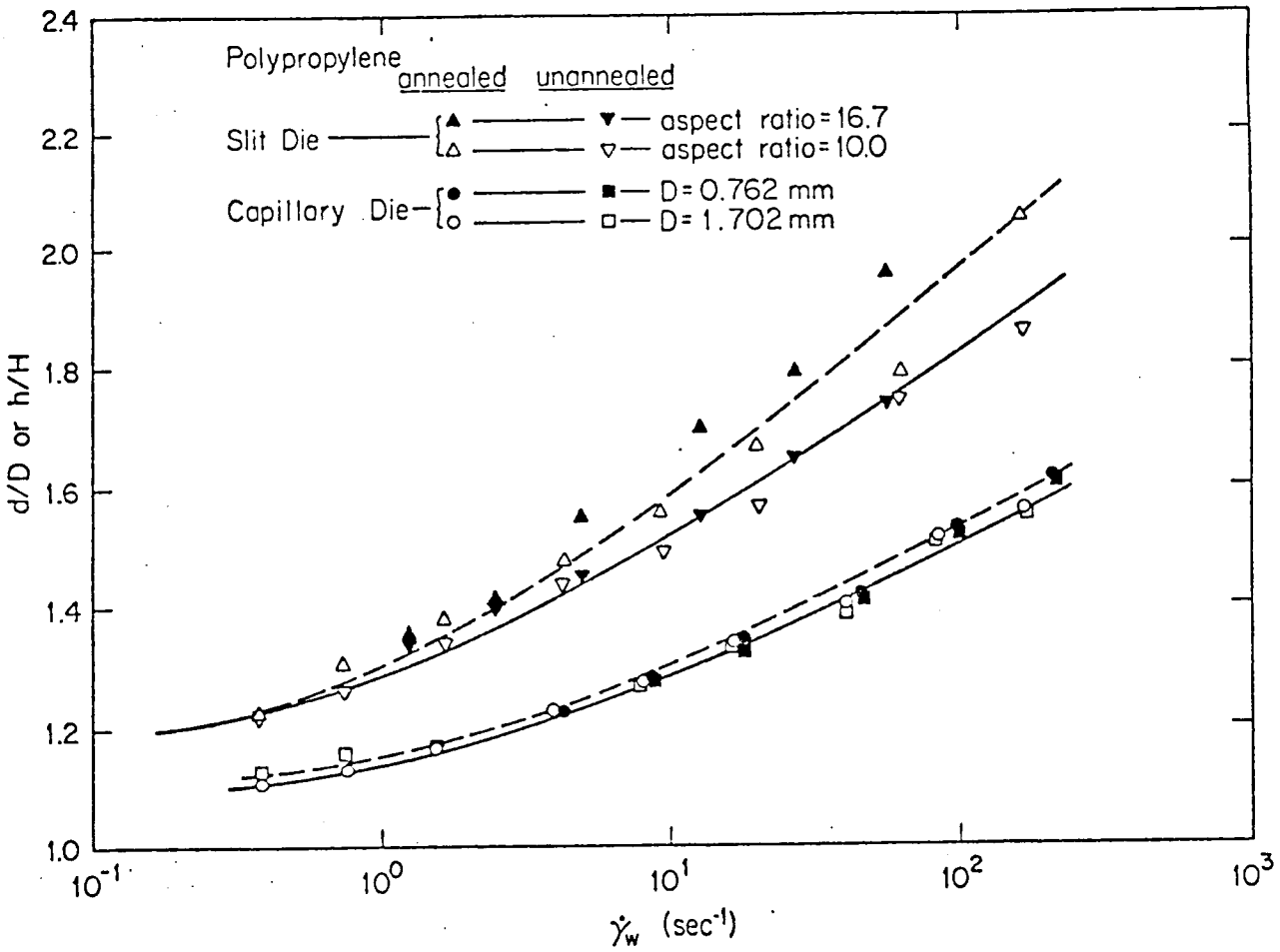

(b) Polypropylene

Figure 5-5. (continued)

Table 5-2. Shear rates and shear stresses at distortion occurrence

Die	Aspect ratio	Slit		Capillary (0.762 mm)
		16.7	10.0	
Polystyrene	$\dot{\gamma}_{crit}(sec^{-1})$	175	650	1054
	σ_{crit}(Pascal)	7.20×10^4	1.05×10^5	1.32×10^5
Polypropylene	$\dot{\gamma}_{crit}(sec^{-1})$	55.8	320	1206
	σ_{crit}(Pascal)	4.07×10^4	7.08×10^4	1.30×10^5

studies. In these papers G was considered to be a constant. We shall not make this restriction in the present studies.

1. Unconstrained recovery from flow

Consider a viscoelastic fluid initially at rest which undergoes a flow history from time zero to time t_R at which it is released from constraints and undergoes an unconstrained recovery. Using the constitutive formulation described in the previous section, we may write the stress and the recovered fluid as:

$$\underset{\sim}{\sigma}(t) = -p\underset{\sim}{I} + \underbrace{\int_0^{t-(t_R+\delta t_R)} m_1(z)\, \underset{\sim}{c}^{-1}(z)\, dz}_{\text{period of delayed recovery}} + \underbrace{\int_{t-(t_R+\delta t_R)}^{t-t_R} m_1(z)\, \underset{\sim}{c}^{-1}(z)\, dz}_{\text{period of instantaneous recovery}} + \underbrace{\int_{t-t_R}^{t} m_1(z)\, \underset{\sim}{c}^{-1}\, dz}_{\text{period of flow}} + \underbrace{\int_{t}^{\infty} m_1(z)\, \underset{\sim}{c}^{-1}\, dz}_{\text{period prior to flow}} \qquad (5\text{-}1)$$

$\underset{\sim}{\sigma}(t)$ is identically zero for recovery from homogeneous deformations, but not in recovery from complex flow fields as would exist in the fluid emerging from a die. For a Maxwellian fluid, i.e. one in which m(z) consists of single exponential there will be no delayed recovery (see Lodge (129)), but note that this also directly follows from the mechanical spring-dashpot Maxwell model (197). This allows us to simplify Eq. (5-1) to

$$\underset{\sim}{\sigma} = - p\underset{\sim}{I} + \int_{t-t_R}^{\infty} m_1(z)\ \underset{\sim}{c}^{-1}(z)\ dz \qquad (5\text{-}2)$$

This formulation is awkward because the reference state is unknown. It is useful to change the reference state using a matrix $\underset{\sim}{Q}$ which transforms the configuration to that existing before the recovery. We may write

$$\underset{\sim}{Q}\ (\underset{\sim}{\sigma} + p\underset{\sim}{I})\ \underset{\sim}{Q}^T = \int_{t-t_R}^{\infty} m_1(z)\ \underset{\sim}{Q}\ \underset{\sim}{c}^{-1}\ \underset{\sim}{Q}^T\ dz \qquad (5\text{-}3)$$

Consider the long duration simple shear flow of a polymer melt. Here

$$\underset{\sim}{Q}\ \underset{\sim}{c}^{-1}\ \underset{\sim}{Q}^T = \begin{vmatrix} 1+\dot{\gamma}^2 z^2 & \dot{\gamma} z & 0 \\ \dot{\gamma} z & 1 & 0 \\ 0 & 0 & 1 \end{vmatrix} \qquad (5\text{-}4)$$

Substitution into Eq. (5-4) and integrating yields

$$\underset{\sim}{Q}\ (\underset{\sim}{\sigma}+p\underset{\sim}{I})\ \underset{\sim}{Q}^T = G \begin{vmatrix} 1+2\tau_{eff}{}^2\dot{\gamma}^2 & \tau_{eff}\dot{\gamma} & 0 \\ \tau_{eff}\dot{\gamma} & 1 & 0 \\ 0 & 0 & 1 \end{vmatrix} \qquad (5\text{-}5)$$

2. Extrudate swell from long die

We now seek to apply the ideas in this paper to predict swell from various types of dies. It is readily possible to consider slit and annular dies.

The recovery may be expressed in the form

$$x_1(t) = \alpha_1\, x_1(t_R) - g(x_2)$$

$$x_2(t) = \alpha_2\, x_2(t_R)$$

$$x_3(t) = x_3(t_R) \tag{5-6}$$

where $g(x_2)$ is a shearing deformation and the three axes x_1, x_2, x_3 are mutually perpendicular.

$$\underset{\sim}{Q}(\underset{\sim}{\sigma} + p\underset{\sim}{I})\,\underset{\sim}{Q}^T = \begin{vmatrix} \frac{1}{\alpha_1^2}(\sigma_t + p) + \hat{g}^2 p & \frac{p\hat{g}}{\alpha_2} & 0 \\ \frac{p\hat{g}}{\alpha_2} & \frac{p}{\alpha_2^2} & 0 \\ 0 & 0 & p \end{vmatrix} \tag{5-7}$$

Comparison of Eqs. (5-5) and (5-7) leads to

$$\frac{1}{\alpha_1^2}(\sigma_t + p) + \hat{g}^2 p = G\,(1 + 2\tau_{eff}^2\dot{\gamma}^2) \tag{5-8a}$$

$$\frac{p\hat{g}}{\alpha_2} = G\,\tau_{eff}\dot{\gamma} \tag{5-8b}$$

$$\frac{p}{\alpha_2^2} = G \tag{5-8c}$$

A similar set of equations may be developed for the case of $\xi = -2$. The Eq. (5-8b,c) may be used to eliminate $\hat{g}$ and p from Eq. (5-8a) to give

$$\frac{1}{\alpha_1^2}\left(\sigma_t + G\,\alpha_2^2\right) + G\,\tau_{eff}^2\dot{\gamma}^2 = G\left(1 + 2\,\tau_{eff}^2\dot{\gamma}^2\right) \tag{5-9a}$$

or

$$\frac{\alpha_2^2}{\alpha_1^2} + \frac{\sigma_t}{G}\frac{1}{\alpha_1^2} = 1 + \tau_{eff}^2\dot{\gamma}^2 \tag{5-9b}$$

To proceed further, we must integrate Eq. (5-9b) across the cross section of the exiting stream. Tanner integrates Eq. (5-9a) across the cross section, while White and Roman integrate Eq. (5-9b) in the case of capillary flow. If we choose the former procedure we obtain after Tanner:

$$\left(G\,\frac{1}{\alpha_1^2}\,\alpha_2^2\right) + \left(\sigma_t\,\frac{1}{\alpha_1^2}\right) = \left(G + \frac{\sigma_{12}^2}{G}\right) \tag{5-10a}$$

where we take

$$\left(G\,\frac{1}{\alpha_1^2}\,\alpha_2^2\right) = G\,\frac{1}{\alpha_1^2}\,B^2 \tag{5-10b}$$

while if we choose the latter:

$$\overline{\frac{1}{\alpha_1^2}\,\alpha_2^2} + \overline{\left(\frac{\sigma_t}{G}\,\frac{1}{\alpha_1^2}\right)} = \overline{\left(1 + \frac{\sigma_{12}^2}{G^2}\right)} \tag{5-10c}$$

where the bar indicates a cross-sectional average and we have noted that the swell B will be the integral of α_2 across the cross section.

To proceed further we must relate α_2 and α_1 and determine the appropriate cross-sectional averages. In doing so we need to say more about G. In Tanner's original work and later studies of White (263) and White and Roman (270), the quantity G was taken as a constant. As first shown by Utracki, Bakerdjian and Kamal (248) it is however possible to take into consideration more complex behavior.

Presuming N_1 function to be

$$N_1 = A \sigma_{12}^{a} \tag{2-25}$$

where A and a depend on molecular weight distribution. For the rheological model used in this study

$$N_1 = 2 G \tau_{eff}^{2} \dot{\gamma}^2 = \frac{2\sigma_{12}^{2}}{G} \tag{5-11a}$$

implying that

$$G = \frac{2}{A} \sigma_{12}^{2-a} \tag{5-11b}$$

and

$$\frac{G + \sigma_{12}^{2}/G}{G} = \frac{\frac{A}{2} \sigma_{12}^{a} + \frac{2}{A} \sigma_{12}^{2-a}}{\frac{2}{A} \sigma_{12}^{2-a}} \tag{5-12a}$$

$$1 + \frac{\sigma_{12}^{2}}{G^2} = 1 + \frac{A^2 \sigma_{12}^{2a-2}}{4} \tag{5-12b}$$

The same procedures may be used for complex N_1- σ_{12} relations such as the Dietz-White-Clark relation (70).

We shall only consider cases here in which no tensile force is applied to the exiting stream. This will be taken to imply that

$$(\sigma_t \frac{1}{\alpha_1^2}) = 0 \qquad (5\text{-}13a)$$

or

$$(\frac{\sigma_t}{G} \frac{1}{\alpha_1^2}) = 0 \qquad (5\text{-}13b)$$

If G is not constant, this is not strictly the case for Eq. (5-13b).

To obtain particular results we must define the geometry and relate α_1 to α_2. We presume the melt emerging from a slit exhibits recovery in only one direction (the direction of shear) rather than equally in all directions as occurs for flow out of a cylindrical die.

3. Slit dies

For an infinite aspect ratio slit die with wall separation distance H continuity demands

$$\alpha_1 = \frac{1}{\alpha_2} \qquad (5\text{-}14)$$

Further using Eqs. (5-12) and (5-13) we may rewrite Eq. (5-10a) as

$$B^4 = \frac{\frac{1}{H}\int_0^H (\frac{A}{2}\sigma_{12}^{\ a} + \frac{2}{A}\sigma_{12}^{\ 2-a})\, dx_2}{\frac{1}{H}\int_0^H (\frac{2}{A}\sigma_{12}^{\ 2-a})\, dx_2}$$

$$= \frac{\int_0^{\sigma_w} (\frac{A}{2}\sigma_{12}^{\ a} + \frac{2}{A}\sigma_{12}^{\ 2-a})\, d\sigma_{12}}{\int_0^{\sigma_w} (\frac{2}{A}\sigma_{12}^{\ 2-a})\, d\sigma_{12}}$$

$$= 1 + \frac{(3-a)}{4\,(1+a)}\,[A(\sigma_{12})_w^{\,a-1}]^2$$

$$B = \left[1 + \frac{(3-a)}{4\,(1+a)}\left(\frac{N_{1w}}{(\sigma_{12})_w}\right)^2\right]^{1/4} \qquad (5\text{-}15a)$$

From Eq. (5-10c)

$$B^4 = \frac{1}{H}\int_o^H \left[1 + \frac{\sigma_{12}^{\,2}}{G^2}\right] dx_2$$

$$= \frac{1}{(\sigma_{12})_w}\int_o^{(\sigma_{12})_w} \left[1 + \frac{\sigma_{12}^{\,2}}{G^2}\right] d\sigma_{12}$$

$$= 1 + \frac{[A\,(\sigma_{12})_w^{\,a-1}]^2}{4\,(2a-1)}$$

$$B = \left[1 + \frac{1}{4\,(2a-1)}\left(\frac{N_{1w}}{(\sigma_{12})_w}\right)^2\right]^{1/4} \qquad (5\text{-}15b)$$

where the linear variation of σ_{12} with x_2 has been used to carry out the integration.

4. Capillary dies

For swell from a capillary die we have

$$\alpha_1 = \frac{1}{\alpha_2^2} = \frac{1}{B^2} \qquad (5\text{-}16)$$

Again from Eqs. (5-10a), (5-12) and (5-13)

$$B^6 = \frac{\int_o^R 2\pi r\,\left(\frac{A}{2}\,\sigma_{12}^{\,a} + \frac{2}{A}\,\sigma_{12}^{\,2-a}\right) dr}{\int_o^R 2\pi r\,\left(\frac{2}{A}\,\sigma_{12}^{\,2-a}\right) d\dot{\gamma}}$$

$$= 1 + \frac{(4-a)}{4\,(2+a)} \left[A\,(\sigma_{12})_w^{a-1}\right]^2$$

$$B = \left[1 + \frac{(4-a)}{4\,(2+a)} \left(\frac{N_{1w}}{(\sigma_{12})_w}\right)^2\right]^{1/6} \qquad (5\text{-}17a)$$

From Eq. (5-10b)

$$B^6 = \frac{1}{\pi R^2} \int_0^R 2\pi r \left[1 + \frac{\sigma_{12}^2}{G^2}\right] dr$$

$$= 1 + \frac{\left[A(\sigma_{12})_w^{a-1}\right]^2}{4a}$$

$$B = \left[1 + \frac{1}{4a} \left(\frac{N_{1w}}{(\sigma_{12})_w}\right)^2\right]^{1/6} \qquad (5\text{-}17b)$$

The viscous swell, C_{slit} may add to Eq. (5-15) for slit and, C_{cap} may add to Eq. (15-17) for capillary.

If we follow the specific formulation of Tanner and White and Roman with constant modulus G, we predict the swell to be of form for each geometry to be

$$\frac{h}{H} = B_{slit} = \left[1 + \frac{1}{12} \left(\frac{N_{1w}}{\sigma_w}\right)^2\right]^{1/4} \qquad (5\text{-}18)$$

$$\frac{d}{D} = B_{cap} = \left[1 + \frac{1}{8} \left(\frac{N_{1w}}{\sigma_w}\right)^2\right]^{1/6} \qquad (5\text{-}19)$$

Note the slit involves a 1/4 power and the capillary a 1/6 power indicating a more rapid rise in swell for the former. Eq. (5-19) is due to Tanner (228). Huilgol (102) has attempted to derive a form for B for a slit using the above methods. However, he considers recovery in all directions rather than in one direction. He obtains a 1/6 rather than a 1/4 power in Eq. (5-18).

C. INTERPRETATION OF EXPERIMENTS

Dimensional analysis considerations suggest plotting the swell B against the Weissenberg number (270, 263) N_1/σ_{12} is evaluated at the die wall. This is shown in Figure 5-6.

To represent the variation of normal stresses we utilized the empirical power law relation of Eq. (2-25) (p. 13). This expression was found to be a useful representation by Oda, White and Clark (180) for commercial polystyrene melts as shown in Figure 3-2 (p. 42). Here A is 3.47×10^{-3} (pascal) and a is 1.66 for moderate molecular weight distribution polystyrene melts. For polypropylene used in this study A is 0.0229 and a is 1.47. The $N_1 - \sigma_{12}$ data described in this dissertation and most data considered by Oda et al. (180) are low shear rate cone and plate results. They were obtained in shear rate ranges below that used in most extrusion studies. Dietz, White and Clark (70) in studying the $N_1 - \sigma_{12}$ data obtained by Wales (256) on a Dow Styron 678 over a wide range of shear rates by both cone-plate and flow birefringence (in the high shear rate range) found that it required a double power law to fit it, i.e.

$$N_1 = A_1 \sigma_{12}^{a_1} \qquad \sigma_{12} < \sigma_c \qquad (5\text{-}20a)$$

$$N_1 = A_2 \sigma_{12}^{a_2} \qquad \sigma_{12} > \sigma_c \qquad (5\text{-}20b)$$

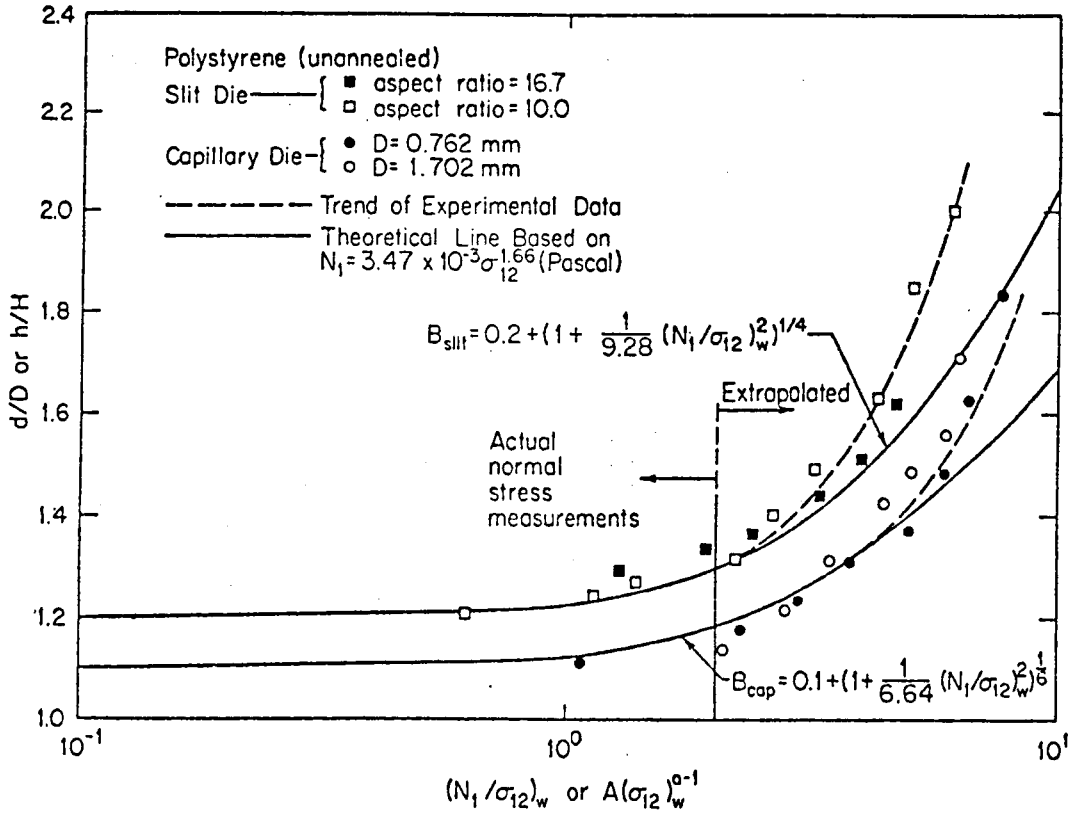

(a) polystyrene

Figure 5-6. Extrudate swell for slit and capillary dies as a function of ratio of principal normal stress difference to shear stress at the die wall.

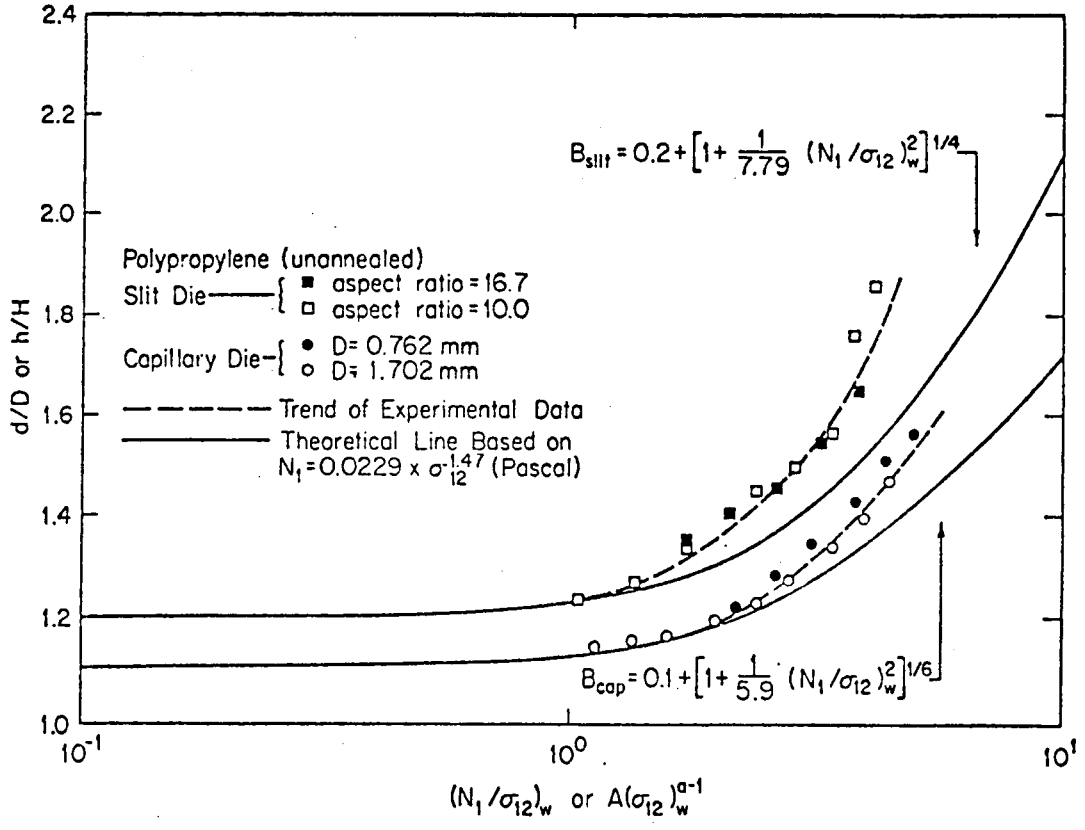

(b) polypropylene

Figure 5-6. (Continued)

where A_1 and a_1 are the values of Oda et al. and A_2 is 1.40×10^{-5} and a_2 is 2.18. If σ_w is less than σ_c, Eqs. (5-17) to (5-19) remain valid. If σ_w is greater than σ_c we obtain using the White-Roman procedure:

$$B_{slit} = C_{slit} + \left[1 + \frac{(a_2-a_1)A_2^2}{2(2a_1-1)(2a_2-1)} \sigma_c^{2a_2-2} \frac{\sigma_c}{\sigma_w} + \frac{A_2^2}{4(2a_2-1)} \sigma_w^{2a_2-2}\right]^{1/4} \quad (5\text{-}21)$$

and

$$B_{cap} = C_{cap} + \left[1 + \frac{(a_2-a_1)A_2^2}{4a_1a_2} \sigma_c^{2a_2-2} \left(\frac{\sigma_c}{\sigma_w}\right)^2 + \frac{A_2^2}{4a_2} \sigma_w^{2a_2-2}\right]^{1/6} \quad (5\text{-}22)$$

As a_2 is greater than a_1, Eqs. (5-21) and (5-22) predict larger swell than Eqs. (5-17) and (5-19).

The above equations generally predict the swell from the slit die is larger than the capillary swell and increases more rapidly with extrusion rate. This is what observed in Figure 5-4 (p. 75) and Figure 5-5 (p. 77). Careful inspection of the derivation of the theory strongly suggests that the inequality is inherent in the geometry and not limited to a particular theory. It is associated with the dimensionality of recovery. Swell from a slit die is one dimensional while that from a capillary is two dimensional.

in Figure 5-6, we plot unannealed B_{slit} and B_{cap} as a function of N_1/σ_{12} determined from actual measurements at low deformation rates and from Eq. (2-25) (p. 13) at high deformation rates. The reason for using unannealed extrudates is based on the experiences of White and Roman (270) who noted that annealing of polyethylenes which have large delayed recovery led to enormous discrepancies.

The theory of Tanner which suggests plots of this type are based on a Maxwell model that has no delayed recovery. Annealing in essence brings out the delayed recovery due to the distribution of relaxation times. The instantaneous recovery seems to correlate with the mean relaxation time computed from normal stress-shear stress ratios. To some extent we are using arbitrary air quenched extrudates for comparison.

Any agreement between the above theories and experiment requires one to take C_{slit} to be 0.2 and C_{cap} to be about 0.1. The agreement with Eqs. (5-17) and (5-19) is reasonably good at low deformation rates but B for both die cross sections increases too rapidly at high deformation rates. This is especially true for the polypropylene.

The failure of Eqs. (5-17) and (5-19) at higher shear rates suggests the use of Eqs. (5-29) and (5-30) in their place. We have done this with the polystyrene melt and plot B_{slit} and B_{cap} vs. σ_w in Figure 5-7. We

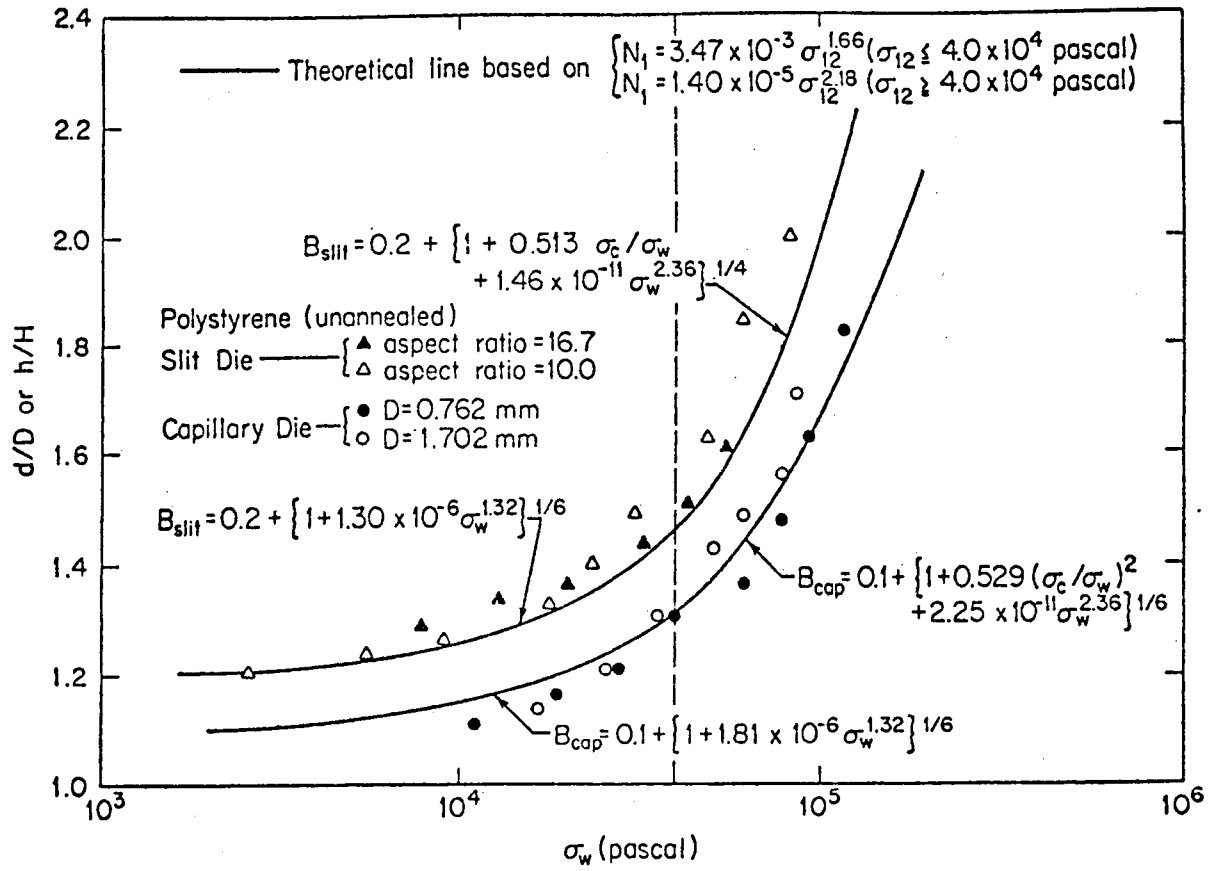

Figure 5-7. Plot of extrudate swell for slit and capillary dies vs. die wall shear stress for polystyrene comparison with Eqs. (5-21) and (5-22).

also include curves calculated from Eqs. (5-21) and (5-22). The agreement between theory and experiment is greatly improved.

D. CONCLUSIONS

1. Generally extrudate swell from a slit is greater than that from a capillary die. This would appear to be because the melt emerging from a slit exhibits recovery in only one direction rather than equally in all direction as occurs for flow out of a capillary die.
2. At low die wall shear rates it goes to a value of about 1.2 as opposed to about 1.1 found for capillary dies.
3. The unconstrained elastic recovery theory for simple shear flow is reasonably good in representing experimental data for swell from slit and capillary dies.
4. Deviation between experimental data and theoretical equation may be due to (i) inadequate representation of N_1 function from low shear rate data while the swell is determined at higher shear rates (ii) over-simplified constitutive model (iii) the approximated averaging across the cross-section and other unknown effect.

In the next chapter, we will generalize this study to short slit and capillary dies which are more realistic in practical applications. In Chapter 7, we will consider the more complex geometries, i.e. rectanglar and trapezoidal dies.

CHAPTER 6

EXTRUDATE SWELL FROM SHORT SLIT AND CAPILLARY DIES

In the preceding chapter, we have studied extrudate swell emerging from slit and capillary dies. Here we are moving further to handle this swell problem of short slit and capillary dies, specifically for the extremely case of L/H equal to zero (i.e. zero length dies).

In the present chapter we carry out an experimental and theoretical study of swell from short capillary and slit dies. The magnitude of swell is studied as a function of extrusion rate (die wall shear rate) and die entrance geometry. A swell theory based upon Lodge (129) and White's analysis (263) for unconstrained elastic recovery from constant elongational flow is developed and compared with experiment.

A. EXPERIMENTAL

1. Materials

The PS and PP melts used in the previous chapters will again be used here. The rheological properties of these polymers are described by Figure 3-1 to 3-3 (pp. 41 - 43).

2. Dies and extrusion apparatus

The various dies used in this study are tabulated in Table 6-1. Dies of varying length and entrance geometry have been investigated. The cross sections are of both slit and capillary type. The extrudate swell measurements were made at 180°C in an Instron capillary rheometer.

3. Experimental procedures

In our earlier study, we found the melt streams especially from slit dies badly necked down due to gravity at low die wall shear rates. Therefore, all the data collected in this paper have wall shear rate higher than 1 sec^{-1}. Extrudates directly cooled in the air were measured with a micrometer to determine the diameter (for the capillary) and center thickness (for the slit). For long slit and capillary we use the data from Chapter 5.

The room temperature data were normalized to 180°C by using a density factor $[\rho(20°C)/\rho(180°C)]^{1/3}$ (1.027 for polystyrene and 1.057 for polypropylene).

B. RESULTS

Extrudate swell is plotted as a function of die length for the PS for capillary and slit dies in Figure 6-1. We contrast swell from long ($L/D, L/H \to \infty$) and short ($L/D, L/H \to 0$) dies with 180°C entrance angle for both PS and PP in Figure 6-2. It may be seen that swell decreases

Table 6-1. Dimensions of dies for experiment in Ch. 6

Slit dies:

H (mm)	Aspect Ratio	L/H		
		1	2	3
0.381	16.7	12.53	20.00	29.87
0.635	10.0	12.00	18.18	24.08

Capillary dies:

Diameter (mm)	L/D			
	1	2	3	4
0.762	8.00	11.95	15.97	---
1.702	5.02	9.98	15.04	20.02

Slit Orifice: L/H = 0 H = 0.394 mm

aspect ratio 8.0

entrance angle 180°

Capillary Orifice: L/D = 0

Entrance angle	180°	120°	90°	60°	30°
Diameter (mm)	1.575	1.575	1.575	1.549	1.575

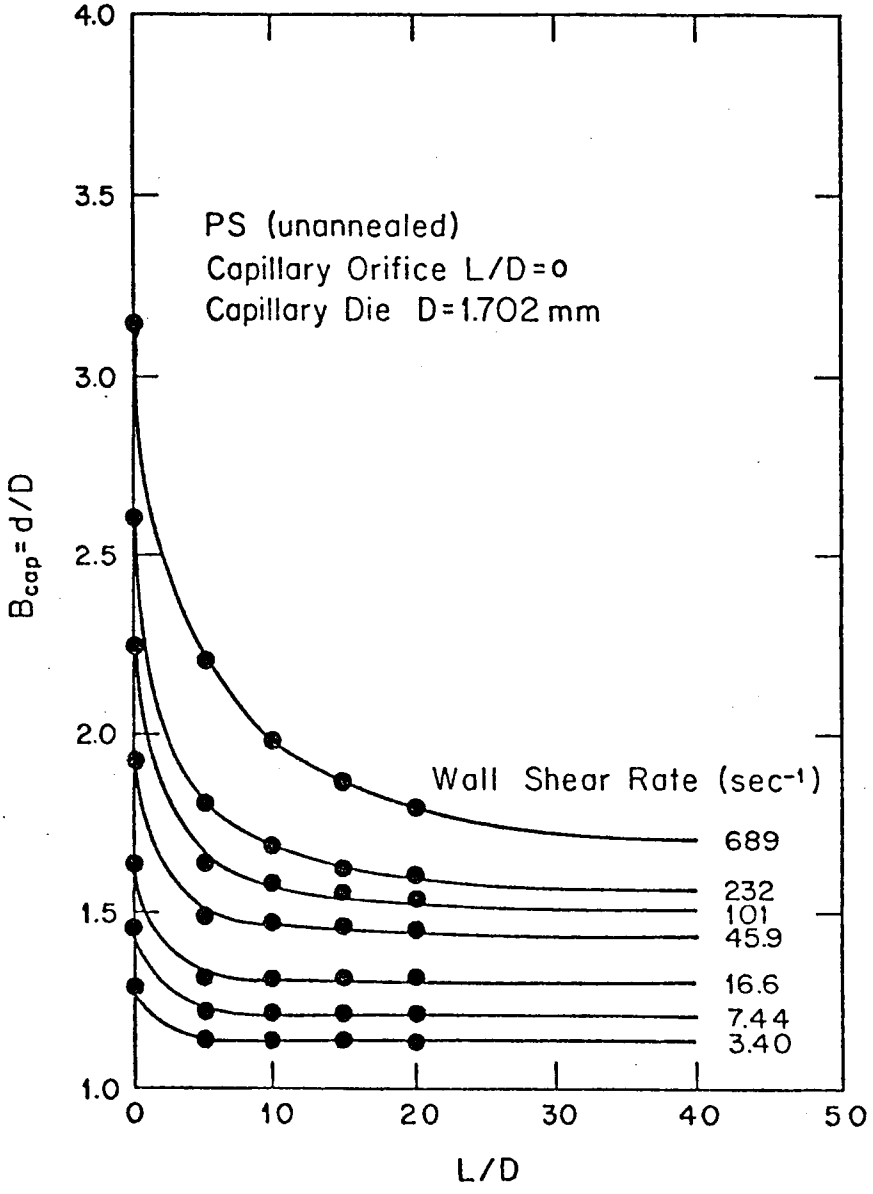

(a) capillary dies

Figure 6-1. Extrudate swell B as a function of die length for PS.

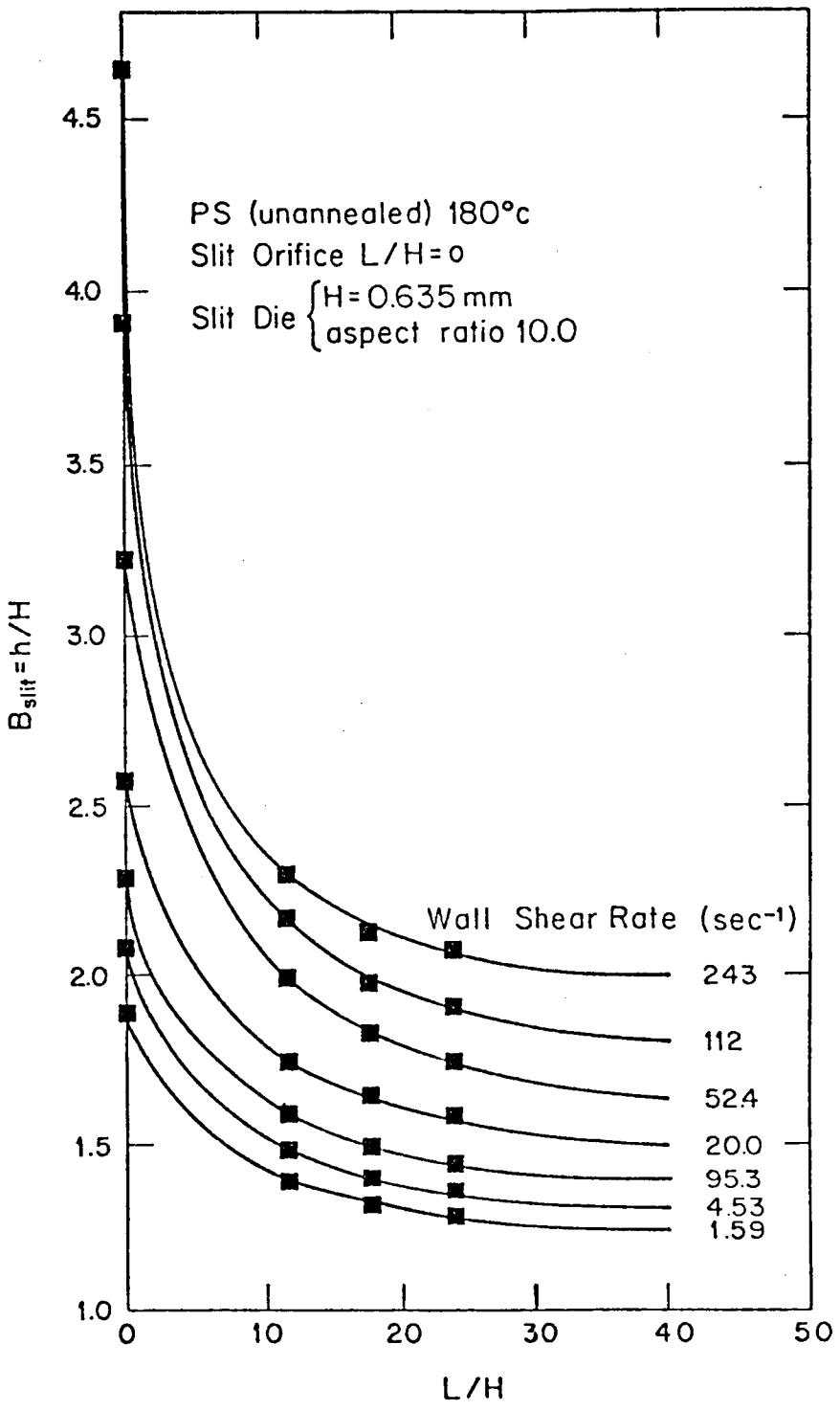

(b) slit dies

Figure 6-1. (Continued)

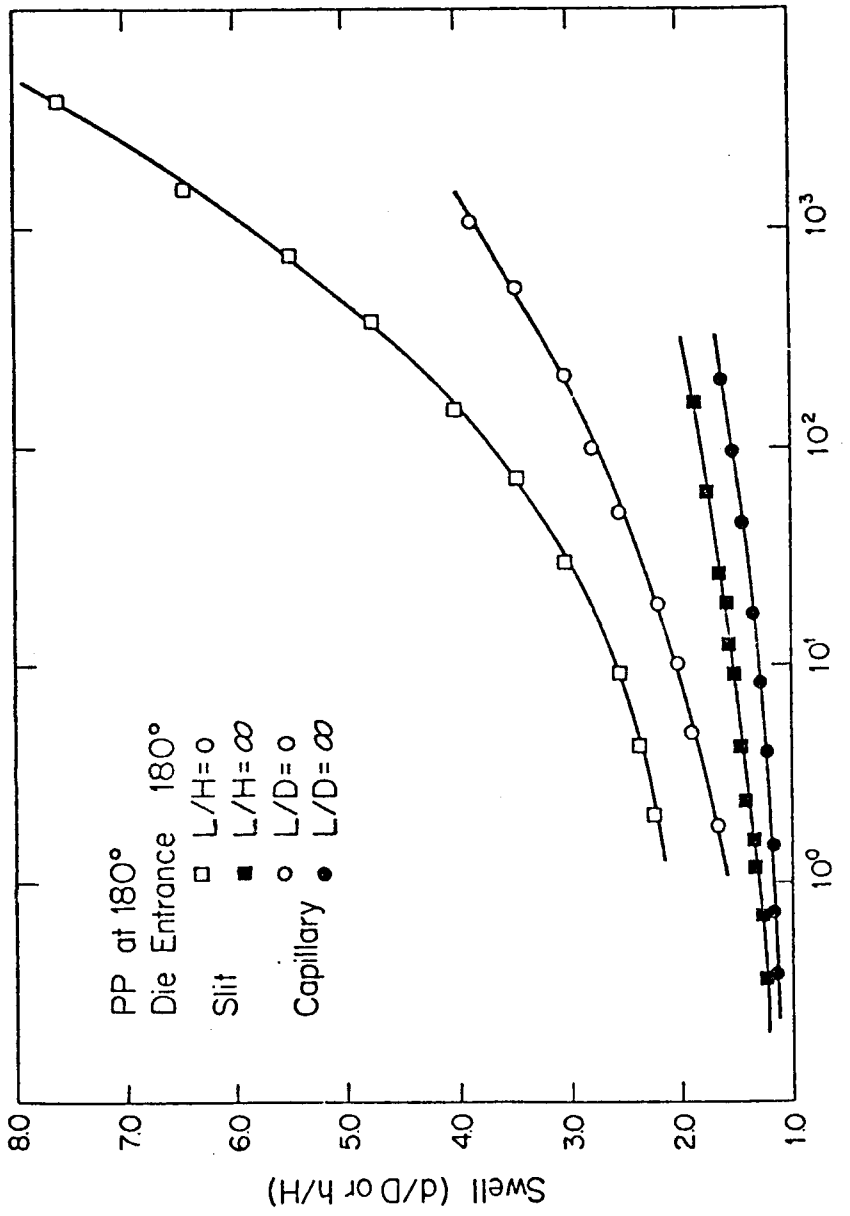

Figure 6-2. Comparison of extrudate swell B from short (L/D, L/H→0) and long (L/D, L/H→∞) slit and capillary dies.

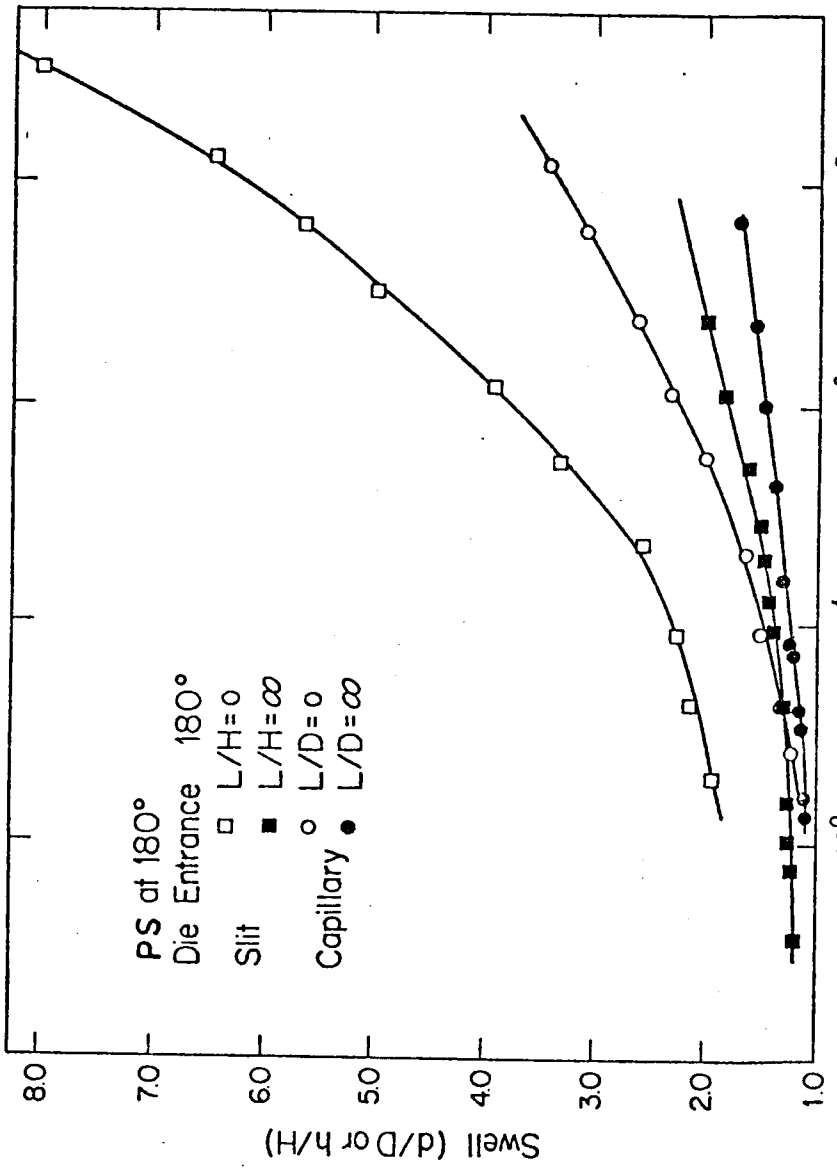

(b) PS

Figure 6-2. (Continued)

with increasing die length for both cross sections. Swell is in all cases higher for the slit die. The level of swell at constant $\dot{\gamma}_w$ is greater for the PP relative to the PS for the short capillary dies.

The influence of die entry geometry on swell is shown in Figures 6-3 and 6-4. It is found that decreasing the entrance angle at constant L/D or L/H from 180° decreases extrudate swell. This is clearly seen in Figure 6-3 for PP. In the case of PS, shown in Figure 6-4 the same trend exists, except cross-overs appear for the 120° and 90° entrance angles.

C. DISCUSSION AND ANALYSIS

1. Die entry flow

The extrudate swell from short dies should be determined from the character of the entrance flow. As this is the only flow history these melts know, it is thus of value to discuss the entrance flow behavior of PS and PP. There have been numerous observations of die entry flow in melts, of which we may cite Tordella (241) on low density polyethylene (LDPE), Ballenger and White (12) for PS, PP and LDPE and by White and Kondo (267) for LDPE, PS and HDPE. Vortex like flows in the die corners are observed for the LDPE and PS which increase in size with extrusion rate. This is illustrated in Figure 6-5. Bagley and

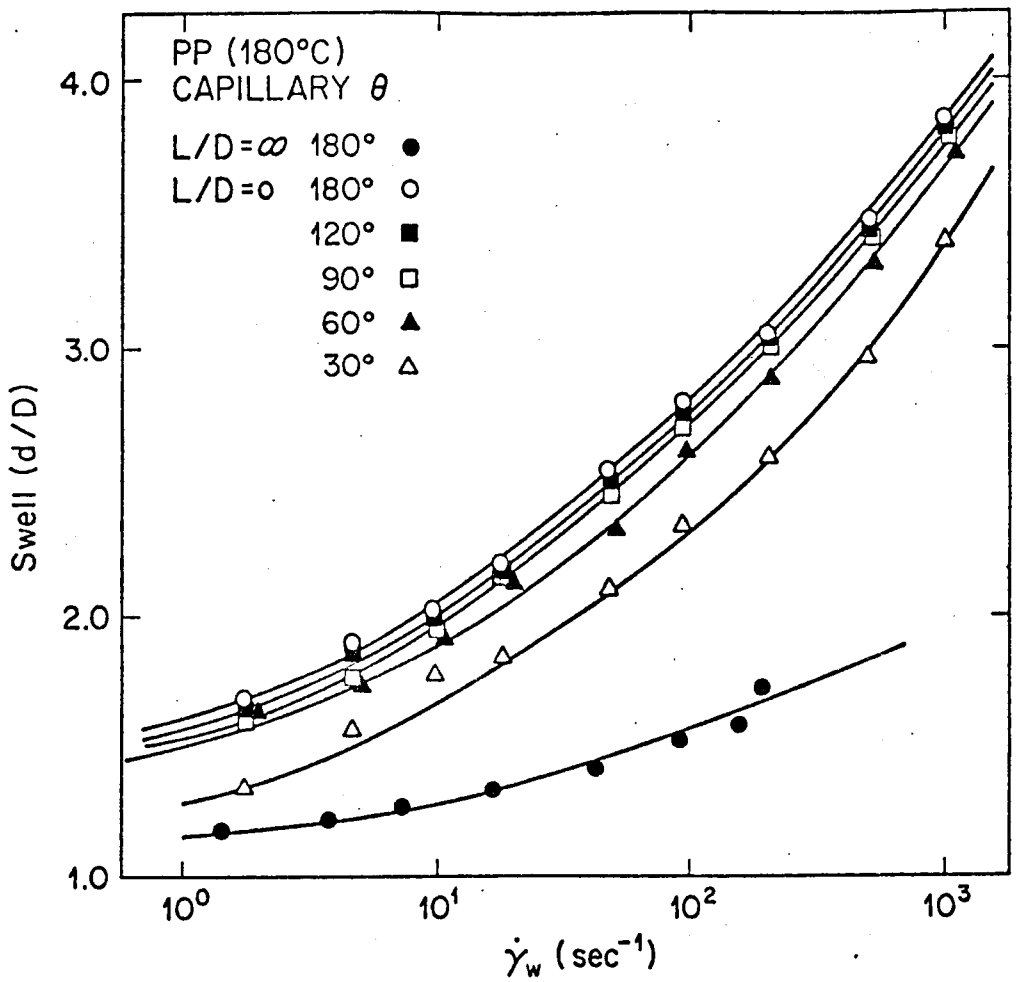

Figure 6-3. Influence of die entry geometry on extrudate swell of PP.

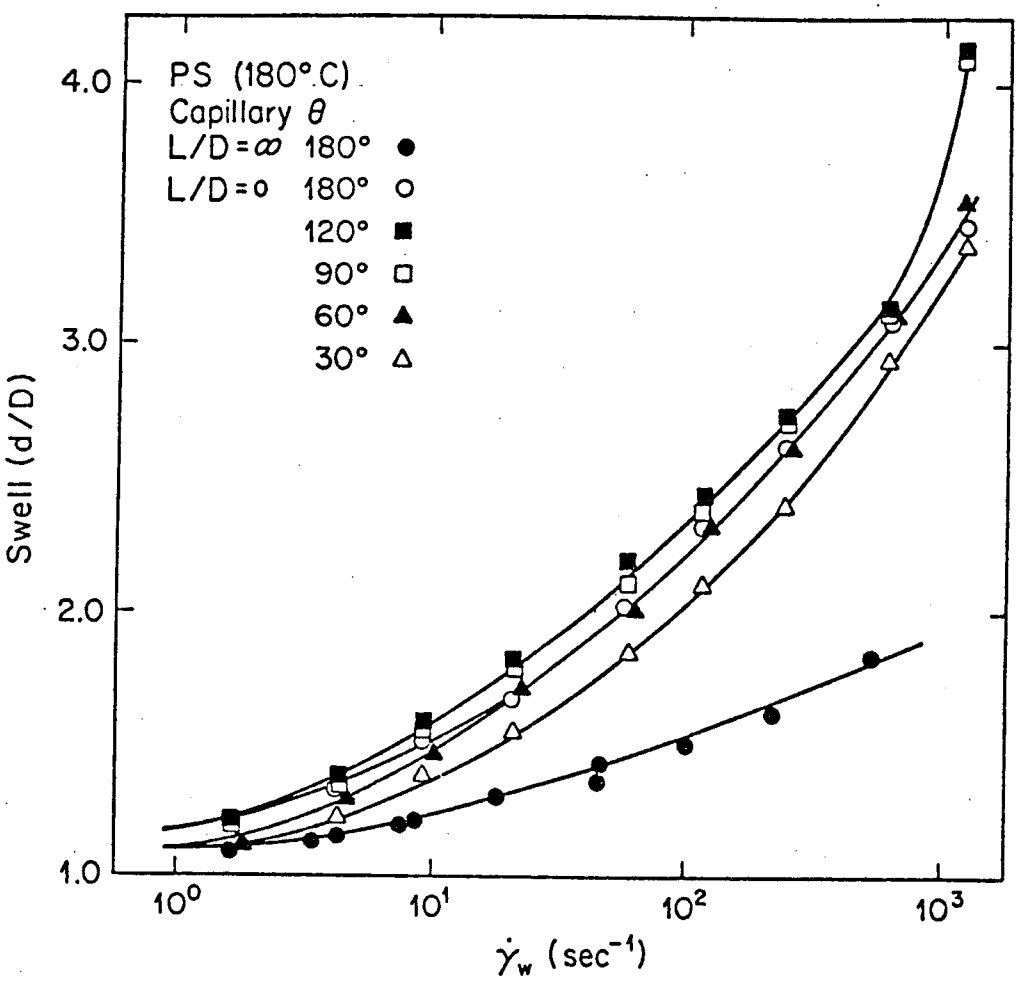

Figure 6-4. Influence of die entry geometry on extrudate swell of PS.

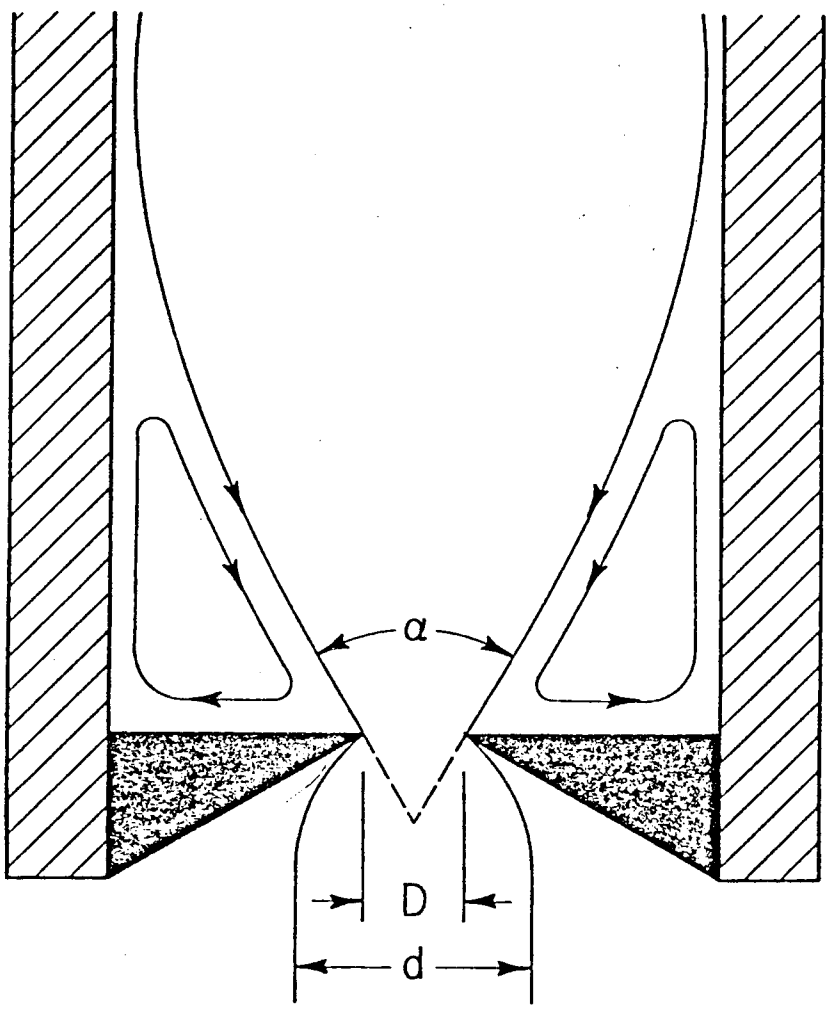

Figure 6-5. Elongational flow character of die entrance region.

Schreiber (9) and White and Kondo (267) have noted a reduction in vortex size with tapering of the die entry.

Of the polymer melts considered in the present study, the PS should have significant vortices. Indeed observations of vortices have been made by White and Kondo (267) on this particular PS. The PP probably exhibits none. There are thus large differences in their die entry flows and histories as the melts emerge from short dies. The PS experiences a more "purer" elongational flow than the PP.

The reasons for these different entrance flow characteristics may be traced to the elongational flow characteristics of the two melts. To surmise the relative response of these two melts we may look to the studies of Ide and White (105) on similar melts. PS exhibits an elongational viscosity function which is constant and $3\eta_0$ at low deformation rates and is an increasing function of elongation rate, while PP appears to be a decreasing function. The large and rising elongational viscosity gives rise to an incompatible stress field in the converging entrance flow. The vortices arise as a stress relief mechanism. This view is expressed by White and Kondo (267).

2. Dimensional analysis

The simplest approach to the problem of extrudate swell rests on dimensional analysis arguments. Clearly swell from short dies should depend on geometry and the

appropriate dimensionless groups representing rheological response. This would be the Weissenberg number, $\tau_{ch}(V_{ch}/L_{ch})$ (267, 272, 164, 26) where τ_{ch} is a characteristic time, V_{ch} a characteristic velocity and L_{ch} a characteristic length.

$$\lim_{L\to 0} B = B\left(\tau_{ch}\frac{V_{ch}}{L_{ch}}\ ,\ \begin{array}{l}\text{dimensionless ratios}\\ \text{of viscoelastic consti-}\\ \text{tutive parameters}\end{array}\ ,\ \theta\right) \qquad (6\text{-}1)$$

where θ is the die entrance angle.

Theories of extrudate swell from long dies are usually expressed in terms of Weissenberg numbers of form (270, 228):

$$\tau_{ch}\frac{V_{ch}}{L_{ch}} = \bar{\tau}\dot{\gamma}_w = \frac{(N_1)_w}{2(\sigma_{12})_w\dot{\gamma}_w}\dot{\gamma}_w = \frac{(N_1)_w}{2(\sigma_{12})_w} \qquad (6\text{-}2)$$

where $\dot{\gamma}_w$ is wall shear rate.

For extrudate swell from short slit and capillary dies the ratio V_{ch}/L_{ch} should be given be the elongation rate $\partial V_1/\partial x_1$ defined as

$$\frac{V_{ch}}{L_{ch}} = \dot{\gamma}_{E1} = \frac{\partial V_1}{\partial x_1} = \frac{d[Q/A]}{dx_1} = -\frac{Q}{A^2}\frac{dA}{dx_1} \qquad (6\text{-}3)$$

The value of A for capillary and slit dies are of form

$$\underline{\text{capillary}} \quad A = \pi\,(r\tan\tfrac{\theta}{2})^2 \qquad (6\text{-}4a)$$

$$\underline{\text{slit}} \quad A = 2Wr\tan\tfrac{\theta}{2} \qquad (6\text{-}4b)$$

where $r = -X_1$ is a radius vector pointed backward into the die entry region. From Eqs. (6-3) and (6-4)

$$\underline{\text{capillary}} \quad \dot{\gamma}_{E1C}(r) = \left(\frac{\partial V_1}{\partial x_1}\right)_{cap}(r) = \frac{2Q}{\pi r^3 \tan^2\frac{\theta}{2}} \tag{6-5a}$$

$$\underline{\text{slit}} \quad \dot{\gamma}_{E1S}(r) = \left(\frac{\partial V_1}{\partial x_1}\right)_{slit}(r) = \frac{Q}{2Wr^2\tan\frac{\theta}{2}} \tag{6-5b}$$

It is to be noted that these expressions for $\dot{\gamma}_{E1}$ vary with position in the die entry.

To evaluate τ_{ch} we again use shear flow data, i.e.

$$\tau_{ch} = \bar{\tau} = \frac{N_1}{2\sigma_{12}\dot{\gamma}_{12}} \tag{6-6}$$

This is plotted in Figure 6-6 to interpret elongational and die entry flow we consider $\bar{\tau}$ to depend on the second invariant of the rate of deformation tensor II_d ($tr\underset{\sim}{d}^2$). Thus for elongational flow in a capillary entrance

$$\dot{\gamma}_{E2C} = \dot{\gamma}_{E3c} = -\frac{1}{2}\dot{\gamma}_{E1c}, \quad II_d = \frac{3}{2}\dot{\gamma}_{E1c}^2 \tag{6-7a}$$

and for the entry to a slit

$$\dot{\gamma}_{E2s} = -\dot{\gamma}_{E1s}, \quad \dot{\gamma}_{E3} = 0, \quad II_d = 2\dot{\gamma}_{E1s}^2 \tag{6-7b}$$

while for shear flow

$$II_d = \frac{1}{2}\dot{\gamma}^2 \tag{6-7c}$$

Equating Eqs. (6-7a, b, c) gives the correspondence of $\bar{\tau}$ values from shear flow to the entrance flows, i.e.

$$\bar{\tau}(\dot{\gamma}) = (\sqrt{3}\,\dot{\gamma}_{E1c}) = \bar{\tau}(2\dot{\gamma}_{E1s}) \tag{6-8}$$

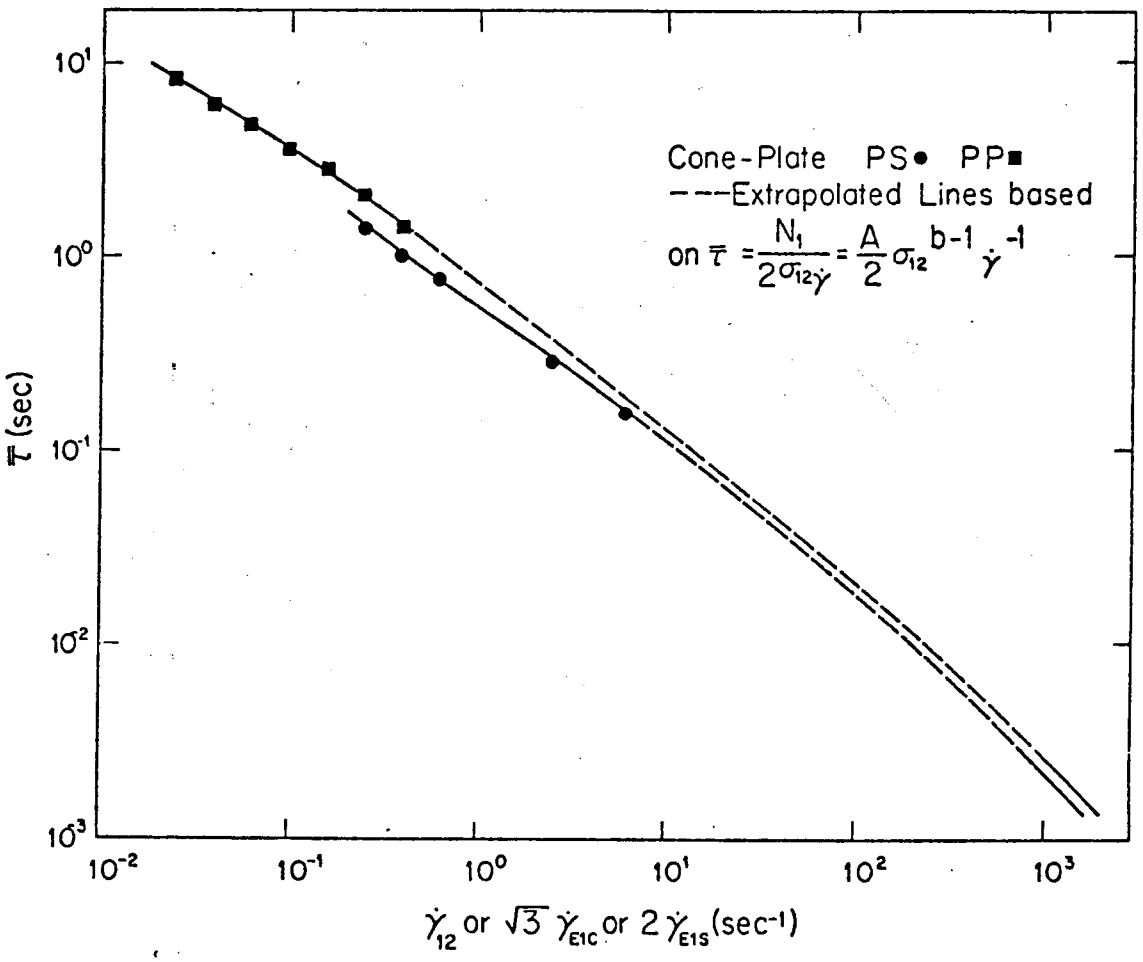

Figure 6-6. $\bar{\tau} = N_1/2\sigma_{12}\dot{\gamma}$ as a function of $\dot{\gamma}$ for PS and PP.

To obtain $\bar{\tau}(\dot{\gamma}_E)$ it was necessary to extrapolate $\tau(\dot{\gamma})$ data as discussed in Chapter 5. Since the characteristic time constant is a decreasing function of elongation rate, the Weissenberg number should increase more linearly than the elongation rate along the streamline.

We have developed dimensional analysis correlations for the swell from tapered entry capillary dies. Based on the above dicussions and taking an averaging process for this accelerating elongational flow, we define the characteristic dimensionless group as half of Weissenberg number at exit.

$$\tau_{ch} \frac{V_{ch}}{L_{ch}} = \frac{1}{2} \bar{\tau}(\dot{\gamma}_{El}) \left[\dot{\gamma}_{El}(\text{exit})\right] \tag{6-9a}$$

i.e. we take for the capillary r = $[(D/2)/\tan(\theta/2)]$

$$\dot{\gamma}_{Elc}(\text{exit}) = \frac{16Q}{\pi D^3} \tan\frac{\theta}{2} \tag{6-9b}$$

for slit r = $[(H/2)/\tan(\theta/2)]$

$$\dot{\gamma}_{Els}(\text{exit}) = \frac{2Q}{WH^2} \tan\frac{\theta}{2} \tag{6-9c}$$

where H is the slit thickness.

In Figure 6-7 we plot B as a function of $\tau_{ch}\ V_{ch}/L_{ch}$ for the 30° and 120° angle capillaries. We find that for the 30° angle the PP and PS data correlate well. This is not the case for the 120° angle or for the 180° angle. These discrepancies probably arise from the existence of vortices in the case of PS. The question of how to remedy these problems in terms of dimensionless groups may be

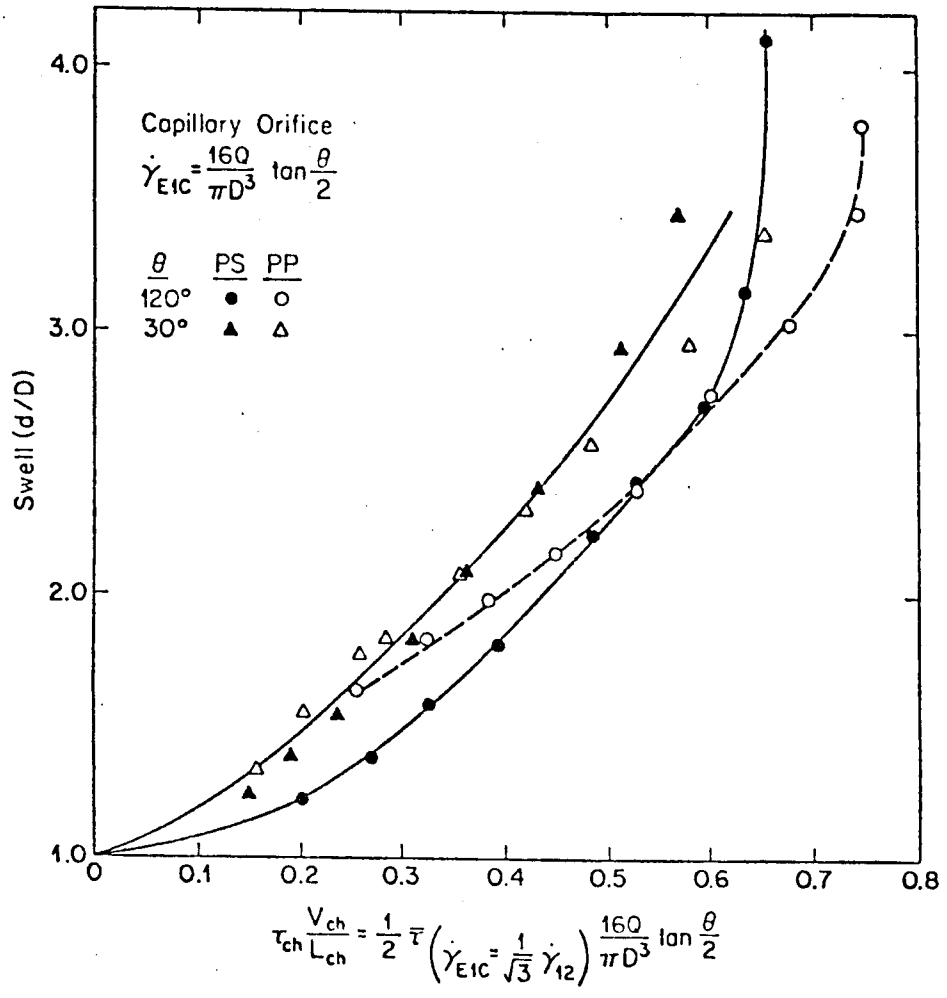

Figure 6-7. Plot B vs. Weissenberg number $\tau_{ch}\ V_{ch}/L_{ch}$ for 30° and 120° angle dies.

answered from the work of White and Konda (267). They use the deformation rate dependence of the relaxation time as the additional parameter in correlating vortex size. The different dependence of $\bar{\tau}(\dot{\gamma})$ for PS and PP is shown in Figure 6-6. As pointed out by Ide and White (104) small changes in $\bar{\tau}(\dot{\gamma})$ can induce large variations in elongational flow behavior. White and Konda (267) found similar response in die entrance flow. The development of high elongational viscosity and large vortices is associated with a weaker $\bar{\tau}(\dot{\gamma})$ dependence as found in PS.

D. THEORY OF EXTRUDATE SWELL FROM SHORT DIES

Our arguments here use the unconstrained recovery theory of swell originally due to Tanner (228) which is an outgrowth of the earlier considerations of three dimensional elastic recovery by Lodge (129). Basically we consider the flow in the die entry region to be elongational in character and shear flow contribution is small as shown in Figure 3-5 (p. 51). The particular formulation we use is similar to that of White's analysis (263) of unconstrained recovery from constant elongational flow of a viscoelastic fluid.

We use a single integral constitutive equation of form (263, 26, 270)

$$\underset{\sim}{\sigma} = - p \underset{\sim}{I} + \int_0^\infty m_1(\tau) \underset{\sim}{c}^{-1} \, dz \qquad (6\text{-}10)$$

where

$$c_{ij}^{-1} = \frac{\partial x_i}{\partial x_a} \frac{\partial x_j}{\partial x_a}$$

and

$$m_1(z) = \frac{G}{\tilde{\tau}_{eff}} e^{-z/\tilde{\tau}_{eff}} \qquad (6\text{-}11)$$

represents a Maxwellian relaxation function. x_i is the instantaneous position and x_a the past configuration in Cartesian coordinates.

We consider the die entrance flow to be of long duration and elongational in character. We write

$$\frac{dx_1}{dt} = \dot{\gamma}_{E1} x_1 , \qquad \frac{dx_2}{dt} = \dot{\gamma}_{E2} x_2 \qquad (6\text{-}12)$$

which leads to

$$x_1(t) = x_1(o) e^{\int \dot{\gamma}_{E1} ds} , \quad x_2(z) = x_2(o) e^{\int \dot{\gamma}_{E2} ds} \qquad (6\text{-}13)$$

Let us write Eq. (6-1) (p. 107) in the form so that it represents the melt after it has exited from the die and exhibited swell. We introduce matrix $\underset{\sim}{Q}$ which transforms back to the system of coordinates before the swell to simplify kinematic considerations. This leads to

$$\underset{\sim}{Q} (\underset{\sim}{\Sigma} + p\underset{\sim}{I}) \underset{\sim}{Q}^T = \int_o^\infty m_1(z) \underset{\sim}{Q} \underset{\sim}{c}^{-1} \underset{\sim}{Q}^T dz \qquad (6\text{-}14)$$

For such an elongational flow, we may write

$$\underset{\sim}{Q}\,\underset{\sim}{c}^{-1}\,\underset{\sim}{Q}^{T} = \begin{vmatrix} \lambda_1^2 & 0 & 0 \\ 0 & \lambda_2^2 & 0 \\ 0 & 0 & 1 \end{vmatrix} \tag{6-15}$$

where

$$\lambda_1 = e^{\int \dot{\gamma}_{E1}\,dz}, \qquad \lambda_2 = e^{\int \dot{\gamma}_{E2}\,dz} \tag{6-16}$$

The swell has the form

$$x_1(t_r) = \frac{1}{\alpha_1}\,x_1(t)\ ,$$

$$x_2(t_r) = \frac{1}{\alpha_2}\,x_2(t)\ ,$$

$$x_3(t_r) = x_3(t) \tag{6-17}$$

There is no shear recovery. This allows us to specify $\underset{\sim}{Q}$ and the left hand side of Eq. (6-14)

$$\underset{\sim}{Q}(\underset{\sim}{\sigma}+p\underset{\sim}{I})\,\underset{\sim}{Q}^{T} = \begin{vmatrix} \frac{1}{\alpha_1^2}(\sigma_{11}+p) & 0 & 0 \\ 0 & \frac{p}{\alpha_2^2} & 0 \\ 0 & 0 & 1 \end{vmatrix} \tag{6-18}$$

From the full Eq. (6-14)

$$\frac{1}{\alpha_1^2}(\sigma_{11}+p) = \int_o^\infty \frac{G}{\tau_{eff}}\,e^{-z/\tau_{eff}}\,\lambda_1^2\,dz = I_1 \tag{6-19a}$$

$$\frac{p}{\alpha_2^2} = \int_o^\infty \frac{G}{\tau_{eff}}\,e^{-z/\tau_{eff}}\,\lambda_2^2\,dz = I_2 \tag{6-19b}$$

Substitution of Eq. (6-19a) into Eq. (6-19b) gives

$$\frac{1}{\alpha_1^2}\sigma_{11} + \frac{\alpha_2^2}{\alpha_1^2} I_2 = I_1 \tag{6-20}$$

Integration across the cross section and taking the integral of σ_{11} to be zero gives

$$\left(\overline{\frac{\alpha_2^2}{\alpha_1^2}}\right) = \int_o^A \frac{\alpha_2^2}{\alpha_1^2}\,da = \frac{\int_o^A I_1\,da}{\int_o^A I_2\,da} \tag{6-21}$$

$$= \frac{\int_o^A \int_o^\infty e^{-\left[z/\tau_{eff} + 2\int \dot{\gamma}_{E1} dz\right]}\,dz\,da}{\int_o^A \int_o^\infty e^{-\left[z/\tau_{eff} + 2\int \dot{\gamma}_{E2} dz\right]}\,dz\,da} \tag{6-22}$$

Generally the integration across the area may be cancelled out leaving the kernel function.

For a capillary

$$\alpha_1 = \frac{1}{\alpha_2^2} \tag{6-23a}$$

$$\frac{\alpha_2^2}{\alpha_1^2} = B^6 \tag{6-23b}$$

$$\dot{\gamma}_{E2c} = -\frac{1}{2}\dot{\gamma}_{E1c} \tag{6-23c}$$

This leads to

$$B = \left[\frac{\int_o^\infty e^{-\left[z/\tau_{eff} + 2\int_o^z \dot{\gamma}_{E1c} dz'\right]}\,dz}{\int_o^\infty e^{-\left[z/\tau_{eff} - \int_o^z \dot{\gamma}_{E1c} dz'\right]}\,dz}\right]^{1/6} \tag{6-24}$$

For a slit

$$\alpha_1 = \frac{1}{\alpha_2} \tag{6-25a}$$

$$\frac{\alpha_2^2}{\alpha_1^1} = B^4 \tag{6-25b}$$

$$\dot{\gamma}_{E2} = -\dot{\gamma}_{E1} \tag{6-25c}$$

This leads to

$$B = \left[\frac{\int_o^\infty e^{-\left[z/\tau_{eff} + 2\int \dot{\gamma}_{Els} dz\right]} dz}{\int_o^\infty e^{-\left[z/\tau_{eff} - 2\int \dot{\gamma}_{Els} dz\right]} dz} \right]^{1/4} \tag{6-26}$$

We now seek to approximate Eq. (6-17) so that we may integrate the integrals. If we take kinematics to be independent of cross section and independent of time with

$$\int \dot{\gamma}_{E1} \, dz = \Gamma_1 z \tag{6-27}$$

This leads to, for a capillary die

$$B^6 = \frac{1 + \tau_{eff}\Gamma_{1c}}{1 - 2\tau_{eff}\Gamma_{1c}} \tag{6-28}$$

For the slit die

$$B^4 = \frac{1 + 2\tau_{eff}\Gamma_{1s}}{1 - 2\tau_{eff}\Gamma_{1s}} \tag{6-29}$$

z represents a dummy time variable. Here $\dot{\gamma}_{E1c}$ and $\dot{\gamma}_{Els}$ are as defined in the previous section. τ_{eff} may be equated to $\bar{\tau}$ for Maxwellian fluids.

Eqs. (6-28) and (6-29) predict the qualitative trends of our experimental data with melt elasticity through $\bar{\tau}$ and increasing elongation rate raising extrudate swell. Swell from slit dies is predicted to be larger than that from capillary dies.

To properly use the above equations, we should have a true elongational flow distinct from a mixed shear and elongational flow. Such elongational flows are observed in LDPE and PS as mentioned earlier, but not in PP. The PS melt used in this paper was among those investigated by White and Kondo (267) in their study of die entrance flow patterns. It is possible from their correlation to know the value of entrance angle α (as defined in Figure 6-5 (p. 105). $\dot{\gamma}_{Elc}$ is taken as $16Q/\pi D^3 \tan(\alpha/2)$. In Figure 6-8, we compare Eq. (6-28) with experiment using this data. The agreement is very good.

In order to make comparison with the PP data, we should have to include combined shear and elongational flow as exists in the Harrison solution (98) for flow in a cone.

E. CONCLUSIONS

1. The extrudate swell from short dies is much larger than from long dies. Swell decreases with decreasing die entrance angle in tapered dies.

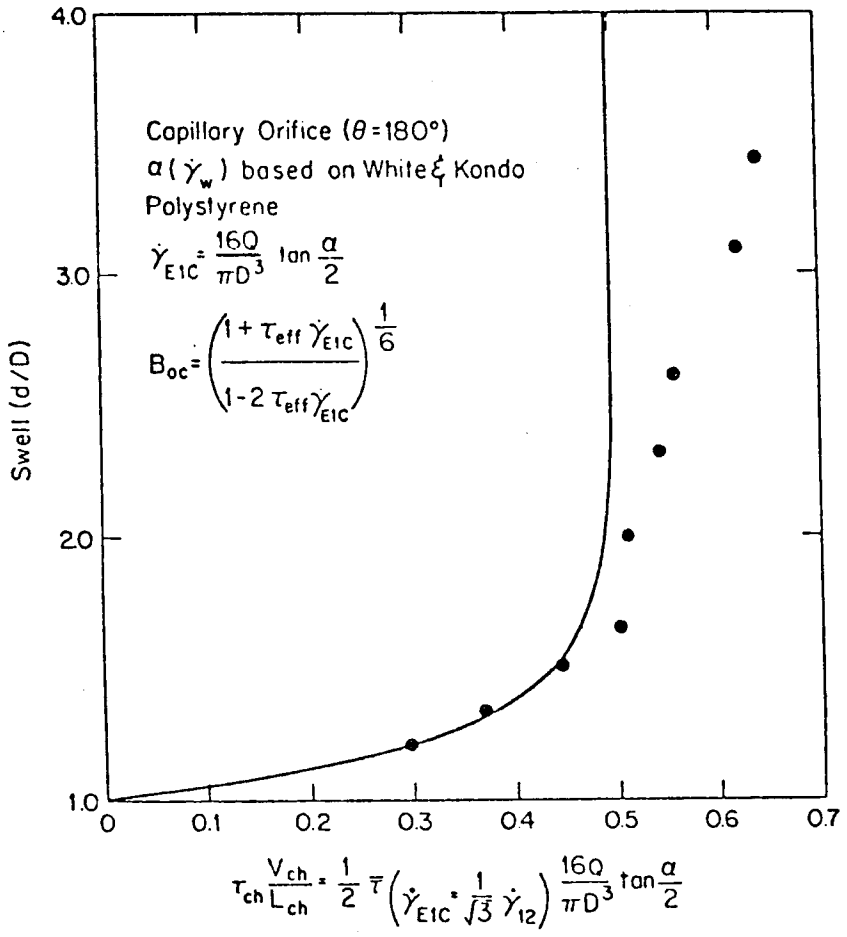

Figure 6-8. Comparison of theory and experiment for swell of PS from a 180° entrance angle die.

2. Again, slit die swell is always larger than capillary die swell.
3. Correlations of extrudate swell data with the Weissenberg number are described.
4. An extrudate swell theory based on recovery from elongational flow appears able to adequately describe the swell from short dies.

In this chapter, we have done critical study of extrudate swell of short slit and capillary dies. In the next chapter we will move to study extrudate swell of complex dies.

CHAPTER 7

EXTRUDATE SWELL FROM DIES OF COMPLEX GEOMETRIES

In Chapter 4, we have studied flow rate-pressure loss for rectangular and trapezoidal dies. In Chapter 5 and 6, we have investigated extrudate swell from long and short slit and capillary dies. In this chapter, we consider the application of the extrudate swell theory to dies of more complicated cross-sectional geomtries.

A. THEORY

In order to consider extrudate swell, we must be more specific and general with regard to constitutive equations considered. We consider here only the case of viscoelastic fluids and we approach the problem of extrudate swell through consideration of unconstrained elastic recovery. Following the earlier studies of this problem by Tanner (228), White and Roman (270) (compare Chapters 5 and 6 of this dissertation), we will use a general single integral constitutive equation of form,

$$\underset{\sim}{\sigma} = - p \underset{\sim}{I} + \int_0^\infty m(\tau) \left[\left(1 + \frac{\epsilon}{2}\right) \underset{\sim}{C}^{-1} + \frac{\epsilon}{2} \underset{\sim}{C} \right] dz \qquad (7\text{-}1)$$

where

$$C_{ij}^{-1} = \frac{\partial x_i}{\partial x_a} \frac{\partial x_j}{\partial x_a}, \qquad C_{ij} = \frac{\partial x_a}{\partial x_i} \frac{\partial x_a}{\partial x_j},$$

and

$$m(z) = \frac{G}{\tau_{eff}} e^{-z/\tau_{eff}}$$

represents a Maxwellian relaxation function. x_i is the instantaneous position and $\bar{x}_a$ the past configuration in Cartesion coordinates.

Consider the unconstrained recovery of such a fluid from a flow within a die with velocity field $V_1(x_2, x_3)$. The Finger and Cauchy deformation tensor for such a flow in terms of a Cartesian coordinate of this type is,

$$\underset{\sim}{C}^{-1} = \begin{vmatrix} 1+\dot{\gamma}_2^2 z^2+\dot{\gamma}_3^2 z^2 & \dot{\gamma}_2 z & \dot{\gamma}_3 z \\ \dot{\gamma}_2 z & 1 & 0 \\ \dot{\gamma}_3 z & 0 & 1 \end{vmatrix} \qquad (7\text{-}2)$$

$$C = \begin{vmatrix} 1 & -\dot{\gamma}_2 z & -\dot{\gamma}_3 z \\ -\dot{\gamma}_2 z & 1+\dot{\gamma}_2^2 z & 0 \\ -\dot{\gamma}_3 z & 0 & 1+\dot{\gamma}_3^2 z \end{vmatrix} \qquad (7\text{-}3)$$

where

$$\dot{\gamma}_2 = \frac{\partial V_1}{\partial x_2}, \qquad \dot{\gamma}_3 = \frac{\partial V_1}{\partial x_3}$$

We write Eq. (7-1) for $\underset{\sim}{\sigma}(t_R)$ to represent the stress and deformation field in the melt emerging from the die a moment before recovery swelling and $\underset{\sim}{\sigma}(t)$ to represent the stress field in the extrudate a moment after recovery. The deviatoric stress $\underset{\approx}{P}(t_R)$ at time t_R is equal to $\underset{\sim}{Q}\ \underset{\approx}{P}(t)\ \underset{\sim}{Q}^T$

where $\underset{\sim}{Q}\,\underset{\sim}{Q}^T$ represents recovery tensor for the extrudates. This suggests

$$\underset{\sim}{Q}\,(\underset{\sim}{\tau}(t) + p\underset{\sim}{I})\,\underset{\sim}{Q}^T = \int_0^\infty m(z)\,\left[(1+\tfrac{\epsilon}{2})\underset{\sim}{C}^{-1} + \tfrac{\epsilon}{2}\underset{\sim}{C}\right] dz$$

$$= G(1+\tfrac{\epsilon}{2}) \begin{vmatrix} 1+2\tau_{eff}^2(\dot\gamma_2^2+\dot\gamma_3^2) & \tau_{eff}\dot\gamma_2 & \tau_{eff}\dot\gamma_3 \\ \tau_{eff}\dot\gamma_2 & 1 & 0 \\ \tau_{eff}\dot\gamma_3 & 0 & 1 \end{vmatrix}$$

$$+ G\,\tfrac{\epsilon}{2} \begin{vmatrix} 1 & -\tau_{eff}\dot\gamma_2 & -\tau_{eff}\dot\gamma_3 \\ -\tau_{eff}\dot\gamma_2 & 1+2\tau_{eff}^2\dot\gamma_2^2 & 0 \\ -\tau_{eff}\dot\gamma_3 & 0 & 1+2\tau_{eff}^2\dot\gamma_3^2 \end{vmatrix} \qquad (7\text{-}4)$$

Eq. (7-4) represents a basis for computing elastic recovery and extrudate swell. It is necessary to first specify the kinematics of the recovery. We take this to be,

$$x_1(t) = \alpha_1 x_1(t_R) - g(x_2,x_3)\ ,$$

$$x_2(t) = \alpha_2 x_2(t_R)\ ,$$

$$x_3(t) = \alpha_3 x_3(t_R) \qquad (7\text{-}5)$$

Following similar procedures in Chapter 5 leads to

$$\underset{\sim}{Q}\,\underset{\sim}{Q}^T = \frac{\partial x_i(t_R)}{\partial x_a(t)}\,\frac{\partial x_j(t_R)}{\partial x_a(t)} \qquad (7\text{-}6a)$$

$$\underset{\sim}{Q} = \begin{vmatrix} \frac{1}{\alpha_1} & \hat{g}_2/\alpha_1 & \hat{g}_3/\alpha_1 \\ 0 & \frac{1}{\alpha_2} & 0 \\ 0 & 0 & \frac{1}{\alpha_3} \end{vmatrix} \tag{7-6b}$$

$$\hat{g}_2 = \frac{\partial g}{\partial x_2}, \qquad \hat{g}_3 = \frac{\partial g}{\partial x_3} \tag{7-6c}$$

This allows us to write the left hand side of Eq. (7-4) as

$$\underset{\sim}{Q}\,(\underset{\sim}{\sigma}+p\underset{\sim}{I})\,\underset{\sim}{Q}^T = \begin{vmatrix} (\sigma_t+p)\frac{1}{\alpha_1^2}+p(\frac{\hat{g}_2^2}{\alpha_1^2}+\frac{\hat{g}_3^2}{\alpha_1^2}) & \frac{p\hat{g}_2}{\alpha_1\alpha_2} & \frac{p\hat{g}_3}{\alpha_1\alpha_3} \\ \frac{p\hat{g}_2}{\alpha_1\alpha_2} & \frac{p}{\alpha_2^2} & 0 \\ \frac{p\hat{g}_3}{\alpha_1\alpha_3} & 0 & \frac{p}{\alpha_3^2} \end{vmatrix} \tag{7-7}$$

Equating Eq. (7-4) and Eq. (7-7) we get

$$\frac{\sigma_t}{\alpha_1^2} + \frac{p}{\alpha_1^2}(1+\hat{g}_2^2+\hat{g}_3^2) = G\,[1 + \epsilon + (2+\epsilon)\tau_{eff}^2(\dot{\gamma}_2^2+\dot{\gamma}_3^2)] \tag{7-8a}$$

$$\frac{p}{\alpha_2^2} = G\,(1 + \epsilon + \epsilon\tau_{eff}^2\dot{\gamma}_2^2) \tag{7-8b}$$

$$\frac{p}{\alpha_3^2} = G\,(1 + \epsilon + \epsilon\tau_{eff}^2\dot{\gamma}_3^2) \tag{7-8c}$$

$$\frac{p\hat{g}_2}{\alpha_1\alpha_2} = G\,\tau_{eff}\dot{\gamma}_2 = \sigma_{12} \tag{7-8d}$$

$$\frac{p\hat{g}_3}{\alpha_1\alpha_3} = G\,\tau_{eff}\dot{\gamma}_3 = \sigma_{13} \tag{7-8e}$$

Solving Eqs. (7-8a - e) and applying the relation

$$\alpha_1 = \frac{1}{\alpha_2 \alpha_3} \tag{7-9}$$

we get

$$\frac{\sigma_t}{G}\alpha_2^2\alpha_3^2 + \alpha_2^4\alpha_3^2\,(1+\epsilon+\epsilon\tau_{eff}^2\dot{\gamma}_2^2) = (1+\epsilon) + (2+\epsilon)\,\tau_{eff}^2(\dot{\gamma}_2^2+\dot{\gamma}_3^2) - \frac{\tau_{eff}^2\dot{\gamma}_2^2}{1+\epsilon+\epsilon\tau_{eff}^2\dot{\gamma}_2^2} - \frac{\tau_{eff}^2\dot{\gamma}_3^2}{1+\epsilon+\epsilon\tau_{eff}^2\dot{\gamma}_3^2} \tag{7-10}$$

and

$$\frac{\alpha_3^2}{\alpha_2^2} = \frac{1+\epsilon+\epsilon\tau_{eff}^2\dot{\gamma}_2^2}{1+\epsilon+\epsilon\tau_{eff}^2\dot{\gamma}_3^2} \tag{7-11}$$

Substituting Eq. (7-11) into Eq. (7-10) leads

$$\alpha_2^6\frac{(1+\epsilon+\epsilon\tau_{eff}^2\dot{\gamma}_2^2)^2}{(1+\epsilon+\epsilon\tau_{eff}^2\dot{\gamma}_3^2)} = -\frac{\sigma_t}{G}\alpha_2^4\frac{(1+\epsilon+\epsilon\tau_{eff}^2\dot{\gamma}_2^2)}{(1+\epsilon+\epsilon\tau_{eff}^2\dot{\gamma}_3^2)} + (1+\epsilon) + (2+\epsilon)\,\tau_{eff}^2(\dot{\gamma}_2^2+\dot{\gamma}_3^2) - \frac{\tau_{eff}^2\dot{\gamma}_2^2}{1+\epsilon+\epsilon\tau_{eff}^2\dot{\gamma}_2^2} - \frac{\tau_{eff}^2\dot{\gamma}_3^2}{1+\epsilon+\epsilon\tau_{eff}^2\dot{\gamma}_3^2} \tag{7-12}$$

$$\alpha_3^6\frac{(1+\epsilon+\epsilon\tau_{eff}^2\dot{\gamma}_3^2)^2}{(1+\epsilon+\epsilon\tau_{eff}^2\dot{\gamma}_2^2)} = -\frac{\sigma_t}{G}\alpha_3^4\frac{(1+\epsilon+\epsilon\tau_{eff}^2\dot{\gamma}_3^2)}{(1+\epsilon+\epsilon\tau_{eff}^2\dot{\gamma}_2^2)} + (1+\epsilon) + (2+\epsilon)\,\tau_{eff}^2(\dot{\gamma}_2^2+\dot{\gamma}_3^2) - \frac{\tau_{eff}^2\dot{\gamma}_2^2}{1+\epsilon+\epsilon\tau_{eff}^2\dot{\gamma}_2^2} - \frac{\tau_{eff}^2\dot{\gamma}_3^2}{1+\epsilon+\epsilon\tau_{eff}^2\dot{\gamma}_3^2} \tag{7-13}$$

Eqs. (7-12) and (7-13) are more general solution of extrudate swelling. ϵ could appear from experiment to be a coefficient with a negative value and may be a complex function. Along a symmetrical center line (x_2, 0), where $\alpha_3 = 1$, $\dot{\gamma}_3 = 0$, also assuming $\epsilon \doteq 0$, we get

$$\alpha_2^4 = -\frac{\sigma_t}{G}\alpha_2^2 + 1 + \tau_{eff}^2\dot{\gamma}_2^2 \qquad (7\text{-}14)$$

This is also the slit swell equation getting from Chapter 5. Similarly, along a symmetrical center line (0, x_3), where $\alpha_2 = 0$ and $\dot{\gamma}_2 = 0$, we can get

$$\alpha_3^4 = -\frac{\sigma_t}{G}\alpha_3^2 + 1 + \tau_{eff}^2\dot{\gamma}_3^2 \qquad (7\text{-}15)$$

Eqs. (7-14) and (7-15) suggests that along a symmetrical center line, we can use the slit swell equation developed in Chapter 5. To evaluate swell other than the symmetrical center lines, we have to use Eqs. (7-12) and (7-13) which are very complex. But we may apply an approximate procedure to predict the swell on the corners of a rectangular die by assuming $\epsilon = 0$, which leads

$$\alpha_2^6 = \alpha_3^6 = -\frac{\sigma_t}{G}\alpha_2^4 + 1 + \tau_{eff}^2\dot{\gamma}_2^2 + \tau_{eff}^2\dot{\gamma}_3^2 \qquad (7\text{-}16)$$

The swell at corners of a rectangular die can be evaluated by

$$B_2 = \left[\int_0^1 \alpha_2^6(x_2, w/2)\, d\frac{x_2}{H/2}\right]^{1/6} \qquad (7\text{-}17)$$

$$B_3 = \left[\int_0^1 \alpha_3^{\,6}(H/2, x_3)\, d\frac{x_3}{w/2} \right]^{1/6} \qquad (7\text{-}18)$$

This leads (assuming $\int \sigma_t\, dx_2 = 0$),

$$B_2 = \left[\int_0^1 \left(1 + \frac{\sigma_{12}^{\,2}}{G^2} + \frac{\sigma_{13}^{\,2}}{G^2}\right) d\frac{x_2}{H/2} \right]^{1/6} \qquad (7\text{-}19)$$

$$B_3 = \left[\int_0^1 \left(1 + \frac{\sigma_{12}^{\,2}}{G^2} + \frac{\sigma_{13}^{\,2}}{G^2}\right) d\frac{x_3}{w/2} \right]^{1/6} \qquad (7\text{-}20)$$

B. EXPERIMENTAL

1. Materials

The PS and PP melts used in previous chapters will again be used here. The rheological properties of these polymers are described by Figure 3-1 to 3-3 (pp. 41 - 43).

2. Dies

Dies with a range of cross sections were used in these experiments. This has been summarized in Table 4-1 (p. 61).

3. Extrudate swell

Polymer melts were extruded vertically downward out of an Instron capillary rheometer into air. The extrudates were cut at a distance of two inches below the die.

The dimensions of the air frozen extrudates were measured by micrometer and then corrected to 180°C by a density factor $[\rho(30°C) / \rho(180°C)]^{1/3}$, i.e. 1.027 for polystyrene and 1.057 for polypropylene. The extrudates

were annealed in silicone oil bath at 170°C for 2 minutes to observe the shape and dimension changes.

C. RESULTS AND INTERPRETATION

The shapes of extrudates emerging from dies of varying cross section are shown in Figure 7-1. Annealing of extrudates results in changes of shape are shown in Figure 7-2. Generally, annealing increases the dimension but also induces flatting on one side. This is because following annealing in silicone oil, the samples were placed on a flat paper.

The flow rate-pressure loss data were collected simultaneously. This has been reported in Chapter 4.

We measured the dimension of extrudate from rectangular die in x_2 and x_3 directions along the center lines. The extrudate swell is then defined as

$$B_2(x_3=0) = h/H \tag{7-21}$$

$$B_3(x_2=0) = w/W \tag{7-22}$$

We also measured the dimension of extrudate swell from trapezoidal die in the x_2 direction along the center line. The extrudate swell is defined as in Eq. (7-22).

We try to plot the above defined extrudate swell with that from slit and capillary dies as a function of their wall shear stresses. For trapezoidal die, the wall shear stress σ_{12} (H/2, 0) is chosen approximately to be,

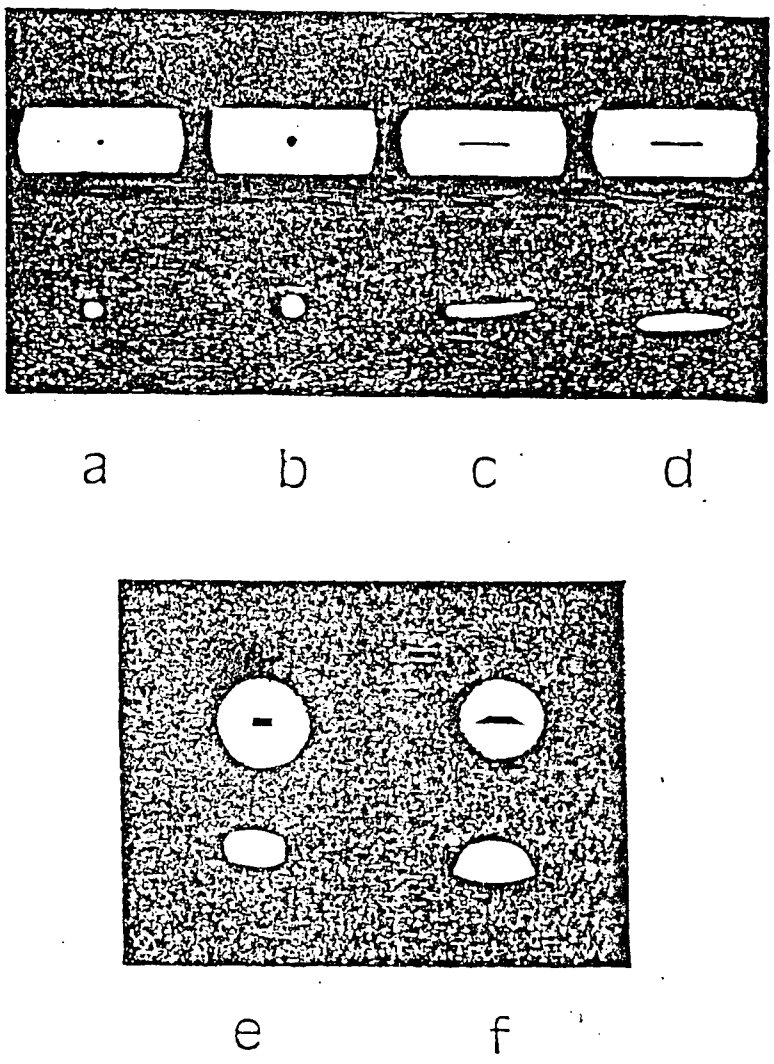

Figure 7-1. Die and extrudate cross sections for capillary: (a) D = 0.762 mm, (b) D = 1.702 mm; for slit: (c) aspect ratio 16.7, (d) aspect ratio 10.0; (e) rectangle, (f) trapezoid.

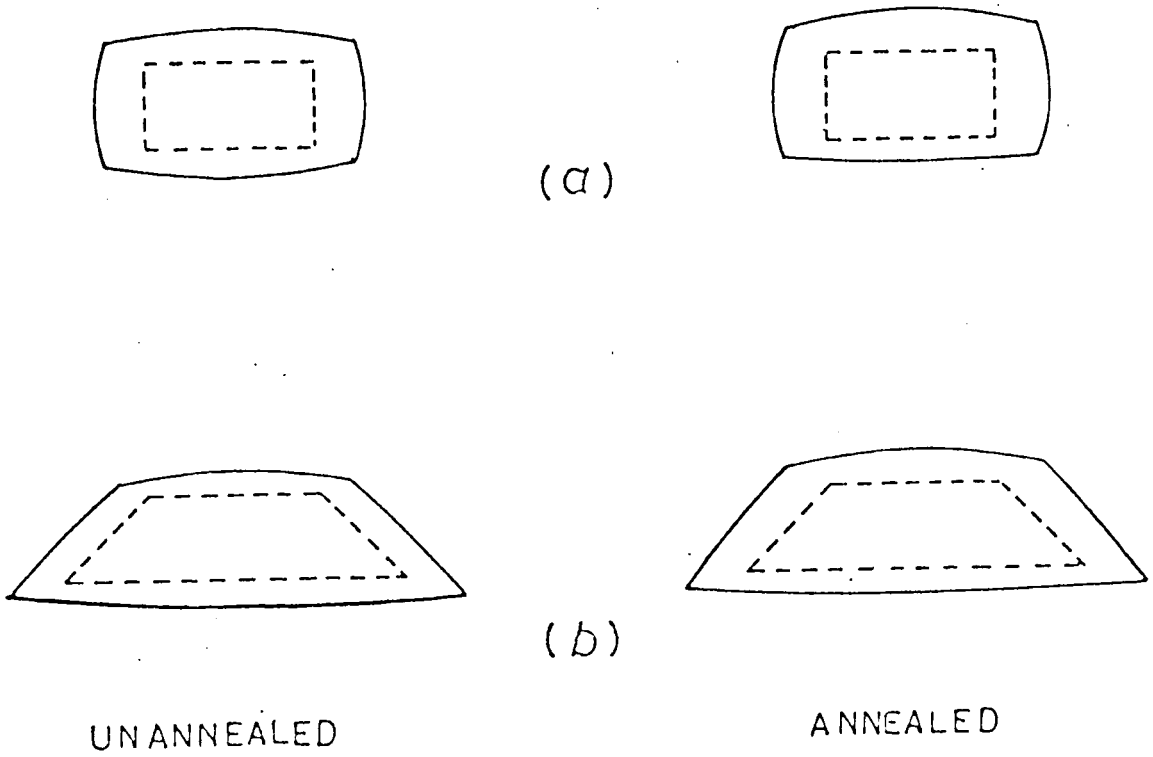

Figure 7-2. Comparison between unannealed and annealed extrudate dimension for (a) rectangular (b) trapezoidal dies.

$$\sigma_{12}\,(H/2,\ 0) = \frac{\Delta P_{die} H}{2L} \tag{7-23}$$

For the rectangular die, we introduce the following procedures to get a reasonable estimation of wall shear stresses $\sigma_{13}\,(0,\ w/2)$ and $\sigma_{12}\,(H/2,\ 0)$ and the ratio of these two stresses.

The equation of motion Eq. (4-3) (p. 54) can be rewrite as the form,

$$\frac{\Delta P_{die}}{L} = \frac{\partial \sigma_{12}}{\partial x_2} + \frac{\partial \sigma_{13}}{\partial x_3} \tag{7-24}$$

σ_{12} and σ_{13} are position dependent with

$$\sigma_{12}\,(x_2,\ 0) = \frac{x_2}{H/2}\,\sigma_{12}\,(H/2,\ 0) \tag{7-25}$$

$$\sigma_{13}\,(0,\ x_3) = \frac{x_3}{w/2}\,\sigma_{13}\,(0,\ w/2) \tag{7-26}$$

At (0, 0)

$$\frac{\Delta P_{die}}{2L} = \frac{\sigma_{12}(H/2,0)}{H} + \frac{\sigma_{13}(0,w/2)}{w} \tag{7-27}$$

let,

$$C_1 = \sigma_{13}\,(0,\ w/2)\ /\ \sigma_{12}\,(H/2,\ 0) \tag{7-28}$$

then

$$\frac{\Delta P_{die} H}{2L} = \left(1 + \frac{C_1}{\phi}\right)\sigma_{12}\,(H/2,\ 0) \tag{7-29}$$

where $\phi = w/H$. This leads

$$\sigma_{12}\,(H/2,\ 0) = \left(\frac{1}{1 + \frac{C_1}{\phi}}\right)\left(\frac{\Delta P_{die} H}{2L}\right) \tag{7-30}$$

$$\sigma_{13}(0, w/2) = \frac{C_1}{1 + \frac{C_1}{\phi}} \frac{\Delta P_{die} H}{2L} \qquad (7\text{-}31)$$

C_1 may mainly depend on the rheological properties of the polymer melts and the aspect ratio of the conduit. Based on power law model C_1 can be evaluated from,

$$C_1 = \frac{\sigma_{13}(0,w/2)}{\sigma_{12}(H/2,0)} = \left[\frac{\dot{\gamma}_{13}(0,w/2)}{\dot{\gamma}_{12}(H/2,0)}\right]^n \qquad (7\text{-}32)$$

Based on Eq. (7-32) and Boussinesq's solution (3) of the velocity profile from a Newtonian rectilinear flow, C_1 found to be a constant value 0.542 for a rectangular conduit of $\phi = 2$. Similarly, based on Arai and Toyota's numerical solution (2) of a power law fluid with n = 0.4 in a rectangular conduit of $\phi = 2$, C_1 calculated to be 0.842.

The polypropylene used in this study close to be a power law fluid with n = 0.412. Therefore, we chose $C_1 = 0.842$ for polypropylene. Polystyrene used in this study close to be a power law fluid at high shear rate with n = 0.357 and a Newtonian fluid at low shear rate. We chose C_1 to be 0.842 at high shear rate and 0.542 at low shear rate.

We plot extrudate swell vs. wall shear stress behaviors in Figure 7-3 for polystyrene and Figure 7-4 for polypropylene. The solid lines in Figure 7-3 are theoretical lines described in Figure 5-7 (p. 93). Generally the extrudate swell of center lines from rectangular and

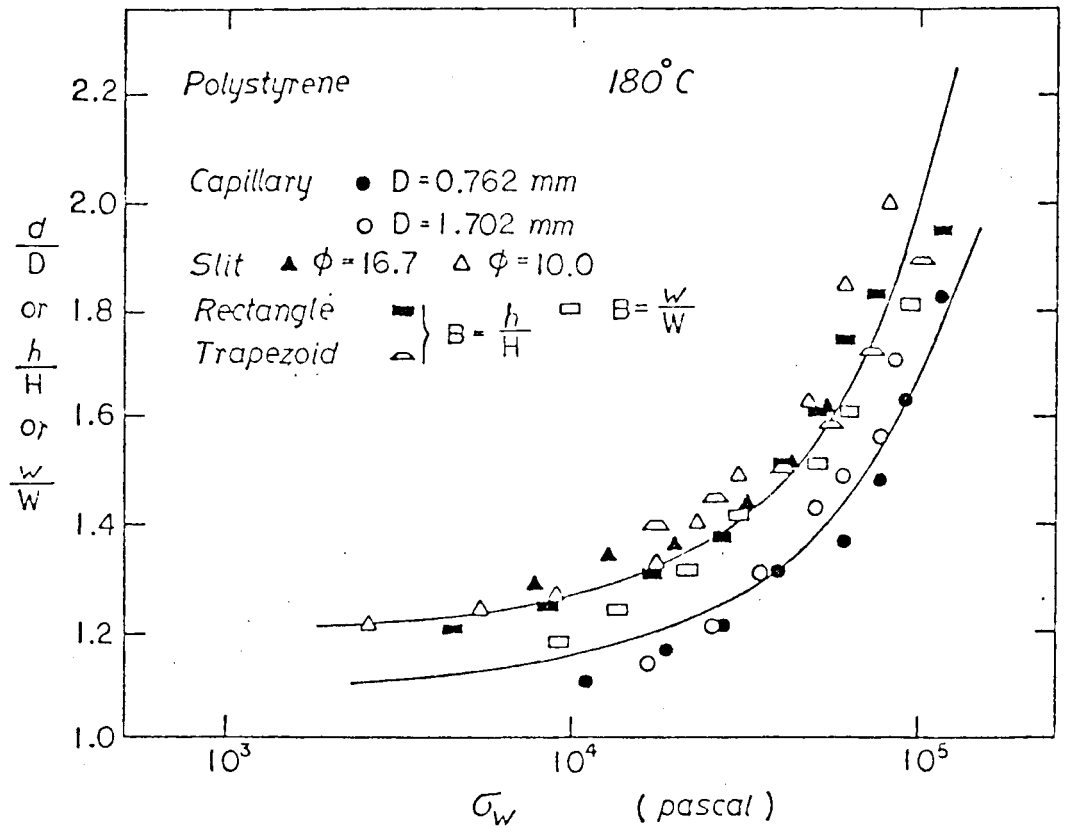

Figure 7-3. Extrudate swell-wall shear stress behaviors for polystyrene of various die geometries.

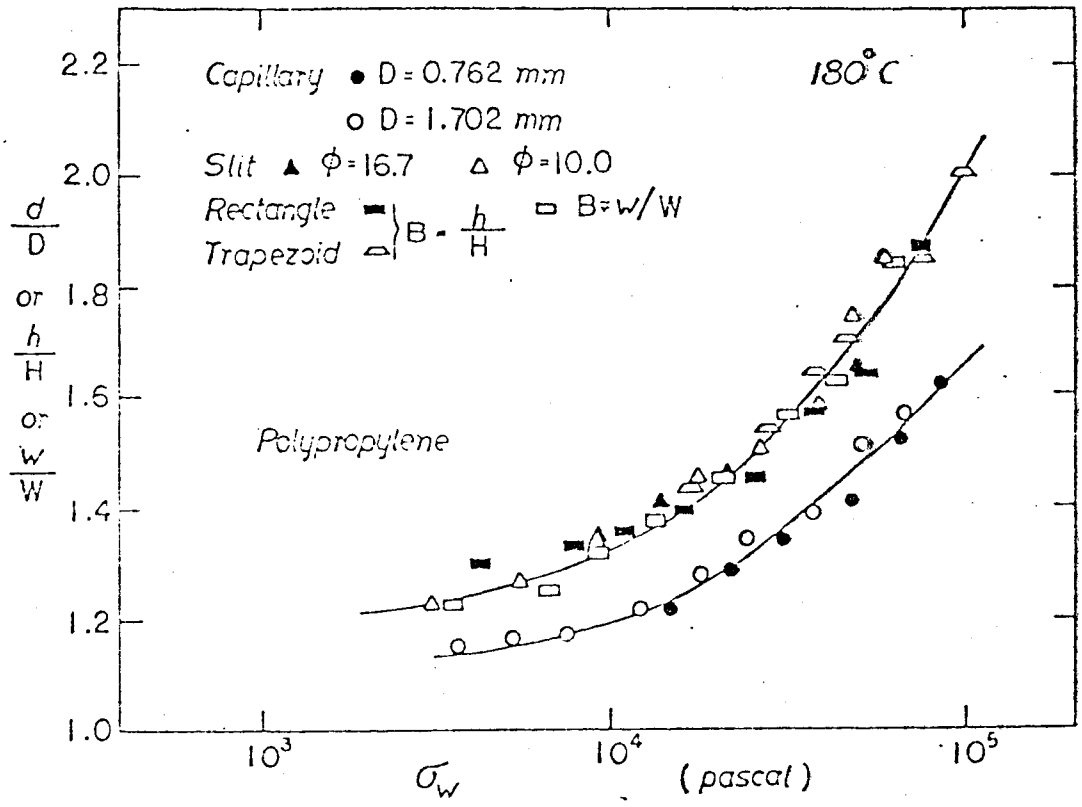

Figure 7-4. Extrudate swell-wall shear stress behaviors for polypropylene of various die geometries.

trapezoidal dies tends to behave like slit dies. This is because along those center lines which divide two equivalent sides, there is only one direction shear stress, i.e. simple shear flow.

For the swell along those symmetrical center lines where exhibit simple shear flow, Eqs. (7-14), (7-15) (p. 125) and those slit swell equations described in Chapter 5 should be able to represent the behavior. For the swell other than those symmetrical center lines, Eqs. (7-12) and (7-13) (p. 124) may be able to represent the behavior through very complicate averaging and integrating procedures across the cross sections.

We will try to work out a swell function at the corner of a rectangular conduit because it is comparatively simpler. Let, approximately,

$$\left| \sigma_{12}^2 + \sigma_{13}^2 \right| (x_2, w/2) = \left[\frac{x_2}{H/2} \sigma_{13} (0, w/2) \right]^2 \qquad (7\text{-}33)$$

$$\left| \sigma_{12}^2 + \sigma_{13}^2 \right| (H/2, x_3) = \left[\frac{x_3}{w/2} \sigma_{12} (H/2, 0) \right]^2 \qquad (7\text{-}34)$$

If G is a constant value, putting Eqs. (7-33) and (7-34) into Eqs. (7-19) and (7-20) (p. 126) to get

$$B_2 = C_2 + \left[1 + \frac{1}{3G^2} \sigma_{13}^2 (0, w/2) \right]^{1/6} \qquad (7\text{-}35)$$

$$B_3 = C_3 + \left[1 + \frac{1}{3G^2} \sigma_{12}^2 (H/2, 0) \right]^{1/6} \qquad (7\text{-}36)$$

To evaluate swell in the corners for the trapezoidal die is more difficult. However, we may do it roughly by

(1) using Eq. (7-36) to calculate B_3 (2) using slit swell equation developed in Chapter 5 for B_2 and assuming

$$\sigma_{12}(H/2, x_3) = \frac{w/2 + b - x_3}{w/2 + b} \sigma_{12}(H/2, 0) \qquad (7\text{-}37)$$

This leads to

$$B_2 = C_2 + \left\{1 + \frac{1}{3G^2}\left[\sigma_{12}(H/2,0)\,\frac{w/2+b-x_3}{w/2+b}\right]^2\right\}^{\frac{1}{4}} \qquad (7\text{-}38)$$

There are two different sets of corners for trapezoidal die, i.e. $(H/2, \pm W/2)$ and $(-H/2, \pm (W/2+b))$. For latter corners, $B_2 = 0$ as predicted by the above equation.

We contrast the measured extrudate shapes of polystyrene with predictions from Eq. (5-15b) (p. 86) for symmetrical center lines and Eqs. (7-35), (7-36) and (7-37) for corners in Figure 7-5 for rectangular dies and Figure 7-6 for trapezoidal dies at $\Delta P_{die} H/2L = 1.1 \times 10^5$ pascal. Generally the predicted shape is consistent with the observed shape but a little smaller. Reasons for this quantitative deviation should be the same as those described in the conclusions of Chapter 5.

D. CONCLUSIONS

1. Along the symmetrical center lines the extrudate swell from rectangular and trapezoidal dies show similar behavior as that from slit die. This may be generally valid for a range of die geometries.

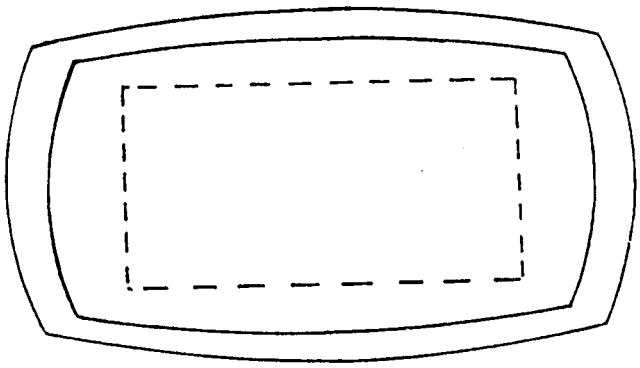

Figure 7-5. Comparison of predicted (inner solid line) observed (outer solid line) PS extrudate dimension from rectangular die at $\Delta P_{die} H/2L = 1.1 \times 10^5$ pascal.

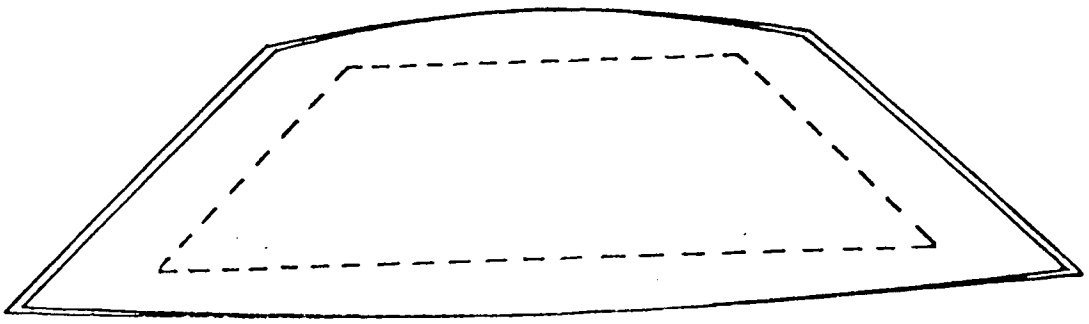

Figure 7-6. Comparison of predicted (inner solid line) observed (outer solid line) PS extrudate dimension from trapezoidal die at $\Delta P_{die} H/2L = 1.1 \times 10^5$ pascal.

2. Extrudate swell due to recovery from complex stress field has been formulated. This involves solving complicate shear stress field in order to get the detail extrudate dimension, and a more general constitutive equation which include both Finger and Cauchy tensor must be applied.

In the next chapter, we will study extrudate swell for filled polymer melt systems.

CHAPTER 8

EXTRUDATE SWELL OF FILLED POLYMER MELTS

In the preceding chapters, we have studied extrudate swell of pure polymer melts emerging from dies of various geometries. In this chapter, we will study extrudate swell for filled polymer melts. From all previous studies (as described in Chapter 2), it is seen that increasing filler loading decreases extrudate swell. The explanation of this phenomenon had been centered on relating swell to filler volume fraction or effective volume fraction. But so far, there is no satisfactory rheological explanation based on constitutive model of these systems.

A. THEORETICAL

1. Constitutive equation of filled polymers

If we assume that the polymer compounds can be represented by a modified Maxwell model following White (301) and Lobe and White (127) as shown in Figure 8-1, where the slider has a yield value Y, it can only move forward and block the recovery. Therefore the only possible recovery is due to string G_1.

Usually, the applied stress is larger than $\bar{Y}$. If we consider the case $\sigma > \bar{Y}$, the strain γ at time t can be represented as

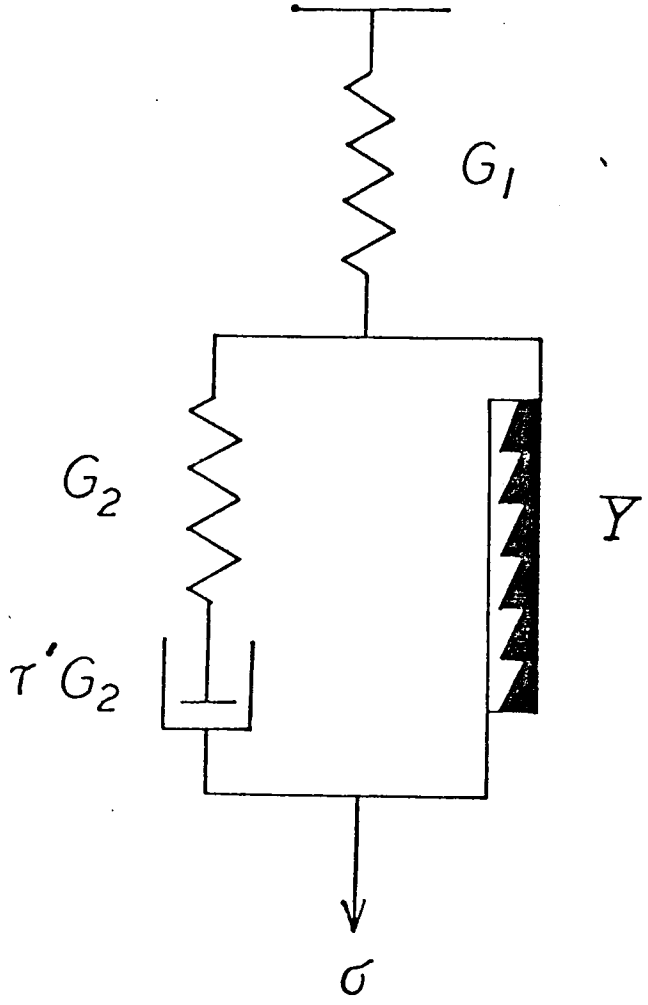

Figure 8-1. Model for filled polymer melts.

$$\gamma = \frac{\sigma}{G_1} + \frac{\sigma - \bar{Y}}{G} + \int_o^t \frac{\sigma - \bar{Y}}{G_2 \tau'} dt' \tag{8-1}$$

Differentiating the above equation with time and rearranging the terms, we can get

$$\frac{\bar{Y}}{G_2 \tau'} + \dot{\gamma} = \left(\frac{G_1 + G_2}{G_1 G_2}\right) \dot{\sigma} + \frac{1}{G_2 \tau'} \sigma \tag{8-2}$$

Solve the above first order ordinary differential equation, we get

$$\sigma = \int_{-\infty}^{t} (\bar{Y} + G_2 \tau' \dot{\gamma}) e^{-\frac{G_1 (t-t')}{(G_1+G_2)\tau'}} \frac{1}{\tau'} \left(\frac{G_1}{G_1+G_2}\right) dt' \tag{8-3}$$

Integrate the above equation by parts and choose present state to be the reference state, we get

$$\sigma = \bar{Y} + \int_o^{\infty} \frac{G}{\tau} \gamma e^{-\frac{z}{\tau}} dz \tag{8-4}$$

$$G = \frac{G_1 G_2}{(G_1+G_2)} \tag{8-5a}$$

$$\tau = \tau'(G_1+G_2)/G_1 \tag{8-5b}$$

$$z = t - t' \tag{8-5c}$$

Now we need to generalize the above equation to a three dimensional constitutive equation. Following the work of White and Lobe (301) and White (127) for the Schwedoff model (as described in Chapter 2) we have the form

$$\underset{\sim}{\sigma} = -p\underset{\sim}{I} + \underset{\sim}{P} \tag{8-6}$$

i) as $tr\underset{\sim}{P}^2 < 2Y^2$

$$\underset{\sim}{\sigma} = -p\underset{\sim}{I} + G_1 \underset{\sim}{\tilde{C}}^{-1}$$

$$\text{where } \underset{\sim}{\tilde{C}}^{-1} = \underset{\sim}{C}^{-1} - \frac{1}{3} tr\, \underset{\sim}{C}^{-1}\underset{\sim}{I} \tag{8-7}$$

ii) as $tr\underset{\sim}{P}^2 > 2Y^2$

$$\underset{\sim}{\sigma} = -\underset{\sim}{I} + \left(1 + \frac{\bar{Y}}{\sqrt{\frac{1}{2}trH^2}}\right)\underset{\sim}{H}$$

$$\text{where } \underset{\sim}{H} = \int_0^\infty \mu_1 \left(\underset{\sim}{C}^{-1} - \frac{1}{3}[tr\underset{\sim}{C}^{-1}]\underset{\sim}{I}\right) dz \tag{8-8}$$

Here $\underset{\sim}{P}$ is the deviatoric stress tensor, the strain tensor may be a combination of the Finger deformation tensor and Cauchy deformation tensor as in many constitutive models. Here, for simplicity, we use Finger tensor $\underset{\sim}{C}^{-1}$ only. $\mu_1(z)$ is the memory function of the filled polymer melt. Based on the model shown in Figure 8-1 and Eq. (8-4) we choose $\mu_1(z)$ to be

$$\mu_1 = \frac{G}{\tau} e^{-z/\tau} \tag{8-9}$$

For a steady simple shear flow

$$\underset{\sim}{C}^{-1} = \begin{vmatrix} 1+\dot{\gamma}^2 z^2 & \dot{\gamma} z & 0 \\ \dot{\gamma} z & 1 & 0 \\ 0 & 0 & 1 \end{vmatrix} \tag{8-10}$$

$$\underset{\sim}{C}^{-1} - \frac{1}{3}[\mathrm{tr}\,\underset{\sim}{C}^{-1}]\underset{\sim}{I} = \begin{vmatrix} \frac{2}{3}\dot{\gamma}^2 z^2 & \dot{\gamma} z & 0 \\ \dot{\gamma} z & -\frac{1}{3}\dot{\gamma}^2 z^2 & 0 \\ 0 & 0 & -\frac{1}{3}\dot{\gamma}^2 z^2 \end{vmatrix} \qquad (8\text{-}11)$$

and,

$$\underset{\sim}{H} = G \begin{vmatrix} \frac{4}{3}\tau^2\dot{\gamma}^2 & \tau\dot{\gamma} & 0 \\ \tau\dot{\gamma} & -\frac{2}{3}\tau^2\dot{\gamma}^2 & 0 \\ 0 & 0 & -\frac{2}{3}\tau^2\dot{\gamma}^2 \end{vmatrix} \qquad (8\text{-}12a)$$

$$\underset{\sim}{P} = \left(1 + \frac{\bar{Y}}{G\tau\dot{\gamma}\sqrt{1+\frac{4}{3}\tau^2\dot{\gamma}^2}}\right)\underset{\sim}{H} \qquad (8\text{-}12b)$$

The shear stress and principal normal stress difference have the forms

$$\sigma_{12} = \left(1 + \frac{\bar{Y}}{G\tau\dot{\gamma}\sqrt{1+\frac{4}{3}\tau^2\dot{\gamma}^2}}\right) G\tau\dot{\gamma} \qquad (8\text{-}13a)$$

$$N_1 = P_{11} - P_{22} = \left(1 + \frac{\bar{Y}}{G\tau\dot{\gamma}\sqrt{1+\frac{4}{3}\tau^2\dot{\gamma}^2}}\right) 2G\tau^2\dot{\gamma}^2 \qquad (8\text{-}13b)$$

Note that at low shear rates

$$\lim_{\dot{\gamma}\to 0} \sigma_{12} = \bar{Y} \qquad (8\text{-}14a)$$

$$\lim_{\dot{\gamma}\to 0} N_1 = 2\bar{Y}\tau\dot{\gamma} = 0 \qquad (8\text{-}14b)$$

The viscosity goes to infinity at small shear rates according to Eq. (8-14a). The N_1 - σ_{12} relationship is

$$\frac{N_1}{2\sigma_{12}^2/G} = \left(\frac{1}{1 + \frac{\bar{Y}}{G\tau\dot{\gamma}\sqrt{1+\frac{4}{3}\tau^2\dot{\gamma}^2}}} \right) \tag{8-15}$$

The right hand side of Eq. (8-15) is 1 for a Maxwell model constitutive equation with $\bar{Y}$ zero. With a yield value $\bar{Y}$, this number is 1 as $\dot{\gamma}\to\infty$ and 0 as $\dot{\gamma}\to 0$. The influence of the yield value would appear to be to decrease N_1 at fixed σ_{12}.

For an uniaxial elongational flow with a constant elongational rate $\dot{\gamma}_{11} = \dot{\varepsilon}$ and $\dot{\gamma}_{22} = \dot{\gamma}_{33} = -1/2\ \dot{\varepsilon}$ where

$$\underset{\sim}{C}^{-1} = \begin{vmatrix} e^{2\dot{\varepsilon}z} & 0 & 0 \\ 0 & e^{-\dot{\varepsilon}z} & 0 \\ 0 & 0 & e^{-\dot{\varepsilon}z} \end{vmatrix} \tag{8-16}$$

Again using the Maxwellian relaxation function of Eq. (8-9) we may show that for a long duration steady flow we have:

$$\underset{\sim}{C}^{-1} - \tfrac{1}{3}[\mathrm{tr}\underset{\sim}{C}^{-1}]\underset{\sim}{I} = \begin{vmatrix} \frac{2}{3}(e^{2\dot{\varepsilon}z} - e^{-\dot{\varepsilon}z}) & 0 & 0 \\ 0 & -\frac{1}{3}(e^{2\dot{\varepsilon}z} - e^{-\dot{\varepsilon}z}) & 0 \\ 0 & 0 & -\frac{1}{3}(e^{2\dot{\varepsilon}z} - e^{-\dot{\varepsilon}z}) \end{vmatrix} \tag{8-17}$$

and

$$\underset{\sim}{H} = G \begin{vmatrix} \frac{2\tau\dot{\varepsilon}}{(1+\tau\dot{\varepsilon})(1-2\tau\dot{\varepsilon})} & 0 & 0 \\ 0 & \frac{-\tau\dot{\varepsilon}}{(1+\tau\dot{\varepsilon})(1-2\tau\dot{\varepsilon})} & 0 \\ 0 & 0 & \frac{-\tau\dot{\varepsilon}}{(1+\tau\dot{\varepsilon})(1-2\tau\dot{\varepsilon})} \end{vmatrix} \tag{8-18}$$

The tensile stress acting on the filament being extended is

$$\sigma_t = \sigma_{11} - \sigma_{22} \qquad (\because \sigma_{22} = 0)$$

$$= \left(1 + \frac{\bar{Y}}{G\sqrt{3\left[\frac{\tau\dot{\varepsilon}}{(1+\tau\dot{\varepsilon})(1-2\tau\dot{\varepsilon})}\right]^2}}\right)\left(\frac{3G\tau\dot{\varepsilon}}{(1+\tau\dot{\varepsilon})(1-2\tau\dot{\varepsilon})}\right) \qquad (8\text{-}19)$$

For low deformation rates:

$$\lim_{\dot{\varepsilon}\to 0} (\sigma_{11} - \sigma_{22}) = \bar{Y}\sqrt{3} \qquad (8\text{-}20)$$

while for high deformation rates:

$$\lim_{\dot{\varepsilon}\to \frac{1}{2\tau}} (\sigma_{11} - \sigma_{22}) \to \infty \qquad (8\text{-}21)$$

The elongational viscosity is

$$x = \frac{\sigma_{11}-\sigma_{22}}{\dot{\varepsilon}} = \frac{\bar{Y}\sqrt{3}}{\dot{\varepsilon}} + \frac{3G\tau}{(1+\tau\dot{\varepsilon})(1-2\tau\dot{\varepsilon})} \qquad (8\text{-}22)$$

The elongational viscosity goes to infinity at both small ($\dot{\varepsilon}\to 0$) and large ($\dot{\varepsilon}\to\frac{1}{2\tau}$). However, as indicated by Ide and White (104), the high deformation rate behavior may be modified by the deformation rate dependence of τ and elongational viscosity does not necessarily go to infinity.

2. Elastic recovery of filled polymers

a. General

We will discuss elastic recovery for filled polymers in this section based on the constitutive model developed by White (301) as described in the previous section.

We think the elastic recovery of a filled polymer such as represented by the model in Figure 8-1 (p. 140) and Eqs. (8-6) and (8-7) is quite different compared to a Maxwell viscoelastic fluid as studied in Chapter 5 to 7. Here, for filled polymers, the elastic recovery can only happen in the gel with modulus G_1. The gel G_2 and viscous portion $G\underset{\sim}{\tau}'$ are associated with yield value $\bar{Y}$ and will not respond to recovery. This can be also explained in the constitutive equation (Eq. (8-7)). As $tr\underset{\sim}{P}^2 < 2Y^2$ which is the case when the stress is made zero or isotropic at any instant following an arbitrary flow history, the deviatoric stresses depend only on G_1. Another important concept we must bear in mind is that we can treat filled polymer melts as incompressible fluids which means that $\alpha_1\alpha_2\alpha_3 = 1$, where α_1, α_2, α_3 denote recovery in 1, 2, 3 - direction respectively. Generally, $\alpha_1 < 1$ and α_2 or $\alpha_3 > 1$. We will use the two major concepts to develop formulations for constrained recovery, unconstrained recovery and extrudate swell in the following sections.

b. Constrained simple shear recovery

We consider a constrained recovery from steady shear flow; i.e. in the shearing of a liquid contained in the gap between two surfaces in relative motion, recovery is measured by releasing one surface to move freely and not allow any change in the gap of the shearing surfaces.

The instantaneous shear recovery of a filled polymer melt should be

$$Sr = \sigma_{12}/G_1$$

$$= (1 + \bar{Y}^*)\, G\tau\dot{\gamma}/\, G_1 \qquad (8\text{-}23)$$

where

$$\bar{Y}^* = \frac{\bar{Y}}{G\tau\dot{\gamma}\sqrt{1 + \frac{4}{3}\tau^2\dot{\gamma}^2}} \qquad (8\text{-}24)$$

Based on Eqs. (8-13a) and (8-13b), Eq. (8-23) can be rearranged to give the instantaneous shear recovery to be

$$Sr = \left(\frac{N_1}{2\sigma_{12}}\right)(1 + \bar{Y}^*)\,\frac{G}{G_1} \qquad (8\text{-}25)$$

The above equation seems to correspond to the major character of elastic recovery of filled polymers: the rapid decrease in elastic recovery with increasing filler loading.

c. Unconstrained recovery

i. General

In the preceeding section, we have studied constrained recovery of filled polymers which is a comparatively simpler case because recovery is only allowed in 1 - direction. In this section we will develop a general formulation for unconstrained recovery of filled polymer systems. Unconstrained recovery, also known as free recovery, involves recovery in the flow direction and also in directions perpendicular to the flow direction.

The history of a filled viscoelastic fluid defined by Eqs. (8-7) and (8-8) prior to the ultimate recovery can be divided into three periods:

1. period of steady flow ($z=\infty$ to tr)
2. period of instantaneous recovery ($z=tr$ to $tr+\delta$)
3. period of delayed recovery ($z=tr+\delta$ to 0)

We would expect delayed recovery to be zero from our mechanical model and it will be neglected. At recovery,

$$\underset{\sim}{\sigma} = \underset{\sim}{o} = -p_1\underset{\sim}{I} + G_1\underset{\sim}{\tilde{C}}^{-1}\Big|_{rec} = -p\underset{\sim}{I} + \left(1+\frac{\bar{Y}}{\sqrt{\frac{1}{2}tr\underset{\sim}{H}^2}}\right)\underset{\sim}{H} \qquad (8\text{-}26a)$$

Here p_1 is an isotropic stress in elastic recovery and p is an isotropic stress in a viscoelastic flow. Therefore, p_1 and p should be in general different. This leads,

$$\underset{\sim}{\tilde{C}}^{-1}\Big|_{rec} = \frac{1}{G_1}\left(1+\frac{\bar{Y}}{\sqrt{\frac{1}{2}tr\underset{\sim}{H}^2}}\right)\underset{\sim}{H} + p_1'\underset{\sim}{I} \qquad (8\text{-}26b)$$

where

$$p_1' = (p_1 - p)/G_1 \qquad (8\text{-}26c)$$

The above equation suggests the formulation for the unconstrained recovery to be,

$$\underset{\sim}{\tilde{C}}^{-1}\Big|_{rec} = \frac{1}{G_1}\left[\left(\frac{\bar{Y}}{\sqrt{\frac{1}{2}tr\underset{\sim}{H}^2}}\right)\underset{\sim}{H} + \underset{\sim}{H}\right]_{\substack{steady\\flow}} + p_1'\underset{\sim}{I} \qquad (8\text{-}27)$$

where

$$\underset{\sim}{H} = \int_{t-tr}^{\infty}\frac{G}{\tau}e^{-z/\bar{\tau}}\,\underset{\sim}{\tilde{C}}^{-1}\,dz \qquad (8\text{-}28a)$$

$$\tilde{\underset{\sim}{C}}^{-1} = \underset{\sim}{C}^{-1} - \frac{1}{3}(tr\underset{\sim}{C}^{-1})\ \underset{\sim}{I} \qquad (8\text{-}28b)$$

Let Q be a transformation matrix between the final state and the flow.

$$\underset{\sim}{Q}\ \underset{\sim}{Q}^{T} = \frac{\partial X_i(tr)}{\partial X_a(t)}\ \frac{\partial X_j(tr)}{\partial X_a(t)} \qquad (8\text{-}29)$$

where tr is the time at a moment before the recovery and t is the time at a moment after the recovery. This leads

$$\tilde{\underset{\sim}{C}}^{-1}\Big|_{rec} = \underset{\sim}{Q}\ \underset{\sim}{Q}^{T} - \frac{1}{3}(tr\underset{\sim}{Q}\underset{\sim}{Q}^{T})\ \underset{\sim}{I} \qquad (8\text{-}30)$$

The above form is due to that det $C^{-1}\big|_{rec}$ must be equal to det $C^{-1}\big|_{\text{steady flow}}$. Based on Eqs. (8-27) and (8-30), we may give general formulation for the instantaneous unconstrained recovery of filled polymer systems.

$$\underset{\sim}{Q}\ \underset{\sim}{Q}^{T} - \frac{1}{3}(tr\underset{\sim}{Q}\underset{\sim}{Q}^{T})\ \underset{\sim}{I} = \frac{1}{G_1}\left[\left(\frac{\bar{Y}}{\sqrt{\frac{1}{2}tr\underset{\sim}{H}^2}}\right)\underset{\sim}{H} + \underset{\sim}{H}\right]_{\substack{\text{steady}\\ \text{flow}}} + p'\underset{\sim}{I} \qquad (8\text{-}31)$$

ii. Uniaxial elongational flow

Consider the instantaneous recovery after a steady elongational flow of constant elongtional rate $\dot{\varepsilon}$. $\underset{\sim}{H}$ is already developed in Eq. (8-18) and

$$\frac{\bar{Y}}{\sqrt{\frac{1}{2}trH^2}} = \frac{\bar{Y}}{G\sqrt{3\left[\frac{\tau\dot{\varepsilon}}{(1+\tau\dot{\varepsilon})(1-2\tau\dot{\varepsilon})}\right]^2}} = \bar{Y}_{el}^{\,*} \qquad (8\text{-}32)$$

The kinematics of recovery are:

$$X_1(t) = \alpha_1\ X_1(tr) \qquad (8\text{-}33a)$$

$$X_2(t) = \alpha_2 \, X_2(tr) \tag{8-33b}$$

$$X_3(t) = \alpha_3 \, X_3(tr) \tag{8-33c}$$

where $\alpha_2 = \alpha_3 = 1/\sqrt{\alpha_1}$. This leads

$$Q \, Q^T = \begin{vmatrix} \frac{1}{\alpha_1^2} & 0 & 0 \\ 0 & \alpha_1 & 0 \\ 0 & 0 & \alpha_1 \end{vmatrix} \tag{8-34}$$

and

$$\tilde{\tilde{C}}^{-1}\Big|_{rec} = \begin{vmatrix} \frac{2}{3}\frac{1}{\alpha_1^2} - \frac{2}{3}\alpha_1 & 0 & 0 \\ 0 & \frac{1}{3}\alpha_1 - \frac{1}{3}\frac{1}{\alpha_1^2} & 0 \\ 0 & 0 & \frac{1}{3}\alpha_1 - \frac{1}{3}\frac{1}{\alpha_1^2} \end{vmatrix} \tag{8-35}$$

Solving Eq. (8-31) based on Eqs. (8-18) (p. 144) and (8-35), we get

$$\frac{1}{\alpha_1^2} - \alpha_1 = (1+\bar{Y}_{el}^{\,*}) \, \frac{G}{G_1} \left[\frac{3\tau\dot{\varepsilon}}{(1+\tau\dot{\varepsilon})(1-2\tau\dot{\varepsilon})} \right] \tag{8-36}$$

or

$$\alpha_2^4 - \frac{1}{\alpha_2^2} = (1+\bar{Y}_{el}^{\,*}) \, \frac{G}{G_1} \left[\frac{3\tau\dot{\varepsilon}}{(1+\tau\dot{\varepsilon})(1-2\tau\dot{\varepsilon})} \right] \tag{8-37}$$

Here $\alpha_1 < 1$ denotes the retraction in the flow direction and $\alpha_2 > 1$ denotes swell in the transverse direction.

The level of retraction α_1 or swell α_2 increases with increasing elongational rate $\dot{\varepsilon}$. α_2 decreases with increasing filler loading through its effect on the G/G_1 ratio.

iii. Shear flow

Consider the instantaneous recovery after a steady shear flow of constant shear rate $\dot{\gamma}$. $\underset{\sim}{H}$ of this kind of flow is already developed in Eq. (8-12a) (p. 143) and

$$\frac{\bar{Y}}{\sqrt{\frac{1}{2}\mathrm{tr}H^2}} = \frac{\bar{Y}}{G\tau\dot{\gamma}\sqrt{1+\frac{4}{3}\tau^2\dot{\gamma}^2}} = \bar{Y}_{sh}^{*} \tag{8-38}$$

The kinematics of recovery are:

$$X_1(t) = \alpha_1 X_1(tr) - g \tag{8-39a}$$

$$X_2(t) = \alpha_2 X_2(tr) \tag{8-39b}$$

$$X_3(t) = \alpha_3 X_3(tr) \tag{8-39c}$$

This leads

$$\underset{\sim}{Q}\,\underset{\sim}{Q}^{T} = \begin{vmatrix} \frac{1}{\alpha_1^2}(1+g^2) & \frac{\hat{g}}{\alpha_1\alpha_2} & 0 \\ \frac{\hat{g}}{\alpha_1\alpha_2} & \frac{1}{\alpha_2^2} & 0 \\ 0 & 0 & \frac{1}{\alpha_3^2} \end{vmatrix} \tag{8-40a}$$

$$\hat{g} = \frac{\partial g}{\partial X_2} \tag{8-40b}$$

and

$$\frac{1}{3}(\mathrm{tr}\underset{\sim}{Q}\underset{\sim}{Q}^{T}) = \frac{1}{3}\left(\frac{1}{\alpha_1^2} + \frac{1}{\alpha_2^2} + \frac{1}{\alpha_3^2} + \frac{\hat{g}^2}{\alpha_1^2}\right) \tag{8-41}$$

This leads the left hand side of Eq. (8-31) to be,

$$\begin{vmatrix} \frac{2}{3}\left(\frac{1}{\alpha_1^2}+\frac{\hat{g}^2}{\alpha_1^2}\right)-\frac{1}{3}\left(\frac{1}{\alpha_2^2}+\frac{1}{\alpha_3^2}\right) & \frac{\hat{g}}{\alpha_1\alpha_2} & 0 \\ \frac{\hat{g}}{\alpha_1\alpha_2} & \frac{2}{3}\frac{1}{\alpha_2^2}-\frac{1}{3}\left(\frac{1}{\alpha_1^2}+\frac{1}{\alpha_3^2}+\frac{\hat{g}^2}{\alpha_1^2}\right) & 0 \\ 0 & 0 & \frac{2}{3}\frac{1}{\alpha_3^2}-\frac{1}{3}\left(\frac{1}{\alpha_1^2}+\frac{1}{\alpha_2^2}+\frac{\hat{g}^2}{\alpha_1^2}\right) \end{vmatrix} \tag{8-42}$$

Solving Eq. (8-31) based on Eqs. (8-12) (p. 143) and (8-42),

$$\frac{1}{\alpha_1^2}-\frac{1}{\alpha_2^2}+\frac{g^2}{\alpha_1^2}=2\frac{G}{G_1}\left(1+\bar{Y}_{sh}^*\right)\tau^2\dot{\gamma}^2=\frac{N_1}{G_1} \tag{8-43a}$$

$$\frac{\hat{g}}{\alpha_1\alpha_2}=\frac{G}{G_1}\left(1+\bar{Y}_{sh}^*\right)\tau\dot{\gamma}=\frac{\sigma_{12}}{G_1} \tag{8-43b}$$

Substituting Eq. (8-43b) into Eq. (8-43a), leads to

$$\frac{1}{\alpha_1^2}-\frac{1}{\alpha_2^2}=\frac{N_1}{G_1}-\frac{\sigma_{12}^2}{G_1^2}\alpha_2^2 \tag{8-44}$$

or, since $\alpha_1 = 1/\alpha_2\alpha_3$,

$$\alpha_2^2\alpha_3^2-\frac{1}{\alpha_2^2}=2\lambda\tau^2\dot{\gamma}^2-\lambda^2\tau^2\dot{\gamma}^2\alpha_2^2 \tag{8-45a}$$

where

$$\lambda=\frac{G}{G_1}\left(1+\bar{Y}_{sh}^*\right)=\frac{G_2\left(1+\bar{Y}_{sh}^*\right)}{(G_1+G_2)}$$

$$=\frac{G}{G_1}\left[1+\left(\frac{\bar{Y}}{G\tau\dot{\gamma}\sqrt{1+\frac{4}{3}\tau^2\dot{\gamma}^2}}\right)\right] \tag{8-45b}$$

Note

$$\frac{\bar{Y}}{\eta(V/L)}=\frac{\bar{Y}}{G\tau\dot{\gamma}}=\text{Bingham number} \tag{8-46a}$$

If we note that

$$W_s=\tau\dot{\gamma}=\text{Weissenberg number} \tag{8-46b}$$

Eq. (8-45) becomes

$$\alpha_2^2\alpha_3^2 - \frac{1}{\alpha_2^2} = 2\lambda W_s^2 - \lambda^2 W_s^2\alpha_2^2 \qquad (8\text{-}47)$$

The above equation indicates the elastic recovery from shear flow is a function of W_s, Weissenberg number and λ. With increasing filler loading, λ, which is less than 1, will tend to 0 and substantially reduce in recovery. Eq. (8-47) is implicit for evaluating recovery.

In a simple shear flow with an infinite dimension in the 3 - direction where $\alpha_3 = 1$, Eq. (8-47) becomes

$$\alpha_2^2 - \frac{1}{\alpha_2^2} = 2\lambda W_s^2 - \lambda^2 W_s^2\alpha_2^2 \qquad (8\text{-}48)$$

or

$$\alpha_2^4[1 + \lambda^2 W_s^2] - \alpha_2^2\, 2\lambda W_s^2 - 1 = 0 \qquad (8\text{-}49)$$

This may be solved to give

$$\alpha_2 = \frac{1}{\alpha_1} = \left(\frac{\lambda W_s^2 + \sqrt{\lambda^2 W_s^4 + \lambda^2 W_s^2 + 1}}{1 + \lambda^2 W_s^2}\right)^{\frac{1}{2}} \doteq \sqrt{\frac{2\lambda W_s^2}{1 + \lambda^2 W_s^2}} \qquad (8\text{-}50)$$

d. Extrudate swell

Extrudate swell of polymer melt systems from a die flow, generally called die swell, is an example of a complicated unconstrained recovery because the shear rate in the die depends on the position. To predict die swell, one must consider not only local elastic recovery but on mass balance in each local element which may involve extensive numerical procedure. However, here we will

develop approximate swell formulations of filled polymer melt systems for simple die flows, i.e. capillary and slit dies. For these die flows, the shear stress is distributed linearly with zero at die center and maximum at die wall. Near the center portion, shear stress is smaller than yield value $\bar{Y}$. In this region, the shear rate is zero and the extrudate dimension should remain unchanged. Only beyond this region will the extrudate swell dimension due to elastic recovery, i.e. die swell. Since the shear rate is varying from the center to the wall of a die and the level of elastic recovery depends on the magnitude of shear rate, the elastic recovery, or swell, is varying at different postions with zero at die center and maximum at die wall. Therefore, to evaluate die swell, involves an averaging procedure, i.e.

$$B_2 = \frac{1}{A}\int_o^A \alpha_2 \, da \tag{8-51}$$

where a is the small area element.

i. For the capillary die,

$$B_{cap} = \frac{1}{\pi R^2}\int_o^R \alpha_2 \, 2\pi r \, dr \tag{8-52a}$$

ii. For the slit die,

$$B_{slit} = \frac{1}{H/2}\int_o^{H/2} \alpha_2 \, dX_2 \tag{8-52b}$$

The elastic recovery at every local area is represented by Eq. (8-47). For filled, especially highly filled

polymers λ is a small value. Taking $\lambda \to \epsilon$, Eq. (8-47) becomes

i. For the capillary, $\alpha_2 = \alpha_3 = 1/\sqrt{\alpha_1}$

$$\alpha_2^6 - 1 = 2 W_s^2 \epsilon \alpha_2^2 - W_s^2 \epsilon^2 \alpha_2^4 \tag{8-53a}$$

ii. For the slit, $\alpha_3 = 1$, $\alpha_2 = 1/\alpha_1$

$$\alpha_2^4 - 1 = 2 W_s^2 \epsilon \alpha_2^2 - W_s^2 \epsilon^2 \alpha_2^4 \tag{8-53b}$$

Since $\epsilon \to 0$, we can apply perturbation method and assume

$$\alpha_2 = \alpha_2^{(0)} + \alpha_2^{(1)}\epsilon + \alpha_2^{(2)}\epsilon^2 + O(\epsilon^3) \tag{8-54}$$

This leads,

i. For the capillary die,

$$\epsilon^0: \alpha_2^{(0)} - 1 = 0 \tag{8-55a}$$

$$\epsilon^1: 6[\alpha_2^{(0)}]^5 \alpha_2^{(1)} = 2 W_s^2 [\alpha_2^{(0)}]^2 \tag{8-55b}$$

$$\epsilon^2: 6[\alpha_2^{(0)}]^4[\alpha_2^{(1)}]^2 + 6[\alpha_2^{(0)}]^5\alpha_2^{(2)} = 4 W_s^2 \alpha_2^{(0)}\alpha_2^{(1)} - W_s^2[\alpha_2^{(0)}]^4 \tag{8-55c}$$

$$\alpha_2 = 1 + \frac{W_s^2}{3}\lambda + \left(\frac{W_s^4}{9} - \frac{W_s^2}{6}\right)^2 + O(\lambda^3) \tag{8-56}$$

ii. For the slit die,

$$\epsilon^0: \alpha_2^{(0)} - 1 = 0 \tag{8-57a}$$

$$\epsilon^1: 4[\alpha_2^{(0)}]^3 \alpha_2^{(1)} = 2 W_s^2 [\alpha_2^{(0)}]^2 \tag{8-57b}$$

$$\epsilon^2: 4[\alpha_2^{(0)}]^2[\alpha_2^{(1)}]^2 + 4[\alpha_2^{(0)}]^3\alpha_2^{(2)} = 4 W_s^2 \alpha_2^{(0)}\alpha_1^{(1)} - W_s^2[\alpha_2^{(0)}]^4 \tag{8-55c}$$

$$\alpha_2 = 1 + \frac{W_s^2}{2}\lambda + \frac{1}{4}(W_s^4 - W_s^2)\lambda^2 + O(\lambda^3) \qquad (8\text{-}58)$$

The swell in slit die is higher than in capillary die. Based on Eqs. (8-13a), (8-13b) and (2-25) (p. 143, p. 143, p. 13), W_s may have the form

$$W_s = \tau\dot{\gamma} = \frac{N_1}{2\sigma_{12}} = \frac{A}{2}\sigma_{12}^{a-1} \qquad (8\text{-}59)$$

Taking the averaging procedure by approximately assuming λ is a constant, leads to

i. For capillary

$$B_{cap} = C_{cap} + 1 + \int_{\bar{Y}}^{\sigma_w}\left[\frac{A^2}{12}\sigma_{12}^{2a-2}\lambda + \left(\frac{A^4}{144}\sigma_{12}^{4a-4} - \frac{A^2}{24}\sigma_{12}^{2a-2}\right)\lambda^2\right] 2\frac{\sigma}{\sigma_w^2}\,d\sigma + O(\lambda^3) \qquad (8\text{-}60)$$

or

$$B_{cap} = C_{cap} + 1 + \frac{A^2}{12a}\left(\sigma_w^{2a-2} - \frac{\bar{Y}^{2a}}{\sigma_w^2}\right)\lambda + \left[\frac{A^4}{144(2a-1)}\left(\sigma_w^{4a-4} - \frac{\bar{Y}^{4a-2}}{\sigma_w^2}\right) - \frac{A^2}{24a}\left(\sigma_w^{2a-2} - \frac{\bar{Y}^{2a}}{\sigma_w^2}\right)\right]\lambda^2 + O(\lambda^3) \qquad (8\text{-}61)$$

ii. For the slit,

$$B_{slit} = C_{slit} + 1 + \int_{\bar{Y}}^{\sigma_w} \left[\frac{A^2}{8}\sigma_{12}^{2a-2}\lambda + \left(\frac{A^4}{64}\sigma_{12}^{4a-4} - \frac{A^2}{16}\sigma_{12}^{2a-2}\right)\lambda^2\right]\frac{1}{\sigma_w}\,d\sigma + O(\lambda^3) \qquad (8\text{-}62)$$

or

$$B_{slit} = C_{slit} + 1 + \frac{A^2}{8(2a-1)}\left(\sigma_w^{2a-2} - \frac{\bar{Y}^{2a-1}}{\sigma_w}\right)\lambda + \left[\frac{A^4}{64(4a-3)}\left(\sigma_w^{4a-4} - \frac{\bar{Y}^{4a-3}}{\sigma_w}\right) - \frac{A^2}{16(2a-1)}\left(\sigma_w^{2a-2} - \frac{\bar{Y}^{2a-1}}{\sigma_w}\right)\right]\lambda^2 + O(\lambda^3) \qquad (8\text{-}63)$$

where C_{cap} and C_{slit} are viscous swell for the capillary die and slit die respectively which may also depend on the filler loading of the polymer compounds.

B. EXPERIMENTAL

1. Materials

The materials used in this study are two typical rubber compounds, tread and side wall SBR compounds. The recipe is shown in Table 3-1 (p. 45). The rheological properties were measured by Instron capillary viscometer at high shear rate and sandwich plate is low shear rate.

The viscosity-shear rate behavior and viscosity-shear stress behavior are shown in Figure 8-2 and 8-3.

The data of PS/TiO_2 system by Minagawa and White (187) has been replotted in different way to provide more complete information.

2. Apparatus and experimental procedures

Extrudate swell measurements were made at 80°C in an Instron capillary rheometer. The dies used had both rectangular and circular cross sections as shown in Table 8-1.

The extrudate swell of the polymer emerging from the slit die were values measured at the center of the cross section and for capillary measured the diameter by micrometer.

Different die length was used for each set of measurements. Die swell vs. L/D plots are used to extrapolate the data to get the die swell of infinite length B. An example of this procedure is described in Figure 8-4.

The wall shear rate and shear stress for both capillary and slit die are determined by the same way described in Chapter 5.

C. RESULTS AND DISCUSSION

1. General

The swell vs. wall shear stress behavior for both capillary and slit data is shown in Figure 8-5 for side

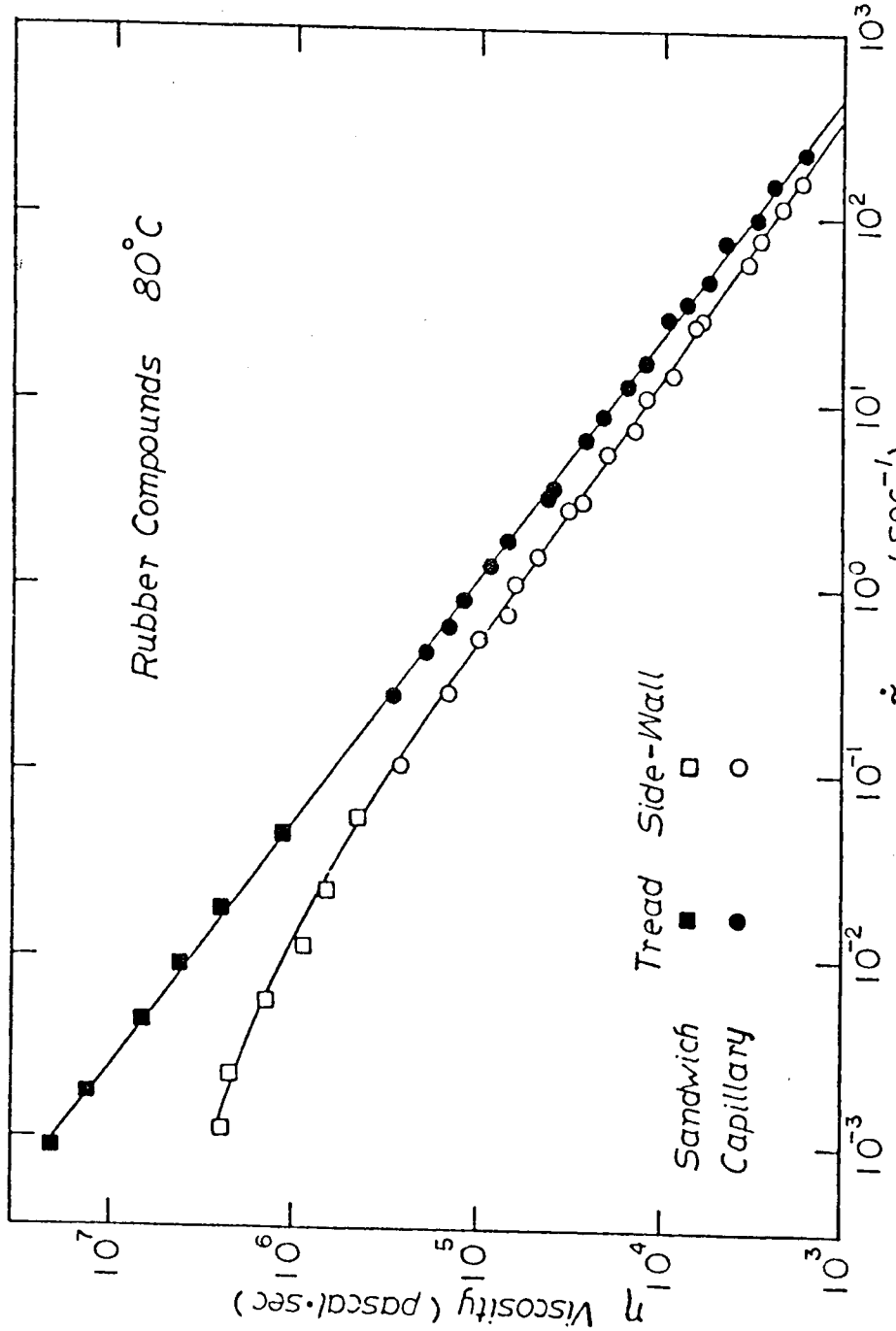

Figure 8-2. Viscosity-shear rate behavior for the rubber compounds used.

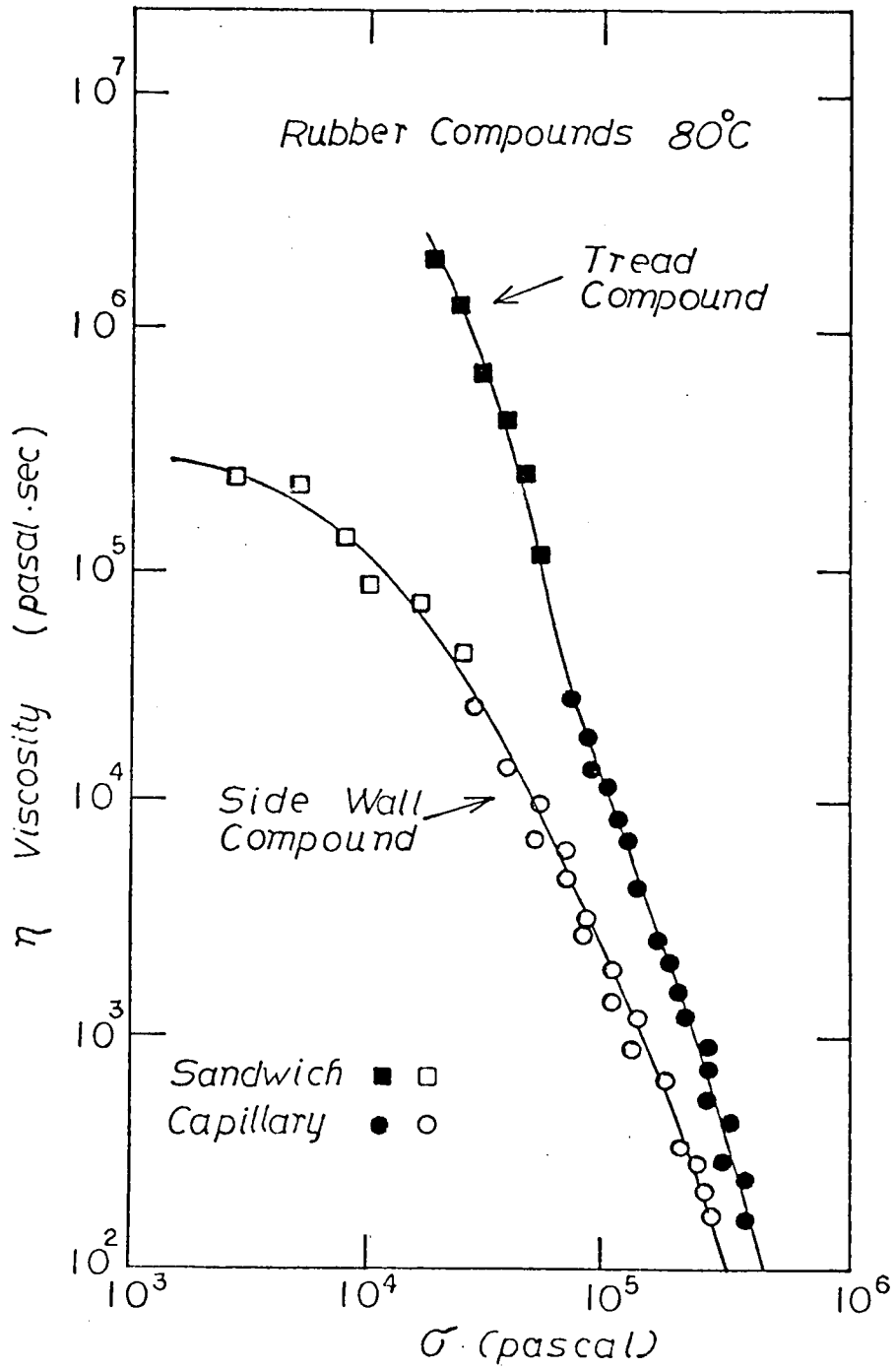

Figure 8-3. Viscosity-shear stress behavior for the rubber compounds used.

Table 8-1. Dimensions of dies for experiment in Ch. 8

Slit dies:

H (mm)	Aspect Ratio	L/H		
		1	2	3
0.381	16.7	12.5	20.0	29.9
0.635	10.0	12.0	18.2	24.1

Capillary dies:

Diameter (mm)	L/D		
	1	2	3
1.473	4.90	10.0	20.0
2.057	5.03	9.81	19.1

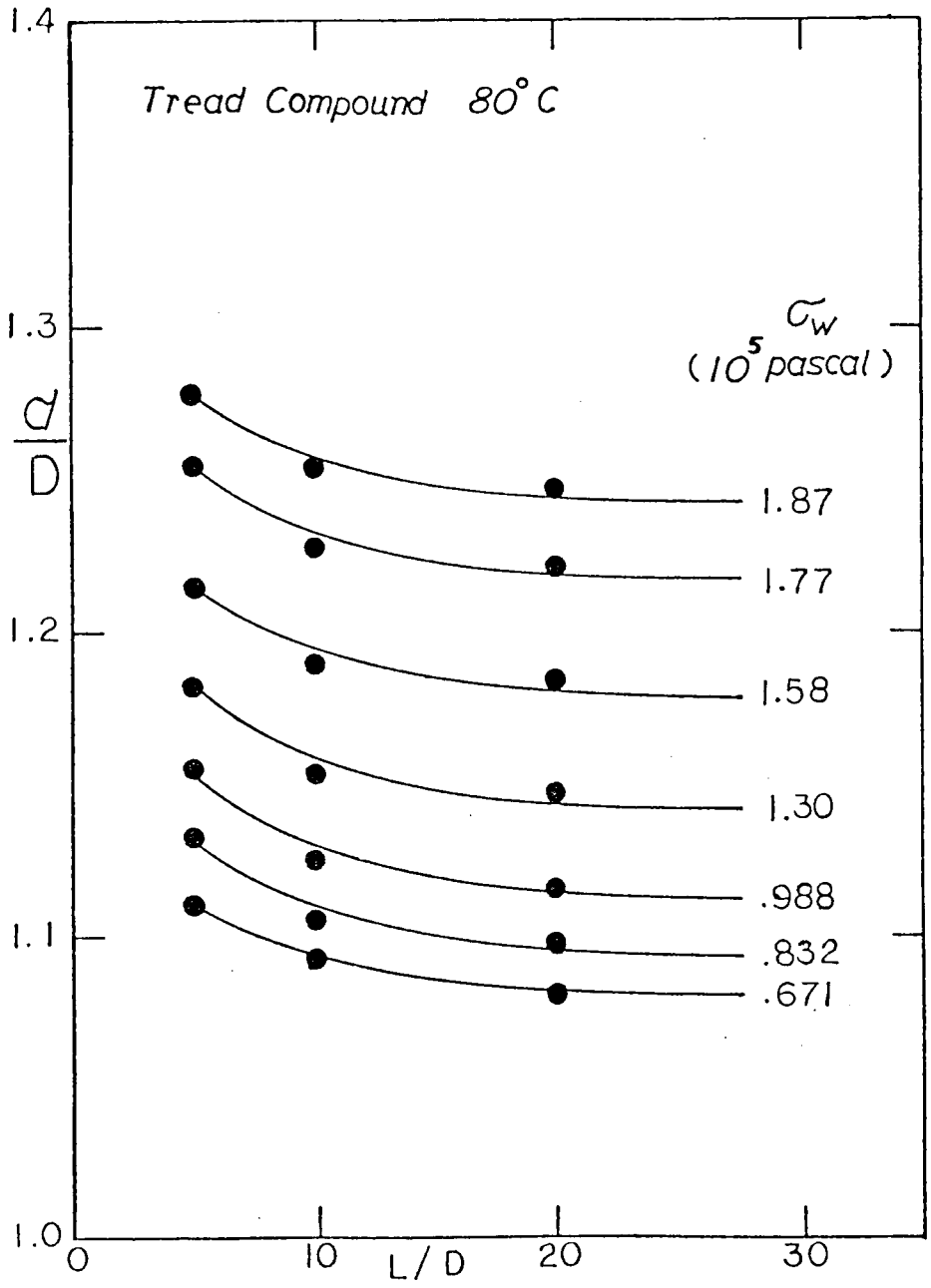

Figure 8-4. Capillary extrudate swell as a function of die length for tread compound.

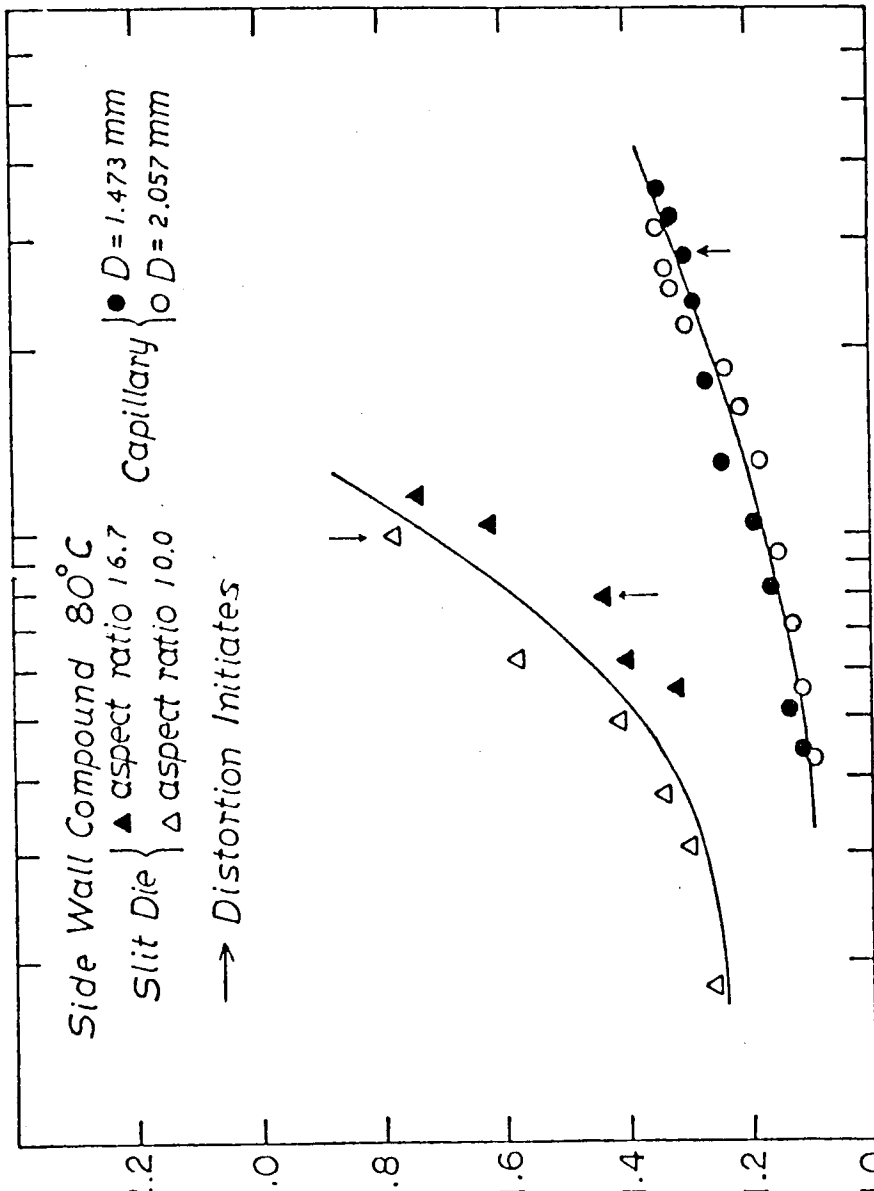

Figure 8-5. Extrudate swell-wall shear stress for side wall compound.

wall compound and Figure 8-6 for tread compound. Generally the slit die swell is much higher than capillary die swell at same wall shear stress. At low die wall shear stress slit die swell goes to a value of about 1.2 as opposed to about 1.1 for capillary die swell.

The slit die swell data suffer in accuracy, especially for the tread compound because of serious distortion at all wall shear stresses used.

Rubber compounds tend to slip in the cone-plate rheometer even at the lowest rotation speed. Therefore we could not obtain N_1 - σ_{12} behavior for rubber compounds.

In order to broaden our experimental evidence, we introduce and rework the data presented by Minagawa and White (187). The polystyrene used by these authors was Dow Styron 678U which is also studied extensively in previous chapters. Here we replot their rheological data in viscosity-shear stress and N_1-shear stress behaviors as shown in Figure 8-7 for 0, 14.3 and 24 volume percent TiO_2 polystyrene compounds. For pure polystyrene a Newtonian viscosity is observed at low shear rate or stress. Increasing TiO_2 loading increases low shear viscosity and yield value. For 24% TiO_2/PS compound, the yield value is about 500 pascal which is comparatively very small to the usually operating wall shear stress ($10^4 \sim 10^5$ pascal). Another interesting phenamenon is that the compound tends to have similar N_1 - σ_{12} behavior to the pure polymer at

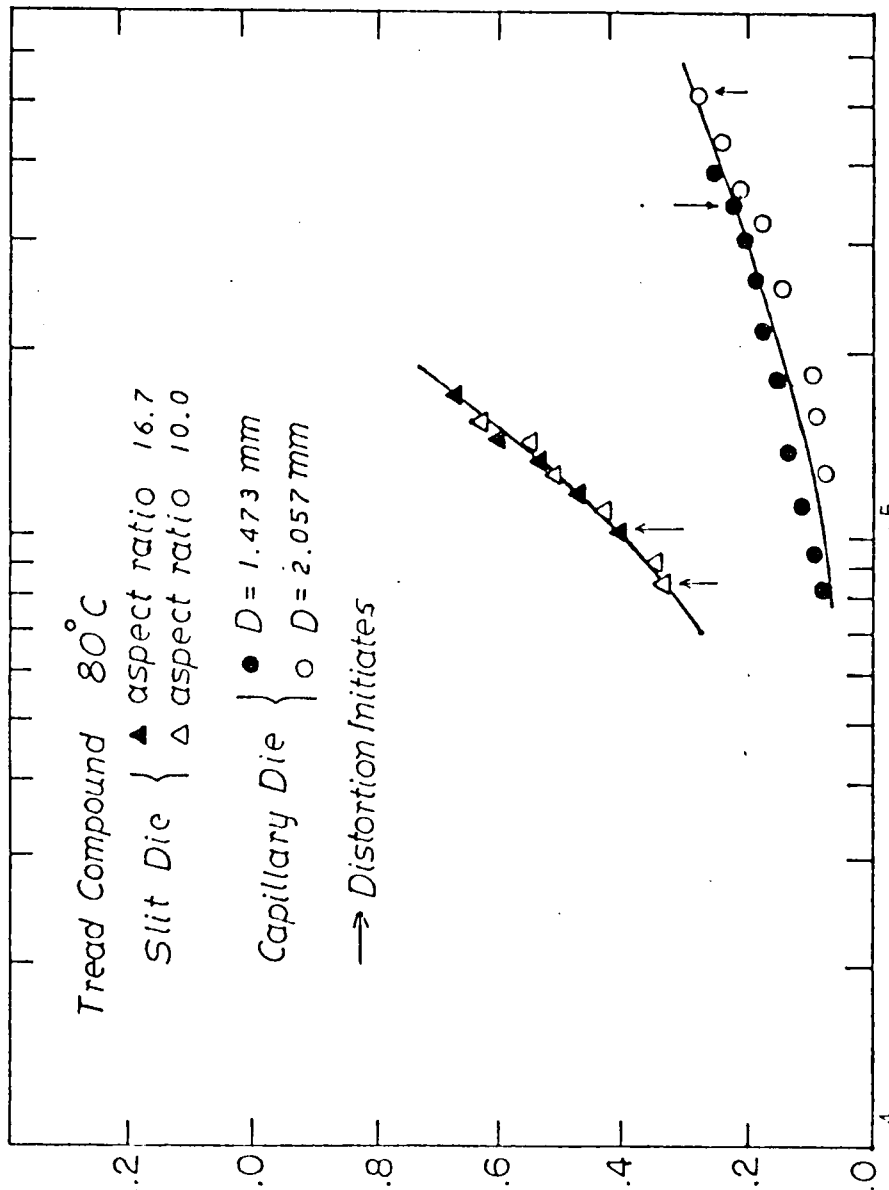

Figure 8-6. Extrudate swell-wall shear stress for tread compound.

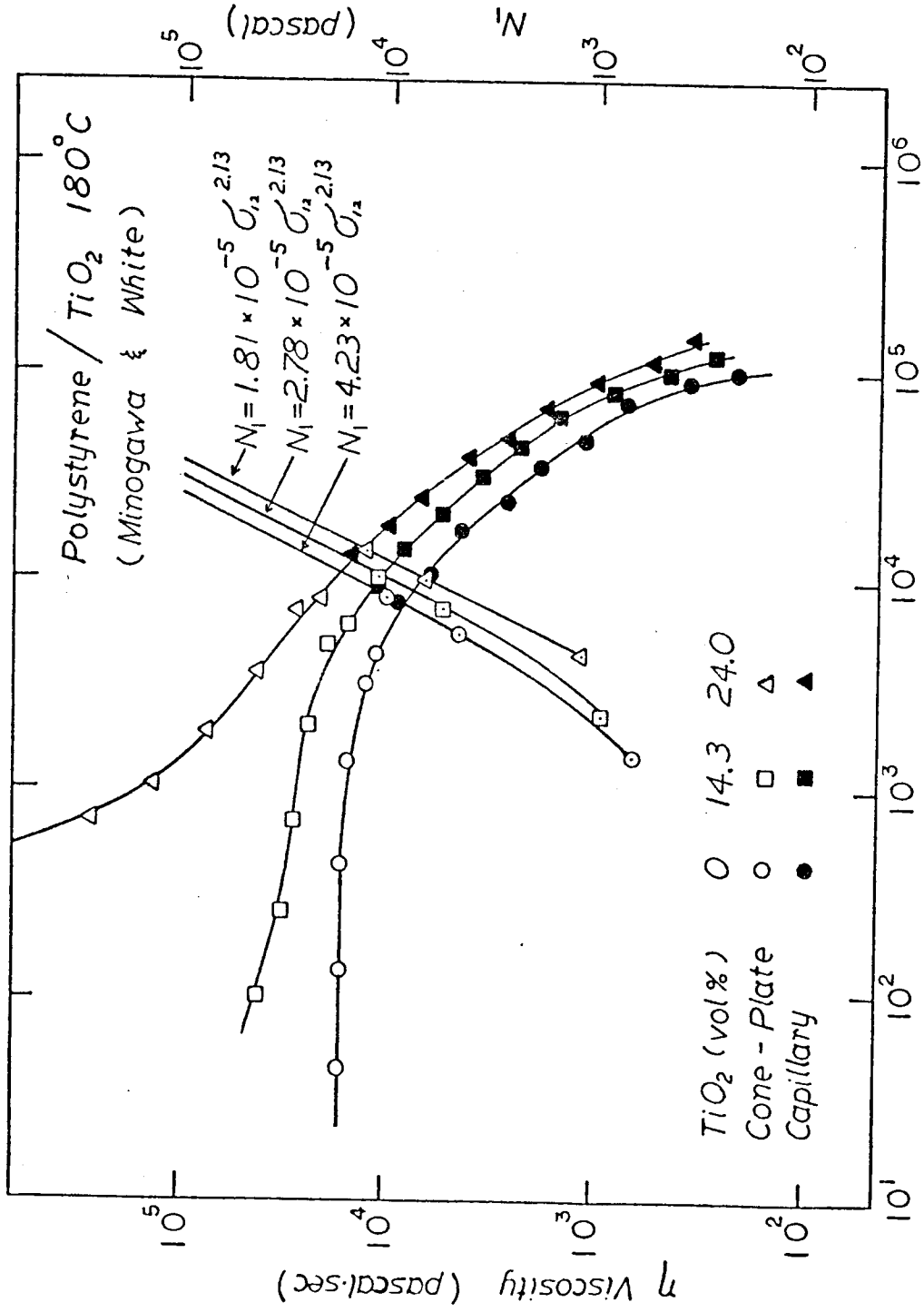

Figure 8-7. Viscosity and principal normal stress difference as a function of shear stress for TiO_2 filled polystyrene with various solid volume fraction.

the same stresses. A power law relation of Eq. (2-25) (p. 13) is applicable:

$$N_1 = A \sigma_{12}^{a} \qquad (2\text{-}25)$$

where the power index a tends to remain constant at about 2 while the N_1 function or A decreases as we increase filler loading.

The capillary die swell B - $(\sigma_{12})_w$ behavior is shown on Figure 8-8. Again we see that die swell decreases as we increase filler loading. If we plot swell - $(N_1/\sigma_{12})_w$ behavior as Figure 8-9, it is seen that the swell data of various loadings is getting closer. However, the decreasing of N_1 function in increasing TiO_2 loading in polystyrene alone is not enough to explain the decrease of extrudate swell.

The available data in the literature (38, 141, 187, 294) generally show less significant changes of the N_1 function as opposed to rapidly decreasing extrudate swell with increasing filler loading.

2. Comparison with theory

Eqs. (8-61) and (8-63) (p. 156, p. 157) can be used to predict extrudate swell from capillary and slit dies for filled, especially highly filled polymer melt systems which have small λ values. At this time, we have no direct measurement for G/G_1 ratio or λ values. Based on Eq. (8-61) (p. 156) and Figures (8-6) and (8-7) of

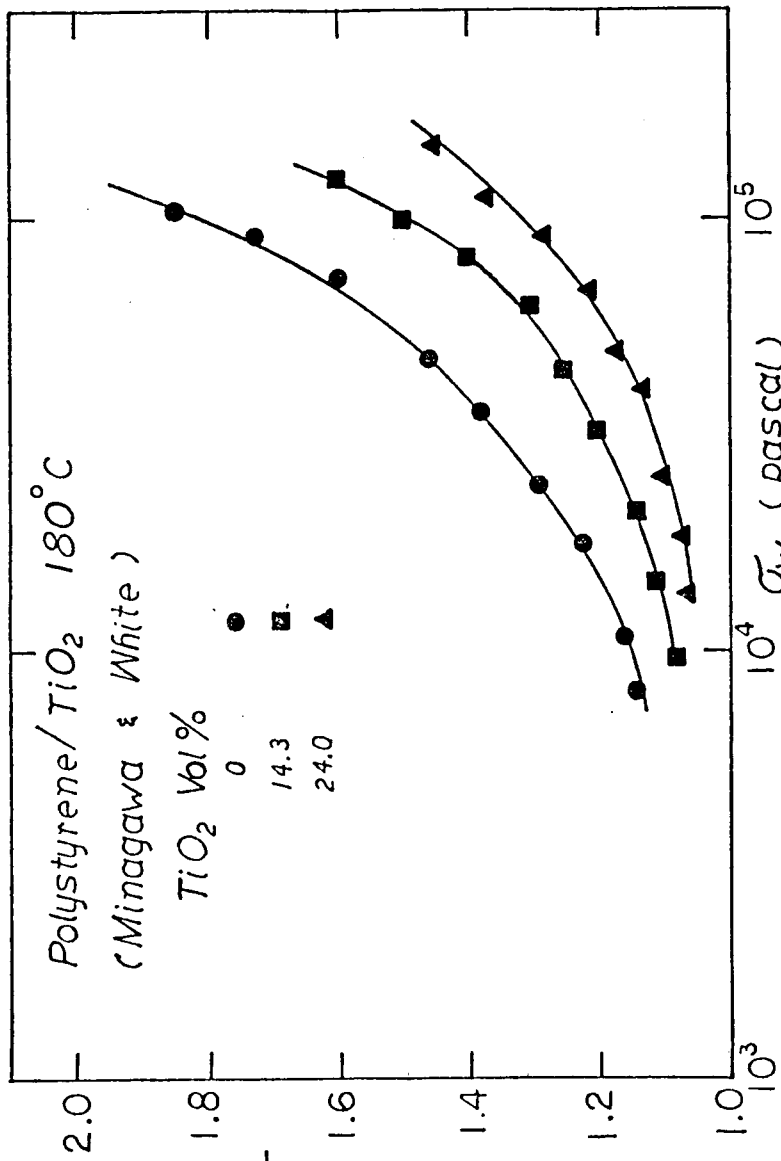

Figure 8-8. Extrudate swell-wall shear stress behavior for TiO_2 filled polystyrene with various solid volume fraction.

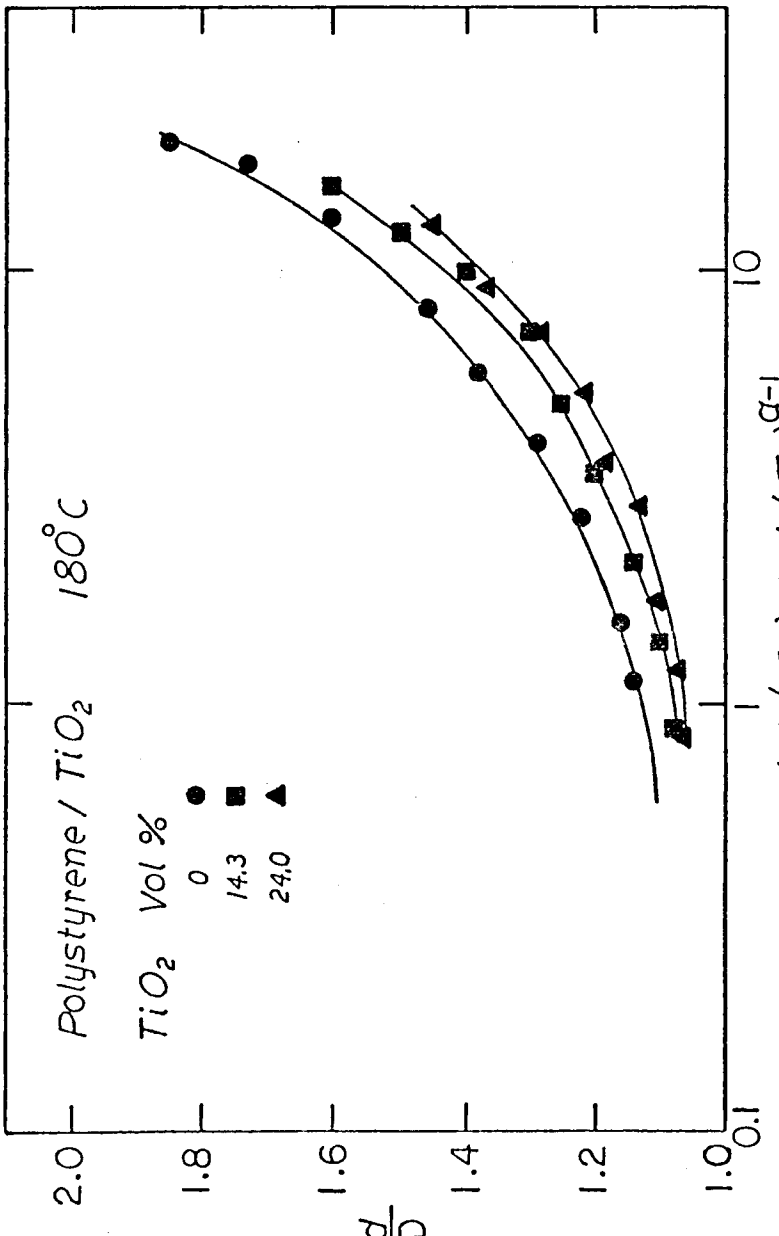

Figure 8-9. Extrudate swell as a function of ratio of principal normal stress difference to shear stress at the die wall.

polystyrene/TiO_2 compounds and taking $C_{cap} \rightarrow 0$, $\bar{Y} \rightarrow 0$, we found the λ value is really small, about 0.1 or less, as assumed in our theoretical derivation.

D. CONCLUSIONS

1. Equations for elastic recovery of filled polymer melts have been developed based on the constitutive model proposed by White and Lobe.
2. The recoverable strain has been considered to have higher elastic modulus than overall elastic modulus of filled polymer melt systems which explains the rapid decrease in extrudate swell as increasing filler loading.
3. Extrudate swell equations for capillary and slit dies have been developed for highly filled polymer melt systems and contrasted with experiment.

CHAPTER 9

SCREW EXTRUSION OF RUBBER COMPOUNDS

The screw extrusion of rubber compounds is different from that of thermoplastics. Rubber compounds are never crystalline or glassy solids but always very viscous liquids or soft solid (with a yield value). There should be no melting region in the screw extrusion.

In principle, therefore, the study of rubber extrusion should be less complicated. However, the plasticating screw extrusion of thermoplastics has been well studied as mentioned in the literature survey. This is not the case for rubber extrusion. This is probably due to the different natures of the industries and preponderance of chemists and compounders rather than engineers working with processing.

There are several basic purposes for investigating the extrusion of rubber compounds: (i) rational design of screw extruders, (ii) to control temperature build-up to avoid any scorch--"prevulcanization", (iii) to reproducibly produce uniform smooth extrudates, (iv) to obtain higher production rate with lower power consumption. This chapter is devoted to a basic study of the extrusion of rubber compounds.

A. GENERAL

In the extrusion of rubber essentially we are feeding a melt into the hopper. There should not be a melting mechanism along the screw extrusion. The behavior is in many senses different from that of plasticating extrusion of solid plastics. At the hopper, the feeding mechanism is quite different for extrusion of plastics. Usually, plastics are fed in as pellets or powers where the major driving force is its own gravity. Rubber compounds are a very high viscous melt or a soft solid and exhibit a yield value, especially at low temperature. In the feeding region, melts or rubber compounds unlike pellets tend to stick to the hopper wall and require applying forces. Generally it is easier to feed as continuous strips. One should expect that feeding may be a complicated problem for rubber compounds. It is well known that rubber compounds slip when one attempts to induce shear flow at low inpressed pressure. Therefore, following the hopper, we should have a short plug conveying zone. Further down the screw the flow will probably evolve into a traditional metering region flow of the type considered by various researchers.

The transfer capacity of these three zones (i.e. feeding zone, plug conveying zone and melt conveying zone) may be different with one controlling the whole operation. In this study a joint plug and melt conveying model will be presented.

B. THEORETICAL MODEL

The melt conveying in screw extrusion has traditionally been considered as melt conveying in a rectangular channel with screw surface stationary and barrel or top plate moving along and perpendicular to the channel.

As the rubber properties are always continuous unlike plastics, which exhibit phase transformation along the length of one screw, we should be able to develop a single model with evolving parameters to represent the entire screw. Different asymptotes of this model will be applicable in different regions. The general model proposed here involves apply:

1. lubrication approximation neglecting normal stresses,
2. a constitutive model for filled polymers developed in Chapter 8 which includes a yield value,
3. more general boundary conditions which include slip.

The field equations are: (refer Figure 9-1)

$$0 = -\frac{\partial p}{\partial x} + \frac{\partial \sigma_{xy}}{\partial y} + \frac{\partial \sigma_{xz}}{\partial z} \tag{9-1}$$

$$0 = -\frac{\partial p}{\partial y} + \frac{\partial \sigma_{yz}}{\partial z} \tag{9-2}$$

$$0 = -\frac{\partial p}{\partial z} + \frac{\partial \sigma_{zy}}{\partial y} \tag{9-3}$$

$$\rho C_p\left(V_x\frac{\partial T}{\partial x} + V_y\frac{\partial T}{\partial y} + V_z\frac{\partial T}{\partial z}\right) = k\left(\frac{\partial^2 T}{\partial y^2} + \frac{\partial^2 T}{\partial z^2}\right) + \eta(II_d, T)II_d \tag{9-4}$$

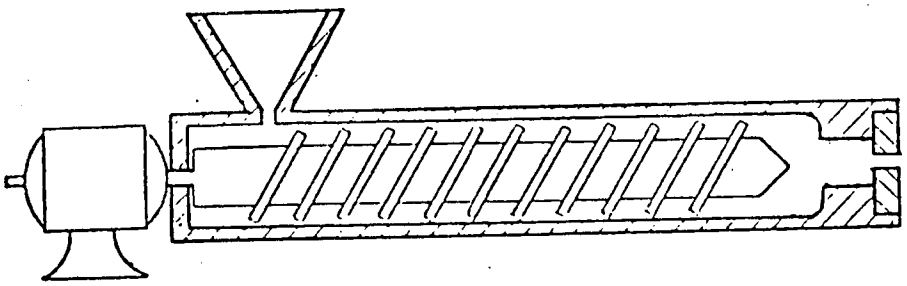

Screw Extruder

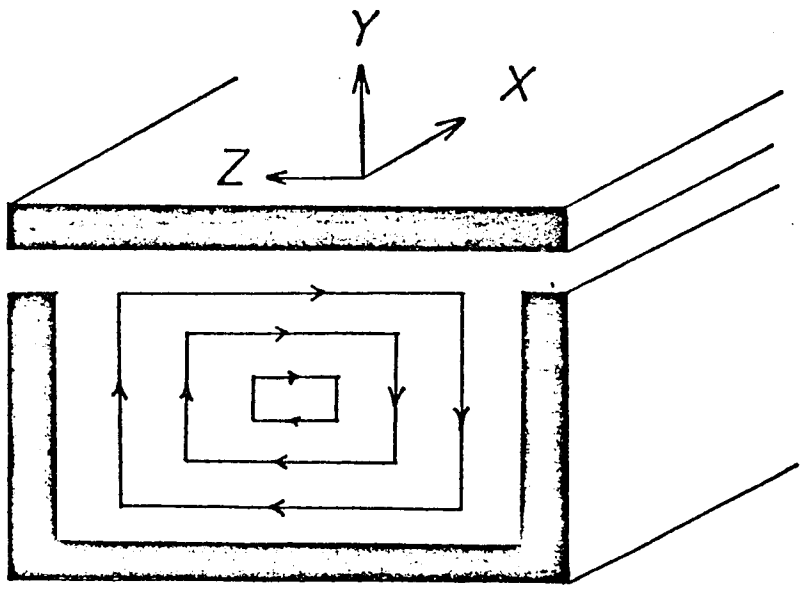

Figure 9-1. Rectanglized screw channel.

Flow rate

$$Q = 2\int_o^H \int_o^{W/2} V_x \, dy \, dz \tag{9-5}$$

and

$$0 = \int_{-w/2}^{+w/2} V_y \, dz \tag{9-6a}$$

$$0 = \int_o^H V_z \, dy \tag{9-6b}$$

These are the same as would apply in a metering region model. However, the constitutive equations and the boundary conditions we consider are different. Based on Chapter 8, the constitutive model for filled polymer melts should include a yield value which may be temperature and shear rate dependent with higher value at low temperature and low shear rate. Here, we use the same model proposed by White.

$$\underset{\sim}{\sigma} = -p\underset{\sim}{I} + \left(1 + \frac{\bar{Y}}{\sqrt{\frac{1}{2}tr\underset{\sim}{H}^2}}\right)\underset{\sim}{H} \tag{9-7a}$$

$$\underset{\sim}{H} = \int_o^\infty \frac{G}{\tilde{\tau}} e^{-z/\tilde{\tau}} \left(\underset{\sim}{C}^{-1} - \frac{1}{3}tr\underset{\sim}{C}^{-1}\underset{\sim}{I}\right) dz \tag{9-7b}$$

or

$$\underset{\sim}{H} = \underset{\sim}{H}' - \frac{1}{3}tr\underset{\sim}{H}'\underset{\sim}{I} \tag{9-7c}$$

where

$$H' = G \begin{vmatrix} 1+\dot{\gamma}_{12}^2\tilde{\tau}^2+\dot{\gamma}_{13}^2\tilde{\tau}^2 & \dot{\gamma}_{12}\tilde{\tau} & \dot{\gamma}_{13}\tilde{\tau} \\ \dot{\gamma}_{12}\tilde{\tau} & 1+\dot{\gamma}_{23}^2\tilde{\tau}^2 & \dot{\gamma}_{23}\tilde{\tau} \\ \dot{\gamma}_{13}\tilde{\tau} & \dot{\gamma}_{32}\tilde{\tau} & 1+\dot{\gamma}_{32}^2\tilde{\tau}^2 \end{vmatrix} \tag{9-7d}$$

so,

$$\underset{\sim}{H} = G\tau \begin{vmatrix} \frac{\tau}{3}\left(2\dot{\gamma}_{12}^2+2\dot{\gamma}_{13}^2-\dot{\gamma}_{23}^2-\dot{\gamma}_{32}^2\right) & \dot{\gamma}_{12} & \dot{\gamma}_{13} \\ \dot{\gamma}_{12} & \frac{\tau}{3}\left(2\dot{\gamma}_{23}^2-\dot{\gamma}_{12}^2-\dot{\gamma}_{13}^2-\dot{\gamma}_{32}^2\right) & \dot{\gamma}_{23} \\ \dot{\gamma}_{12} & \dot{\gamma}_{32} & \frac{\tau}{3}\left(2\dot{\gamma}_{32}^2-\dot{\gamma}_{12}^2-\dot{\gamma}_{13}^2-\dot{\gamma}_{23}^2\right) \end{vmatrix} \tag{9-7e}$$

$$\sqrt{\tfrac{1}{2}\mathrm{tr}\underset{\sim}{H}^2} = G\tau\phi = \eta\phi \tag{9-7f}$$

where

$$\phi = \sqrt{\tfrac{1}{2}\mathrm{tr}\underset{\sim}{H}^2}/G\tau \tag{9-7g}$$

ϕ is a complicated function of strain rates. Here η is a viscosity function which generally can be represented perhaps by a non-isothermal power law model,

$$\eta = K\, II_d^{\frac{n-1}{2}} \tag{9-7h}$$

$$II_d = 2d_{ij}d_{ji} \tag{9-7i}$$

$$d_{ij} = \tfrac{1}{2}\left(\frac{\partial v_i}{\partial x_j} + \frac{\partial v_j}{\partial x_i}\right) \tag{9-7j}$$

and

$$K = C_o e^{-a(T-T_o)} \tag{9-7k}$$

where n is the power law index and a is the temperature sensitivity of polymers. The boundary conditions we consider are:

for the temperature:

$$\text{barrel } T(H,x) = T_b(x) \tag{9-8a}$$

$$\text{screw } \frac{\partial T}{\partial y}(0,x) = 0 \qquad (9\text{-}8b)$$

$$\frac{\partial T}{\partial z}(\pm\frac{W}{2},y,x) = 0 \qquad (9\text{-}8c)$$

For velocities at boundaries are more complicated. The boundary at the screw surface or the barrel surface can be considered as an interface of polymer solid and metal. Chung et al (45) have studied the friction factor of this kind of interface. More recent studies have been made by Klein (115). Generally they found the friction factor of a polymer solid-metal interface increases with increasing displacement rate or relative velocity difference of these two inter surfaces. This phenamenon may be due to that the polymer solid is viscoelastic in nature and shows some viscous character even in the solid state. This should be more so for rubber compounds which behave like a solid especially at low temperatures due to high yield values and more like a viscous liquid at high temperatures where they possess lower yield value. We may write the force balance by the constitutive equations at the two displacing interfaces of metal vs. solid-like polymer melt as ($i \neq j$)

$$\sigma_{ij} = J(V_{ui}-V_{li})n_j = (1 + \frac{\bar{Y}}{\eta\dot{\gamma}})\,\eta\dot{\gamma}_{ij}\Big|_{wall} \qquad (9\text{-}9a)$$

where V_{ui} and V_{li} are velocity in i - direction for upper and lower surfaces respectively. n_j denotes the surface where the displacement is taking place. J is an interface parameter which may be a function of the pressure, temperature

and the character of the interface and also $\sqrt{(V_{ui}-V_{li})^2}$. $\dot{\gamma}_{ij}\big|_{wall}$ is the shear rate at the wall. Rearranging Eq. (9-9a), we get

$$\Delta V_i\Big|_{slip} n_j = \alpha_{surface}\left(\frac{\partial V_i}{\partial x_j}\right)_{at\ boundary} \qquad (9\text{-}9b)$$

$$\alpha_{surface} = \frac{Y}{\phi J} + \frac{\eta}{J} \qquad (9\text{-}9c)$$

where α surface is the slip parameter at the boundary surface. We denote α_b for barrel surface and α_s for screw surface. This slip parameter which determines the level of slip should increase with increasing viscosity and yield value and should decrease with increasing in J and strain rate. It may also depend on pressure, shear stress, temperature and surface character. Near the hopper, the slip parameter may be larger because of low pressures, low termperature and high yield value at this region. This would give rise to a plug conveying region. Further down the screw, the slip parameter may become so small that the flow will be a traditional metering or melt conveying region. For the whole region, we can apply general boundary conditions:

$$V_x(H,x) = \pi DN\cos\theta - \alpha_b\left(\frac{\partial V_x}{\partial y} + \frac{\partial V_x}{\partial z}\right)_{(H,x)}$$

$$V_y(H,x) = 0$$

$$V_z(H,x) = \pi DN\sin\theta - \alpha_b\left(\frac{\partial V_z}{\partial y} + \frac{\partial V_z}{\partial x}\right)_{(H,x)}$$

$$V_x(0,x) = \alpha_s\left(\frac{\partial V_x}{\partial y} + \frac{\partial V_x}{\partial z}\right)_{(0,x)}$$

$$V_y(0,x) = 0$$

$$V_z(0,x) = \alpha_s\left(\frac{\partial V_z}{\partial y} + \frac{\partial V_z}{\partial x}\right)_{(0,x)}$$

$$V_x(\pm\frac{w}{2},y,x) = \alpha_s\left(\frac{\partial V_x}{\partial y} + \frac{\partial V_x}{\partial z}\right)_{(\pm w/2,y,x)}$$

$$V_y(\pm\frac{w}{2},y,x) = \alpha_s\left(\frac{\partial V_y}{\partial z} + \frac{\partial V_y}{\partial x}\right)_{(\pm w/2,y,x)}$$

$$V_z(\pm\frac{w}{2},y,x) = 0 \qquad (9\text{-}10)$$

where, N = screw rotating speed

p = pressure

w = width of screw flight

H = height of screw flight

V = velocity

T = temperature

θ = screw helical angle

D = diameter of screw

The rheological parameters generally depend on temperature. K is already given by Eq. (9-7k). Y is given by

$$Y = Y_o e^{-b(T-T_o)} \qquad (9\text{-}11a)$$

For surface, this may be

$$\alpha = \alpha_o e^{-c(T-T_o)} \qquad (9\text{-}11b)$$

Increasing temperature decreases viscosity and slip at boundary srufaces.

The prediction of temperature build-up needs a complete solution of all equations of motion and energy of Eqs. (9-1) to (9-4) (p. 173). Generally, complicated numerical calculation with high speed computer should be carried out. Even so, up to date there is no solution of solving the complete model listed in Eqs. (9-1) to (9-4) (p. 173). One must sacrifice one part or the other. Extensive work was reported by Zamodits and Pearson (281) in which they built up a computer program to solve the 2-dimensional non-isothermal problem. Martin (136) further developed the program to include heat convection in the energy equation. Before one does serious numerical computation, it is necessary to have a more fundamental understanding of the screw extrusion of rubber compounds.

In the following, we introduce an approximate treatment, which should help reduce the problem. Let us consider an infinitesimal area at barrel surface (refer to Figure 9-2) where the local power consumption can be represented as

$$\begin{aligned}\vec{f}\cdot\vec{v}\,dx\,dz &= f\cos\psi\,\pi DN\,dx\,dz \\ &= f\cos\psi\,(\cos\theta\,\vec{x} + \sin\theta\,\vec{z})\cdot\pi DN \\ &\quad (\cos\theta\,\vec{x} + \sin\theta\,\vec{z})\,dx\,dz \\ &= f\cos\psi\,\pi DN\cos^2\theta + f\cos\psi\,\pi DN\sin^2\theta \qquad (9\text{-}12)\end{aligned}$$

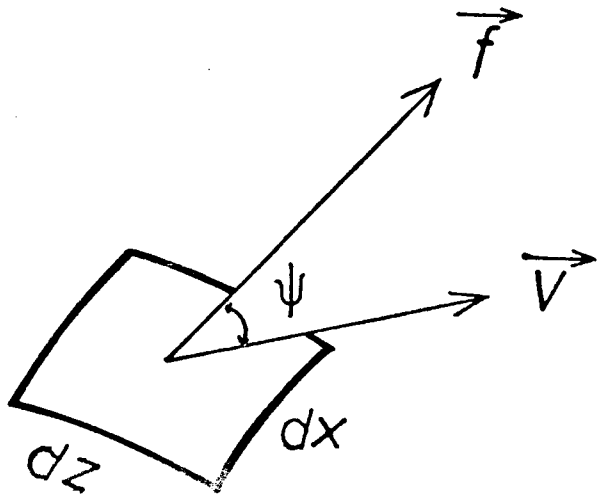

Figure 9-2. An infinitesimal element at barrel surface.

where $\vec{f}$ is the force per unit area, ψ is the angle between force and velocity directions. The first term on the right hand of Eq. (9-12) is the power consumption of motion in the principal direction and the next term is the power consumption of motion in the transverse direction. Therefore the ratio of power consumed in the principal to the transverse direction is equal to $\tan^2\theta$. If we approximately assume this relation holds throughout the whole region. The heat generating term is Eq. (9-4) (p. 173) can be represented as

$$\sigma_{ij}\frac{\partial v_i}{\partial x_j} = \eta(II_d, T)\, II_d$$

$$= (1 + \tan^2\theta)\eta\left[\left(\frac{\partial V_x}{\partial y}\right)^2 + \left(\frac{\partial V_x}{\partial z}\right)^2\right] \qquad (9\text{-}13)$$

Since V_y and $\partial T/\partial z$ are small, we can neglect $V_y(\partial T/\partial y)$ and $V_z(\partial T/\partial z)$ in the energy equation. This reduces field equations to

$$0 = -\frac{\partial p}{\partial x} + \frac{\partial \sigma_{xy}}{\partial y} + \frac{\partial \sigma_{xz}}{\partial z} \qquad (9\text{-}1)\ (p.\ 173)$$

$$\rho C_p V_x \frac{\partial T}{\partial x} = k\frac{\partial^2 T}{\partial y^2} + \eta(II_d, T)\, II_d \qquad (9\text{-}14)$$

$$II_d = (1 + \tan^2\theta)\left[\left(\frac{\partial V_x}{\partial y}\right)^2 + \left(\frac{\partial V_x}{\partial z}\right)^2\right] \qquad (9\text{-}15)$$

where θ is the screw helical angle. Although the above equations are still very complicated but it is already only 1/3 of scale of the original one. This scale of numerical

computation has been done by Martin (136). The output rate (Q) and temperature (T) build-up should be a function of G (pressure to shear stress dimensionless group), Br (Brinkman number), Pe (Pelect number) and aspect ratio. However, those dimensionless groups need to be modified due to Eq. (9-28). They should be represented as in the following

$$G = \frac{(\Delta p/L)\, H^{1+n}}{2C_o(\pi DN\cos\theta)^n(1+\tan^2\theta)^{(n-1)/2}} \tag{9-16}$$

$$Br = aC_o(1+\tan^2\theta)^{(n+1)/2}(\pi DN\cos\theta)^{n+1}H^{1-n}/k \tag{9-17}$$

$$Pe = \rho C_p(\pi DN\cos\theta)H/k \tag{9-18}$$

In the following sections, we will develop solutions for a simplified case by neglecting transverse flows, the effect in z-direction and temperature. This leads

$$0 = -\frac{\partial p}{\partial x} + \frac{\partial \sigma_{xy}}{\partial y} \tag{9-19a}$$

$$V_x(H) = \pi DN\cos\theta - \alpha_b\left(\frac{\partial V_x}{\partial y}\right)_{(H)} \tag{9-19b}$$

$$V_x(0) = \alpha_s\left(\frac{\partial V_x}{\partial y}\right)_{(0)} \tag{9-19c}$$

1. Isothermal Newtonian model

For a Newtonian isothermal case, we have

$$\sigma_{xy} = \mu\left(\frac{\partial V_x}{\partial y}\right) \tag{9-20}$$

and α_s, α_b are constants. The solution is:

$$\bar{u} = 0.5\, G_r\, \bar{y}^2 + \left(\frac{1-0.5G_r-\alpha_b^* G_r}{1+\alpha_s^*+\alpha_b^*}\right) \bar{y}$$

$$+ \alpha_s^* \left(\frac{1-0.5G_r-\alpha_b^* G_r}{1+\alpha_s^*+\alpha_b^*}\right) \tag{9-21}$$

where

$$\bar{u} = V_x/\pi DN\cos\theta$$

$$\bar{y} = y/H$$

$$G_r = \left(\frac{\Delta p}{L}\right) \frac{H^2}{\mu \pi DN\cos\theta}$$

$$\alpha_s^* = \alpha_s/H$$

$$\alpha_b^* = \alpha_b/H \tag{9-22}$$

and the dimensionless flow rate Q^* is

$$Q^* = Q/wH\pi DN\cos\theta$$

$$= \frac{0.5+\alpha_s^*}{1+\alpha_s^*+\alpha_b^*} - \left(\frac{(0.5+\alpha_s^*)(0.5+\alpha_b^*)}{1+\alpha_s^*+\alpha_b^*} - \frac{1}{6}\right) G_r \tag{9-23}$$

If $\alpha_s^* = \alpha_b^* = 0$, i.e. non-slip condition, Eq. (9-23) reduces to

$$Q^* = \frac{1}{2} - \frac{1}{12} G_r \tag{9-24}$$

or

$$Q = \frac{wH\pi DN\cos\theta}{2} - \frac{\Delta p w H^3}{12\mu L} \tag{9-25}$$

Eq. (9-17) is the same as the existing solution in the literature for isothermal Newtonian metering flow.

In Figure 9-3, we plot the velocity profile for (a) $\alpha_b^* = \alpha_s^* = 0$, (b) $\alpha_b^* = 0$, $\alpha_s^* = 1$, (c) $\alpha_b^* = 1$, $\alpha_s^* = 0$ and (d) $\alpha_b^* = \alpha_s^* = 1$ at various pressure gradient conditions. As $G_r \geq 1/(0.5+\alpha_b^*)$, backward flow starts to occur. Therefore, we compare situations where G_r is below and above this value. Generally, increasing pressure gradient decreases flow rate and having less slip at barrel than the screw surface will be favorable to the overall flow rate. This is because the shear stress at barrel surface is the driving force and the stress at screw surface and the increasing pressure are the retarding forces.

In Figure 9-4, we compare Q^* vs. G_r behavior for isothermal Newtonian flow at various barrel and screw surface slippage conditions. Generally slip at both surfaces would decrease the capacity to build up pressure. Slip at the barrel is especially unfavorable to flow rate and pressure build-up capability.

The slip parameter might be presumed to depend on pressure as

$$\alpha^* = \alpha^o e^{-p/p^*} \tag{9-26}$$

where p^* is a characteristic pressure. With the above condition, the slippage would be higher near the hopper and lower at the end of the screw. The pressure gradient for a Newtonian flow along a screw channel is,

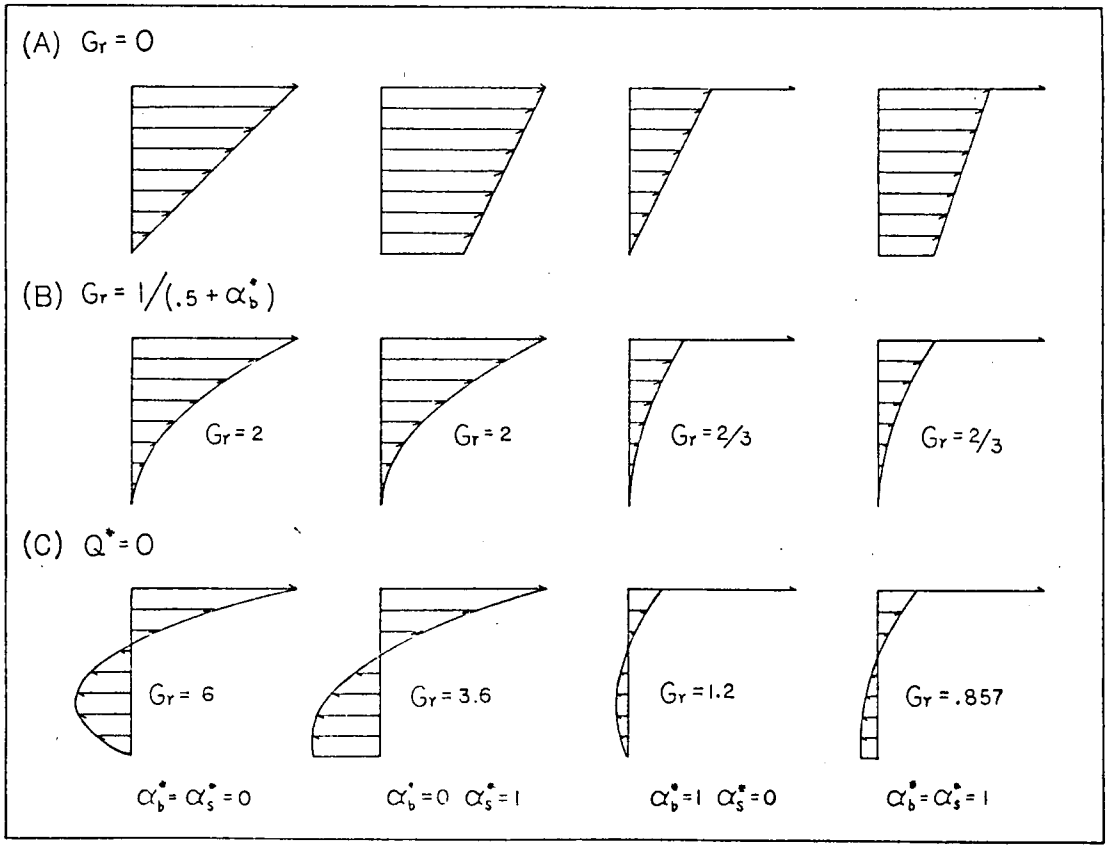

Figure 9-3. Flow patterns of isothermal flow in screw channel with various slip conditions.

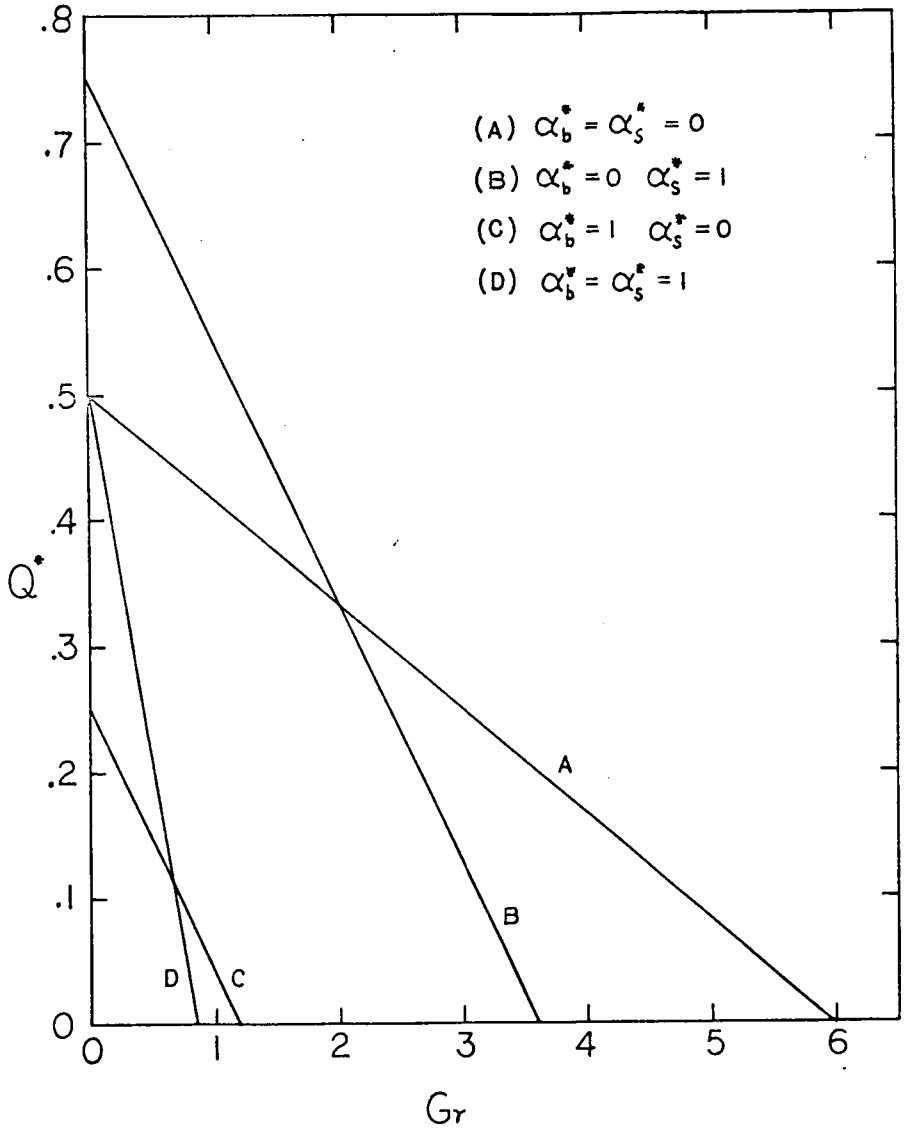

Figure 9-4. Comparison of Q^* vs. G_r behaviors of isothermal Newtonian flow at various barrel and screw surface slippage conditions.

$$\frac{\partial p}{\partial x} = \left(\frac{3 + 6\alpha_s^* - 6Q^*(1+\alpha_s^*+\alpha_b^*)}{0.5 + 2\alpha_s^* + 2\alpha_b^* + 6\alpha_s^*\alpha_b^*}\right)\left(\frac{\mu\pi DN\cos\theta}{H^2}\right) \qquad (9\text{-}27)$$

Based on Eqs. (9-18) and (9-19) a numerical computation has been performed for our 3/4" laboratory screw as an example, i.e.

$w = 1.524$ cm

$H = 0.381$ cm

$D = 1.905$ cm

$L = 76.2$ cm

$\theta = 17.7°$

$N = 50$ RPM

$\mu = 1.0 \times 10^4$ pascal-sec

The Runge-Kutta numerical scheme and a computer are used to carry out the calculation. We plot in Figure 9-5 Q^* vs. G_r for three different slip conditions: (a) $\alpha_b^o = 0$, $\alpha_s^o = 1$, (b) $\alpha_b^o = 1$, $\alpha_s^o = 0$ and (c) $\alpha_b^o = \alpha_s^o = 1$. Generally for $\underline{p}^*$ to be very large (e.g. $> 10^7 \sim 10^9$ pascal), the influence of pressure in slippage is negligible, and for small $\underline{p}^*$ (e.g. $< 10^4 \sim 10^5$ pascal), it behaves as if non-slip at surfaces.

2. Isothermal Bingham model

Our general constitutive model represented by Eq. (9-9a) can be simplified to the Bingham model as

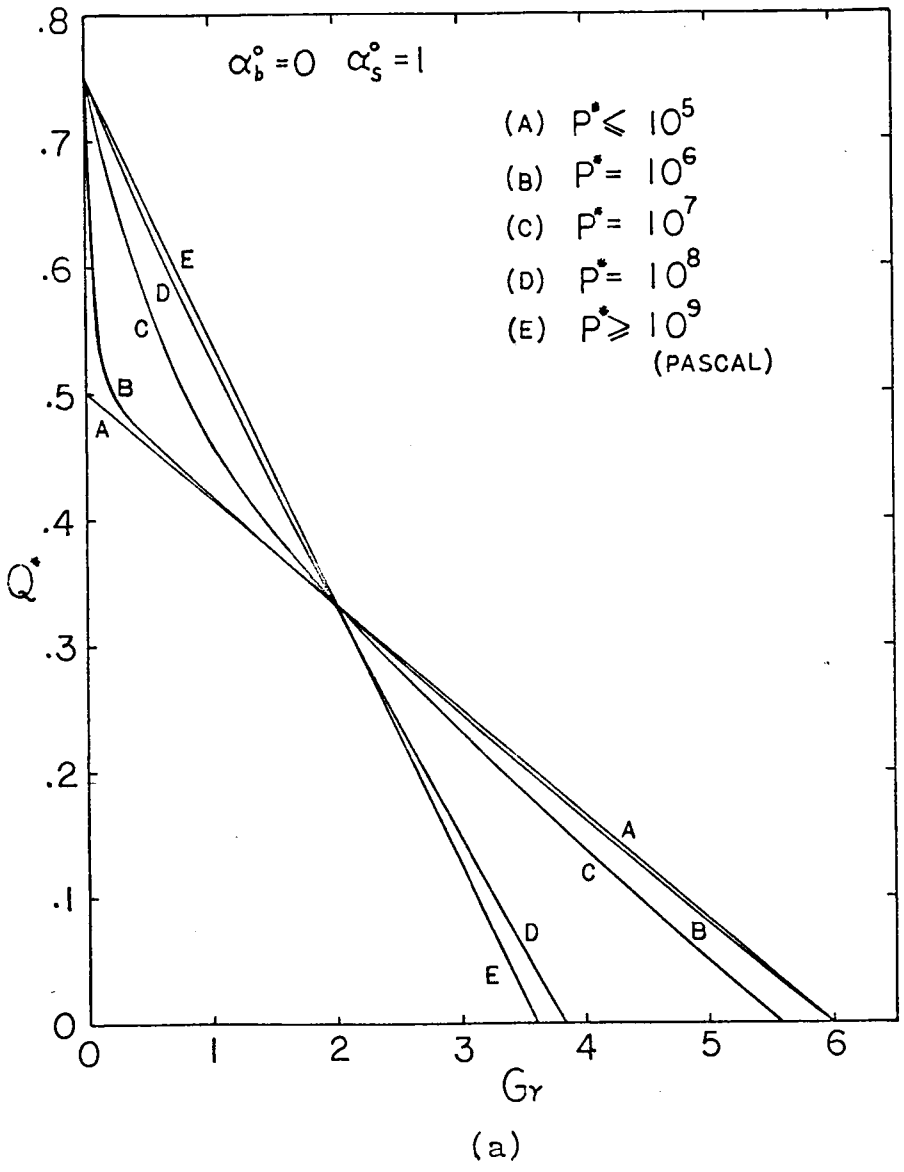

(a)

Figure 9-5. Comparison of Q^* vs. G_r behaviors of isothermal flow in screw channel with variable slip conditions.

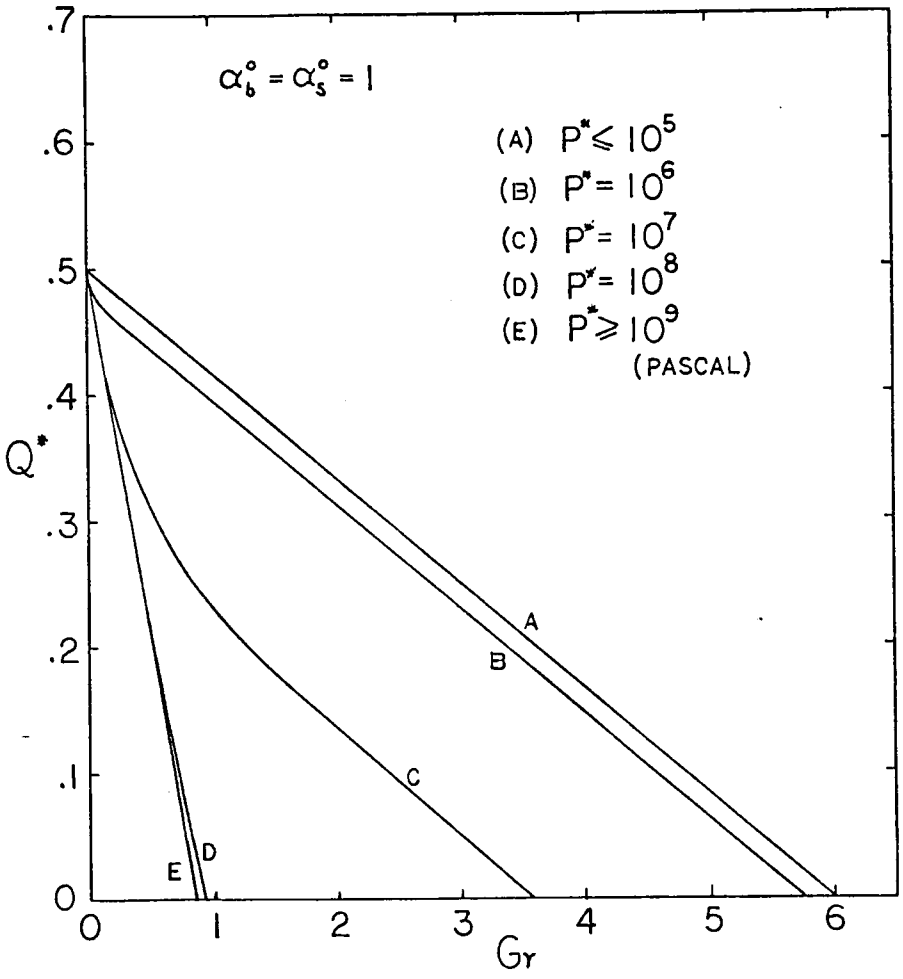

(b)

Figure 9-5. (continued)

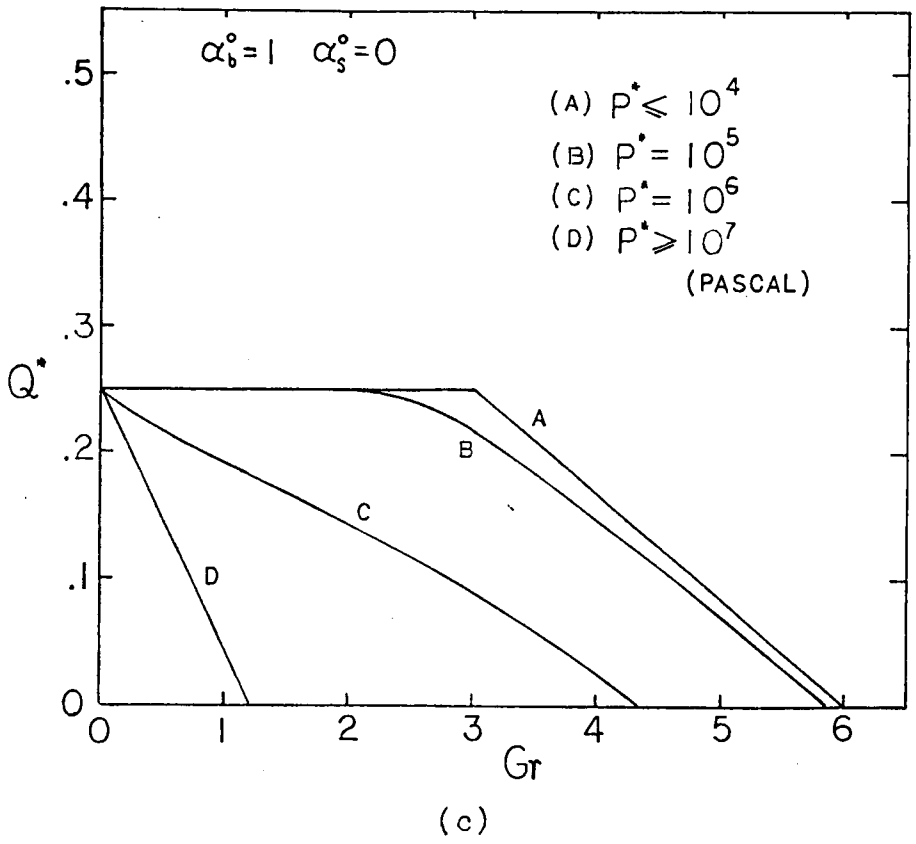

(c)

Figure 9-5. (continued)

$$\sigma_{xy} = \pm \bar{Y} + \mu\left(\frac{\partial V_x}{\partial y}\right)$$

$$\text{where} \begin{cases} + \bar{Y} \text{ for } \left(\frac{\partial V_x}{\partial y}\right) > 0 \\ - \bar{Y} \text{ for } \left(\frac{\partial V_x}{\partial y}\right) < 0 \end{cases} \qquad (9\text{-}28)$$

Screw extrusion of Bingham fluid with non-slip at wall had been studied by Mori and Ototoke (125). Here, we will generalize this problem to include slip at boundaries.

(i) For the case $(\sigma_{xy})_{y=0} > \bar{Y}$, the dimensionless velocity profile and flow rate are represented by Eqs. (9-21) and (9-22) (p. 184).

(ii) For the case $(\sigma_{xy})_{y=0} \leqslant \bar{Y}$, the dimensionless velocity profile is,

$$\bar{\mu} = \bar{C} \qquad \text{as } \bar{y} \leqslant \delta$$

$$\bar{\mu} = \frac{G_r}{6}(1-\delta)^3 + \bar{C} \qquad \text{as } \delta \leqslant \bar{y} \leqslant 1 \qquad (9\text{-}29a)$$

and the dimensionless flow rate is

$$Q^* = \frac{G_r}{6}(1-\delta)^3 + \bar{C} \qquad (9\text{-}29b)$$

where

$$\delta = 1 + \alpha_b^* = \sqrt{\alpha_b^{*2} + (2-\bar{C})/G_r}$$

$$\bar{C} = V_x\Big|_{y=o} / \pi DN\cos\theta \qquad (9\text{-}29c)$$

(iii) If both shear stresses at barrel and screw surfaces are smaller than yield value, the rubber compound will be extruded like pure plug conveying. And the velocity

of this plug will depend on shear stress at boundaries and the parameter J of Eq. (9-9a) (p. 177).

(iv) For the case $(\sigma_{xy})_{y=0} \leq -\bar{Y}$ and the dimensionless velocity profile is,

at $\delta_1 \leq \bar{y} < 1$

$$\bar{u} = 1 + G_r\left[\frac{\bar{y}^2}{2} - \delta_1\bar{y} - \alpha_b^*(1-\delta_1) - (\tfrac{1}{2}-\delta_1)\right] \quad (9\text{-}30a)$$

$$Q_1^* = (1-\delta_1) + Gr\left[\tfrac{1}{6}(1-\delta_1^3) - \tfrac{1}{2}\delta_1(1-\delta_1^2) - \alpha_b^*(1-\delta_1)^2 - (0.5-\delta_1)(1-\delta_1)\right] \quad (9\text{-}30b)$$

at $\delta_2 \leq \bar{y} \leq \delta_1$

$$\bar{u} = -G_r\delta_2\left(\frac{\delta_2}{2} + \alpha_s^*\right) \quad (9\text{-}30c)$$

$$Q_2^* = -G_r\bar{Y}'\delta_2\left(\frac{\delta_2}{2} + \alpha_s^*\right) \quad (9\text{-}30d)$$

at $0 \leq \bar{y} \leq \delta_2$

$$\bar{u} = G_r\left(\frac{\bar{y}^2}{2} - \delta_2\bar{y} - \delta_2\alpha_s^*\right) \quad (9\text{-}30e)$$

$$Q_3^* = -G_r\left(\tfrac{1}{3}\delta_2^3 + \alpha_s^*\delta_2^2\right) \quad (9\text{-}30f)$$

and the overall dimensionless flow rate is

$$Q^* = Q_1^* + Q_2^* + Q_3^*$$

where

$$\delta_1 = (0.5 + \alpha_b^* - \bar{Y}'^2/2 + \alpha_z^*\bar{Y}' - 1/G_r)/(1 + \alpha_s^* + \alpha_b^* - \bar{Y}')$$

$$\delta_2 = (0.5 + \alpha_b^* + \bar{Y}'^2/2 - \bar{Y}' - \alpha_b^*\bar{Y}' - 1/G_r)/(1 + \alpha_s^* + \alpha_b^* - \bar{Y}')$$

$$\bar{Y}' = \frac{2\bar{Y}}{(\frac{\partial p}{\partial x})\ H}$$

$$\delta_2 = \delta_1 - \bar{Y}' \qquad (9\text{-}30g)$$

Some qualitative dimensionless velocity profile of screw extrusion of a material with yield value and slip at boundaries are plotted in Figure 9-6 for various conditions.

In the above analyses, if we take $\alpha_s = \alpha_b = 0$, we will get solutions for Bingham fluid with non-slip at boundaries. In Figure 9-7, we compare Q^* vs. G_r behaviors of Newtonian and Bingham fluids at non-slip at boundaries. Figure 9-7 shows the yield value can cause higher pressure building capability. But this advantage may be cancelled out by inducing slip at boundaries due to the yield value in filled polymer systems.

3. Modelling of feed region

At the hopper where the screw is exposed, the rubber compound is pushed by the flight of the screw. The feeding rate can be represented as, for a hopper opening parallel to the screw flight:

$$Q = N\ W\ (\frac{\pi D^2}{4} - \frac{\pi(D-2h)^2}{4})/\ 2\cos\theta$$

$$= \pi NWH(D-H)/2\cos\theta \qquad (9\text{-}31)$$

for hopper opening perpendicular to the screw as shown on Figure 9-8

$$Q = \frac{\pi}{2}\ NWH\ (D-H) \qquad (9\text{-}32)$$

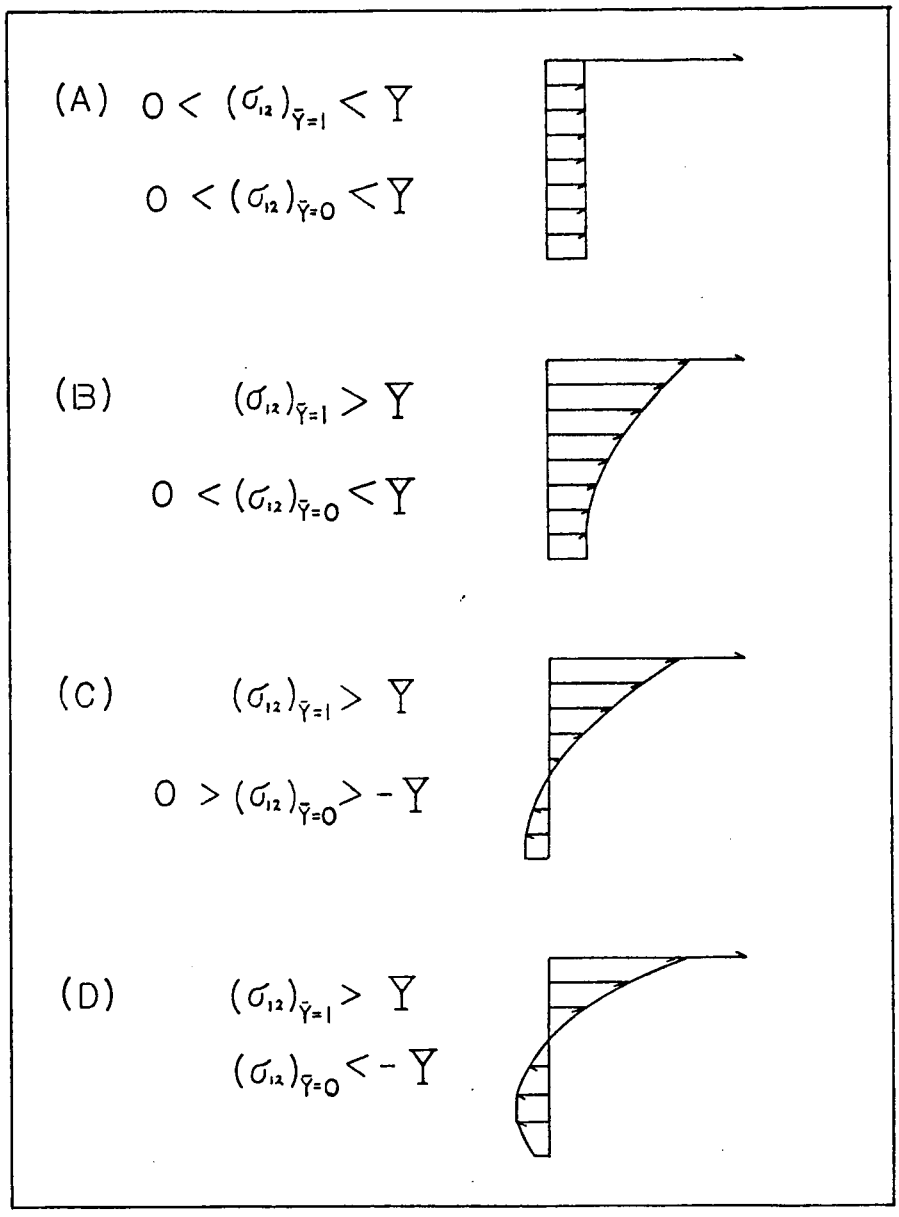

Figure 9-6. Flow patterns of Bingham fluid in a screw channel at various conditions.

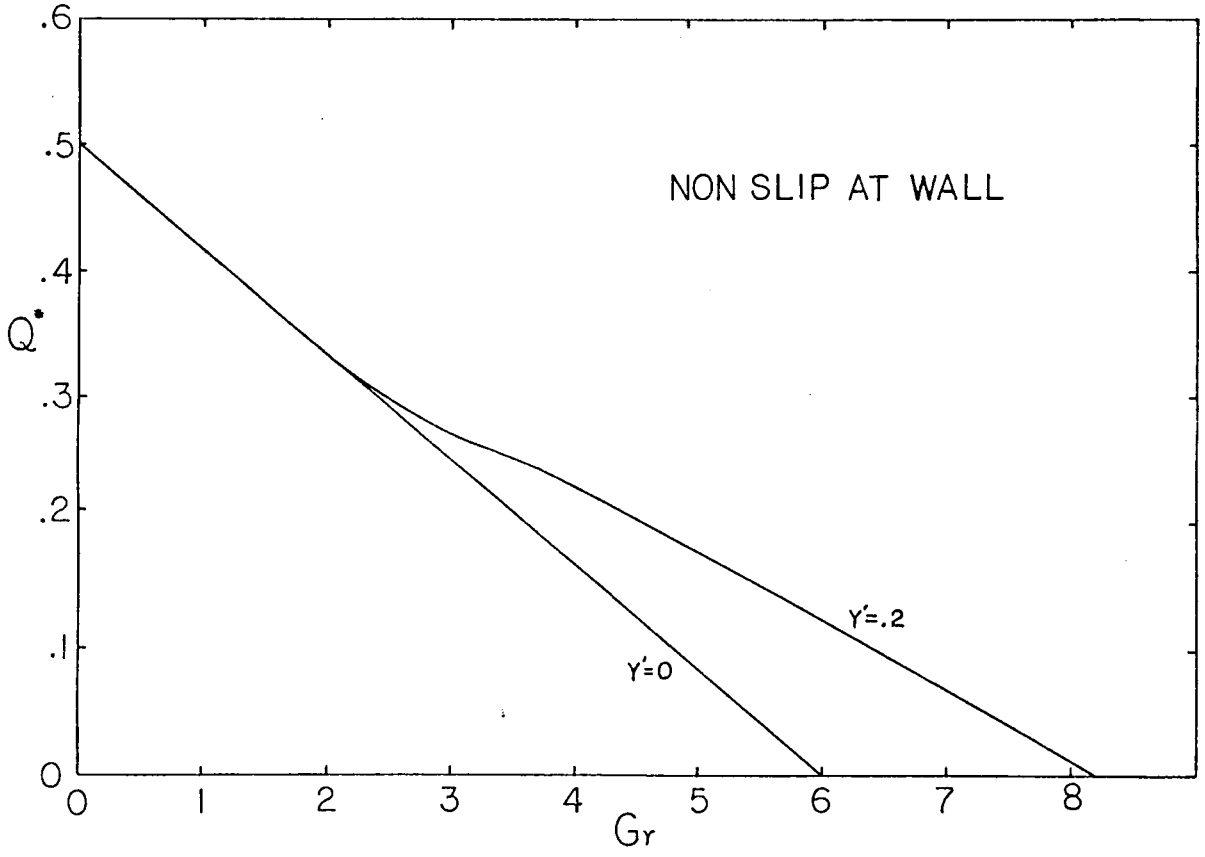

Figure 9-7. Comparison of Q^* vs. G_r behaviors between Newtonian and Bingham fluid and non-slip at wall.

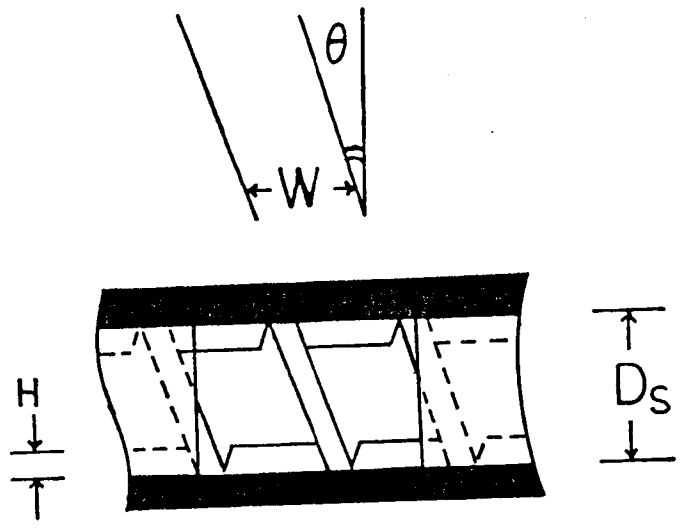

Figure 9-8. Rectangular opening at the screw hopper.

Eq. (9-31) represents the feeding rate at the hopper before going into the extruder and has a form very close to a pure drag flow in the extruder. This feeding mechanism from a normal push by the screw flight may cause a problem in extruding rubber compounds. Unlike plastic pellets or powders, rubber compounds studied here are not loose particles but a continuous body with contact on both barrel and screw surfaces and, therefore, the barrel driving mechanism which should drive the rubber compound foreward in the helical direction tends to take place immediately after the flight normal pushing feed mechanism. This means the same surface of barrel right next to the hopper to be a resistant surface for the feeding mechanism and a driving surface for the plug conveying mechanism. And, since these two driving mechanisms are perpendicular and conflicting to each other, we may get a poorer pumping capacity in the screw extrusion of rubber compounds.

C. EXPERIMENTAL

1. Experimental procedure

The instrument used in this study is a Brabender extruder which has been described in detail in Chapter 3. The materials used here are tread and side-wall SBR compounds as described in Chapter 3 and Chapter 8. They were fed into the hopper of the extruder at hot or cold temperature and at irregular pieces or longitudinal strips.

Hot feed is done by heating the rubber compounds in a heated steel box to the temperature about 80°C before feeding into the hopper. Cold feed is done by feeding compounds into the hopper at room temperature (about 30°C).

The temperature at the die surface was controlled at 100°C. The barrel surface was controlled at 100°C (hot barrel) or 30°C (cold barrel) by circulating constant flow rate cooling water and automatically adjusted electric heating on the barrel surface.

Two plastics, polystyrene (Dow Styron 678U) and polypropylene (Hercules 6523F), were studied for comparison, in both cases barrel and die at 200°C. Data of output rate (cm^3/min), head pressure (psi) and rotation speed (RPM) were recorded. The output rate was determined by first measuring the weight in an extrusion period of about 1-5 min. This gave the quantity in gram/min. It was then divided by density at 100°C (1.11 g/cm^3 for tread and 1.08 g/cm^3 for side wall compounds). The head pressure is the pressure at the end of the screw at the entrance of the die which is shown on a 10,000 psi pressure gauge. The rotation speed is shown on a tachometer which is rotating at the same speed as the shaft by a connected chain belt.

The temperature of the materials should vary from the hopper to the die, and from the barrel surface to the screw. But it is difficult to measure any temperature profile.

2. Results

The tread compound is hard and dry. It is easier to feed in as a continuous strip or short strips with longitudinal shape. It is more difficult to feed it in irregular shaped pieces. We ran experiments by feeding tread compound as both long strips and irregular shaped pieces under different conditions (i.e. cold feed and hot feed) and extruder barrel temperatures. The side wall compound is soft and sticky. It is difficult to feed manually in long strips in our laboratory extruder. We have to tear this compound into small pieces and quickly feed into the hopper manually.

We plot (a) output rate vs. screw speed (RPM), (b) head pressure vs. screw speed in Figure 9-9 for tread compounds and in Figure 9-10 for side wall compounds with various feed conditions and barrel temperatures. Generally, we found (i) that barrel temperature has no significant influence on the final output rate although the head pressure in cold barrel extrusion is substantially higher than that of hot barrel, (ii) hot feed pieces shows higher output rate than for cold feed pieces, (iii) cold feed strips shows the highest output rate for the tread compound. We also fed some strips at side wall compound even although we could not get a complete set of data due to a sticking problem. Feeding side wall compound in strips shows a little higher output rate than feeding in

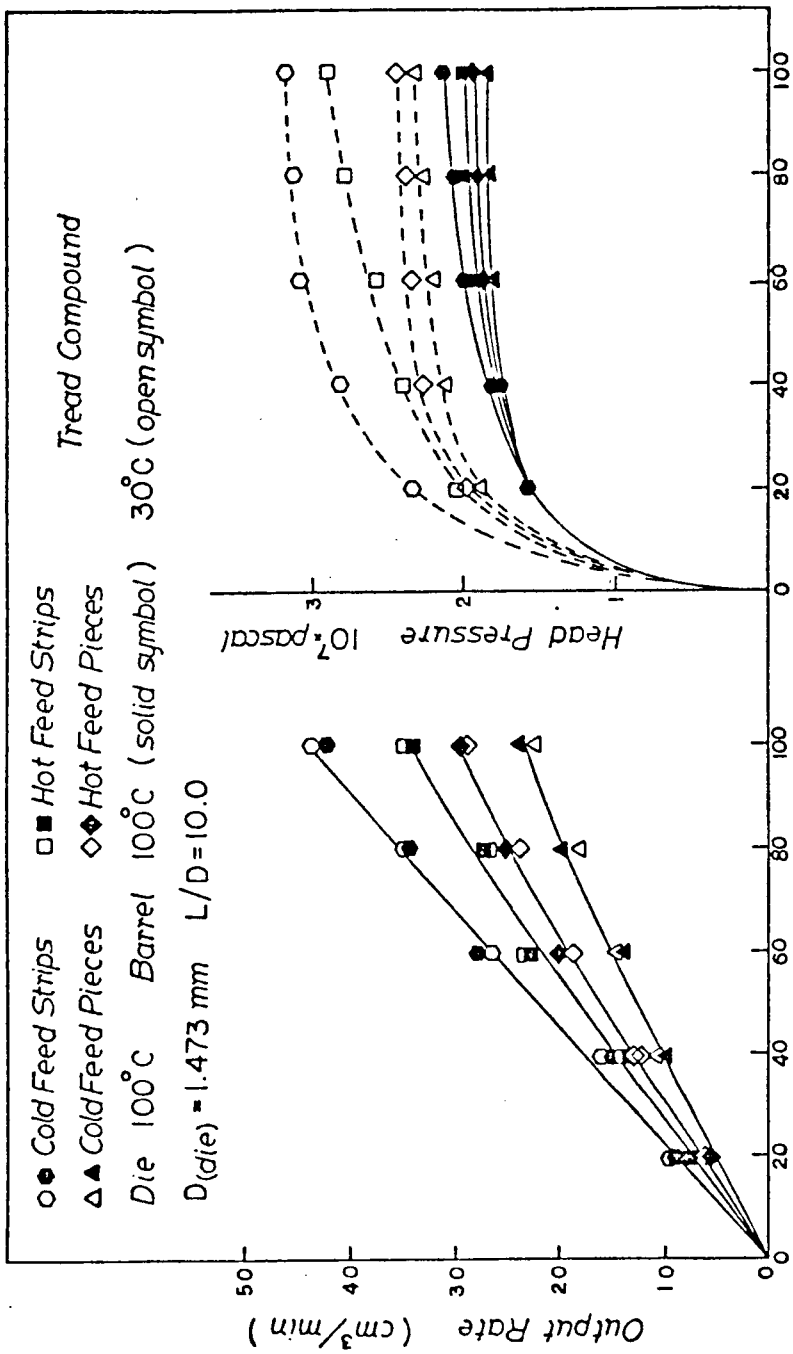

Figure 9-9. (a) Output rate-RPM (b) head pressure-RPM behaviors for the screw extrusion of tread compound at various conditions.

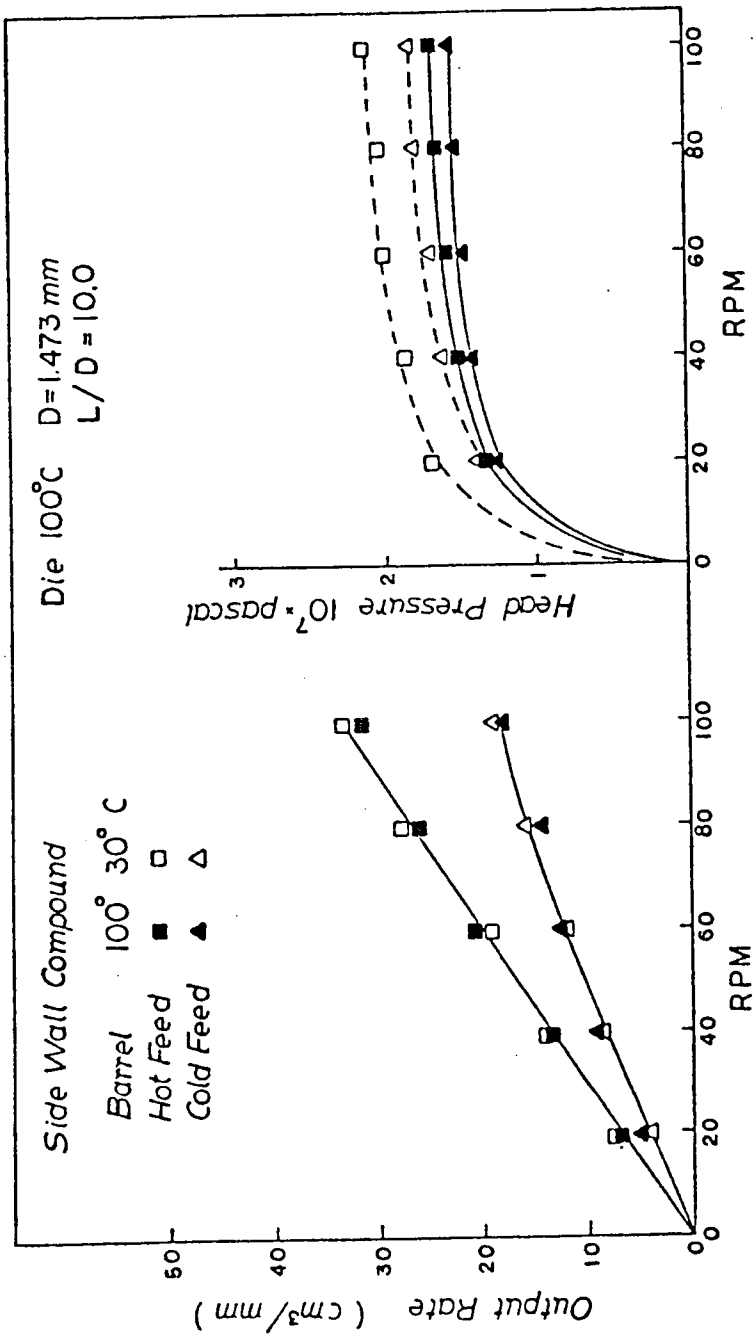

Figure 9-10. (a) Output rate-RPM (b) head pressure-RPM behaviors for the screw extrusion of side wall compound at various conditions.

irregular shaped pieces. It is not as significant for extruding tread compounds. These results are shown in Figure 9-11 to 9-15.

Extrusion experiments were carried out for polystyrene and polypropylene. The results are shown in Figures 9-16 and 9-15. Generally, the plastics show higher output rate and lower head pressure.

D. DISCUSSION

From the experimental results a few pieces of evidence have revealed that the screw extrusion of rubber compounds is quite different from the screw extrusion of plastics. The changing output rate corresponding to changes in methods of feeding confirms our suggestion that the feeding and plug conveying zone is the critical region to the screw extrusion of rubber compounds.

We compare our experimental results by using dimensionless flow rate Q^* as defined by Eq. (9-23) (p.184). Since, our experimental data were collected from a small 3/4" in screw extruder, we may approximately take the barrel temperature to be the polymer temperature and use G_b to be the dimensionless pressure gradient,

$$G_b = G e^{a(T_b - T_o)} \tag{9-33}$$

where T_b is the barrel temperature and a is the temperature

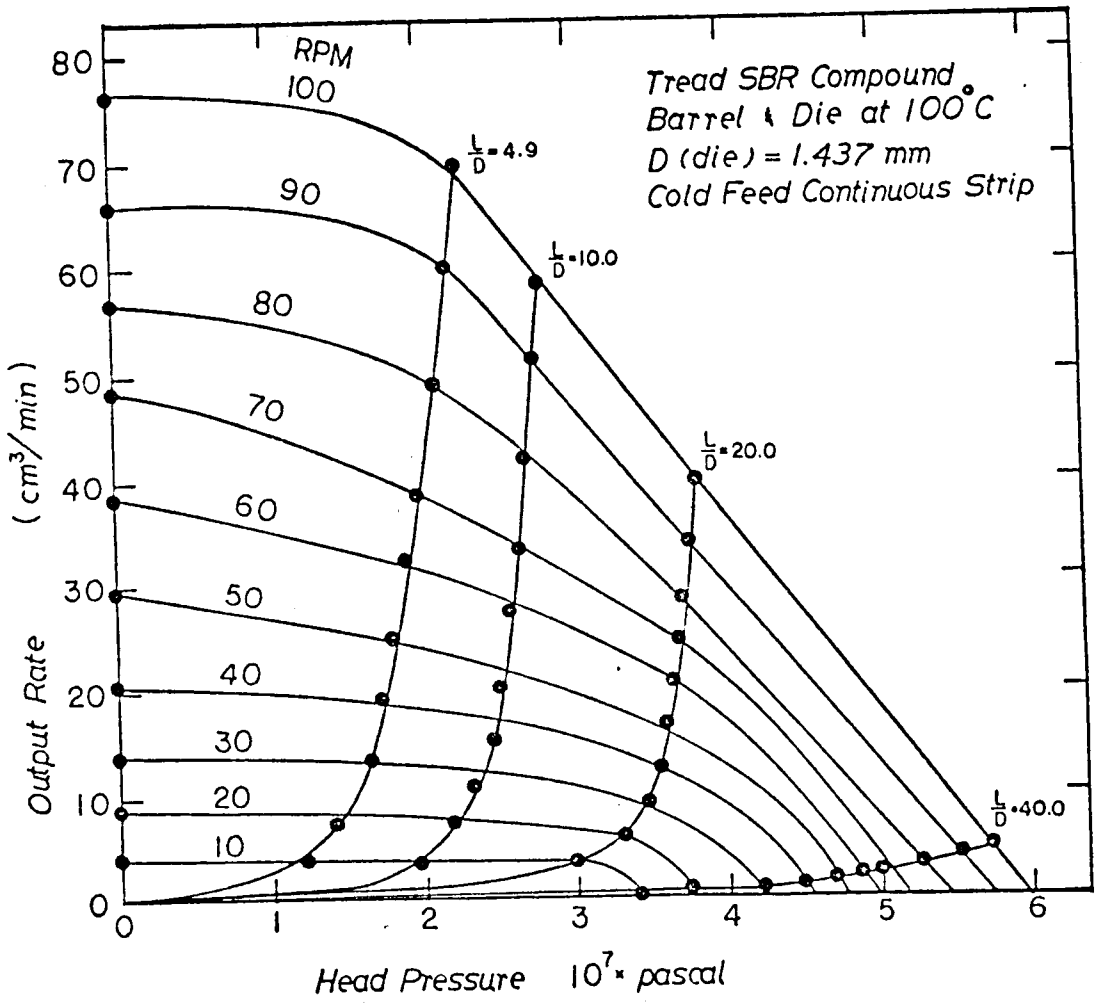

Figure 9-11. Output rate-head pressure behaviors for cold feed continuous strip of tread compound at various RPM.

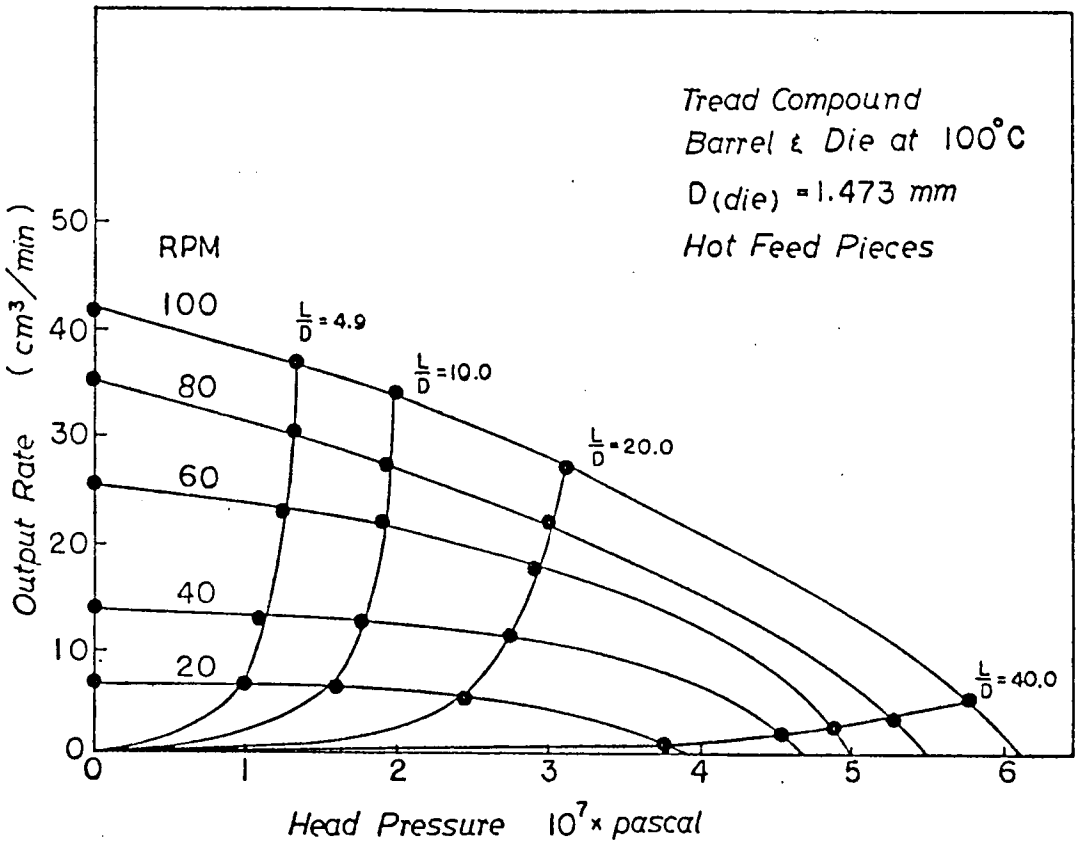

Figure 9-12. Output rate-head pressure behaviors for hot feed pieces of tread compound at various RPM.

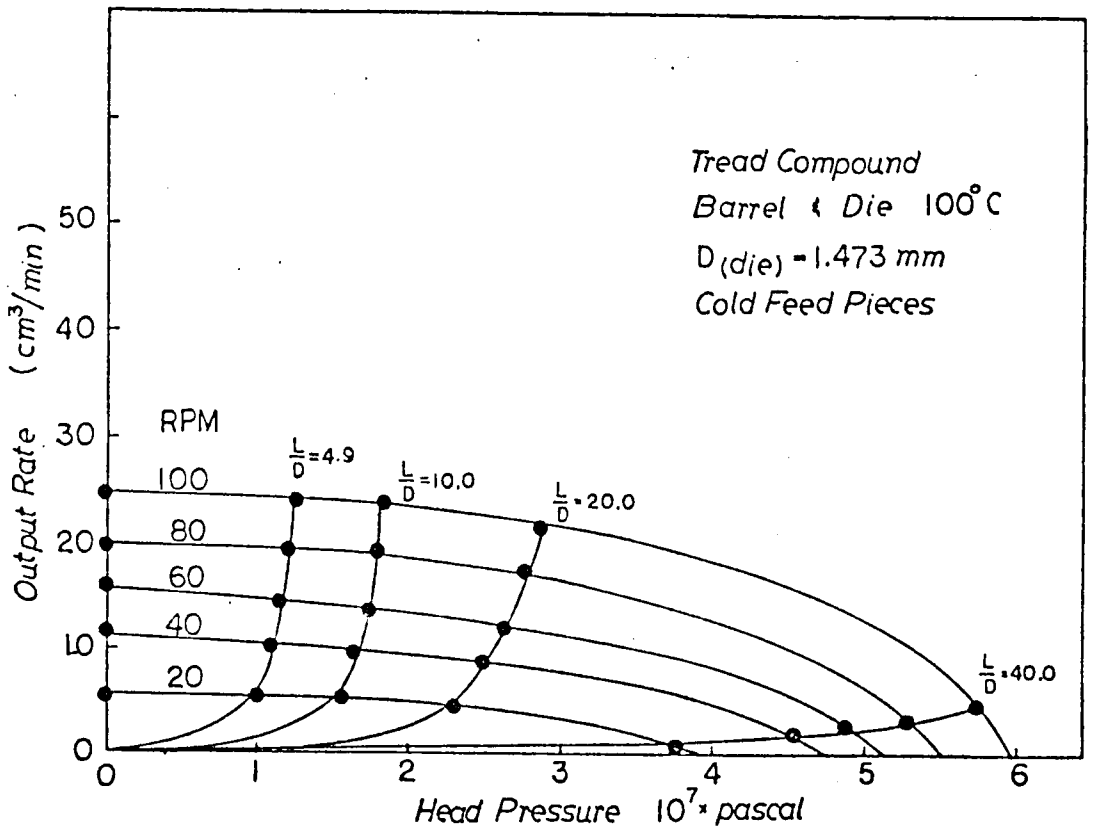

Figure 9-13. Output rate-head pressure behaviors for cold feed pieces of tread compound at various RPM.

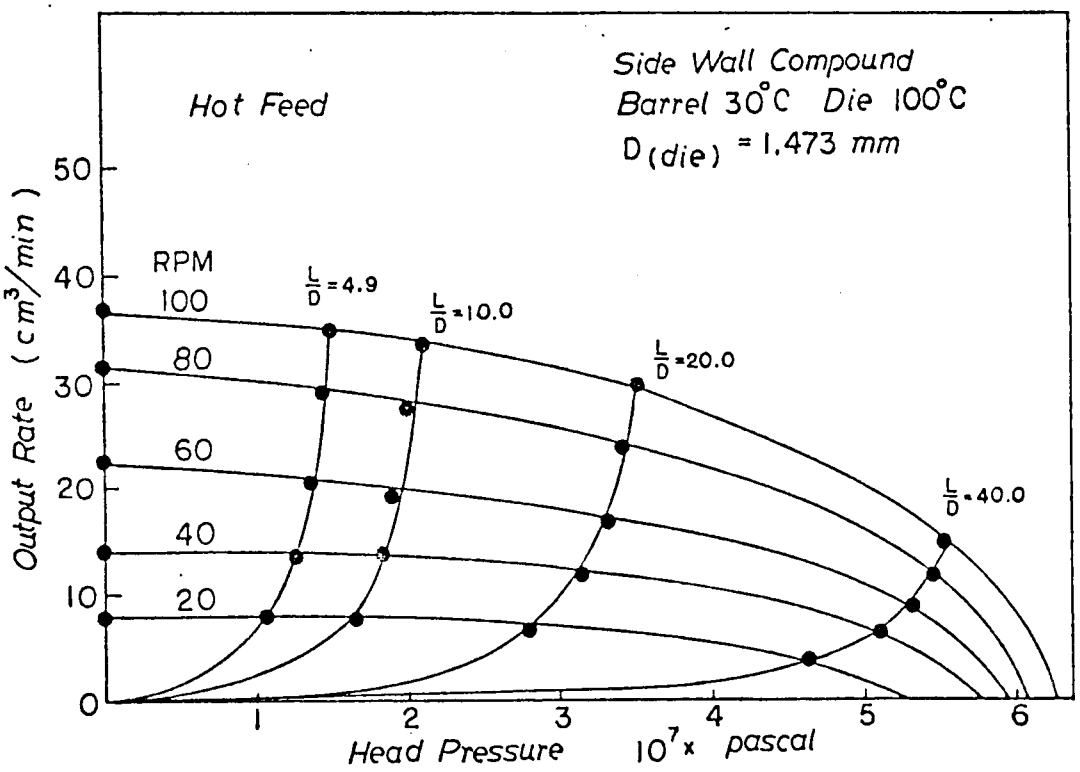

Figure 9-14. Output rate-head pressure behaviors for hot feed side wall compound at various RPM.

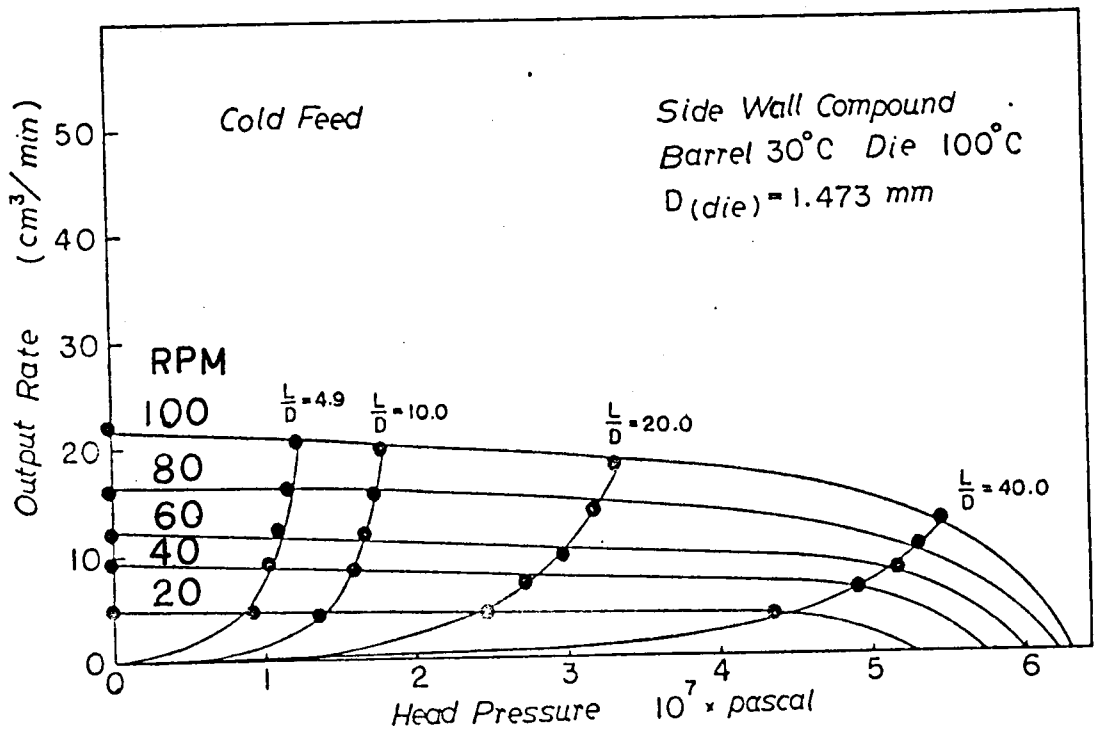

Figure 9-15. Output rate-head pressure behaviors for cold feed side wall compound at various RPM.

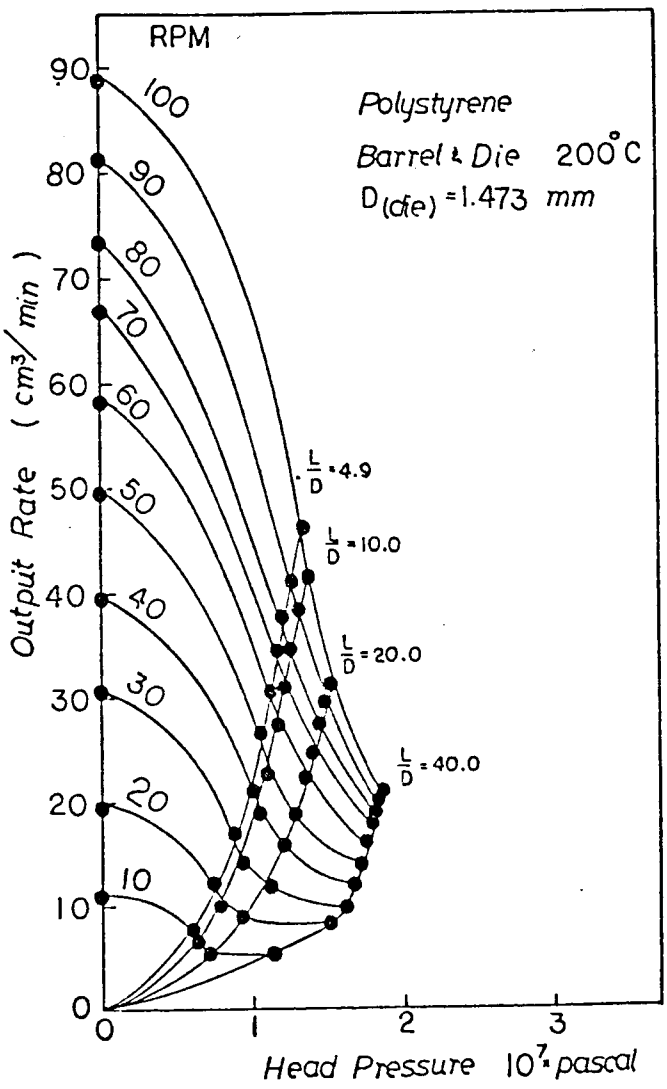

Figure 9-16. Output rate-head pressure behaviors for polystyrene.

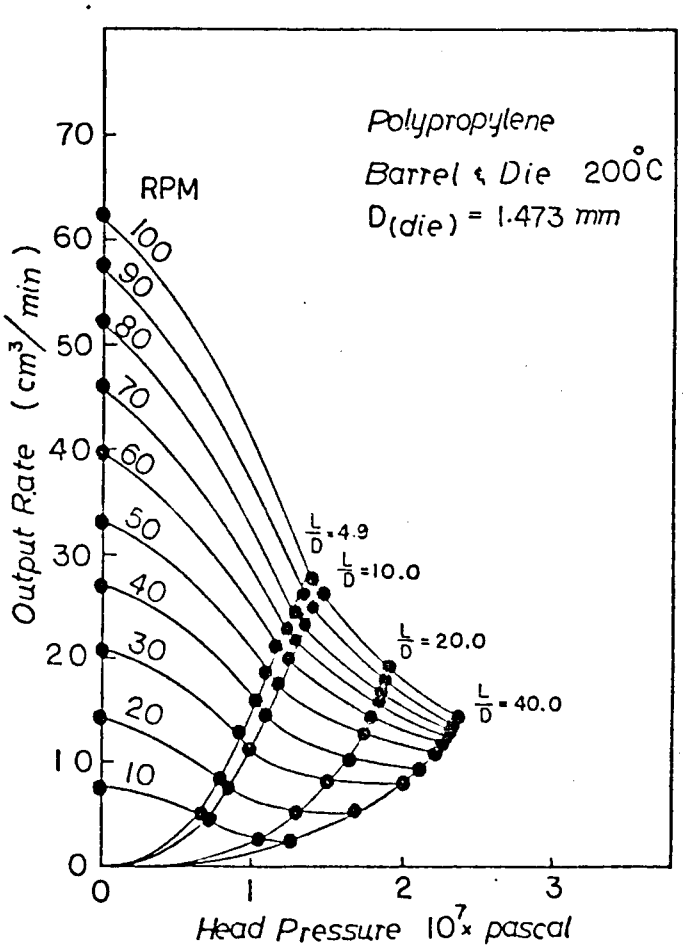

Figure 9-17. Output rate-head pressure behaviors for polypropylene.

sensitivity. G is defined as in Eq. (9-16) (p. 183). The actual G_b formulations found for the various materials are:

$$G_b = 0.722 \times 10^{-7} \Delta p/N^{0.235} \quad \text{(tread compound)}$$

$$G_b = 0.916 \times 10^{-7} \Delta p/N^{0.292} \quad \text{(side wall compound)}$$

$$G_b = 2.35 \times 10^{-7} \Delta p/N^{0.357} \quad \text{(polystyrene)}$$

$$G_b = 2.31 \times 10^{-7} \Delta p/N^{0.389} \quad \text{(polypropylene)} \qquad (9\text{-}34)$$

where Δp is head pressure in pascal and N is rotation speed in RPM.

In Figure 9-18, we compare Q^* vs. G_b behavior for cold feed continuous strip of tread compounds at different RPM. We found increasing screw speed N increases Q^* at lower G_b (<1). This phenomenon is very significiant for the tread compound but not as much for the side wall compound. We also plotted Q^* vs. G_b for various feeding conditions at 60 RPM in Figure 9-19 for the tread compound and Figure 9-20 for the side wall compound. In feeding irregular shape pieces of both tread and side wall compounds, we found hot feed has higher Q^* than cold feed. It is very striking to note here that the method of feeding can change Q^* significantly. Higher Q^* for continuously fed strips of rubber compounds (especially tread compound) may be due to stretch forces induced in this type feeding which promote the extrusion rate. In feeding as irregular

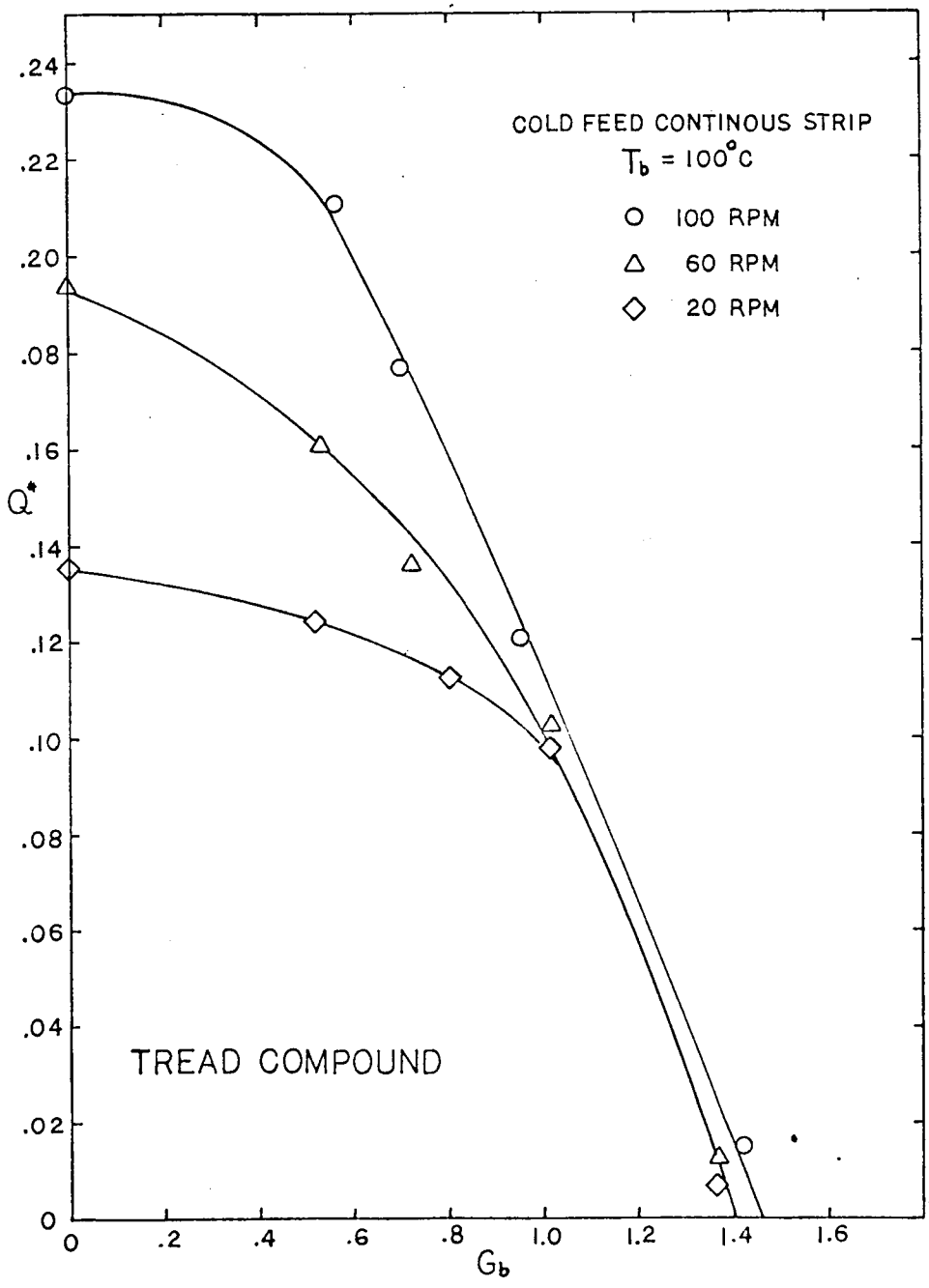

Figure 9-18. Comparison of Q^* vs. G_b behaviors of cold feed continuous strip at various RPM.

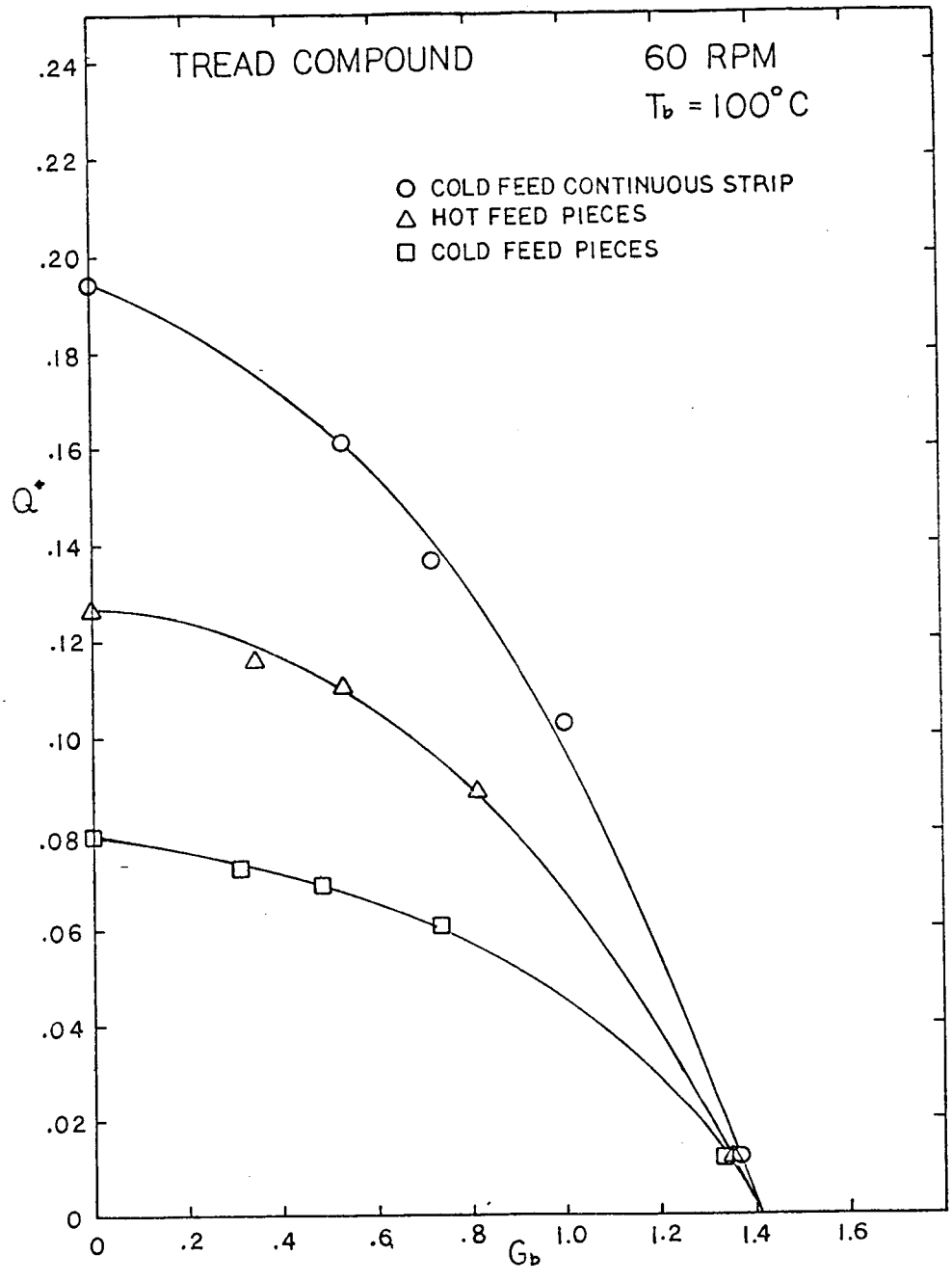

Figure 9-19. Comparison of Q^* vs. G_b behaviors of tread compound at 60 RPM and various feeding conditions.

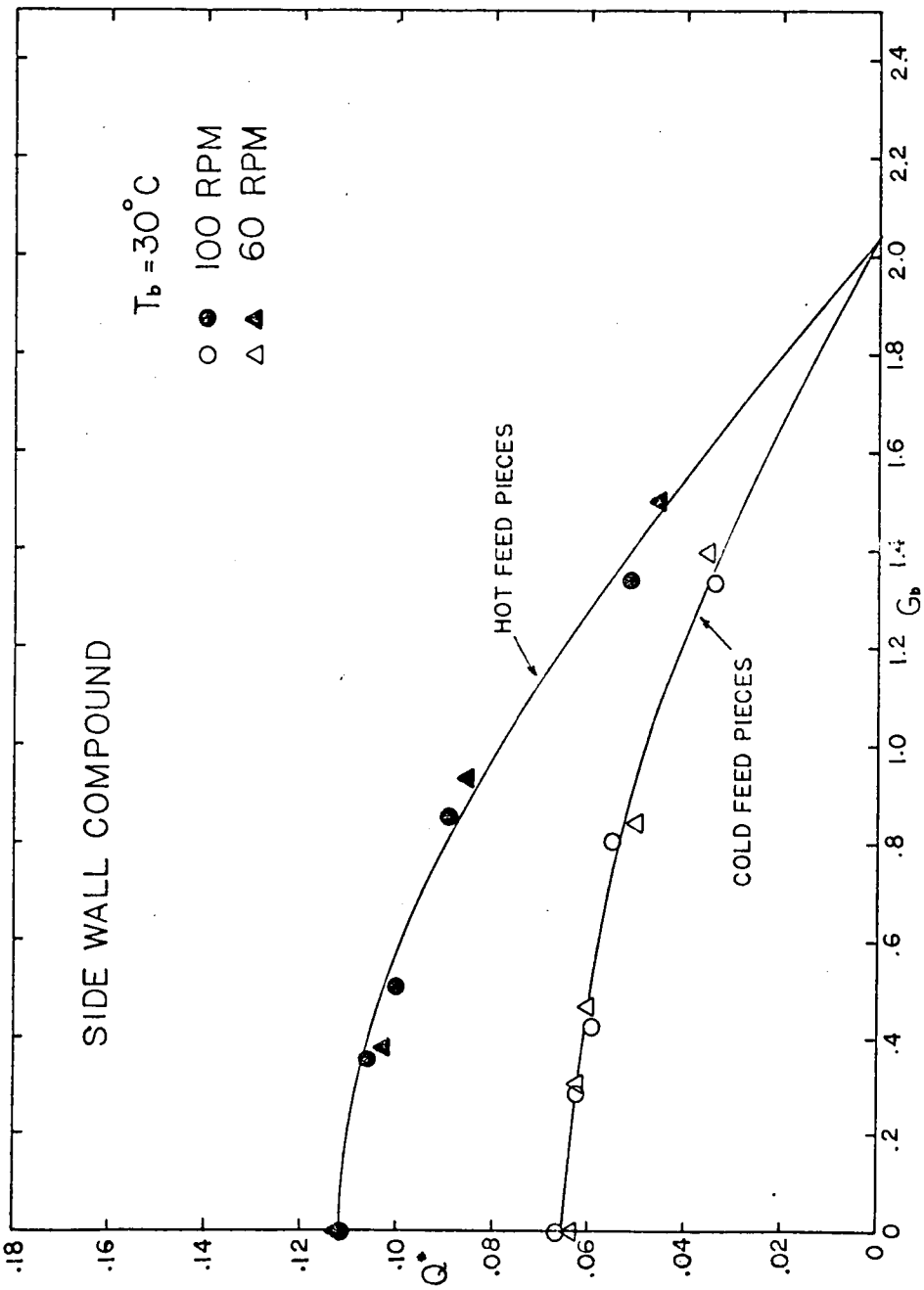

Figure 9-20. Comparison of Q^* vs. G_b behaviors of side wall compound at various RPM and feeding conditions.

pieces, the higher Q^* in hot feed than in cold feed is probably due to less slip of the rubber compounds at the higher material temperature.

Comparing experimental results in Figure 9-18 to 9-20 with theoretical curves in Figure 9-3 (p. 186) suggests the existence of slip at boundaries. The experimental data are for non-isothermal operations. Near the hopper, rubber compounds are colder and have higher viscosity and higher yield values. However, the interface parameter J may not change very much at this lower temperature because as we change barrel temperature, we do not observe significant change in pumping performance.

In feeding rubber compounds, we observed a back flow at the leading edge of hopper as shown in Figure 9-21 where a long strip of rubber compound is fed into the screw channel on the left side of the hopper. The right side of the hopper which precedes the plug conveying zone is filled with a back flow of compound. This backup flow may also be due to poorer pumping capacity at the plug conveying region next to the hopper.

We compare Q^* vs G_b behaviors of polystyrene in Figure 9-22 and polypropylene in Figure 9-23. Since the screw used in this study has constant channel depth, the extrusion of PS and PP here from peaking densities considerations must be controlled by the solid conveying zone.

(a)

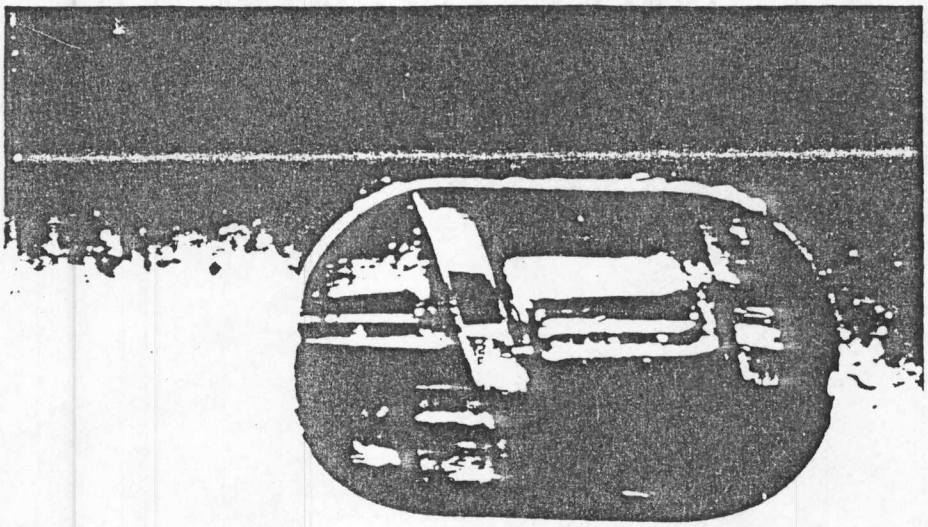

(b)

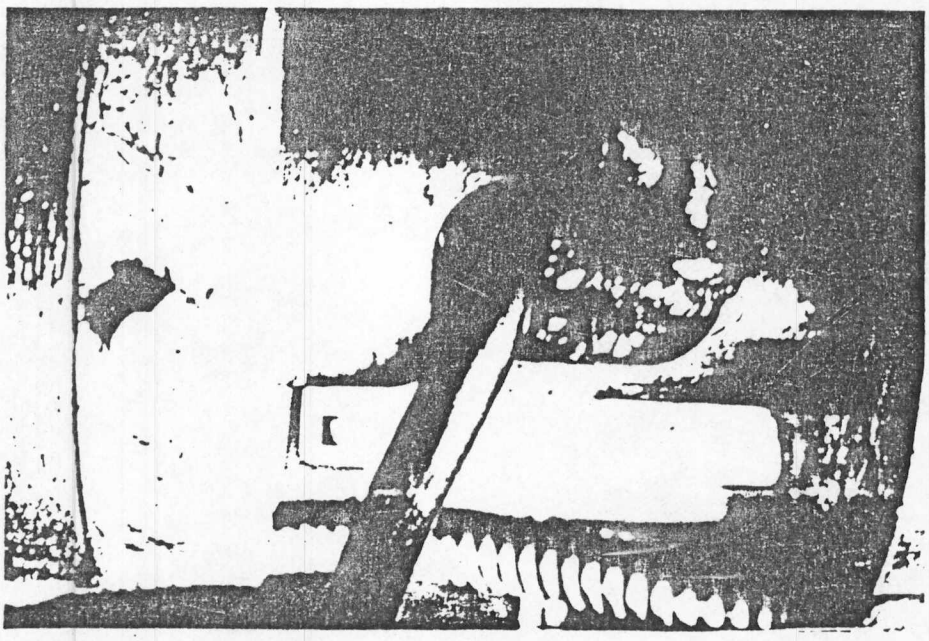

Figure 9-21. (a) Screw opening (b) backup flow at screw opening of rubber compounds.

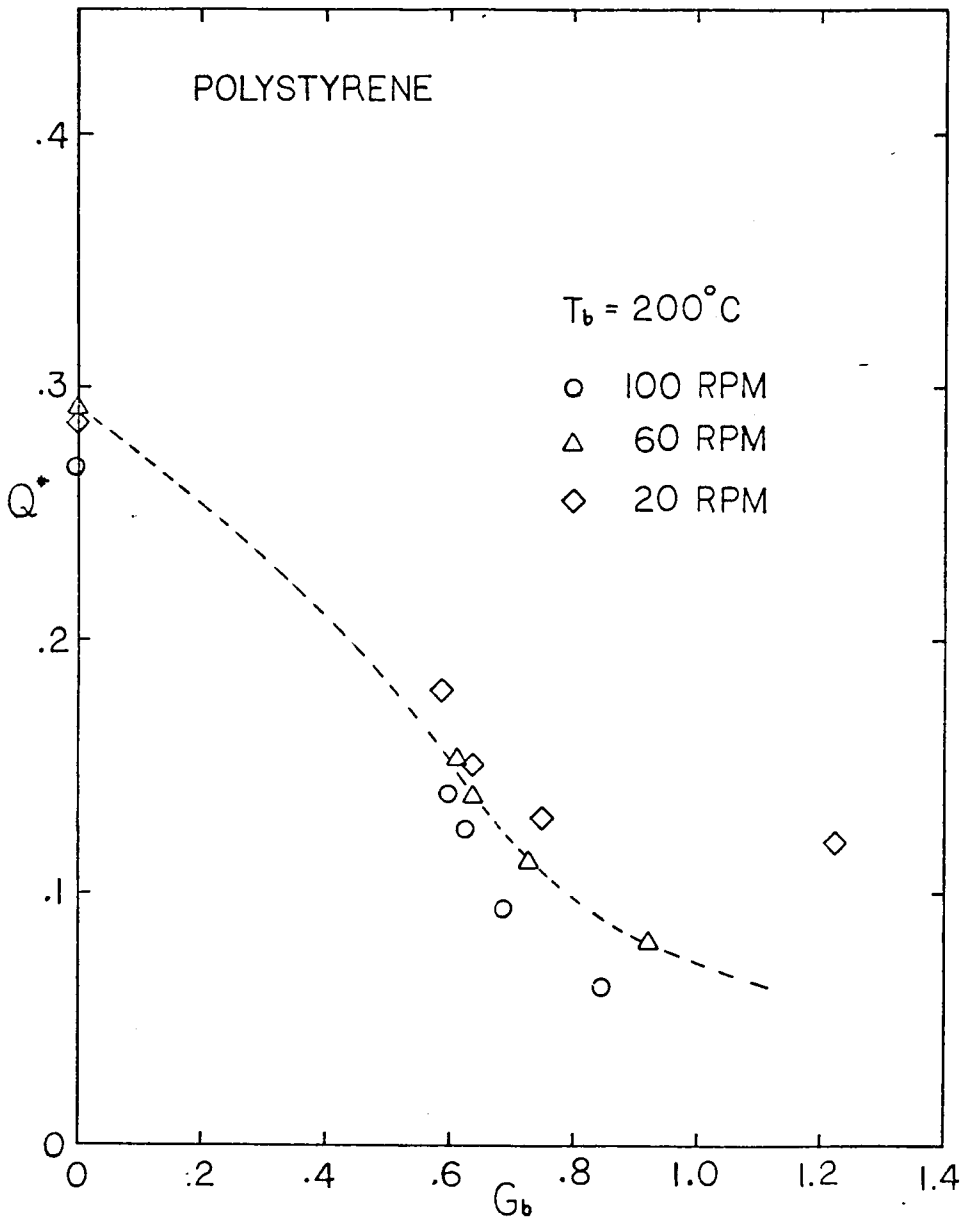

Figure 9-22. Q^* vs. G_b behaviors of polystyrene at various RPM.

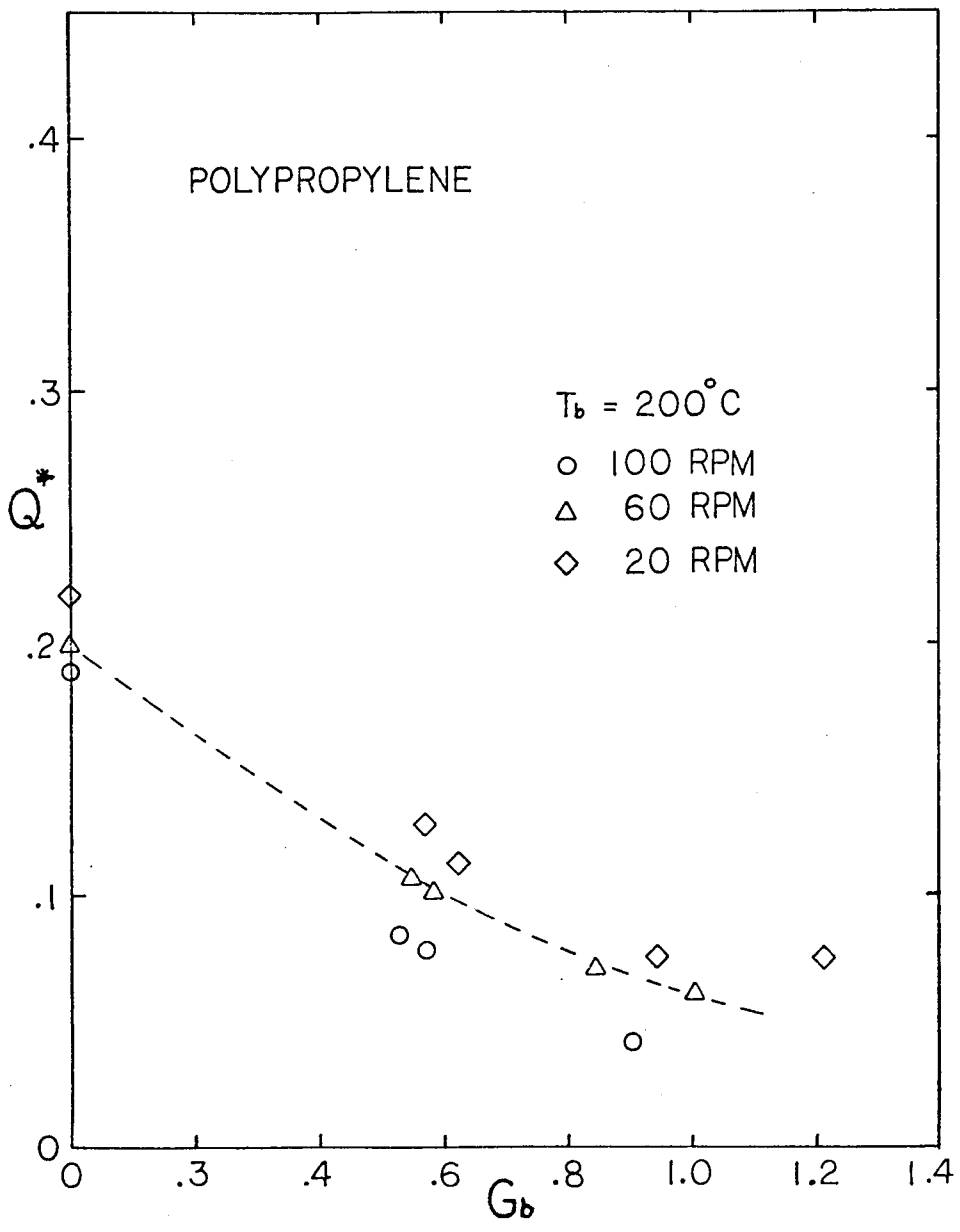

Figure 9-23. Q^* vs. G_b behaviors of polypropylene at various RPM.

Generally, increasing RPM decreases Q^*, opposite to the observation in the extrusion of cold feed continuous strip of tread compound as shown in Figure 9-18 (p. 212), which may be the result of a lower friction coefficient between barrel-pellet and pellet-pellet interfaces at higher screw RPM.

Polystyrene shows higher Q^* (0.3) than polypropylene (0.2) at $G_b = 0$ which is consistent with higher friction coefficient measured in polystyrene than that in polypropylene by Chung el al (45).

E. CONCLUSIONS

1. A theoretical model of screw extrusion based on a constitutive equation of filled polymer melts includes a yield value and slip at boundaries is proposed for the screw extrusion of rubber compounds. It is predicted in the theory, that higher viscosity and larger yield value in the polymer matrix which depend on the filler loading and temperature cause higher slip at boundaries. This seems to be observed in experiments on the screw extrusion of rubber compounds as higher pumping rates result for the feeding of hot pieces compounds compared to the feeding of cold pieces compounds.
2. It is the plug conveying region which starts at the edge of hopper controls the pumping capacity in the

screw extrusion of rubber compounds. Because in this region, rubber compounds have lower temperature, higher viscosity, higher yield value and, therefore, higher slip at barrel and screw surfaces.

3. The feeding mechanism is complicated and also very important to the pumping performance of the screw extrusion of rubber compounds.

LIST OF REFERENCES

LIST OF REFERENCES

1. Andrews, R. D., N. Hofman-Bang and A. V. Tobolsky, J. Poly. Sci., 3, 669 (1948).

2. Arai, T. and H. Toyoda, Proc. 5th Int. Cong. Rheol., ed. by S. Onogi, 4, 461 (1970).

3. Arnold, K. R. and J. R. Street, Proc. 5th Int. Cong. Rheol., ed. by S. Onogi, 4, 377 (1970).

4. Bagchi, A. K. and K. K. Sirkar. "Extrusion Die Swell of Carbon Black Filled Natural Rubber". Chem. Eng. Dept. of Indian Institute of Technology (1978).

5. Bagley, E. B., J. Appl. Phys., 624 (1957).

6. Bagley, E. B. and A. M. Birks, J. Appl. Phys., 31, 556 (1960).

7. Bagley, E. B., A. M. Birks and H. P. Schrieber, J. App. Poly. Sci., 4, 362 (1960).

8. Bagley, E. B. and J. J. Duffey, Trans. Soc. Rheol., 14:4, 545 (1970).

9. Bagley, E. B. and H. P. Schreiber, Trans. Soc. Rheol., 5, 341 (1961).

10. Bagley, E. B., S. H. Storey and D. C. West, J. Appl. Polym. Sci., 7, 1661 (1963).

11. Ballenger, T. F., I. J. Chen, J. W. Crowder, G. E. Hagler, D. C. Bogue, and J. L. White, Trans. Soc. Rheol., 15, 1949 (1971).

12. Ballenger T. F. and J. L. White, Chem. Eng. Sci., 25, 1191 (1970).

13. Ballenger, T. F. and J. L. White, J. Appl. Poly. Sci., 15, 1949 (1971).

14. Barr, R. A. and C. I. Chung, SPE J., 6, 71 (1966).

15. Bernhardt, E. C. and J. M. Mckelvey, SPE J., 10, 419 (1954).

16. Bernstein, B., E. A. Kearsley and L. J. Zapas, Trans. Soc. Rheol., 7, 391 (1963).

17. Bernstein, B., E. A. Kearsley and L. J. Zapas, J. Res. Nat. Bur. Stand., 68B, 103 (1964).

18. Bialas, G. A. and J. L. White, Rubber Chem. & Techn., 42, 3, 675 (1969).

19. Bingham, E. C., "Fluidity and Plasticity". New York, McGraw-Hill, (1922).

20. Bird, R. B., SPE J., 11, (7), 35 (1955).

21. Bird, R. B. and P. J. Carreau, Chem Eng. Sci., 23, 427 (1968). Carreau, P. H., Trans. Soc. Rheol., 16, 99 (1972).

22. Bird, R. B., M. W. Johnson and J. F. Stevenson, Ed. by S. Onogi, Proc. 5th Inst. Conger. Rheol. p. 159. Baltimore, University Park Press, (1970).

23. Bird, R. B., W. E. Stewart, and E. N. Lightfoot, "Transport Phenomena". New York, John Wiley & Sons, (1966).

24. Bogue, D. C., Ind. Eng. Chem. Fund., 5, 253 (1966).

25. Bogue, D. C., Class lecture "Non-Newtonian Fluid Mechanic", Polymer Engineering 5210, The University of Tennessee.

26. Bogue, E. C. and J. L. White, "Engineering Analysis of Non-Newtonian Fluids", NATA Agardograph #144 (1970).

27. Boles, R. L., Ph.D. Dissertation, Dept. of Chem. & Met., U. T. Knoxville (1967).

28. Boles, R. L., H. I. Davis, and D. C. Bogue, Poly. Eng. Sci., 10, 24 (1970).

29. Boltzmann, L. S., Sitzurgber Akad. Wiss. Wien, 70, 275 (1874).

30. Bond, W. N., Phil. Mag., 42 (7), 365 (1951).

31. Boonstra, B. B., "Rubber Technology", 2nd ed., ed. by M. Morton. New York, Van Nostrand, (1970).

32. Boussinesq, M. S., Math. Pures. Appl. 13, 377 (1868).

33. Brinkman, H. C., Appl. Sci. Res., A2, 120 (1951).

34. Brinkman, H. C., J. Chem. Phys., 20, 571 (1952).

35. Broyer, E. and Z. Tadmor, Poly. Eng. Sci., 12, 12 (1972).

36. Carley, J. F., R. S. Mallouk, and J. M. Mckelvey, Ind. Eng. Chem., 45, 974 (1953).

37. Carley, J. F. and J. M. Mckelvey, Ind. Eng. Chem., 45, 989 (1953).

38. Chan, Y., J. L. White and Y. Oyanagi, Poly. Eng. Sci., 18, 268 (1978).

39. Chang, H., and A. S. Lodge, Rheol. Acta., 11, 127 (1972).

40. Chen, I. J.,and D. C. Bogue, Trans. Soc. Rheol. 16, 59 (1972).

41. Chen, I. J., E. E. Hagler, L. E. Abbott, D. C. Bogue and J. L. White, Trans. Soc. Rheol., 16, 473 (1972).

42. Chou, S. I. and A. C. Pipkin, Acta. Mech., 14, 164 (1967).

43. Chung, C. I., Mod. Plastics, 45, 178 (1968).

44. Chung, C. I., SPE J., 26, (5), 32 (1970).

45. Chung, C. I., W. J. Hennessey and M. H. Tusim, Poly. Eng. Sci., 17, (1), 9 (1977).

46. Chung, C. I., R. J. Nichols and G. A. Kruder, Poly. Eng. Sci., 14, (1), 28 (1974).

47. Clegg, P. L., Brit. Plastics, (February), 96 (1966).

48. Cogswell, F. N., Rheol. Acta., 8, 187 (1968).

49. Cogswell, F. N., Rheol. Acta., 8, 190 (1969).

50. Cogswell, F. N., Trans. Soc. Rheol., 16, 383 (1972).

51. Cogswell, F. N., Polym. Eng. Sci., 12, 64 (1972).

52. Cogswell, F. N., Am. Chem. Soc. Symposium on Fiber and Yarn Processing, Phil., April, (1975).

53. Cogswell, F. N., J. Non-Newt. F. M., 2, 37, (1977).

54. Coleman, B. D. and W. Noll, Arch. Rat. Mech. Anal., 6, 355 (1960).

55. Collins, E. A. and J. T. Oetzel, Rubber Age, 102, 64 (1970).

56. Collins, E. A. and J. T. Oetzel, Rubber Age, 103 (1971).

57. Colwell, R. E. and K. R. Nickolls, Ind. Eng. Chem., 51, 841 (1959).

58. Cotten, G. R., Rubber Age, November, 51 (1968).

59. Cox, H. W. and C. W. Macosko, AIChE J., 20, 785 (1974).

60. Crowder, J. W., M. S. Thesis, Chem Eng. U. T. Knoxville (1973).

61. Darnell, W. H. and E. A. J. Mol, SPE J., 12, (4), 20 (1956).

62. Dealy, J. M., Poly. Eng. Sci., 11, 433 (1971).

63. Decker, G. E. and Roth F. L., India Rubber World, 128, 339 (1953).

64. Denn, N. M. and G. Marucci, AIChE J., 17, 101 (1971).

65. Denson, C. D. and R. J. Gallo, Poly. Eng. Sci., 11, 174 (1971).

66. Denson, C. D., W. M. Prest. and J. M. O'Reilly, AIChE J., 15, 809 (1969).

67. den Otter, J. L., J. L. S. Wales and J. Schijf, Rheol. Acta., 6, 205 (1967).

68. den Otter, J. L., Rheol. Acta., 8, 187 (1969). Plast. Poly., 38, 155 (1970).

69. deWitt, T. W., J. Appl. Phys., 26, 889 (1955).

70. Dietz, W., J. L. White and E. S. Clark, Polym. Eng. Sci., 18, 277 (1978).

71. Dillon, J. H. and N. Johnson, Physics, 4, 225 (1933).

72. Dodson, A. G. and P. Townsond and K. Waltors, Computors and Fluids, 2, 317 (1974).

73. Donovan, R. C., D. E. Thomas and L. D. Leversen, Poly. Eng. Sci., 11, 353 (1971).

74. Eccher, S. and W. Valentinotti, Ind. Eng. Chem., 50, 829 (1958).

75. Eisenschitz, R., Koll. Zeit., 54, 184 (1933).

76. Eisenschitz, R., B. Rabinowitch and K. Weissenberg, Mitt. d. deat. Materialprufungsanhalten, 9, 91 (1929).

77. Ericksen, J. L., Quart. Appl. Math., 14, 318 (1956).

78. Forrest, G. and W. L. Wilkinson, Trans. Inst. Chem. Eng., 51, 331 (1973); 52, 10 (1974).

79. Freeman, S. M. and K. Weissenberg, Nature, 161, 324 (1948).

80. Friche, C. A., Poly. Eng. Sci., 6, 135 (1966).

81. Furuta, I., V. M. Lobe and J. L. White, Report No. 53, December (1975), Poly. Sci. & Eng. U. T. Knoxville.

82. Galili, N. and R. Takserman-Krozer, Israel J. Techn., 9, 439 (1971).

83. Gee, R. E. and J. B. Lyon, Ind. Eng. Chem., 49, 956 (1957).

84. Gerard, J. E. and W. Philippoff, Proc. Fourth Int. Cong. Rheol., 2, 77 (1965).

85. GieseKus, H., Rheol. Acta., 4, 85 (1965).

86. GieseKus, H., Rheol. Acta., 7, 127 (1968); 8, 411 (1969).

87. Goldstein, C., Trans. Soc. Rheol., 18, 357 (1974).

88. Graessley, W. W., S. D. Glasscock and R. L. Crawley, Trans. Soc. Rheol., 14:4, 519 (1970).

89. Green, A. E. and R. S. Rivlin, Quart. Appl. Math., 14, 299 (1956).

90. Green, A. E. and R. S. Rivlin, Arch. Rat. Mech. Anal., 1, 1 (1957).

91. Griffith, R. M., Ind. Eng. Chem., 1, 180 (1962).

92. Griffith, R. M., SPE J. 11, 65 (1967).

93. Han, C. D., AIChE J., 17, 1418 (1971): 18, 1286, 19, 649 (1973) and J. Appl. Polym. Sci., 19, 187 (1973).

94. Han, C. D., "Rheology in Polymer Processing". New York, Academic Press, (1976).

95. Han, C. D. and L. H. Drexler, J. Appl. Poly. Sci., 17, 2369 (1973).

96. Han, C. D., K. U. Kim, N. Siskovic and C. R. Huang, J. Appl. Poly. Sci., 17, 95 (1973); Rheol. Acta., 14, 533 (1975).

97. Harmon, D. B., J. Franklin Inst., 259, 519 (1955).

98. Harrison, N., J. Proc. Comp. Phil. Soc., 19, 307 (1919).

99. Hencky, H., ZAMM, 4, 323 (1924).

100. Hohenemser, K. and W. Prager, ZFAMM, 12, 216 (1932).

101. Hopper, J. R., Rubber Chem. Tech., 40, 463 (1972).

102. Huilgol, R. R., "Continuum Mechanics of Viscoelastic Fluid". p. 339. Halsted Press, (1975).

103. Ide, Y. and J. L. White, J. Appl. Poly. Sci., 20, 2511 (1976).

104. Ide, Y. and J. L. White, J. Non-Newt. Fluid Mech., 2, 281 (1977).

105. Ide, Y. and J. L. White, J. Appl. Polym. Sci., 22, 1061 (1978).

106. Janeschitz-Kriegl, H. and Schijf, J. Plastics & Polymers, 37, 523 (1969).

107. Jepson, C. H., Ind. Eng. Chem., 45, 993 (1953).

108. Kacir, L. and Z. Tadmor, Poly. Eng. Sci., 12, 387 (1972).

109. Kaloni, P. N., J. Phys. Soc. Japan, 20, 132 & 610 (1965).

110. Kaufman, M., Plast. Poly., 37, 243 (1969).

111. Klein, I. and D. I. Marshall, Poly. Eng. Sci., 6, 198 (1966).

112. Klein, I. and D. I. Marshall, ed.,,"Computer Programs for Plastics Engineers" (1968).

113. Klein, I. and Z. Tadmor Z, Poly. Eng. Sci., 9, (1), 11 (1969).

114. Klein, I., Poly. Eng. Sci., 15, 444 (1975).

115. Klein, I., Plastics World, 37, 46 (1979).

116. Kobayashi, T. and Tomita, Bull. Jan. Soc. Mech. Eng., 14, 208 (1971); 15, 236 (1972).

117. Kondo, A., Ph.D. Thesis Dept. of Chem. & Met. Eng. U. T. Knoxville (1976).

118. Kraus, G., Polymer Letters, 8, 601 (1970).

119. Kraus, G., J. Appl. Polym. Sci., 15, 1679 (1970).

120. Kraus, G., editor, Reinforcement of Elastomers. New York, Interscience, (1965).

121. Kroesser, F. W. and S. Middleman, Poly. Eng. Sci., 5, 230 (1965).

122. Kruse, R. L., Polymer Letters, Vol. 2, 841 (1964).

123. Langlois, W. E. and R. S. Rivlin, Rend. Math., 22, 169 (1963).

124. LaNieve, H. L. and D. C. Bogue, J. Appl. Poly. Sci., 12, 353 (1968).

125. Lee, B. L. and J. L. White, Trans. Soc. Rheol., 18, 467 (1974).

126. Lindt, J. T., Poly. Eng. Sci., 4, 16, 284 (1976).

127. Lobe, V. M. and J. L. White, "An Experimental Study of the Influence of Carbon Black on the Rheological Properties of a Polystyrene Melt", Polymer Science and Engineering Report No. 118, The University of Tennessee, July, (1978).

128. Lodge, A. S., Trans. Faraday. Soc., 52, 120 (1956).

129. Lodge, A. S., "Elastic Liquids". New York, Academic Press, (1962).

130. Maddock, B. H., SPE J., 15, 383 (1959); 15, 433 (1959).

131. Maerker, L. and W. R. Schowalter, Rheol. Acta., 13, 627 (1974).

132. Malkin, A. Y., V. V. Goncharenko and V. V. Malinovskii, Polymer Mechanics, 12, 439 (1976).

133. Manson, J. A. and L. H. Sperling, "Polymer Blends and Composites", p. 331. New York, Plenum Press, (1976).

134. Marshall, D. I., I. Klein and R. H. Uhl, SPE J., 21, 1192 (1965).

135. Marshall, D. I. and I. Klein, Poly. Eng. Sci., 6, 191 (1966).

136. Martin, B., Plastics and Polymers, 4, 1130 (1970).

137. Matsui, M., M. S. Thesis, Chem. Eng. U. T. Knoxville, (1976).

138. Matsui, M. and D. C. Bogue, Poly. Eng. Sci., 16, 735, (1976).

139. Matsui M. and D. C. Bogue, Trans. Soc. Rheol., 21, 133 (1977); 453 (1977).

140. Matsumoto, T. and D. C. Bogue, J. Poly. Sci.: Physics Ed. 15, 1663 (1977); Trans. Soc. Rheol., 21, 453-468 (1977).

141. Matsumoto, C. Hitomi, and S. Onogi, Trans. Soc. Rheol., 19, 541 (1975).

142. Matsumoto, T., Y. Segawa, Y. Warashina and S. Onogi, Trans. Soc. Rheol., 17, 47 (1973).

143. Matsumoto, T., A. Takashima, T. Masuda, and S. Onogi, Trans. Soc. Rheol., 14, 617 (1970).

144. Maxwell, J. C., Phil. Trans. Roy. Soc., A157, 49 (1867).

145. McCabe, N. and C. C. Mucller, Trans. Sec. Rheol., 5, 329 (1961).

146. McKelvey, J. M., SPE J., 9, (3), 12 (1953).

147. McKelvey, J. M., Ind. Eng. Chem., 46, 660 (1954).

148. McKelvey, J. M., Ind. Eng. Chem., 45, 978 (1953).

149. McKelvey, J. M., in "Rheology", Vol. 3, ed. by F. R. Eirich. Academic Press, (1960).

150. McKelvey, J. M., "Polymer Processing". New York, John Wiley & Sons, (1962).

151. Medalia, A. I., J. Colloid Interf. Sci., 32, (1), 115 (1970).

152. Meissner, J., Rheol. Acta., 8, 78 (1969).

153. Meissner, J., Trans. Soc. Rheol., 13, 123 (1969).

154. Meister, B. J., Trans. Soc. Rheol., 15, 63 (1971).

155. Mendelson, R. A., F. L. Finger and E. B. Bagley, J. Poly. Sci., C35, 177 (1971).

156. Mendelson, R. A. and F. L. Finger, J. Appl. Poly. Sci., 17, 797 (1973).

157. Mendelson, R. A. and F. L. Finger, J. Appl. Poly. Sci., 19, 1061 (1975).

158. Metzner, A. B., Trans. Soc. Rheol., 13, 429 (1969).

159. Metzner, A. B., E. L. Carley, and I. K. Park, Mod. Plastics, 37, 11, 133 (1960).

160. Metzner, A. B., W. T. Houghton, R. E. Hurd and C. C. Wolfe, "Second Order Effects in Elasticity, Plasticity and Fluid Dynamics". Pergammon, (1962).

161. Metzner, A. B., W. T. Houghton, R. A. Sailor and J. L. White, Trans. Soc. Rheol., 5, 133 (1961).

162. Metzner, A. B. and A. P. Metzner, Rheol. Acta., 9, 174 (1970).

163. Metzner, A. B., E. A. Uebler and C. F. Chanman Fong, AIChE J., 15, 750 (1969).

164. Metzner, A. B., J. L. White and M. M. Denn, AIChE J., 12, 863 (1966).

165. Middleman, S., Trans. Soc. Rheol., 9, (1), 83 (1965).

166. Middleman, S., "The Flow of High Polymers". New York, Wiley, (1968).

167. Middleman, S., Trans. Soc. Rheol., 13, 123 (1969).

168. Minagawa, N. and J. L. White, J. Appl. Poly. Sci., 20, 501 (1976).

169. Mohr, W. D. and R. S. Mallouk, Ind. Eng. Chem., 51, 756 (1959).

170. Mooney, M., J. Rheol., 2, 210 (1931).

171. Mooney, M., J. Colloid Sci., 2, 69 (1947).

172. Mooney, M. and S. A. Black, J. Colloid Sci., 7, 204 (1952).

173. Mooney, M., "The Rheology of Raw Elastomers" in "Rheology", Vol. 2, ed. by F. R. Eirich. New York, Academic Press, (1958).

174. Morette, R. A. and C. G. Gogos, Poly. Eng. Sci., 8, 272 (1968).

175. Mori, Y. and N. Ototoke, Chem. Eng. (Japan), 17, 2224 (1953); 18, 221 (1954).

176. Nakajima, N., H. H. Bowerman and E. A. Collins, Rubber Chem. Techn., 46, 417 (1973); Proc. Inter. Rubber Conf., Tokyo, 15-3-20 (1975).

177. Nakajima, N. and M. Shida, Trans. Soc. Rheol., 10, 299 (1966).

178. Nickell, R. E., R. I. Tanner and B. Caswell, J. Fluid Mech., 65, (1), 189 (1974).

179. Noll, W., Arch. Rat. Mech. Anal., 2, 197 (1958).

180.. Oda, K., J. L. White and E. S. Clark, Polym. Eng. Sci., 18, 25 (1978).

181. Oldroyd, J. G., Proc. Camb. Phil. Soc., 43, 100 (1947).

182. Oldroyd, J. G. Proc. Roy. Soc., A200, 523 (1950).

183. Oldroyd, J. G., Quart. J. Mech. Appl. Math., 4, 271 (1951); Proc. Roy. Soc., A245, 278 (1958).

184. Onogi, S., T. Masuda and T. Matsumoto, Trans. Soc. Rheol., 14, 275 (1970).

185. Onogi, S., T. Matsumoto and Y. Warashina, Trans. Soc. Rheol., 17, 175 (1973).

186. Pearson, J. R. A. and R. Trottnow, J. Non-Newt. F. Mech. (in press).

187. Perera, M. G. N. and K. Waltor, J. Non-Newt. F. Mech., 2, 49 (1977); 2, 197 (1977).

188. Philippoff, W. and F. H. Gaskins, Trans. Soc. Rheol., 2 263 (1958).

189. Pigott, W. T., Trans, A. S. M. E., 947 (1951).

190. Pipkin, A. C., Pro. 4th Int. Rheol. (E. H. Lee, ed.) Partl., p. 213. New York, Wiley, (1965).

191. Pliskin, I. and N. Tokita, J. Appl. Polym. Sci., 16, 473 (1972).

192. Rabinowitsch, B., Z. Physik. Chem., A145, 1 (1929).

193. Racin, R. and D. C. Bogue, "Molecular Weight Effects in Die Swell and in Shear Rheology", J. Rheology, 23, (3), 263 (1979).

194. Racin, R., M. S. Thesis, Chem Eng. U. T. Tennessee, (1978).

195. Ramsteiner, F., Kunststoffe, 61, 943 (1971).

196. Reddy, K. R. and R. I. Tanner, "On the Swelling of Extruded Plane Sheets", J. Rheology, 22, (6), 661 (1978).

197. Reiner, M., "Deformation, Strain and Flow". London, Lewis, (1948).

198. Reiner, M., "Lectures on Theoretical Rheology", 3rd ed. North Holland, Amsterdam,((1960).

199. Roman, J. F., "Die Swell in Molten Polymers", M. S. Thesis, U. T. Tennessee, June (1974).

200. Roscoe, R., Phil. Mag. (Ser. 7) Vol. 40, 338 (1949).

201. Rothemeyer, F., Kunststoffe, 59, 333 (1969).

202. Rothemeyer, F., Kunststofftechnik, 9, 235 (1970).

203. Rothemeyer, F., Rheol. Acta., 9, 259 (1970).

204. Rowell, H. S. and D. Finlayson, Engineering, 114, 606 (1922); 12, 249, 385 (1928).

205. Schechter, R. S., AIChE J., 1, 445 (1961).

206. Schneider, K., Kunstoffe, 59, (2), 97 (1969).

207. Schott, H. and W. S. Kaghan, Ind. Eng. Chem., 51, 844 (1959).

208. Schlaffer, W., J. Schijf and H. Janeschitz-Kriegl, Plastics & Polymers, 6, 193 (1971).

209. Schummer, P., Rheol. Acta., 6, 192 (1967).

210. Schummer, P., Rheol. Acta., 7, 271 (1968).

211. Semjonow, V. V., Rheol. Acta., 6, 171 (1967).

212. Shroff, R. N. and M. Shida, Paper presented at the annual meeting of the Society of Plastic Engineering (ANTEC) in Montreal (1977).

213. Shroff, R. N., L. V. Cancio and M. Shida, Trans. Soc. Rheol., 21, 429 (1977).

214. Snyder, J. M. and M. H. Leonard, in "Introduction to Rubber Technology", ed. by M. Morton. New York, Reinhold, (1959).

215. Spencer, R. S. and R. E. Dillon, J. Colloid Sci., 3, 163 (1948).

216. Spencer, R. S. and R. E. Dillon, J. Colloid Sci., 4, 241 (1949).

217. Spriggs, T. W., Chem. Eng. Sci., 20, 931 (1965).

218. Spriggs, T. W. and R. B. Bird, Ind. Eng. Chem. Fund., 4, 182 (1964).

219. Spriggs, T. W., J. D. Huppler and R. B. Bird, Trans. Soc. Rheol., 10 (1966).

220. Street, L. F., Inter. Plastics Eng., 1, 289 (1961).

221. Strauss, K., Acta. Mech., 20, 233 (1974).

222. Tadmor Z., Poly. Eng. Sci., 6, 185 (1966).

223. Tadmor, Z. and E. Broyer, Poly. Eng. Sci., 12, 378 (1972).

224. Tadmor, Z., I. Duvdevani and I. Klein, Ibid 7, 198 (1967); Poly. Eng. Sci., 7, 198 (1967).

225. Tadmor, Z. and I. Klein, Poly. Eng. Sci., 9, (1), 1, (1969).

226. Tadmor, Z. and I. Klein, "Engineering Principles of Plasticating Extrusion" (1970).

227. Tanner, R. I., J. Appl. Polym. Sci., 12, 1649 (1968).

228. Tanner, R. I., J. Poly. Sci., A2, 8, 2067 (1970).

229. Tanner, R. I., Trans. Soc. Rheol., 17, 365 (1973).

230. Tanner, R. I., in "US-Japan Seminar on Polymer Processing and Rheology", ed. by D. C. Bogue, M. Yamamoto and J. L. White, Appl. Polym. Symp., 20, 201 (1973).

231. Thien, N. P. and R. I. Tanner, J. Non-Newt. F. Mech., 2, 353 (1977).

232. Thomas, D. P. and R. S. Hagan, Poly. Eng. Sci., 9, 164 (1969).

233. Tobolsky, A. V., "Properties and Structure and Polymers".

234. Tobolsky, A. V. and G. M. Brown, J. Poly. Sci., 17, 547 (1958).

235. Tobolsky, A. V. and K. Murakami, J. Poly. Sci., 40, 443 (1959).

236. Tokita, N. and I. Pliskin, Rubber Chem. Techn., 46, 1166 (1975).

237. Tokita, N. and R. Scott, Rubber Chem. Techn., 42, 944 (1969).

238. Tokita, N. and J. L. White, J. Appl. Poly. Sci., 10, 1011 (1966).

239. Toor, H. L., Trans. Soc. Rheol., 1, 177 (1957).

240. Tordella, J. P., J. Appl. Phys., 27, 454 (1956).

241. Tordella, J. P., Trans. Soc. Rheol., 1, 203 (1957).

242. Tordella, J. P., J. Appl. Polym. Sci., 1, 215 (1963).

243. Tordella, J. P., in "Rheology", Vol. 5, ed. by F. R. Eirich. New York, Academic Press, (1969).

244. Townsond, P., K. Waltors and W. M. Watorhouse, J. Non-Newt. Fluid Mech., 1, 107 (1976).

245. Truesdall, C. and R. A. Toupin, "The Classical Field Theories", in Hand buch Der Physik, Vol. III. Berlin, Springer, (1960).

246. Ui, J., Y. Ishimru, H. Murakami, N. Fukushima and Y. Mori, SPE Trans., 4, 295 (1964).

247. Uy, W. C. and W. W. Graessley, Macro., 4, 458 (1971).

248. Utracki, L. A., Z. Bakerdjian and M. R. Kamal, J. Appl. Polym. Sci., 19, 431 (1975).

249. Vinogradov, G. V., N. L. Insarova, B. B. Boiko and E. K. Borisenkora, Poly. Eng. Sci., 12, 323 (1972).

250. Vinogradov, G. V., A. Ya Malkin, E. P. Plornikova, D. Yu. Sabsai and N. E. Nikolayava, Int. J. Poly. Mat., 2, 1 (1972).

251. Vlachopoulos, J., Rheol. Acta., 13, 2 (1974).

252. Vlachopoulos, J. and M. Alam, Poly. Eng. Sci., 12, 184 (1972).

253. Vlachopoulos, J. and T. W. Chan, J. Appl. Polym. Sci., 21, 1177 (1977).

254. Vlachopoulos, J., M. Horie and S. Lidorikis, Trans. Soc. Rheol., 16, 669 (1972).

255. Wales, J. L. S., J. L. den Otter and H. Janeschitz-Kriegl, Rheol. Acta., 3, 83 (1963).

256. Wales, J. L. S., "The Application of Flow Birefringence to Rheological Studies of Polymer Melts". Delft, Delft University Press, (1976).

257. Weissberg, H. L., Phys. Fluids, Vol. 5, 1033 (1962).

258. Weissenberg, K., Proc. 1st Int. Rheol. Cong. (1949).

259. Wheeler, J. A. and E. H. Wissler, AIChE J., 11, 207 (1965).

260. Wheeler, J. A. and E. H. Wissler, Trans. Soc. Rheol., 10, 353 (1966).

261. White, J. L., Rubber Chem. Tech., 42, 257 (1969).

262. White, J. L., Appl. Poly. Symp., 20, 155 (1973).

263. White, J. L., Trans. Soc. Rheol., 19, 271 (1975).

264. White, J. L., Ch. 5 "Rubber Science and Technology", ed. by F. R. Eirich, A. M. Gassler and E. G. Konotos (in press).

265. White, J. L., Rubber Chem. Techn., 50, 163 (1977).

266. White, J. L. and J. W. Crowder, J. Appl. Poly. Sci., 18, 1013 (1974).

267. White, J. L. and A. Kondo, J. Non-Newt. Fluid Mech., 3, 41 (1978).

268. White, J. L. and Y. M. Lin, J. Appl. Poly. Sci., 17, 3273 (1973).

269. White, J. L. and A. B. Metzner, J. Appl. Poly. Sci., 8, 1367 (1963).

270. White, J. L. and J. F. Roman, J. Appl. Poly. Sci., 20, 1005 (1976); ibid 21, 869 (1977).

271. White, J. L. and N. Tokita, J. Appl. Poly. Sci., 11, 321 (1967); ibid 11, 321 (1967).

272. White, J. L., J. Non-Newt. Fluid Mech., 5, 177 (1979).

273. Williams, M. C. and R. B. Bird, AIChE J., 12, 1064 (1966).

274. Williams, M. L., R. F. Landel and J. D. Ferry, J. Amer. Chem. Soc., 77, 3701 (1955).

275. Winter, H. H., Poly. Eng. Sci., 15, 2 (1975).

276. Wissler, E. H., Poly. Eng. Sci., 15, 2 (1975).

277. Wortberg, J., P. B. Junk and Menges, SPE Antec Tech. paper, 35, 434 (1977).

278. Worth, R. A., J. Parnaby and H. A. A. Helmy, Poly. Eng. Sci., (17), 257 (1977).

279. Yamamoto, M., J. Phys. Soc. Japan, 11, 413 (1956); 12, 1148 (1957); 13, 1200 (1958).

280. Yamamoto, M., Trans. Soc. Rheol., 15, 783 (1971).

281. Zamodits, H. J. and J. R. A. Pearson, Trans. Soc. Rheol., 13, 357 (1969).

282. Zapas, L. J. and T. Craft, J. Res. Nat. Bur. Stand., 69A, 541 (1965).

283. Zapas, L. J., J. Res. Nat. Bur. Stand., 70A, 525 (1966).

284. Zaremba, S., Bull. Acak. Sci., Cracovie, 594 (1903).

VITA

David C. Huang was born in Chung-Chin, China on May 14, 1947. He was brought to Taiwan during the Chinese civil war in 1949. He attended Min-Tshang Elementary School and Gin-Ko High School in Taipei, graduating from the latter in June 1969.

After serving one year in army as a Chemistry Instructor, he worked two years for Tatung Paint & Varnish Co. where for the first time he was introduced into polymer industry. Between July 1972 and September 1973, he was a teaching assistant in Tatung Institute of Technology. On September 12, 1973, he came to the U.S.A. to attend Stanford University and received Master of Science degree in Chemical Engineering in June 1975.

In September 1975, he entered the Graduate School of the University of Tennessee. He passed his oral examination of dissertation for the Doctor of Philosophy degree in Polymer Engineering in August 1978.